QoS–Constrained Information Theoretic Capacity Maximization in CDMA Systems

by

Arash Abadpour

A thesis submitted to the Faculty of Graduate Studies

in partial fulfillment of the requirements for the degree of

Doctor of Philosophy

Department of Electrical and Computer Engineering

The University of Manitoba

Winnipeg, MB, Canada

THE UNIVERSITY OF MANITOBA

FACULTY OF GRADUATE STUDIES

*****

COPYRIGHT PERMISSION

QoS-Constrained Information Theoretic Capacity Maximization in CDMA Systems

By

Arash Abadpour

A Thesis/Practicum submitted to the Faculty of Graduate Studies of The University of Manitoba in partial fulfillment of the requirement of the degree

Of

Doctor of Philosophy

To the concept of friendship.

Contents

Abbreviations

AWGN Additive White Gaussian Noise

CDMA Code Devision Multiple Access

CSC Classical Single Cell

CSC^{a} Approximation–enabled Classical Single–Cell

DS–CDMA Direct Sequence Code Devision Multiple Access

HDR High Data Rate

MC Multiple–Cell Multiple–Class

MINLP Mixed Integer Nonlinear Programming

MSC Multiple–Class Single–Cell

M^{1}SC Multiple–Class Single–Cell solved using Linear Programming

M^{2}SC Multiple–Class Single–Cell solved using Quadratic Programming

MSC$^{a\nu L_i}$ Generalized Multiple–Class Single–Cell

NSC New Single Cell

N′SC Internal Variant of the NSC utilized within the N^{+}SC

N′SC+c Internal Variant of the NSC utilized within the N^{+}SC

NSC^a Approximation-enabled New Single-Cell

NSC^{f-} New Single-Cell with Concave Utility Function

NSC^{f+} New Single-Cell with Convex Utility Function

NSC$^\alpha$ New Single-Cell with the Utility Function $f(x) = x^\alpha$

N$^+$SC New Enhanced Single Cell

N$^+$SC^a Approximation-enabled New Enhanced Single Cell

OFDMA Orthogonal Frequency Division Multiple Access

OPC Opportunist Power Control

QoS Quality of Service

SIR Signal to Interference Ratio

TDMA Time Division Multiple Access

List of Figures

List of Tables

Abstract

Code Division Multiple Access (CDMA) has proved to be an efficient and stable means of communication between a group of users which share the same physical medium. Therefore, with the rising demand for high–bandwidth multimedia services on mobile stations, it has become necessary to devise methods for more rigorous management of capacity in these systems. While one of the substantial techniques for regulating capacity in CDMA systems is through power control, the mathematical complexity of the regarding model complicates the analysis and the subsequent implementation of useful generalizations and extensions.

In this thesis, the classical problem of capacity optimization in the reverse link of a CDMA system is analyzed. Here, it is shown that the classical formulation of the problem is solvable through examination of a finite set of transmission powers, for which closed forms are given. Although, this method leads to a more accurate and a faster solution to the classical problem, it is noted that the classical problem is very prone to yielding partial solutions in which the calculated system capacity is not realizable in a practical setting. The developed mathematical model, however, is shown to be applicable to more general definitions of the problem.

The major part of this thesis is the analysis of the capacity optimization problem equipped with increasing sets of constraints and utility functions. These features are incorporated into the problem in order to produce solutions deployable in practical systems. Cases of multiple–class systems are also analyzed and more accurate system models are implanted in the problem as well. Subsequently, after single–cell systems are carefully examined, one chapter is devoted to the analysis of multiple–cell systems. These systems are modeled based on an inclusive set of parameters.

For each problem, a solver is developed and experimental results are discussed. Some of the material presented in this thesis has been previously published in a number of articles, as listed in Appendix B.

Chapter 1

Introduction

An essential means of regulating the capacity in CDMA systems is through effective transmission power assignment [1]. The necessity of this issue arises from the fact that, for example, in DS–CDMA systems there is universal frequency reuse, meaning that the same carrier frequency and spectral band are shared in all the cells [2]. Hence, it is important to devise a method which is capable of assigning optimal transmission powers to the mobile stations in accordance with a set of practical constraints as well as a properly–devised objective function (see a survey in [3]). In fact, it has been shown that proper control of the transmission powers of the mobile stations in a cellular system can result in the control and suppression of the interference in the system [4].

The basic approach to the capacity optimization problem is to define a set of constraints and then to find the solution which satisfies all of them at equality. One example of this approach is to find the set of transmission powers which provide a given (often identical) Signal to Interference Ratio (SIR) for all the mobile stations in a cell [5]. For example, in [6], the researchers work on capacity design and call admission control analysis based on a fixed–SIR approach (also see [7, 8]). A comprehensive and generalized treatment of this topic can be found in [9]. It is worth to mention that the fixed–SIR approach is implemented through power control carried out by the individual mobile stations. In this framework power messages transmitted by the base station instruct each mobile station to power either up or down [10]. For a thorough review of control strategies and feedback mechanisms in power control refer to [11].

In an early paper, *Zander* [12] discussed the idea of equalizing the SIR of the signals received from different mobile stations at the base station in a cellular radio system. The suggested target–tracking approach guarantees the same quality of service for all the mobile stations in the system and has been investigated thoroughly in the literature (see [9, 13, 14, 15, 16, 17] as examples among other works). In a system which utilizes the fixed–SIR approach, as the mobile stations undergo the deterioration of the signal received from them at the base station, due to deep fades for example, they increase their transmission power. Equalization of the SIR also helps in dealing with the near–far effect, by enabling the mobile stations far from the base station to achieve the same quality of service that those close to it do [18]. The fact that all the mobile stations in such a system are provided with the same capacity is a direct reflection of the voice–only nature of the earlier CDMA networks [19].

For more work on enhancing system performance through finding optimal values of the system parameters, including the minimum SIR bound, refer to [20] and the references therein. This work is also different from the approaches which model the problem as a non–cooperative game [21, 22, 23, 24] and also the Opportunist Power Control (OPC) approaches such as [25, 26, 27]. In the framework of the OPC, the mobile stations increase their transmission power as they acquire a better link to the base station (also called "multiuser diversity" [28]). Here, we do not consider the issue of optimizing the hand–offs and the underlying trade–off between their cost compared to connection quality either (for details refer to [29, 30]). Furthermore, relatively similar concepts are discussed in capacity optimization for Orthogonal Frequency Division Multiple Access (OFDMA) systems. For example, among other works, joint analysis of channel allocation, modulation level and power control in a multiple–cell OFMDA network is discussed in [31] (refer to [32] for more work on multiple–cell OFDMA systems and to [33, 34] for the analysis of the single–cell ones).

With the introduction of multimedia services to wireless CDMA communications, the goal is no more to provide fixed capacity to all the mobile stations [35], but to maximize the aggregate capacity given a set of constraints [1]. In fact, the addition of other types of services to the conventional voice–only communication channels has urged the need for more control over the rates

at which different mobile stations transmit [36]. This is necessary in order to maximize system performance measures including the aggregate capacity [18]. For an early coverage of managing multiple–rate systems [37] through maintaining fixed chip–rate and different transmission powers refer to [38, 39].

The communication channel, through which the data is transfered, can be defined from different perspectives. In the literature, this channel is defined as, either the physical medium through which the electromagnetic waves are propagated, or the radio channel which also includes the receiver and the transmitter antennas, or the digital channel which includes the modulation and demodulation stages as well [40]. Here, we consider the definition of the communication channel as the radio channel (also see [41]).

The maximization of the capacity, in this thesis, is carried out at the reverse link (uplink), because this link is often the limiting link [42, 43] which has to satisfy stringent requirements [44] as well. In fact, the focus on the reverse link in many of the works cited here, as well as in the present work, is in accordance with what the authors of [45] mention to be the consideration of "the majority of the literature". For example, it is suggested that in the presence of an ideal power control mechanism and hard hand–off, the reverse link limits the system capacity [18]. However, it has to be emphasized that a consensus on this issue does not exist in the literature and some researchers work on the forward link as well (for an example of work on the forward link refer to [46]). For an early coverage of the capacity of the reverse link, accompanied by results gathered from field tests, refer to [47] (also see [48]). Among different channels on the reverse link, this thesis concentrates on the traffic channels, due to the more demanding conditions they need to satisfy in order to establish stable communications [49].

The rest of this chapter is organized as follows. First, in Section 1.1, the literature of capacity analysis at the reverse link in single–cell systems is analyzed. Then, in Section 1.2, multiple–cell systems and the challenges of capacity optimization in them are discussed. This discussion essentially addresses the implications of modeling CDMA systems within multiple–cell frameworks as opposed to the more simplistic single–cell approaches. The chapter then follows with a thorough investigation of the parameters of single–cell CDMA systems as well as

those of the multiple-cell ones, in Section 1.3. This investigation yields SIR models which are used throughout this thesis in formulating different optimization problems. At the end of this chapter, in Section 1.4, the structure of the rest of this thesis is briefly discussed.

1.1 Single-Cell Systems

The maximization of the capacity of the reverse link in this thesis is achieved through controlling the transmission powers of the individual mobile stations. Here, the analysis is first carried out in a single-cell system, by assuming that either there is only one cell in the system or that the activity in other cells can be modeled as fixed interference to the current cell [50].

In this thesis, the term capacity is defined as the rate of transmission of each mobile station. Here, to relate the transmission power to rate, an information theoretic approach is taken [51] (also see [52, 53]) and Shannon's theorem is used [1, 54]. The adoption of the maximum bound given by Shannon's theorem is based on previously-developed models (see [1, 54, 55] for example). This issue will be discussed in more detail later in this section.

The system-wide information theoretic capacity of CDMA systems was first analyzed in [50] and then developed further for multi-user networks in [56]. While these works focus on the set of all capacities, more recent research has benefited from the advances in matched filters [1] and the aggregate capacity has been analyzed [55, 57, 58]. In these works, assuming a sub-optimal coding scheme, the mapping between the SIR and the throughput is determined by the coding strategy.

Subsequently, research in the field has benefited from capitalizing on the assumption of Shannon's capacity. Although, Shannon's theorem gives the maximum bound for the capacity, the existence of coding strategies such as Turbo Coding makes Shannon's bound practically achievable [1]. It should be emphasized that, here, the assumption of Additive White Gaussian Noise (AWGN) [59] is necessary for the adoption of the maximum bound on the system capacity as given by Shannon's theorem [60].

The analysis of the capacity-maximization problem for a particular group of mobile stations is given in many works. However, many of these methods do not have a natural generalization

when different groups of customers are incorporated into the problem [61]. For example, in [62] the authors work on a two-class system in which voice users are guaranteed a minimum quality and data users are provided with the highest possible system capacity.

A general category of the research done on optimizing the transmission powers of the reverse link is based on maximizing capacity-oriented, often similarly-defined, objective functions, subject to different sets of constraints (also see [63]). For example, in [9, 13, 64, 65], the authors work on minimizing the transmitted power subject to a minimum SIR requirement, an approach suitable for fixed-SIR voice-only communications. In [66], the authors work on a similar problem with the difference that they formulate the objective function as representing the throughput for delay-tolerant users. In fact, the major difference between these works is the constraints they use and subsequently how much realistic their solutions become, as a result of the utilized constraints. For example, in [67], the only constraints are a minimum guaranteed SIR and bounds on individual transmission powers. There, first, the problem is constituted as minimizing the aggregate received power. Then, it is reformulated as maximizing the aggregate capacity. A similar problem is looked at in [68], where the authors minimize the aggregate received power in a multiple-cell system subject to power and SIR constraints, where the assignment of the mobile stations to the cells is to be decided as well. A similar problem is treated in [69, 70] in a stochastic framework.

In a recent paper, *Oh* and *Soong* [71] developed a method for optimizing the aggregate reverse link capacity of a CDMA system given a set of constraints. In that work, the study is carried out in a single cell for aggregate system capacity maximization. The constraints of that problem include minimum SIR, maximum and minimum bounds for transmission powers, and maximum bound on the aggregate received power. In fact, one of the main contributions of [71] is the addition of the minimum SIR constraint to the problem. That has primarily been an attempt for resolving the issue of impractical solutions produced earlier, as reported in [57, 58]. For simplicity of reference, throughout this thesis, the problem analyzed in [71] will be addressed as the Classical Single Cell problem (CSC).

One of the major contributions of the work performed in [71] is the reduction of the dimension of the search space. In fact, in a cell which contains M mobile stations, the search space for

the CSC is essentially M–dimensional. However, *Oh* and *Soong* showed that the search can be limited to a multiple of M number of one–dimensional intervals. For that, they utilized a numerical optimization procedure [71].

It is worth to mention that while the approach taken in [71] considers the identity function as the utility identifier, there are sound arguments for the appropriateness of concave utility functions for data communication [72]. For instance, it is suggested that the application of concave utility functions in the aggregate–capacity maximization problem leads to intrinsically more fair capacity distributions [73]. This issue will be treated in Section 3.4.

In contrast with the classical model for the SIR, used in [71] among other works, this thesis also investigates the incorporation of more advanced models, suggested in [57, 74, 75] and elsewhere. These models, however, directly alter the structure of the SIR and thus demand the development of new models to tackle the resulting problems. Here, we also consider different classes of services for different users [76] to collectively set up a problem encompassing an inclusive set of features.

Thorough research has shown that the classical formulation of the capacity maximization problem given in [71] has to be restructured in order to contain more explicit bounds on the unfairness of the system (see the discussions given in [58] for more details). Chapter 3 discusses the new additions to and the alterations of the CSC into new forms which exhibit better properties in terms of fairness, among other factors.

1.2 Multiple–Cell Systems

There are substantial differences when CDMA systems are modeled within a multiple–cell framework (see [45] and the references therein). Among these differences are the presence of inter–cell interference [47], as well as the trade–offs to be dealt with regarding the strength of the pilot signals and the issue of cell placement [45]. In this thesis, we address the task of transmission power assignment in a multiple–cell system when an inclusive SIR model is utilized.

In dealing with the challenges of producing the solution to a multiple–cell problem, some researchers have suggested reduction methods which use approximations in order to reduce a

multiple–cell one to an imaginary single–cell system [77]. This is because one of the main challenges of dealing with the problem in a multiple–cell setting is the fact that interference to the signal received from any mobile station at the corresponding base station includes more than just the transmission powers of all the mobile stations in that same cell. In fact every mobile station in the system can potentially be a source of interference to every other one. From a mathematical point of view, as will be shown later, the primary challenge with the multiple–cell model for the SIR is the existence of extra terms in its denominator. These terms represent entities from outside the corresponding cell. Collective address of these terms plus the background noise as the new imaginary background interference can potentially lead to producing a rough solution for a multiple–cell system through using single–cell solvers. However, the implementation of this scheme demands proper design of an iterative procedure. Among other issues, concerns over stability and convergence of such iterative methods are of grave significance (this issue is fully covered in [78] for a similar problem). The challenging aspects of iterative optimization of the capacity include the need for proper handling of hand–offs [79]. In addition, in some implementations, such as the GSM for example, delays of as long as $500ms$ in the measurement and feedback loop can exist [11]. The integrity and stability of the optimization method in these long–delay scenarios adds to the challenges of using iterative approaches.

Another simplistic approach to direct reduction of a multiple–cell problem into a single–cell one is through the use of the "loading factor". This technique assumes that the intra–cell interference arriving at the base station of a cell can be safely approximated by a fraction of the inter–cell interference in the same cell. In other words, it is suggested that there exists a constant factor δ which when multiplied by the inter–cell interference, can in fact approximate the intra–cell interference [80]. This reduction technique leads to a problem which can be solved by a modified version of a single–cell solver developed later in this thesis. Here, δ is the loading factor, also called the "inter–cell interference factor" (also denoted by g). Equivalently, it is suggested that the intra–cell interference can be taken care of by adding $[\delta M]$ imaginary mobile stations to a cell containing M mobile stations [81].

In this thesis, we use a multiple–cell model which explicitly addresses the inter–cell interfer-

ence without using rough estimations such as the ones mentioned in the above. The algorithm, however, takes advantage of the loading factor, and other approximations, in order to simplify some of the constraints.

The issue of base station assignment is a key factor in optimizing the capacity in a multiple–cell system [82]. In this thesis, we consider the case of each mobile station being connected to only one base station chosen by a separate algorithm [83]. Therefore, the aim of this work is to develop an efficient method for optimizing the transmission powers of the mobile stations assuming that the assignment is already given or that it will be optimized by an algorithm which uses the method developed here within an assignment optimization procedure.

One of the major categories of the research done on power optimization in multiple–cell systems approaches it from a game–theory perspective [76, 82, 84] (also see [23, 85, 86]). For example, in a 2004 paper [79] (an extension to the single–cell work by the same team presented in [87]), the authors aim at achieving a fixed–SIR for all the mobile stations through distributed calculation of the optimal transmission powers. To do so, a closed–loop control mechanism is designed which, for each mobile station, uses a linear combination of its transmission power and a capacity–related term as the cost function. The capacity term in that paper is defined using the Shannon formulation and the paper partly adopts the definition of its cost from earlier works [72, 88].

A comprehensive study of the application of Game Theory–based methods adopted from the field of economics in multiple–cell power control is given in [88]. The aim of these methods is to set up an optimization process through which each mobile station will independently maximize its own utility [88]. The definition of utility in this category is sometimes unique to each paper. The actual implementation of the game is different in different works as well. For example, in [75], the authors extend a centralized game–theory based approach to a decentralized one through implementing a penalty function which will encourage the mobile stations to move towards the point in which every mobile station meets its individually–assigned SIR while minimizing the overall interference to the neighboring cells. In [89] game–theory concepts are utilized for a joint

analysis of the uplink and the downlink simultaneously, where fixed SIR is achieved in a multi–rate system. For more applications of methods borrowed from game theory and microeconomics refer to [90, 91, 92].

In [93, 94], the authors investigate utility–based power allocation for the forward link (downlink) in a multiple–cell CDMA network. The analysis in that work first suggests a solution for the underlying single–cell problem and is then generalized to a two–cell scenario. Subsequently, the authors suggest a signaling–based approach to finding a solution to the problem when a more general setting, containing more than two cells, is to be dealt with. In [77] the authors utilize a model similar to the one implemented in this thesis for the forward link. That work considers the two problems of resource allocation and base station assignment simultaneously, through joint study of powers as well as the utilized rates. The resulting non–convex optimization problem is then dealt with using a distributed algorithm which is based on dynamic pricing. An earlier work on the joint consideration of the transmission powers and the spreading gains for the reverse link in a single–cell setting can be found in [95] as well. The approach taken in that paper is then generalized in [96] to multiple–cell systems. Similar to the case of the early coverage of the CSC [71], the formulation utilized in many of the works cited in the above results in all the mobile stations being forced to transmit at the lowest possible rate while the mobile station which is the closest to the base station will be transmitting at orders of hundreds of times more of capacity (a Time Division Multiple Access (TDMA)–style strategy). This situation is extensively analyzed in [57, 58] and is known to result in a very unfair system, in which guarantees of quality of service are hard to achieve. Nevertheless, taking a similar approach, in [97], the authors work on the joint optimization of transmission powers as well as the corresponding scheduling. The distributed forward link optimization approach presented in that work operates in a multiple–cell system and is based on the idea of switching off the transmission in cells which show poor performance. That approach is assumed to contribute to increasing the aggregate capacity through decreasing the intra–cell interference.

In another attempt, and in continuation of the work done earlier [98, 99], the authors of [100] suggest Mixed Integer Nonlinear Programming (MINLP) as the solver for both single–cell and

multiple–cell problems. There, the challenge of base station assignment is taken into consideration as well and the system is modeled at the reverse link. Other works on capacity maximization for the forward link include [101, 102]. In both these cases a maximum bound on the transmission rates is not considered and thus these approaches yield similar TDMA–type outcomes (for more discussion on the topic refer to [77] and also IS–856 system specifications [103] as well as High Data Rate (HDR) systems [42, 104]).

It is important to emphasize that the work presented in this thesis produces the solution in polynomial time. This solution is often given as a closed form, or alternatively proved to be a member of a finite set, the members of which are given in closed form. Some other algorithms developed in this work utilize numerical search for finding the optimal solution, in which case the algorithm is always proved to be able to find the solution, or an approximation of it, in finite time. This is in contrast to works such as [77] which do not guarantee to always generate the optimal solution.

1.3 System Model

The discussion about the system model utilized in this thesis starts in Section 1.3.1 where a single–cell system model is described. Then, a set of new features adopted from more recent works is presented in Section 1.3.2. These improvements are applied to the single–cell model in order to generalize it and rewrite in the context of multiple–cell scenarios, as presented in Section 1.3.3. The single–cell system presented here is adopted from previous works such as [57].

1.3.1 Single Cell Systems

The maximum bound on the capacity of a single point–to–point communication link is given by the Shannon theorem as [1] (also, see [55]),

$$C = B \log_2 (1 + \gamma) . \tag{1.1}$$

Here, B is the bandwidth and γ is the SIR of the communication link. In the rest of this thesis we omit B knowing that it is a constant multiplier. Hence, here, relative capacities are analyzed. For convenience, the term "relative" will be omitted as well. We emphasize that, in order to produce numbers with the proper unit, the vertical axis of the graphs which carry capacity–related terms should be read as relative to B.

Assume that there are M mobile stations with reverse link gains of $g_1, \cdots, g_M$, all located in the same cell and communicating with the same base station. Throughout this thesis, we will address the sequence $g_1, \cdots, g_M$ as the vector $\vec{\mathbf{g}}$. Similarly, for any other variable which is defined for a set of mobile stations or cells, we will use a similar vector abbreviation, given that it is clear in the context what is being addressed. The assumption of fixed $\vec{\mathbf{g}}$ which only models the path–loss, is based on the assumption that the system is analyzed in time slots of T_s, where $T_s \gg \frac{1}{W}$ (W is the bandwidth), and that the coherence time of the most rapidly varying channel is greater than T_s. Therefore, in each time slot, $\vec{\mathbf{g}}$ can be assumed to be constant [57]. It is also worth to mention that the typical time interval during which the shadowing factor in nearly constant for a mobile station is a second or more [2]. Therefore, the assumption of constant $\vec{\mathbf{g}}$ is in fact valid for algorithms with run–times significantly less than a second. Furthermore, for low to moderate data rates, the inter–symbol interference can be dealt with through channel equalization [41] and thus, multi–path fading can be considered to be flat (constant for all symbols) as well [11]. These assumptions are used in other works, such as [105], as well, where it is assumed that the path gains, the background noise, and the inter–cell interference (in case of multiple–cell systems) are fixed during the time it takes for the solver to produce a solution. In Section 1.3.3 a more general definition of the reverse gains for multiple–cell systems will be given.

We assume that the mobile stations are ordered in such a way that,

$$g_1 > \cdots > g_M, \tag{1.2}$$

and define the power at which the i–th mobile station is transmitting as p_i, for which we have,

$$0 \leq p_i \leq p_{max}, \tag{1.3}$$

for a given p_{max}. While, here, all the mobile stations are assumed to be limited by the same maximum transmission power, this condition can be relaxed in favor of a more general model in which p_i is bounded by p_i^{max}. If this model is to be utilized, the condition given in (1.2) should change to,

$$g_1 p_1^{max} > \cdots > g_M p_M^{max}. \tag{1.4}$$

Although this generalization does exist, for notational convenience, in many cases in this thesis we consider constant p_{max} for all the mobile stations, unless specified otherwise.

Here, the work is carried out in a circular cell of radius $R = 2.5km$. Subsequently, in single–cell models, for the mobile station i at the distance d_i from the base station only the path–loss is considered, and modeled as [106],

$$g_i = C d_i^n. \tag{1.5}$$

For early works on this path–loss model consult [107, 108] and for a comprehensive review of this subject refer to [109]. Here, C and n are constants equal to 7.75×10^{-3} and -3.66, respectively, when d_i is in meters. Equivalently, with d_i in kilometers, C will equal 1.2283×10^{-13} [82] (also see [74, 110]).

Using the notations defined in the above, with a background noise of I, the SIR for the signal transmitted by the i–th mobile station as perceived by the base station is modeled as (see [12, 111] for more details),

$$\gamma_i = \frac{p_i g_i}{I + \sum_{j=1, j \neq i}^{M} p_j g_j}, \tag{1.6}$$

Hence, using Shannon's formula, the capacity of the i-th mobile station is modeled as,

$$C_i = \log_2(1+\gamma_i) = \log_2 \frac{I + \sum_{j=1}^{M} p_j g_j}{I + \sum_{j=1, j\neq i}^{M} p_j g_j}. \tag{1.7}$$

Using (1.7) for computing the aggregate capacity of the system, we have,

$$C(\vec{\mathbf{p}}) = \sum_{i=1}^{M} C_i = \log_2 \frac{\left(I + \sum_{j=1}^{M} p_j g_j\right)^M}{\prod_{i=1}^{M}\left(I + \sum_{j=1, j\neq i}^{M} p_j g_j\right)}. \tag{1.8}$$

Here, $\vec{\mathbf{p}} = (p_1, \cdots, p_M)$ is the vector of all the decision variables of the optimization problem.

Using the definition of the objective function given in (1.8), the CSC uses the constraint given in (1.3) as well as two other ones, to be described here. The first constraint defines a minimum guaranteed SIR, as,

$$\gamma_i \geq \gamma, \forall i. \tag{1.9}$$

Furthermore, in the CSC, in order to suppress interference from one cell to the others, the aggregate received power at the base station is limited as,

$$\sum_{i=1}^{M} p_i g_i \leq P_{max}. \tag{1.10}$$

These constraints can be collectively written as,

$$\begin{cases} \gamma_i \geq \gamma, \forall i, \\ \sum_{i=1}^{M} p_i g_i \leq P_{max}, \\ 0 \leq p_i \leq p_{max}, \forall i. \end{cases} \tag{1.11}$$

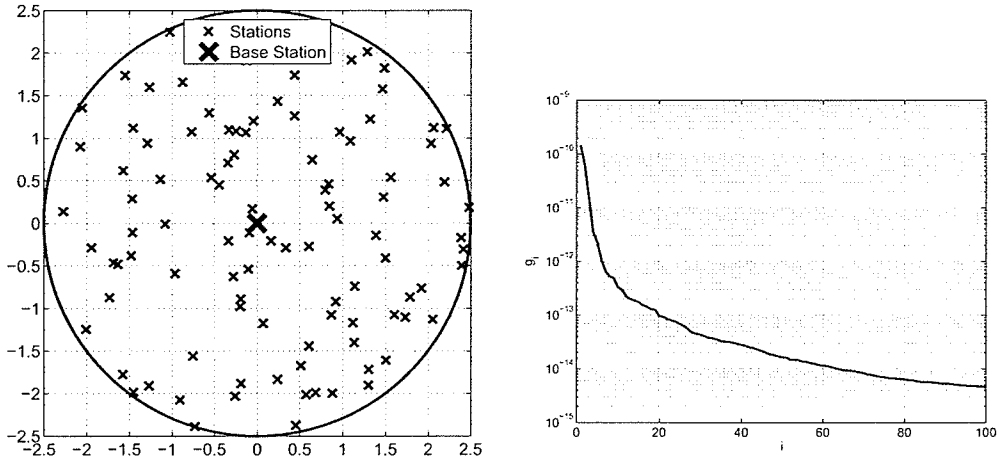

Figure 1.1: *(a) Location of different mobile stations in a sample cell. (b) The corresponding sequence of reverse gains.*

The base parameters used in this study are $\gamma = -30dB$, $I = -113dBm$, $P_{max} = -106dBm$, $p_{max} = 23dBm$ ($p_{max} = 30dBm$ is used in some other works [85]), $M = 10$, $\eta = 0.3$, $\mu = \frac{1}{1.5}$, and $\alpha = 0.7$. These values are partly based on the data given in [74, 82, 85, 112] (the parameters η, μ, and α are defined in this thesis and will be clearly described in Chapter 3). Note that here the values of I and P_{max} comply with the notion of limiting the blocking probability, as defined in [78]. In any experiment, when a parameter is different from the list given in the above, it is mentioned.

The execution times given here are measured on a Pentium IV 3.00GHz personal computer with 1GB of RAM, running Windows xp and MATLAB 7.0.

Figures 1.1–(a) and 1.1–(b) show the location of different mobile stations and the sequence of reverse gains, respectively, in a sample set generated as described in the above. The surrounding circle in Figure 1.1–(a) shows the border of the cell.

1.3.2 Improvements on the Model

In this section, some improvements on the model described in Section 1.3.1 are discussed. The addition of these improvements to the model will be discussed in Section 1.3.3.

It is suggested that at any time each mobile station is only active with the probability equal to ν. Therefore, a more appropriate model for γ_i, originally defined in (1.6), will be as,

$$\gamma_i = \frac{p_i g_i}{I + \nu \sum_{j=1, j\neq i}^{M} p_j g_j}. \tag{1.12}$$

In [74], a proper value for ν in voice systems is suggested to be 0.4. It is worth to mention that another method for modeling ν is the assumption that a cell with M mobile stations in fact only contains $[M\nu]$ mobile stations [81]. In this thesis we will use the formulation given in (1.12) instead.

It is also suggested that a more accurate model for the SIR is to write,

$$\gamma_i = \frac{p_i g_i}{I + \alpha \sum_{j=1, j\neq i}^{M} p_j g_j}. \tag{1.13}$$

Here, α is a constant depending on the characteristics between the spreading codes of the mobile stations. The values of $\alpha = 1$ and $\alpha = \frac{1}{3}$ for synchronous and asynchronous mobile stations are suggested, respectively [57].

While the formulation given in (1.6) models the system at chip level, there is a straightforward extension of this work to symbol level capacity optimization through writing [75, 82, 84, 113],

$$\gamma_i = \frac{L p_i g_i}{I + \sum_{j=1, j\neq i}^{M} p_j g_j}. \tag{1.14}$$

Here,

$$L = \frac{W}{R} > 1, \tag{1.15}$$

is the spreading gain of the CDMA system, in which formulation W is the chip rate and R is the data rate. This formulation can also be extended to multi-rate systems. In doing so, the

SIR model is extended by assuming that the data–rate for the i–th mobile station is denoted by r_i. Therefore,

$$\gamma_i = \frac{L_i p_i g_i}{I + \sum_{j=1, j\neq i}^{M} p_j g_j}. \tag{1.16}$$

where,

$$L_i = \frac{W}{r_i}. \tag{1.17}$$

In a typical system, $W = 10^6 Hz$ and $R = 10^4 bits/second$, thus producing $L = 100$ [85] ($L = 128$ is used in [83]). Note that (1.14) is a special case of (1.16) in which $L_i = L, \forall i$.

Another model, similar to (1.13), in which the cross–correlation of different codes has been taken into consideration models the SIR at the output of the matched filter for the i–th code as [114],

$$\gamma_i = \frac{p_i N_i}{\sum_{j=1, j\neq i}^{M} p_j \frac{\tilde{\rho}_{ij}^2}{N_j} + I}. \tag{1.18}$$

Here, ρ_{ij}^2 is the constant cross–correlation between the i–th and the j–th codes and N_i is the spreading gain for the i–th mobile station. This model, although slightly different from the one used in this thesis, can be rewritten in order to have the same structure analyzed here and thus is solvable through a similar methodology. Here, we do not cover this model.

The formulation given in (1.6) is based on the assumption that the entire power transmitted by the i–th mobile station, here denoted by p_i, is effectively received at the base station, after it is attenuated by the environment. More proper models, such as the one proposed in [115], and further developed in [116], consider the factor ζ_i as the "ratio of useful received power". This factor represents the impairments caused by multiple path, non–constant standing wave ratio, and transmission non–linearities as well as imperfect equalization [116]. In order to properly model the effects of these phenomena, an auto–interference term is added to the denominator

of (1.6) while the nominator is multiplied by ζ_i, collectively yielding,

$$\gamma_i = \frac{\zeta_i p_i g_i}{I + \sum_{j=1, j\neq i}^{M} p_j g_j + (1-\zeta_i) p_i g_i}. \tag{1.19}$$

The factor ζ_i decreases as d_i, the distance between the i–th mobile station and the base station, increases. In other words, if the mobile station is extremely close to the base station then the corresponding ζ_i is very close to one. Similarly, as a mobile station moves towards the edge of cell, the corresponding value of ζ_i approaches ζ_{min}. Nominal values for ζ_{min} are given as 0.75 and 0.9 and ζ_i is modeled as a linear function of d_i [116],

$$\zeta_i = \frac{\zeta_{min} - 1}{R} d_i + 1. \tag{1.20}$$

Here, R is the radius of the cell and d_i is inside the range ($d_i \leq R$).

Through collective incorporation of (1.12), (1.13), (1.16) and (1.19) into the SIR model given in (1.6), the resulting formulation will better represent the physical phenomenon under investigation. To do so, the SIR of the signal transmitted by the i–th mobile station as perceived by the base station will be modeled as,

$$\gamma_i = \frac{L_i \zeta_i p_i g_i}{I + \alpha\nu \sum_{j=1, j\neq i}^{M} p_j g_j + (1-\zeta_i) p_i g_i}. \tag{1.21}$$

The issue with the formulation given in (1.21) is that the existence of the factors $\alpha\nu$ and $\zeta_i L_i$ and the term $(1-\zeta_i) p_i g_i$ disrupts the application of many available approaches as well as some early methods developed in this thesis.

In Section 1.3.3 the SIR model presented here is implemented within the framework discussed in Section 1.3.1 in order to yield a multiple–cell capacity maximization problem.

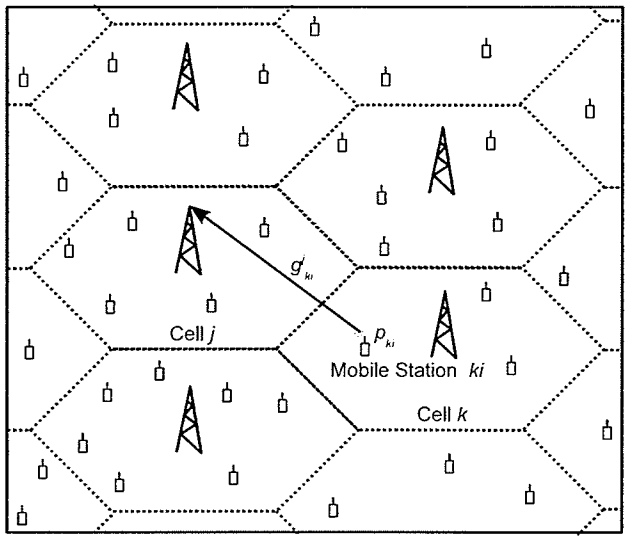

Figure 1.2: *Multiple-cell system model used in this thesis.*

1.3.3 Multiple–Cell Systems

A schematic depiction of the multiple–cell model developed in this section is given in Figure 1.2. This model is the extension of the single–cell model presented in Section 1.3.1, deployed to a multiple–cell scenario after the additions discussed in Section 1.3.2 are applied to it. The model presented in this section is also the generalized form of what is given in [79]. That model is based on the ones given in [75, 84, 89]. Models similar to the one discussed here are used in many other works as well (including [88]). To the best knowledge of the author, the multiple–cell model presented in this thesis is the most inclusive model available in the literature.

Assume that there are K cells, with M_k mobile stations in the k–th cell, $k = 1, \cdots, K$, making a total of,

$$M = \sum_{k=1}^{K} M_k, \tag{1.22}$$

mobile stations. We denote the parameters corresponding to the i–th mobile station in the k–th cell, where $i = 1, \cdots, M_k$, with the subscript ki (when needed, this mobile station will

be addressed as MS_{ki}). For example, the i–th mobile station in the k–th cell transmits at the power p_{ki} and the path gain from this mobile station to the base station at the j–th cell is denoted by g_{ki}^{j}. For convenience, we use g_{ki} when g_{ki}^{k} is referred to. We also assume that the i–th mobile station in the k–th cell is at distance d_{ki} from the k–th base station and define ζ_{ki} using a doubly–indexed extension of (1.20). The underlying assumption here is that every mobile station is connected to only one base station at any given moment (the closest to it in terms of geographical distances) [83].

As opposed to the single–cell model presented in Section 1.3.1, in which g_i only represented the path–loss, in this section a more inclusive model for the $\vec{\mathbf{g}}$ is adopted. From the point of view of the underlying physical model, the quantity g_{ki} can be written as [83],

$$g_{ki} = h_{ki} f_{ki}. \tag{1.23}$$

Here, $0 < h_{ki} < 1$ represents the slow–varying channel gain, excluding any fading, and f_{ki} denotes fast time–scale Rayleigh fading between the i–th mobile station in the k–th cell and the corresponding base station [109]. The assumption here is that $\vec{\mathbf{h}}$ does not change significantly during the time–scale of the analysis. Similarly, $\vec{\mathbf{f}}$ is assumed to be constant during each data frame but varying from one frame to another. In fact, the elements of $\vec{\mathbf{f}}$ are assumed to follow unit mean Rayleigh distributions, or, equivalently, a Rayleigh distribution with the parameter equal to,

$$\sigma = \sqrt{\frac{2}{\pi}}. \tag{1.24}$$

Furthermore, the formulation for h_{ki} is given as [83],

$$h_{ki} = \left(\frac{C}{d_{ki}}\right)^{n} Y_{\sigma}^{-1}. \tag{1.25}$$

Here, d_{ki} is the distance from the i–th mobile station to the base station and $C = 0.1$ and $n = 2.5$ for low density environments are suggested [109] (d_{ki} is in meters). Also, $\log(Y_{\sigma})$ is modeled as

a zero-mean Gaussian random variable with the standard deviation equal to $\tilde{\sigma}$. Here, $\tilde{\sigma} = 0.1$ is used [83]. In dynamic settings, $\vec{\mathbf{f}}$ is produced at each time step, while Y_σ is calculated every 20 time steps, when operating at the refresh rate of $1kHz$ [83].

In order to model the frequency reuse pattern in the system, we define $\theta_{kk'}$ as one if the cells k and k' share the same frequency band and zero otherwise. As a marginal case, in DS-CDMA systems, all the mobile stations communicate at the same frequency band. In other words, the system employs a frequency reuse of one. Therefore, every mobile station is interfering with every other one. Here, in the model, we consider this extreme case. Other cases, in which less number of cells operate on the same frequency band, can be modeled through the same formulation by setting the corresponding $\theta_{kk'}$ equal to zero when the frequency bands used in the two cells k and k' do not collide [11]. Note that, in any setting, θ_{kk} is equal to one for all values of k. Although, here, $\vec{\theta}$ represents the frequency reuse pattern, and thus its elements are assumed to hold binary values, the assumption of binary-valued $\vec{\theta}$ is not essential to the derivations and the subsequent analysis. Therefore, these values can also be used to incorporate other non-binary features, such as the "orthogonality factor" [77], into the model.

Defining the background noise at the k-th cell as I_k, we employ $\theta_{kk'}$ within the framework of an SIR model following the same methodology as (1.21). Doing so, the SIR for of the signal transmitted by the i-th mobile station at the k-th cell as perceived by the base station in that cell is modeled as,

$$\gamma_{ki} = \frac{L_{ki}\zeta_{ki}p_{ki}g_{ki}}{I_k + \alpha\nu\left(\sum\limits_{k'=1,k'\neq k}^{K}\left[\theta_{kk'}\sum\limits_{i'=1}^{M_{k'}}p_{k'i'}g^{k}_{k'i'}\right] + \sum\limits_{i'=1,i'\neq i}^{M_k}p_{ki'}g_{ki'}\right) + (1-\zeta_{ki})\,p_{ki}g_{ki}}. \tag{1.26}$$

Similar models are used in [77, 83, 101, 102], among other works. Note that, in [83] only the effects of the mobile stations at the first-tier neighborhoods are included in the model, while here, the entire network is taken into consideration.

As the equivalent to (1.7) in multiple-cell systems, the relative capacity of the i-th mobile

stations in the k–th cell is defined as,

$$C_{ki} = \log_2 (1 + \gamma_{ki}) . \tag{1.27}$$

Using this model, the general multiple–cell capacity maximization problem solved in this thesis is composed as maximizing,

$$C = \sum_{k=1}^{K} \sum_{i=1}^{M_k} f_{ki} (C_{ki}) , \tag{1.28}$$

subject to,

$$\begin{cases} 0 \leq p_{ki} \leq p_{ki}^{max}, \forall i, k, \\ \gamma_{ki} \geq \gamma_{ki}^{min}, \forall i, k, \\ C_{ki} \leq C_{ki}^{max}, \forall i, k, \\ \alpha\nu \sum_{k'=1}^{K} \left[\theta_{kk'} \sum_{i'=1}^{M_{k'}} p_{k'i'} g_{k'i'}^{k} \right] \leq P_{k}^{max}, \forall k. \end{cases} \tag{1.29}$$

Here, the constants γ_{ki}^{min}, C_{ki}^{max}, and p_{ki}^{max} are the minimum SIR, the maximum capacity, and the maximum transmission power of the i–th mobile station in the k–th cell, respectively, and $f_{ki}(\cdot)$ is the utility function of this mobile station.

Note that the model presented in (1.26) does cover many other single–cell models discussed in this thesis. In order to carry out the reduction, K has to be set equal to one and some of the system parameters may have to be ignored. Moreover, through setting $\theta_{kk'} = \delta_{k=k'}$ and replacing $\alpha\nu$ with $\alpha\nu(1 + \delta)$, the approach of using virtual mobile stations will be simulated. Therefore, the author argues that to his best knowledge the multiple–cell formulation presented and then solved in this thesis is the most general model available in the cited works as well as others not mentioned here.

1.3.4 Fairness Analysis

The analysis of the fairness of the solution to the optimization problem investigated throughout this thesis is an important issue (also see [57, 58]). As will be shown later, for example in Section 3.1, through imposing constraints specifically designed to control the range of the capacity offered to each mobile station the system can be made more fair. To examine this situation, numerical measures for modeling fairness in the system are needed. Therefore, the subtractive unfairness of the system is defined as the difference between the highest and the lowest capacities offered in the system,

$$f = \max\{C_i\} - \min\{C_i\}. \tag{1.30}$$

Similarly, the ratio unfairness of the system is defined as the ratio between these two capacities,

$$\tilde{f} = \frac{\max\{C_i\}}{\min\{C_i\}}. \tag{1.31}$$

Note that f and $\tilde{f}$ are measures of unfairness for the whole system. In contrast, as a measure of fairness specific to each mobile station, we define the capacity share of mobile station i as,

$$\tilde{C}_i = \frac{C_i}{C}. \tag{1.32}$$

In a cell which contains M mobile stations, the closer the values of $\tilde{C}_i$ are to M^{-1}, the less dispersed the range of the capacities is. In this context, the values of $\tilde{C}_i$ constitute a measure of fairness for the system.

These measures will be used throughout this thesis in order to analyze the fairness of the solutions produced by different algorithms.

1.4 Structure of this Thesis

This thesis is essentially composed of different methods building upon their predecessors, each one bringing a new improvement to the task of optimizing the transmission powers in a CDMA

system. The analysis starts from the classical problem which contains a minimal list of constraints as well as a simplistic objective function. This problem is thoroughly discussed in Chapter 2. As a result, the mathematical basis for the analysis of several other generalizations is developed. In addition, the performance of the classical problem is comprehensively investigated (in Section 5.1).

As expected from the reports already available in the literature, the classical formulation produces unrealistically unfair systems. Therefore, the classical problem is gradually redefined in Chapter 3 in order to be equipped with more advanced features. This process starts in Sections 3.1 and 3.2 through the addition of more constraints to the problem. This process provides hard limits on the unfairness of the system and thus makes the results applicable in practice. However, as more features are included in the system, the complexity of the solver increases and no straight–forward method for the addition of new features and constraints into the problem exists. In other words, the addition of a new constraint is only possible through the complete analysis of the new problem from bottom up, and not through a procedure which would build on the existing analysis of the previous problem. Thus, in Section 3.3 a new set of approximations is developed. These approximations produce substitute solvers for the available problems and at the same time provide the opportunity for the algorithmic integration of more advanced features into the problem.

Taking advantage of the developed approximations, the addition of utility functions is investigated in Section 3.4 and it is observed that concave utility functions, which were out of reach in the previous methodology, result in promising systems. Subsequently, multiple–class systems are addressed in Section 3.5 and, finally, as the last addition to the single–cell problem, the underlying SIR model utilized in the multiple–class model is also improved (in Section 3.6).

Using the multiple–class problem formulated at the end of Chapter 3, the model developed in Section 1.3.3 is implemented in Chapter 4 to produce a multiple–cell multiple–class problem. This problem is subsequently solved using some of the mathematical tools developed earlier as well as a few others developed in Chapter 3.

The thesis then continues with comprehensive analysis of all the developed problems in Chapter 5, where different experiments are designed and carried out for each problem. Finally, Chapter 6 outlines the conclusions of this research.

Chapter 2

Classical Single Cell (CSC)

This chapter contains the work carried out on the problem of maximizing the capacity of the reverse link in a single–cell system. The problem analyzed here is the CSC, as introduced in [71, 117]. This section is organized as follows. First, in Section 2.2, we develop a set of linear transformations in order to simplify the CSC formulation. Then, the behavior of the problem in specific hyperplanes is investigated, resulting in a theorem given in Section 2.3. The procedure is then followed in Section 2.4, where the solution is localized to a smaller search space than what has been suggested before, thus producing new tighter bounds on the decision variables. Then, in Section 2.5, we carefully analyze the problem and give a theorem which is used in Section 2.6 in order to propose a new algorithm for accurately finding the solution to the CSC. The coverage of the problem then follows in Section 2.7, where analysis of the computational complexity of the proposed algorithm is presented. Finally, Section 2.8 carries out an analysis on the significance of the value of P_{max}.

2.1 Problem Definition

As mentioned in Section 1.3.1, the CSC problem is defined as finding,

$$\arg_{\vec{\mathbf{p}}} \max \frac{\left(I + \sum_{j=1}^{M} p_j g_j\right)^M}{\prod_{i=1}^{M}\left(I + \sum_{j=1, j\neq i}^{M} p_j g_j\right)}, \tag{2.1}$$

given,

$$0 \leq p_i \leq p_{max}, \forall i, \tag{2.2}$$

$$\frac{p_i g_i}{I + \sum_{j=1, j\neq i}^{M} p_j g_j} \geq \gamma, \forall i, \tag{2.3}$$

$$\sum_{i=1}^{M} p_i g_i \leq P_{max}. \tag{2.4}$$

2.2 Linear Transformation

The first step in this work is to propose a linear transformation which gives an alternative representation of the single–cell problem which is easier to work with. This will also lead to a more convenient solver. In doing so, first, we rewrite (2.3) as,

$$\frac{p_i g_i}{I + \sum_{j=1}^{M} p_j g_j} \geq \varphi = \frac{\gamma}{\gamma + 1}, \forall i. \tag{2.5}$$

Notice that, $0 < \varphi < 1$. Now, substituting,

$$x_i = \frac{p_i g_i}{I}, \tag{2.6}$$

into (2.1) gives,

$$\Delta(\vec{\mathbf{x}}) = \frac{\left(1 + \sum_{j=1}^{M} x_j\right)^M}{\prod_{i=1}^{M}\left(1 + \sum_{j=1, j\neq i}^{M} x_j\right)}, \tag{2.7}$$

where $\vec{\mathbf{x}} = (x_1, \cdots, x_M)$. For the sake of analytical convenience, we transform (2.7) into a more convenient form, shown below, which is to be minimized.

$$\Phi(\vec{\mathbf{x}}) = \frac{\prod_{i=1}^{M}\left(1 + \sum_{j=1}^{M} x_j - x_i\right)}{\left(1 + \sum_{j=1}^{M} x_j\right)^M}. \tag{2.8}$$

This of course assumes that the maximum is finite which is a reasonable assumption. Now, we find the new representations of the constraints using the transformation shown in (2.6). Substituting (2.6) into (2.2) gives,

$$0 \leq x_i \leq l_i, l_i = \frac{p_{max}}{I} g_i, \forall i. \tag{2.9}$$

Note that as $\vec{\mathbf{g}}$ is a vector of descending elements, so is $\vec{\mathbf{I}}$. Here, to comply with the history of the problem, we have assumed that p_{max} is fixed for all the mobile stations. The analysis, however, never in fact depends on this assumption, except for proving that the elements of $\vec{\mathbf{I}}$ are sorted in a descending fashion. Therefore, the analysis given here also applies to the case in which p_{max} is not fixed for all the mobile stations, in which case we will sort the mobile stations in terms of the corresponding values of $p_i^{max} g_i$. Here, p_i^{max} is the maximum transmission power of the i–th mobile station. Hence, the solution given here is more general than the previous discussion given in [71, 117].

Substituting (2.6) into (2.5) gives,

$$\frac{x_i}{1+\sum_{j=1}^{M} x_j} \geq \varphi, \forall i. \tag{2.10}$$

Also, (2.4) becomes,

$$\sum_{i=1}^{M} x_i \leq X_{max}, X_{max} = \frac{P_{max}}{I}. \tag{2.11}$$

To summarize, using the transformation depicted in (2.6), the single–cell problem is reduced to minimizing $\Phi(\vec{\mathbf{x}})$, given in (2.8), subject to,

$$\begin{cases} 0 \leq x_i \leq l_i, \forall i, \\ \frac{x_i}{1+\sum_{j=1}^{M} x_j} \geq \varphi, \forall i, \\ \sum_{i=1}^{M} x_i \leq X_{max}. \end{cases} \tag{2.12}$$

2.3 Working on Specific Hyper–Planes

Here, we investigate the behavior of the problem in specific hyperplanes. This investigation leads to a theorem at the end of this section.

We analyze the behavior of the problem in the hyperplane defined as,

$$\sum_{i=1}^{M} x_i = T, \tag{2.13}$$

for different values of T. In any such hyperplane, the single–cell problem reduces to finding the minimum of,

$$\Phi(\vec{\mathbf{x}}) = (1+T)^{-M} \Phi_T(\vec{\mathbf{x}}), \tag{2.14}$$

where,

$$\Phi_T(\vec{\mathbf{x}}) = \prod_{i=1}^{M} (1 + T - x_i)\,. \tag{2.15}$$

Therefore, for fixed T, the problem which should be solved is the minimization of $\Phi_T(\vec{\mathbf{x}})$. In other words, the single–cell problem can be rewritten as finding T for which the minimum value of $\Phi_T(\vec{\mathbf{x}})$ is the smallest possible.

In the hyperplane indicated in (2.13), the constraints have more convenient formulations. For example, the inequality given in (2.11) changes into a limitation for T as,

$$T \leq X_{max}. \tag{2.16}$$

Also, (2.10) in combination with (2.9), yields,

$$\varphi(1 + T) \leq x_i \leq l_i, \forall i. \tag{2.17}$$

Now, the problem is to minimize (2.15) given that $\vec{\mathbf{x}}$ lies on the hyperplane defined as (2.13). The vector $\vec{\mathbf{x}}$ should also satisfy (2.17). Also, T should not become larger than X_{max}. We know that if the $\vec{\mathbf{x}}$ satisfying (2.13) is the minimizer of (2.8) then it is the minimizer of (2.15), but not vice versa.

Assume that $\vec{\mathbf{x}}$ is the minimizer of (2.15) and consider two distinct values of i and j. Then, rewrite (2.15) in terms of x_i and x_j.

$$\Phi_T(\vec{\mathbf{x}}) = (1 + T - x_i)\,(1 + T - x_j) \prod_{k=1, k\neq i,j}^{M} (1 + T - x_k)\,, \tag{2.18}$$

where the last term (which contains $M - 2$ factors) depends neither on x_i nor on x_j. Hence, for minimizing $\Phi_T(\vec{\mathbf{x}})$, the product of the first and second terms has to be minimized. Here,

$$x_j = T - S - x_i, \tag{2.19}$$

$$S = \sum_{k=1.k\neq i,j}^{M} x_i. \tag{2.20}$$

Now, the function which should be minimized is,

$$f(x_i) = (1 + T - x_i)(1 + T - x_j). \tag{2.21}$$

It can be shown that,

$$f(x_i) = -\left(x_i - \frac{T-S}{2}\right)^2 + (1+T)(S+1) + \left(\frac{T-S}{2}\right)^2. \tag{2.22}$$

Remembering that,

$$x_i - \frac{T-S}{2} = \frac{1}{2}(x_i - x_j), \tag{2.23}$$

it is proved that for minimizing $\Phi_T(\vec{\mathbf{x}})$, x_i and x_j should be as far from each other as possible.

Now, assume that $\vec{\mathbf{x}}$ is a solution to (2.15) that satisfies all the constraints. Furthermore, assume that there are values of i and j, for which there is a value of δ such that replacing x_i and x_j with $x_i^\star = x_i + \delta$ and $x_j^\star = x_j - \delta$ still satisfies all the constraints. Note that this new point is still on the same hyperplane. Also, note that,

$$x_i^\star - x_j^\star = x_i - x_j + 2\delta, \tag{2.24}$$

which means that if the sign of δ is the same as that of $x_i - x_j$, then $x_i^\star$ and $x_j^\star$ have a larger absolute difference than that of x_i and x_j. Based on what was described in the above, this new $\vec{\mathbf{x}}$ will produce a lower value of $\Phi_T(\vec{\mathbf{x}})$, which is a contradiction to what was assumed before. Using this, a theorem is stated.

Theorem: In the solution to the single–cell problem, there can be no pair of x_i and x_j which can increase their absolute distance. We call this pair an extending one if they can do so and the situation is called an extension. Therefore, at the optimal point, the inequalities for $\vec{\mathbf{x}}$ (see (2.17)) should always stop its elements from increasing the distance among themselves.

Proof: This issue will be presented through a graphical visualization. Before that, we know that $\Phi(\vec{\mathbf{x}})$ is independent of the permutations of $\vec{\mathbf{x}}$. Also, rather than the bound for T given in (2.16), the other conditions are on individual elements of $\vec{\mathbf{x}}$ (see (2.17)). Furthermore, in these constraints, the minimum possible values for all the elements $\vec{\mathbf{x}}$ are identical and the set of maximum possible values is given as $\vec{\mathbf{I}}$, the elements of which are sorted in a descending scheme. Hence, it is possible to show the range of x_i as,

$$x_i : [\varphi(1+T) \cdots \leftarrow \times \rightarrow \cdots l_i], \tag{2.25}$$

where $\times$ shows the approximate location of x_i in the interval and the arrows indicate possible movements. Here, we give names for three situations of x_i. In doing so, x_i is called to be at the beginning, at the middle, or at the end if $x_i = \varphi(1+T)$, $\varphi(1+T) < x_i < l_i$, and $x_i = l_i$, respectively.

Now, we use the theorem presented earlier and the proposed visual representation in order to prove the first lemma in [118]. The Lemma states that in the optimum solution there is at most one x_i at the middle. Assuming otherwise, there are x_i and x_j, both at the middle and $i < j$. In this situation, there are two possibilities, $x_i \geq x_j$ or $x_i < x_j$. The first case leads to

$$\begin{array}{l} x_i : [\varphi(1+T) \cdots\cdots\cdots\cdots \times \rightarrow \cdots\cdots\cdots\cdots l_i] \\ x_j : [\varphi(1+T) \cdots\cdots\cdots \leftarrow \times \cdots\cdots\cdots\cdots l_j] \end{array},$$

which is an extension. The later case is similar,

$$\begin{array}{l} x_i : [\varphi(1+T) \cdots\cdots \leftarrow \times \cdots\cdots\cdots\cdots\cdots\cdots l_i] \\ x_j : [\varphi(1+T) \cdots\cdots\cdots\cdots \times \rightarrow \cdots\cdots\cdots\cdots l_j] \end{array} \blacksquare$$

This visually intuitive proof is compared with the one given in [71, 117].

The second lemma in [118] states that in the optimum solution, if there is one x_i at the middle, all x_j for $j > i$ will be at the beginning. Again assume two distinctive x_i and x_j, where $i < j$ and x_i is at the middle. Now, if x_j is at the end, there are two possibilities, namely $x_i \geq l_j$

or $x_i < l_j$. The first one leads to,

$$\begin{array}{l} x_i : [\varphi(1+T) \cdots\cdots\cdots\cdots\cdots\cdots \times \rightarrow \cdots l_i] \\ x_j : [\varphi(1+T) \cdots\cdots\cdots\cdots\cdots \leftarrow \times l_j] \end{array},$$

which is an extension. The second condition leads to an extension as well, although it is not as clear as the previous one is. Writing,

$$\begin{array}{l} x_i : [\varphi(1+T) \cdots\cdots\cdots \times \cdots\cdots\cdots\cdots\cdots\cdots l_i] \\ x_j : [\varphi(1+T) \cdots\cdots\cdots\cdots\cdots \times l_j] \end{array},$$

and replacing x_i and x_j gives,

$$\begin{array}{l} x_i : [\varphi(1+T) \cdots\cdots\cdots\cdots\cdots \times \rightarrow \cdots\cdots\cdots\cdots l_i] \\ x_j : [\varphi(1+T) \cdots\cdots \leftarrow \times \cdots\cdots l_j] \end{array},$$

where the extension is trivial.

Lemma 3 in [118] is refers to the x_i above the one at the middle. The claim is that if x_k is at the middle and for $m < k$, x_m is at the beginning, then for $m < i < k$, x_i can not be at the end. Using the lemmas given in the above, the result is that x_i should always be at the beginning. The situation which this lemma refers to is,

$$\begin{array}{l} x_m : [\varphi(1+T) \times \cdots\cdots\cdots\cdots\cdots\cdots\cdots\cdots\cdots\cdots\cdots\cdots l_m] \\ x_i : [\varphi(1+T) \cdots\cdots\cdots\cdots\cdots\cdots\cdots\cdots \times l_i] \\ x_k : [\varphi(1+T) \cdots\cdots\cdots \times \cdots\cdots\cdots\cdots l_k] \end{array},$$

which changes into the extendable case of,

$$\begin{array}{l} x_m : [\varphi(1+T) \cdots\cdots\cdots\cdots\cdots\cdots\cdots\cdots \times \rightarrow \cdots\cdots l_m] \\ x_i : [\varphi(1+T) \times \cdots\cdots\cdots\cdots\cdots\cdots\cdots\cdots\cdots\cdots l_i] \\ x_k : [\varphi(1+T) \cdots\cdots \leftarrow \times \cdots\cdots\cdots\cdots l_k] \end{array}.$$

Proposition 1 in [118] is now concluded; if there is a solution to the single–cell problem then

it is as,

$$\vec{\mathbf{x}} = (l_1, \cdots, l_{k-1}, x_k, \varphi(1+T), \cdots, \varphi(1+T)) . \tag{2.26}$$

Note that there may be need to switch the elements of $\vec{\mathbf{x}}$ so that the one at the middle separates those at the beginning and those at the end.

2.4 Bounds on x_k

Equation (2.26) gives the structure of the optimum solution to the single–cell problem. This equation reduces the number of the unknowns to two. In this section we reduce the size of the search space by finding appropriate bounds for both k and x_k.

Defining,

$$L = \sum_{i=1}^{k-1} l_i. \tag{2.27}$$

we have,

$$1 + T = \frac{x_k + L + 1}{1 - (M-k)\varphi}. \tag{2.28}$$

As T is always positive, we should have,

$$1 - (M-k)\varphi > 0 \rightarrow k > M - \frac{1}{\varphi}. \tag{2.29}$$

The fact that $1 - (M-k)\varphi$ is positive is used in some of the derivations to be presented.

Working on $x_k \geq \varphi(1+T)$, given in (2.17), results in,

$$x_k \geq \frac{\varphi(L+1)}{1 - (M-k+1)\varphi}. \tag{2.30}$$

We also have,

$$k > M - \frac{1}{\varphi} + 1, \tag{2.31}$$

which makes (2.29) tighter. Similarly, the aggregate power condition gives,

$$x_k \leq (X_{max} + 1)\left[1 - (M - k)\varphi\right] - L - 1. \tag{2.32}$$

According to the structure of $\vec{\mathbf{x}}$ given in (2.26) and because of (2.17), we should have $\varphi(1 + T) \leq l_M$ which gives,

$$x_k \leq l_M \frac{1 - (M - k)\varphi}{\varphi} - L - 1. \tag{2.33}$$

To make the bound in (2.33) positive we should have,

$$k < \frac{1}{\varphi} - \frac{1}{l_M} + 1. \tag{2.34}$$

Using (2.31) we have,

$$M - \frac{1}{\varphi} + 1 < k < \frac{1}{\varphi} - \frac{1}{l_M} + 1. \tag{2.35}$$

Therefore, the constraints are abbreviated in two bounds on x_k,

$$x_k \leq \min \left\{ \begin{array}{l} l_k \\ (X_{max} + 1)\left[1 - (M - k)\varphi\right] - L - 1 \\ l_M \dfrac{1 - (M - k)\varphi}{\varphi} - L - 1 \end{array} \right\}, \tag{2.36}$$

and,

$$x_k \geq \frac{\varphi(L + 1)}{1 - (M - k + 1)\varphi}; \tag{2.37}$$

for those values of k satisfying (2.35). The important fact about the inequalities in (2.35), (2.36), and (2.37) is that they are both necessary and sufficient.

2.5 Spotting the Solution

It was proved in Section 2.3 that the solution to the single–cell problem is structured as (2.26). Now, the question is to find the appropriate values of k and x_k. Here, we assume that we have selected a value of k and produce the optimal choices for x_k.

We know from what was described in Section 2.4 that it is both necessary and sufficient for x_k to satisfy (2.36) and (2.37). In this section we prove that $\Phi(\vec{\mathbf{x}})$ has a very specific behavior in terms of x_k (when other elements of $\vec{\mathbf{x}}$ are selected as in (2.26)). In fact, we prove that the minimum value of $\Phi(\vec{\mathbf{x}})$ happens on a boundary (at a margin). This directly leads to the two choices given in (2.36) and (2.37) for x_k. In this way, the single–cell problem reduces to checking two values for x_k for any value of k (also limited by (2.35)). The importance of this non–iterative method over the numerical one used in previous works is notable. Furthermore, while the proposed method produces the exact solution to the single–cell problem, the approach devised in [71] is only capable of calculating the solution up to some precision.

Equation (2.26) gives,

$$\Phi(\vec{\mathbf{x}}) = \frac{1}{(1+T)^M}\left[\prod_{i=1}^{k-1}(1+T-l_i)(1+T-x_k)\left((1-\varphi)(1+T)\right)^{M-k}\right]. \tag{2.38}$$

Using (2.28) and performing routine algebraic manipulation we have,

$$\Phi(x_k) = C\frac{\prod_{i=1}^{k}(x_k+\beta_i)}{(x_k+\beta)^k}, \tag{2.39}$$

where,

$$C = (M-k)\varphi(1-\varphi)^{M-k}, \tag{2.40}$$

$$\beta_i = \begin{cases} L+1-(1-(M-k)\varphi)\, l_i & i = 1, \cdots k-1 \\ \dfrac{L+1}{(M-k)\varphi} & i = k \end{cases} \tag{2.41}$$

$$\beta = L + 1. \tag{2.42}$$

Note that, here, $\Phi(x_k)$ is referred to, as opposed to $\Phi(\vec{\mathbf{x}})$, because we are dealing with the optimal choice of x_k and hence the other elements of $\vec{\mathbf{x}}$ are calculated based on x_k. Therefore, the problem is to minimize,

$$f(x) = \frac{\prod_{i=1}^{k}(x+\beta_i)}{(x+\beta)^k}, \tag{2.43}$$

where β_i and β are given as (2.41) and (2.42), respectively. Note that with these definitions we have,

$$0 < \beta_1 < \beta_2 < \cdots < \beta_{k-1} < \beta < \beta_k. \tag{2.44}$$

Also, we have,

$$\sum_{i=1}^{k} \beta_i - k\beta = (1-(M-k)\varphi)\left[\frac{1}{(M-k)\varphi} + L\frac{1-(M-k)\varphi}{(M-k)\varphi}\right] > 0. \tag{2.45}$$

Figure 2.1 shows a sample function f when $k = 3$ with values of β_i and β given in the caption are used. Note that, in this example, it is evident that in any interval on the positive side, the minimum value of the function happens at the boundaries. In Appendix A it is proved that this is in fact the case for any choice of the parameters β_i which satisfy (2.44) and for which $\sum_{i=1}^{k} \beta_i - k\beta$ is positive. Using this result, in the next section, we propose an algorithm that computes the value of Φ in less then $2M$ candidate points and finds the optimal solution.

2.6 Details of the Proposed Algorithm

Figure 2.2 shows the detailed structure of the proposed algorithm.

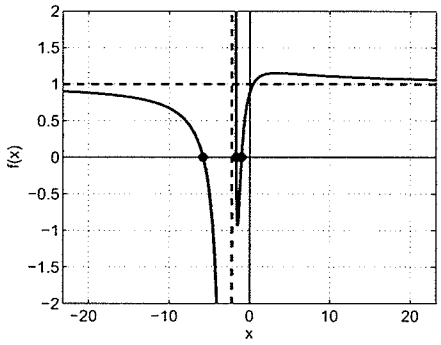

Figure 2.1: *Typical shape of $f(x)$ defined in (2.43) with values of parameters as $\beta_1 = 1.0082$, $\beta_2 = 1.6728$, $\beta_3 = 5.7966$, and $\beta = 2.2310$.*

1. Compute X_{max} using (2.11), φ using (2.5), and $\vec{\mathrm{I}}$ using (2.9).
2. For all k satisfying (2.35), do the followings,
   (a) Compute L using (2.27).
   (b) Compute max_k and min_k using (2.36) and (2.37), respectively.
   (c) If not $max_k \geq min_k \geq 0$ then go to the next value of k, else continue (goto 2d).
   (d) Do the following lines for the two values of $x_k = min_k$ and $x_k = max_k$, separately. Store both Φ and the values of x_i for each trial.
   - Compute T using (2.28).
   - Set $x_i = l_i$ for $i = 1, \cdots, k-1$.
   - Set $x_i = \varphi(1+T)$ for $i = k+1, \cdots, M$.
   - Compute Φ using (2.8).
3. Find the smallest Φ produced at the above and retrieve the corresponding values of x_i.
4. Compute $\vec{\mathbf{p}}$, using (2.6), and return that as well as C.

Figure 2.2: *Details of the algorithm CSC.*

2.7 Computational Cost

Analysis of the proposed algorithm shows that its computational cost equals,

$$\tau = 8\varepsilon M^2 + (16\varepsilon + 4)M + 10, \tag{2.46}$$

flops. Here, εM is the number of values of k for which line 2d in the algorithm depicted in Figure 2.2 is executed. Empirically, for $M \geq 10$ we have $\varepsilon \leq 0.25$. The worst case happens when ε equals one, for which we have,

$$\tau_{CSC} = 8M^2 + 20M + 10, \tag{2.47}$$

flops. As an example, substituting $M = 100$ results in the computational costs of $82K$ and $20K$ flops, for $\varepsilon = 1$ and $\varepsilon = 0.1$, respectively. Here, $\varepsilon = 1$ shows the worst-case, while the other value of ε represents a likely event. On a 1Gfps (one Giga flops per second) processor it takes less than 0.1ms to do the calculations of the proposed algorithm when M equals 100 (0.08 ms and 0.02ms for the worst and the average cases, respectively). As a general measure note that here the computational cost is of order $O(M^2)$.

2.8 Analysis of P_{max}

The only place in the algorithm stated in Section 2.6, where the actual value of P_{max} is important is in line 2b. Using (2.11), and based on (2.36), we can show that the actual value of P_{max} may have an impact on the final solution only if,

$$\frac{X_{max} + 1}{l_M}\varphi < 1 \rightarrow P_{max} < p_{max} g_M \frac{\gamma + 1}{\gamma} - I. \tag{2.48}$$

It is in fact expected that increasing P_{max} from certain limits will make (2.4) redundant.

Chapter 3

Extensions to Single–Cell

Thorough work on the CSC, alongside the analysis of the results presented in Section 5.1, leads to the suggestion that including more constraints in the problem could result in better properties for the solution. In this chapter this approach is first followed in the design of the problem New Single–Cell (NSC), discussed in Section 3.1, and then in the development of problem N^+SC, discussed in Section 3.2. Then, in order to enhance the efficiency of the proposed algorithms, new approximations are employed, resulting in newer versions of all the developed algorithms in Section 3.3. These algorithms are marked with the superscript a, denoting "approximation". The work then continues with incorporating convex and concave utility functions, thus increasing the practicality of the problems, as discussed in Section 3.4. Finally, the case of multiple–class systems is analyzed in Section 3.5 and generalized multiple–class systems are discussed in Section 3.6.

Some of the extensions to the classical single–cell problem developed in this thesis are summarized in Figure 3.1. This figure depicts the different constraints and how they produce newer problems.

3.1 New Single Cell (NSC)

Analysis of the CSC reveals that almost always there is a single mobile station in the cell transmitting at a capacity about fifty times as much as the others, this issue is mentioned

$$\left.\begin{array}{l} \max C(\vec{\mathbf{p}}) = \log_2 \dfrac{\left(I + \sum_{j=1}^{M} p_j g_j\right)^M}{\prod_{i=1}^{M}\left(I + \sum_{j=1, j\neq i}^{M} p_j g_j\right)} \\ \text{given,} \\ 0 \leq p_i \leq p_{max}, \forall i, \\ \gamma_i \geq \gamma, \forall i, \\ \sum_{i=1}^{M} p_i g_i \leq P_{max}, \\ C_i \leq \eta, \forall i, \\ \tilde{C}_i \leq \dfrac{1}{\mu}\dfrac{1}{M}, \forall i. \end{array}\right\} CSC \Bigg\} NSC \Bigg\} N^+SC$$

Figure 3.1: *Some of the extensions to the CSC developed in this thesis.*

by other researchers as well [57, 58]. To resolve this issue, here we add another constraint to the problem and utilize a method similar to what was described in Chapter 2. As a result, the problem New Single-Cell (NSC) is produced. It is worth to mention that the unfairness of the results produced by the CSC was one of the main reasons the authors in [71] devised the minimum SIR constraint. Here, we show that through adding a maximum bound on the capacity of each mobile station there will be an implicit limit on the unfairness of the system, thus resulting in a more practical solution.

This section is organized as follows. First, in Section 3.1.1 the new maximum capacity constraint is introduced and it is shown how it integrates into the whole problem. Then, in Section 3.1.2 we show the structural similarity of the NSC to the CSC. As such, we justify that properties similar to what was proved before for the CSC are still valid. Then, Section 3.1.3 uses these results to propose an algorithm for solving the NSC. The analysis follows in Section 3.1.4 by discussing the computational cost of the proposed algorithm. Finally, Section 3.1.5 shows how in fact the new constraint puts a limit on the unfairness of the system in order to distribute the resources in the system.

3.1.1 Maximum Capacity Bound

Using (1.7), the constraint given in (1.9) gives,

$$C_i \geq -\log_2(1-\varphi). \tag{3.1}$$

Therefore, the value of φ, and equivalently that of γ, determines a minimum for the capacity of each mobile station. However, using Taylor Series we know that for a small values of x,

$$\log_2(1-x) \simeq -\frac{1}{\ln(2)}x. \tag{3.2}$$

Hence, we have the approximate form,

$$C_i \geq \frac{1}{\ln(2)}\varphi. \tag{3.3}$$

This means that φ directly imposes a minimum bound on the capacity of each mobile station.

Following the same line of reasoning, we propose to add the constraint given below to those presented in (1.3), (1.9), and (1.10),

$$C_i \leq \eta, \forall i. \tag{3.4}$$

Here, we will work on (3.4) to show that this constraint will in fact control the unfairness of the solution.

According to (1.7), and using the linear transformation of the search-space discussed in Section 2.2, while also using (2.13), the new constraint mandates,

$$\frac{1+T}{1+T-x_i} \leq 2^{\eta}, \forall i. \tag{3.5}$$

Continuing with (3.5) and defining

$$\omega = 1-2^{-\eta}, \tag{3.6}$$

We have,

$$x_i \leq \omega(1+T), \forall i, \tag{3.7}$$

which is similar to the left side of (2.17) except for the fact that the previous one put an upper bound on x_i, as opposed to the lower bound given in (2.17). Note that $\omega > \varphi$ is a necessary condition for the existence of any solution.

3.1.2 Spotting the Solution

In Section 3.1.1, the NSC was formulated as minimizing $\Phi(\bar{\mathbf{x}})$, given in (2.8), subject to,

$$\begin{cases} 0 \leq x_i \leq l_i, \forall i, \\ \varphi \leq \dfrac{x_i}{1 + \sum_{j=1}^{M} x_j} \leq \omega, \forall i, \\ \sum_{i=1}^{M} x_i \leq X_{max}. \end{cases} \tag{3.8}$$

To solve this problem, we use the same method of performing the analysis in specific hyperplanes developed in Section 2.3. The similarity of the structural arrangement of the search space of the current problem to the one given in (2.17) mandates an optimal $\bar{\mathbf{x}}$ which has a structure similar to (2.26). Note that, here, for some values of i, the maximum bound for $x_j (j \geq i)$ is given by $\omega(1+T)$ and not by l_j. Nevertheless, the same pyramid-like structure of the search space, generated by the descending upper bounds, is still valid. Hence, in accordance with (2.26), it is inferred that the optimal solution to the single-cell problem when the new constraint is included, is given by,

$$\bar{\mathbf{x}} = \Big(\omega(1+T), \cdots, \omega(1+T), l_{j+1}, \cdots, l_{k-1}, x_k, \varphi(1+T), \cdots, \varphi(1+T)\Big). \tag{3.9}$$

Note the similarity between this vector and the structure of the solution to the CSC given in (2.26).

Comparing (3.9) with (2.26) reveals that in the NSC there are two values of j and k which have to be found while in the CSC we were only faced with k (see Section 2.5). Hence, it is anticipated that the solver for this problem will be of a higher order (the computational cost of this algorithm is discussed in Section 3.1.4).

Using (3.9) we have,

$$1+T=\frac{x_k+\sum_{i=j+1}^{k-1} l_i+1}{1-[j\omega+(M-k)\varphi]}=\frac{1}{\psi}(x_k+L+1). \tag{3.10}$$

Here,

$$L=\sum_{i=j+1}^{k-1} l_i, \tag{3.11}$$

$$\psi=1-[j\omega+(M-k)\varphi]\,. \tag{3.12}$$

Note that both ψ and L depend on j and k but not on x_k.

Routine derivation shows that in order to fulfill all the constraints we should have,

$$x_k\le \min\left\{\begin{array}{l} l_k \\ \dfrac{\omega}{\psi-\omega}(L+1)\dfrac{1}{1-[\psi<\omega]} \\ \psi\min\left\{\dfrac{1}{\omega}l_j\dfrac{1}{1-[j=0]},\dfrac{1}{\varphi}l_M,X_{max}+1\right\}-(L+1)\end{array}\right\}, \tag{3.13}$$

$$x_k\ge \max\left\{\begin{array}{l}\left(\dfrac{\psi}{\omega}l_{j+1}-(L+1)\right)(1-[k\le j+1]) \\ \dfrac{\varphi}{\psi-\varphi}(L+1)\end{array}\right\}. \tag{3.14}$$

Here, for any logical statement P, $[P]$ is one if P holds and zero otherwise [119].

It is informative to investigate the case of large η. Assuming $\eta=\infty$ leads to $\omega=1$, in which

case the maximum constraint in fact becomes trivial. Using (3.12) we have,

$$\psi - \omega = -(M-k)\varphi < 0, \tag{3.15}$$

and also $j = 0$. Hence, this case results in (3.13) converting to,

$$x_k \leq \min \left\{ \begin{array}{l} l_k \\ \\ (1-(M-k)\varphi) \min \left\{ \begin{array}{l} \frac{1}{\varphi} l_M \\ X_{max}+1 \end{array} \right\} - (L+1) \end{array} \right\}, \tag{3.16}$$

which is identical to the maximum limit in the CSC. Also, (3.14) changes to,

$$x_k \geq \max \left\{ \begin{array}{l} \left((1-(M-k)\varphi)\, l_1 - (L+1)\right)\left(1-[k \leq j+1]\right) \\ \dfrac{\varphi(L+1)}{1-(M-k+1)\varphi} \end{array} \right\}, \tag{3.17}$$

which is not identical to its counterpart in the case of CSC in its current form. A closer look, however, reveals that if $k \geq 2$ then using (3.11),

$$L = \sum_{i=1}^{k-1} l_i \geq l_1 \geq (1-(M-k)\varphi)\, l_1. \tag{3.18}$$

Hence, the first term in (3.17) is in fact negative. On the contrary, if $k < 2$ then $k < j+1$ which eliminates the first condition. Hence, (3.17) converts to,

$$x_k \geq \frac{\varphi(L+1)}{1-(M-k+1)\varphi}, \tag{3.19}$$

which is identical the one developed in the case of the CSC. Therefore, as expected, as η tends to infinity the NSC converges to the CSC.

Substituting (3.9) into (2.8) we have,

$$\Phi(\vec{\mathbf{x}}) = \left(\frac{1+T-\omega(1+T)}{1+T}\right)^j \prod_{i=j+1}^{k-1} \left(\frac{1+T-l_i}{1+T}\right)\left(\frac{1+T-x_k}{1+T}\right) \tag{3.20}$$

$$\left(\frac{1+T-\varphi(1+T)}{1+T}\right)^{M-k}.$$

Now, using (3.10) we have,

$$\Phi(\vec{\mathbf{x}}) = \frac{c\psi}{1-\psi}\prod_{i=j+1}^{k-1}\left(\frac{\frac{1}{\psi}(x_k+L+1)-l_i}{\frac{1}{\psi}(x_k+L+1)}\right)\left(\frac{\frac{1}{\psi}(x_k+L+1)-x_k}{\frac{1}{\psi}(x_k+L+1)}\right). \tag{3.21}$$

Here, c is a constant defined as.

$$c = \frac{1-\psi}{\psi}(1-\omega)^j(1-\varphi)^{M-k}. \tag{3.22}$$

Continuing with (3.21) we have,

$$\Phi(\vec{\mathbf{x}}) = c\frac{\prod_{i=1}^{n}(x_k+\beta_i)}{(x_k+\beta)^n}. \tag{3.23}$$

Here, we have $n = k - j$ and,

$$\beta_i = \begin{cases} L+1-\psi l_{j+i} & i = 1.\cdots n-1 \\ \dfrac{L+1}{1-\psi} & i = n \end{cases}. \tag{3.24}$$

$$\beta = L+1. \tag{3.25}$$

Notice that,

$$0 < \beta_1 < \beta_2 < \cdots < \beta_{n-1} < \beta < \beta_n. \tag{3.26}$$

$$\sum_{i=1}^{n}\beta_i - n\beta = (n-1)(L+1) - \psi L + \frac{L+1}{1-\psi} - n(L+1) = \frac{\psi(\psi L+1)}{1-\psi} > 0. \tag{3.27}$$

Hence, according to the theorem given in Section 2.5, it is inferred that the minimum value of Φ happens when x_k accepts one of the boundary values given in (3.13) and (3.14).

3.1.3 Details of the Proposed Method

Figure 3.2 shows the detailed structure of the proposed algorithm.

3.1.4 Computational Cost

Analysis of the computational cost of the algorithm depicted in Section 3.1.3 shows that it demands,

$$\tau = \frac{16}{3}\varepsilon M^3 + \frac{53\varepsilon + 2}{3}M^2 - 23\varepsilon M + 6. \tag{3.28}$$

flops. Here, ε is the portion of trials for which ϕ is in fact computed. The worst case, setting $\varepsilon = 1$, gives,

$$\tau = \frac{16}{3}M^3 + \frac{55}{3}M^2 - 23M + 6, \tag{3.29}$$

flops. However, for a typical system, as described in Section 1.3.1, ε is 0.2. On a 1Gfps (one Giga flops per second) processor, the proposed algorithm takes less than 6ms when M equals 100 (5.5ms and 0.6ms for the worst case and the bast one). Note that here the computational cost is of order $O(M^3)$ compared to the $O(M^2)$ algorithm given for the CSC. In fact, this was expected because the main "for" loop in Figure 3.2 contains two variables each one ranging somewhere between 0 and M. In Section 5.2 we show that the acceptable results of this algorithm compensates for its higher computational cost. Note that the computational cost of the new algorithm is almost $\frac{2}{3}M$ times the CSC.

3.1.5 Fairness Analysis

Using (3.4) and (3.6) we know that,

$$\max\{C_i\} \leq \eta = -\log_2(1-\omega), \tag{3.30}$$

1. Compute X_{max} using (2.11), φ using (2.10), ω using (3.6), and $\vec{\mathbf{I}}$ using (2.12).
2. Report ''Error'' if $\omega < \varphi$.
3. For all j from 0 to M and for all k from $j + 1$ to M do the followings,
   (a) Compute ψ using (3.12).
   (b) If not $\psi > \varphi$ then go to Line 3 and start over for new values of j and k, else continue to Line 3c.
   (c) Compute L as (3.11).
   (d) Compute max_x and compute min_x using (3.13) and (3.14), respectively.
   (e) If not $max_x \geq min_x \geq 0$ then go to Line 3 and start over for new values of j and k, else continue to Line 3f.
   (f) Do the following lines for the two values of $x_k = min_x$ and $x_k = max_x$, separately. Store both Φ and the values of x_i for each trial.
      - Compute T using (3.10).
      - Set $x_i = \omega(1+T)$ for $i = 1, \cdots, j$.
      - Set $x_i = l_i$ for $i = j+1, \cdots, k-1$.
      - Set $x_i = \varphi(1+T)$ for $i = k+1, \cdots, M$.
      - Compute Φ using (2.8).
4. Find the smallest Φ produced at the above and retrieve the corresponding values of x_i.
5. Compute $\vec{\mathbf{p}}$, using (2.6), and return them as well as C.

Figure 3.2: *Details of the algorithm NSC.*

$$\min\{C_i\} \geq -\log_2(1-\varphi), \tag{3.31}$$

Hence,

$$f \leq -\log_2(1-\omega) + \log_2(1-\varphi) = \log_2\left(\frac{1-\varphi}{1-\omega}\right). \tag{3.32}$$

Using this equation, after φ is selected, the appropriate ω, and hence η, which result in a desired unfairness can be calculated. Furthermore, it is shown that the unfairness of the system is controllable after the new constraint is added.

For the second unfairness measure define in (1.31) we have,

$$\tilde{f} = \frac{\max\{C_i\}}{\min\{C_i\}} \leq \frac{-\log_2(1-\omega)}{-\log_2(1-\varphi)}. \tag{3.33}$$

Note that both terms $-\log_2(1-\omega)$ and $-\log_2(1-\varphi)$ are positive. Again, the new constraint puts a limit on the ratio unfairness.

Equations (3.30) and (3.31) can be used to give approximations for f and $\tilde{f}$ as well. Here, we use the notations $f^\star$ and $\tilde{f}^\star$ for the maximum expected subtractive and ratio unfairness measures, respectively, given γ and η. By calculating these two values, maximum values for f and $\tilde{f}$ can be guaranteed. Using (3.32) we have,

$$f^\star = \log_2\left(\frac{1-\varphi}{1-\omega}\right) = \log_2\left(\frac{2^\eta}{1+\gamma}\right) = \eta - \log_2(1+\gamma) \simeq \eta - \frac{1}{\ln 2}\gamma. \tag{3.34}$$

Here, we have used the fact that if γ is very small then $\ln(1+\gamma) \simeq \gamma$. Equation (3.34) shows that the maximum possible subtractive unfairness is a linear function of η and γ. Although, γ has a negative contribution to $f^\star$ (with a coefficient of about 1.44), according to the fact that γ is negligible, we know that η is the main factor which determines $f^\star$.

Using (3.33) we also have,

$$\tilde{f}^\star = \frac{\log_2(1-\omega)}{\log_2(1-\varphi)} = \frac{\eta}{\log_2(1+\gamma)} \simeq \frac{\eta}{\gamma}\ln 2. \tag{3.35}$$

The two equations (3.34) and (3.35) relate $f^\star$ and $\tilde{f}^\star$ to γ and η. However, the operation can be performed in the other direction as well, namely, values of γ and η which yield desired values of $f^\star$ and $\tilde{f}^\star$ can be calculated. Solving (3.34) and (3.35) for γ and η we have,

$$\gamma = 2^{\frac{f^\star}{\tilde{f}^\star - 1}} - 1 \simeq \frac{f^\star}{\tilde{f}^\star - 1} \ln 2, \tag{3.36}$$

$$\eta = \frac{f^\star \tilde{f}^\star}{\tilde{f}^\star - 1}. \tag{3.37}$$

Note that $f^\star \geq 0$ and $\tilde{f}^\star \geq 1$, by definition.

As a numerical example, setting $\gamma = -50dB$ and $\eta = 0.3$ we will have $f^\star = 0.30$ and $\tilde{f}^\star = 65.76$. Compared to Table 5.1, in which $f = 0.25$ and $\tilde{f} = 6.02$, we will infer that $f^\star$ is in fact a good approximation. Also, while $\tilde{f}^\star$ is still a conservative value, the system is in fact more fair than this approximation. Similarly, selecting $f^\star = 5$ and $\tilde{f}^\star = 0.2$ yields $\gamma \simeq -30dB$ and $\eta = 0.25$. The formulation can also be used for determining the value of η which gives $\tilde{f}^\star = 3$ for $\gamma = -50dB$ (the answer is $\eta = 0.014$ for which $f^\star = 0.0091$).

3.2 New Enhanced Single Cell (N^+SC)

The capacity shares of the mobile stations in a system constitute a set of non-negative numbers with a total of one. Therefore, in a system which depends on all the mobile stations evenly we will have,

$$\tilde{C}_i = \frac{1}{M}. \tag{3.38}$$

Here, $\tilde{C}_i$ is the capacity share and is defined (1.32). Looking from the point of view of the mobile stations, this system is allocating identical capacities to all the mobile stations. However, this ideal case may not be practically acceptable because the system tends to acquire more revenue from giving service to those who are capable of receiving it, in our case those who are closer to

the base station and have larger values of g_i. On the other hand, very high values of $\tilde{C}_i$ denote the extreme dependence of the system on one particular mobile station. In fact, losing such a mobile station will results in a loss of revenue with the factor of $1-\tilde{C}_i$. Therefore, it is necessary to be able to control the maximum range for the elements of $\tilde{\tilde{\mathbf{C}}}$. Note that, even though in such a system no minimum bound for the elements of $\tilde{\tilde{\mathbf{C}}}$ is devised, the maximum capacity share and the minimum capacity bounds result in an implicit bound on the minimum capacity share of the individual mobile stations.

This section is organized as follows. First, in Section 3.2.1, a new maximum capacity share constraint is introduced and it is shown how it integrates into the NSC. Then, Section 3.2.2 analyzes the new bound and demonstrates how the dimension of the search space can be reduced. The analysis then follows, in Section 3.2.3, where a theorem is proved which produces a finite set which is guaranteed to contain the optimal solution. Then, an algorithm is proposed which solves the NSC equipped with the new constraint, resulting in the problem which is called the N^+SC. Finally, Section 3.2.4 gives a maximum bound for the computational cost of the proposed algorithm.

3.2.1 Maximum Capacity Share Bound

To make the maximum limit for the elements of $\tilde{\tilde{\mathbf{C}}}$ independent from the number of the mobile stations, we compare $\tilde{C}_i$ with M^{-1} in a condition formulated as,

$$\tilde{C}_i \leq \frac{1}{\mu}\frac{1}{M}, 0 \leq \mu \leq 1. \tag{3.39}$$

Working on (3.39) and applying (2.6) on (1.7) and (1.8) and using (3.39) and (2.13) we will have,

$$M\mu \log_2 \frac{1+T}{1+T-x_i} \leq \log_2 \frac{(1+T)^M}{\prod_{j=1}^{M}(1+T-x_j)}. \tag{3.40}$$

Following this analysis by writing the power share of the i-th mobile station as,

$$\tilde{x}_i = \frac{x_i}{I + \sum_{j=1}^{M} x_j} = \frac{x_i}{1+T}, \tag{3.41}$$

Equation (3.40) changes into,

$$(1-\tilde{x}_i)^{M\mu} \geq \prod_{j=1}^{M}(1-\tilde{x}_j) \rightarrow 1 - M\mu\tilde{x}_i + \Delta_1 \geq 1 - \sum_{j=1}^{M}\tilde{x}_j + \Delta_2. \tag{3.42}$$

Here, both Δ_1 and Δ_2 are terms including the product of two or more of the elements of $\vec{\mathbf{x}}$, where $\tilde{x}_i \in [\varphi, \omega]$. For typical values of $\gamma = -30dB$ and $\eta = 0.3$ this interval becomes $[0.03, 0.19]$. Due to the fact that $\tilde{x}_i \ll 1$, it is possible to ignore terms including powers of two and more in (3.42) and following some routine derivation write the approximate form,

$$x_i \leq \frac{1}{M\mu}T. \tag{3.43}$$

We will empirically show that this is a valid approximation.

In summary, the N^+SC problem can be written as minimizing $\Phi(\vec{\mathbf{x}})$, given in (2.8), subject to,

$$\begin{cases} 0 \leq p_i \leq p_{max}, \forall i, \\ \gamma \leq \dfrac{p_i g_i}{I + \sum\limits_{j=1, j\neq i}^{M} p_j g_j} \leq 2^{\eta} - 1, \forall i, \\ \sum\limits_{i=1}^{M} p_i g_i \leq P_{max}, \\ p_i g_j \leq \dfrac{1}{M\mu}\sum\limits_{j=1}^{M} p_j g_j. \end{cases} \tag{3.44}$$

3.2.2 Limiting the Search Space

Combining all the constraints for x_i we have,

$$\varphi(1+T) \leq x_i \leq \min\left\{l_i, \omega(1+T), \frac{1}{M\mu}T\right\}, \forall i. \tag{3.45}$$

Hence, according to the descending pattern of $\vec{\mathbf{g}}$, and hence that of $\vec{\mathbf{I}}$, the search space has a pyramid structure, and therefore the optimal solution to the N$^+$SC can be written as,

$$\vec{\mathbf{x}} = (\omega(1+T), \cdots, \omega(1+T), l_{j+1}, \cdots, l_{k-1}, x_k, \varphi(1+T), \cdots, \varphi(1+T)), \tag{3.46}$$

if,

$$\frac{1}{M\mu}T \geq \omega(1+T). \tag{3.47}$$

$$\vec{\mathbf{x}} = \left(\frac{1}{M\mu}T, \cdots, \frac{1}{M\mu}T, l_{j+1}, \cdots, l_{k-1}, x_k, \varphi(1+T), \cdots, \varphi(1+T)\right), \tag{3.48}$$

if,

$$\frac{1}{M\mu}T < \omega(1+T). \tag{3.49}$$

Here, the appropriate values of j, k, and x_k have to be found in order to make $\vec{\mathbf{x}}$ conform to all the constraints. The rest of this section discusses the conditions that make $\vec{\mathbf{x}}$ an acceptable solution to the N$^+$SC. Here, we first find a subset of the search space in which all the constraints are satisfied. Then, in the next section, the value of x_k is analyzed and a theorem is proved.

Working on (3.46) and (3.48) we have,

$$1+T = \frac{1}{\psi}(x_k + L + 1). \tag{3.50}$$

Here,

$$L = \sum_{i=j+1}^{k-1} l_i, \tag{3.51}$$

$$\psi = 1 - [j\omega + (M-k)\varphi], \tag{3.52}$$

Similarly, working on $\frac{1}{M\mu}T \geq \omega(1+T)$ leads to,

$$T \geq \frac{\omega M\mu}{1-\omega M\mu}. \tag{3.53}$$

which also needs $\omega M\mu < 1$. Substituting (3.50) into (3.53) we have,

$$x_k \geq \psi\frac{1}{1-\omega M\mu} - (L+1). \tag{3.54}$$

As (3.46) is identical to the pattern of the solution to the NSC we conclude that one solution to the N^+SC is the solution which comes from the NSC given that (3.54) is also added to the set of conditions. We will call this algorithm as the NSC+c.

Note that if $M\mu \leq 1$ then (3.43) becomes trivial. In this situation the N^+SC reduces to an ordinary NSC.

Now, we consider (3.48). We have,

$$1 + T = \frac{1}{\psi}(x_k + L + \alpha). \tag{3.55}$$

Here, L is identical to what is defined in (3.51) and,

$$\alpha = 1 - \frac{j}{M\mu}, \tag{3.56}$$

$$\psi = 1 - \left[\frac{j}{M\mu} + (M-k)\varphi\right]. \tag{3.57}$$

Note that although using the same symbol, ψ has two different definitions in (3.52) and (3.57). We use the same symbol for two different identities because they are used in separate algorithms. Now, working on $\frac{1}{M\mu}T < \omega(1+T)$ gives either $\omega M\mu > 1$ or,

$$T \leq \frac{\omega M\mu}{1-\omega M\mu} \rightarrow x_k \leq \psi\frac{1}{1-\omega M\mu} - (L+\alpha). \tag{3.58}$$

Note that (3.54) and (3.58) are the two sides of the same inequality in two different setups and hence lead to two different conditions.

Routine derivation shows that to make (3.48) comply with all the constraints we should have,

$$x_k \geq \max\left\{ \begin{array}{l} (\psi(M\mu l_{j+1}+1) - (L+\alpha))(1-[k \leq j+1]) \\ \frac{\varphi}{\psi-\varphi}(L+\alpha) \end{array} \right\}. \tag{3.59}$$

$$x_k \leq \min\left\{ \begin{array}{l} \psi \min\left\{ \begin{array}{l} X_{max}+1 \\ \frac{M\mu l_j+1}{1-[j=0]} \\ \frac{1}{\varphi} l_M \end{array} \right\} - (L+\alpha) \\ \frac{L+\alpha-\psi}{M\mu\psi-1}\frac{1}{1-[M\mu\psi<1]} \\ l_k \end{array} \right\}. \tag{3.60}$$

We call the algorithm which finds the optimum solution given these constraints the N′SC. Note that this is not an independent algorithm and will be used inside another algorithm. When (3.58) is added to the search space for the N′SC, we call the new algorithm as the N′SC+c.

What was performed so far aimed at finding the search space in which all the constraints are satisfied. The next step in this analysis is to spot the optimal solution in the search space. Working on the N^+SC, we know that if $M\mu \leq 1$ is satisfied then the solution can be sought for using the NSC algorithm, because the new maximum capacity share constraint becomes trivial. Furthermore, we know that when $\omega M\mu < 1$ the solution is the one given by either the NSC equipped with the extra inequality (3.54) or by the N′SC equipped with (3.58). On the other

1. If $M\mu < 1$ then solve the NSC.
2. Else, if $\omega M\mu < 1$ Then
   (a) Solve the NSC+c.
   (b) Solve the N'SC+c.
3. Else, solve the N'SC.
4. Find the best outcome.

Figure 3.3: *Details of the algorithm N^+SC.*

hand, if $\omega M\mu \geq 1$, the solution comes from the N'SC (see the comments before (3.58)). The pseudo-code of this algorithm is shown in Figure 3.3. Note that each algorithm, namely the NSC or the N'SC, have their own search space and also their own structure of the vector $\vec{\mathbf{x}}$, as shown in (3.46) and (3.48).

3.2.3 Spotting the Solution

In Section 3.2.2 the search space was limited by a set of inequalities to satisfy all the constraints. Therefore, it was proven than the optimal solution is one of the points of the given search space, which still is infinite. However, in the case of the NSC it was proved that x_k should accept one of the boundary values, leading to a finite set of possible solutions from which the optimal one is selected. The basis of that argument is a theorem proved in Section 2.5. In this section we will prove a theorem more general than the one proved previously, the new theorem will prove that for the case of the N'SC too the value of x_k must be equal to one of the boundaries.

Looking at Figure 3.3 we are concerned with solving the NSC or the N'SC either solely by themselves or when an extra inequality for x_k is included in the problem as well. The theorem proved in Section 2.5 shows that for the NSC structure of $\vec{\mathbf{x}}$, which is given in (3.46), having $l \leq x_k \leq L$, which complies with all the constraints, the optimal solution is produced by either $x_k = l$ or $x_k = L$. Hence, we should produce $\vec{\mathbf{x}}$ for both of these choices and then find the value of the function at that point. Iterating this check for all the possible values of j and k we will have a list of possible solutions, one of which is the optimal one. Here, we will prove that with

the structure of $\vec{\mathbf{x}}$ which is given in (3.48) the same condition applies. So, again, we should only check a finite number of possibilities and then find the optimal solution among them. In the following parts of this section we will prove a theorem which allows us to do so.

Using the structure of $\vec{\mathbf{x}}$ for the N′SC given in (3.46) and (3.48), we have,

$$\Phi(\vec{\mathbf{x}}) = \frac{(1-\varphi)^{M-k}}{(1+T)^k}\left(1+T-\frac{1}{M\mu}T\right)^j \prod_{i=j+1}^{k-1}(1+T-l_i)\,(1+T-x_k)\,. \tag{3.61}$$

Defining,

$$\beta = L + \alpha, \tag{3.62}$$

$$\beta_i = \begin{cases} L+\alpha+\dfrac{\psi}{M\mu-1} & i=1,\cdots,j \\ L+\alpha-\psi l_i & i=j+1,\cdots,k-1 \\ \dfrac{L+\alpha}{1-\psi} & i=k \end{cases}, \tag{3.63}$$

we can write,

$$\Phi(\vec{\mathbf{x}}) = Cf(x_k), \tag{3.64}$$

where,

$$f(x) = \frac{\prod_{i=1}^{k}(x+\beta_i)}{(x+\beta)^k}. \tag{3.65}$$

Here, C is a positive constant. Using (3.63) and (3.62) we can show that all the elements of $\vec{\beta}$ and also β are positive.

Assume that we have shown that $f'(x)$ cannot become zero twice. Also, note that the smallest of all the elements of $\vec{\beta}$ and β is β_{j+1}. Hence, the largest zero of $f(x)$, after which it neither gets zero nor goes to infinity, is $-\beta_{j+1}$. Knowing that $\lim_{x\to\infty} f(x) = 1$, we infer that $f'(-\beta_{j+1})$

should be positive. Because, otherwise, for a positive ε the value of $f(-\beta_{j+1}+\varepsilon)$ becomes negative. Then the continuous function f has different signs in the interval $[-\beta_{j+1}+\varepsilon, \infty]$ and hence there should be at least one x in this interval for which $f(x)$ gets zero, something we know is impossible. Knowing $f'(-\beta_{j+1})$ is positive, for $f(x)$ to have a local minimum inside $[-\beta_{j+1}, \infty]$ we should have a point c in this interval in which $f'(c)=0$ and $f'(c^-)<0$. Now, the continuous function $f'(x)$ accepts two different signs in the two margins of $[-\beta_{j+1}, c]$ and hence should have a zero in between. Having proved that $f'(x)$ cannot have two zeros in $[-\beta_{j+1}, \infty]$ we know that this is impossible. Hence, we know that in any interval $[l, L]$ on the positive side, the minimum value of $f(x)$ happens in a boundary, and not a point inside the interval. Now, we prove that $f'(x)$ cannot become zero twice in the interval $[0, \infty]$.

We assume that there are at least two distinct solutions for $f'(x)=0$. Therefore,

$$f'(x)=f(x)\left(\sum_{i=1}^{k}\frac{1}{x+\beta_i}-\frac{k}{x+\beta}\right)=0\rightarrow\sum_{i=1}^{k}\frac{1}{x+\beta_i}=\frac{k}{x+\beta}. \tag{3.66}$$

Minor algebraic manipulations give,

$$x+\beta=\left(\frac{1}{k}\sum_{i=1}^{k}\frac{}{x+\beta_i}\right)^{-1}. \tag{3.67}$$

We know that if for continuous functions $f(x)$ and $g(x)$ there are two distinct solutions to $f(x)=g(x)$ for $x\in[a,b]$ then there is a solution for $f'(x)=g'(x)$ in the same interval. Hence, having two solutions to (3.67), there should be a solution for,

$$\frac{1}{k}\sum_{i=1}^{k}\frac{1}{x+\beta_i}=\left(\frac{1}{k}\sum_{i=1}^{k}\frac{1}{(x+\beta_i)^2}\right)^{\frac{1}{2}}. \tag{3.68}$$

Here, we use the general mean theorem stated as follows. Assume that the positive values of $x_1,\cdots,x_n$ are given and define $\vec{\mathbf{x}}=(x_1,\cdots x_n)$. Now defining,

$$M^r(\vec{\mathbf{x}})=\left(\frac{1}{n}\sum_{i=1}^{n}x_i^r\right)^{\frac{1}{r}}. \tag{3.69}$$

the general mean theorem states that for $r < s$ we have $M^r(\vec{\mathbf{x}}) \leq M^s(\vec{\mathbf{x}})$. The equality happens when all the elements of $\vec{\mathbf{x}}$ are all identical. Hence, (3.68) may only happen if $x + \beta_i = x + \beta_j$ for all values of i and j. This needs all the elements of $\vec{\beta}$ to be identical, contradicting their definition given in (3.63). Hence, we have proved that the solution to the N'SC happens in one of the bounds given in (3.59) and (3.60) and nowhere in between. Note that this is a property of the structure of $\vec{\mathbf{x}}$ and not any particular bounds. Hence, including other bounds for x_k does not contradict these results, as long as the interval remains on the positive side. Therefore, the same theorem applies to the NSC+c and to the N'SC+c, as well.

In order to execute the code given in Figure 3.3 one should only find the respective boundaries for x_k, construct the vector $\vec{\mathbf{x}}$ and then find the value of the aggregate capacities. Then, a comparison over all the possibilities gives the optimal solution. The essence of this algorithm is identical to the one given for the CSC (see Section 2.6) and the NCS (see Section 3.1.3) while the structure of $\vec{\mathbf{x}}$ and also the boundaries are vastly different in each of these algorithms.

3.2.4 Computational Cost

Using Figure 3.3 we know that,

$$\tau_{N^+SC} = 1 + \max \left\{ \begin{array}{l} \tau_{NSC} \\ 1 + \max \left\{ \begin{array}{l} \tau_{NSC} + \tau_{N'SC} + 2M^2 - 2M + 2 \\ \tau_{N'SC} \end{array} \right\} \end{array} \right\}. \tag{3.70}$$

Here, τ_P is the computational cost of the algorithm P (in flops) for solving a problem including M mobile stations. Hence, at the worst case,

$$\tau_{N^+SC} = \frac{32}{3}M^3 + \frac{128}{3}M^2 - 52M + 20, \tag{3.71}$$

which is almost twice as much as the computational cost of the NSC (see Section 3.1.4). Still, the computational cost of the new algorithm is of order $O(M^3)$.

3.3 Application of the Approximations

In this section, we use approximations in order to reduce the computational cost of finding the aggregate capacity for a given x_k. Also, new shorter proofs for the established theorems are given.

This section is organized as follows. First, in Section 3.3.1, the algorithms proposed in Chapter 2 and Sections 3.1 and 3.2 are looked at through a unifying approach, yielding the concept of a "typical algorithm". Then, giving an approximation for the aggregate capacity in Section 3.3.2 and using a theorem proved in Section 3.3.3 the basis for the new analysis is stated. These results are used in Section 3.3.4 to propose substitute approximate algorithms.

3.3.1 Typical Algorithm

The three algorithms of the CSC, the NSC, the N$^+$SC, and also the internal algorithm the N$'$SC, have a similar structure. In fact, the analysis always shows that there is a value of k, or a pair of j and k, for which the vector $\vec{\mathbf{x}}$ is linearly calculated based on x_k. Then, the problem is to find the best k, or k and j, and then spot the best x_k. For each problem it has independently been proved that having fixed k, and also j if applicable, x_k should accept either the smallest or the largest value allowed by the boundaries. This way, in each algorithm the two functions θ and Θ which depend on k, and j if applicable, and the system parameters are derived. Then, the question is to iterate over all values of k, and j if applicable, and to set $x_k = \theta$ and $x_k = \Theta$ and gather all possible results. Then, the best solution is selected.

3.3.2 Approximations

Except for the CSC, γ_i is always a member of $[\gamma, 2^\eta - 1]$ and therefore, using nominal values of $\gamma = -30dB$ and $\eta = 0.3$, approximating $\ln(1+\gamma_i)$ with γ_i carries less than 10% error. Hence, we write,

$$C_i \simeq \frac{1}{\ln 2}\gamma_i = \frac{1}{\ln 2}\frac{x_i}{1+T-x_i} = \frac{1}{\ln 2}\frac{\frac{x_i}{1+T}}{1-\frac{x_i}{1+T}}. \tag{3.72}$$

We know that $\frac{x_i}{1+T}$ belongs to $[\varphi, \omega]$. For the mentioned values of γ and η we have $\varphi = 0.03$ and $\omega = 0.19$. Hence, we approximate C_i as,

$$C_i \simeq \frac{1}{\ln 2} \frac{x_i}{1+T} \left(1 + \frac{x_i}{1+T}\right). \tag{3.73}$$

A closer look into (3.72) and (3.73) reveals that here we are using the approximation,

$$\log_2 \left(1 + \frac{x}{1-x}\right) \simeq \frac{1}{\ln 2} x\,(1+x)\,, \tag{3.74}$$

for $x = \frac{x_i}{1+T}$. We know that for the cases of the NSC and the N^+SC x belongs to $[\varphi, \omega]$. Calculating the right and the left sides of (3.74) for different values of x and drawing them on the same axes, as shown in Figure 3.4–(a), we investigate the properness of this approximation. Figure 3.4–(b) shows that for the cases of the NSC and the N^+SC, the shaded area, the approximation results in less than 8% error. Also, for these two problems the exact value is always less than the approximated one. However, for highly impartial CSC solutions, for which x may go over 0.7, the approximation may fall below the exact value. Note that, generally, the approximation generates less than 10% error, independent of the algorithm. This approach is partially based on the analysis given in [120].

Using (3.73) we have,

$$C \simeq \frac{1}{\ln 2} \left(\frac{T}{T+1} + \frac{\sum_{i=1}^{M} x_i^2}{(1+T)^2} \right) = \frac{1}{\ln 2} \left(1 + \frac{\sum_{i=1}^{M} x_i^2}{(1+T)^2} - \frac{1}{1+T} \right). \tag{3.75}$$

Equation (3.75) shows that for fixed T the maximum value of $C(\vec{\mathbf{x}})$ happens when $\sum_{i=1}^{M} x_i^2$ is maximum. Assuming that all the elements of $\vec{\mathbf{x}}$ are fixed except for x_j and x_k, while we should have,

$$x_j + x_k = T - \sum_{i=1, i\neq j, i\neq k}^{M} x_i^2 = S, \tag{3.76}$$

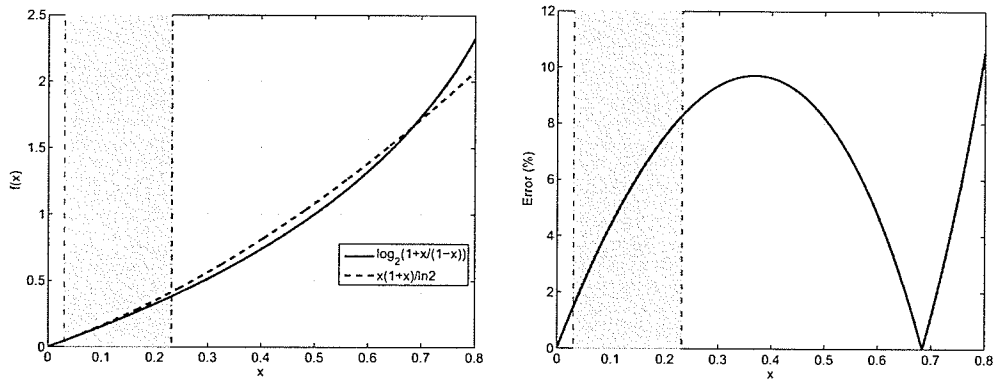

Figure 3.4: *Investigation of the properness of (3.74). (a) The two sides of (3.74). (b) The relative error induced by using the approximation given in (3.74). The shaded area shows the working interval for the cases of the NSC and the N^+SC.*

the problem reduces to looking for the maximum value of $x_j^2 + x_k^2$. Now, according to,

$$2(x_j^2 + x_k^2) = (x_j + x_k)^2 + (x_j - x_k)^2, \tag{3.77}$$

the maximum happens when x_j and x_k are at the most possible absolute distance. This is another proof for the theorem proved in Section 2.5.

Note that the approximation given in (3.75) is also helpful in fast calculation of the value of C for a given $\vec{\mathbf{x}}$. As described in Section 3.3.1, the typical algorithm includes finding bounds for the x_k, for different values of k, and j if applicable, and then finding the aggregate capacity at the bounds. Using the approximation given here this process can be accelerated. Note that using this method, the calculation of the boundaries is still being carried out precisely according to the exact formulation. Therefore, if the approximate algorithm does not fail in finding the best k, and j if applicable, the values of $p_1, \cdots, p_M$ will be exactly accurate. The actual worry here is that the approximation may deviate the algorithm from finding the best k, or j, and hence give a wrong result. Here, we assume that the approximation does not change two values of C for two different vectors $\vec{\mathbf{p}}$ in a way that the better situation becomes worse. Assuming this, after $\vec{\mathbf{p}}$ is determined $\vec{\mathbf{C}}$ is calculated again in order to yield the exact result. Through

experimental analysis we will empirically show that the approximate algorithm does give the exact solution, with a negligible probability of erratic behavior. After producing the correct $\vec{\mathbf{p}}$, and the approximate value of C, we will recalculate C using the precise formulation. This will result in finding the precise value of C.

3.3.3 Theorem

Assume that values of a, b and c are given and that the function $f(x)$ is defined as,

$$f(x) = \frac{x^2 + ax + b}{(x+c)^2}, x \in R^+ \cup \{0\}. \tag{3.78}$$

Also, assume that we know that c is positive. In fact, this function has one singularity on $x = -c$, which is on the negative side. Also, we know that $\lim_{x\to\infty} f(x) = 1$ and,

$$f'(x) = \frac{(2c-a)x + (ac-2b)}{(x+c)^3}. \tag{3.79}$$

Hence, for $x > -c$ the value of $f'(x)$ gets zero at most once. Although, we do not yet know the sign of $\lim_{x\to -c} f(x)$, it is identical to the sign of $c^2 - ac + b$. Assume that this value is positive, meaning $\lim_{x\to -c} f(x) = +\infty$. We claim that for any interval on the positive side, say $[\theta, \Theta]$, the maximum value of $f(x)$ in $[\theta, \Theta]$ is either $f(\theta)$ or $f(\Theta)$.

We will show that given the specified conditions, $f(x)$ has one of the typical shapes depicted in Figure 3.5. Note that for $x \in [0, \infty]$ both $f(x)$ and $f'(x)$ are continuous. Furthermore, the fact that $\lim_{x\to -c} f(x) = +\infty$ implies that $\lim_{x\to -c} f'(x) = -\infty$. Also, we know that, $\lim_{x\to\infty} f'(x) = 0$. Hence, for positive values of x, the value of $f(x)$ is negative, converging to zero at $+\infty$. We know that this function can at most get zero once during this process. Hence, there are two possibilities. First, $f'(x)$ is always negative, except for at infinity in which it becomes zero (the dashed line in Figure 3.5). Second, it is negative then gets zero and positive and then it returns to zero (the solid line in Figure 3.5). For any $f(x)$ which has either of the shapes shown in Figure 3.5 we observe that for any interval on the positive side the maximum

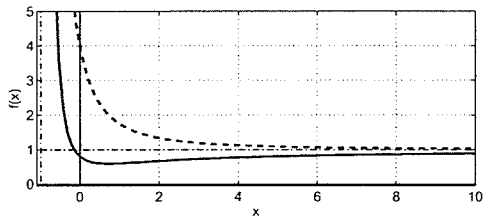

Figure 3.5: *Possible shapes of the function $f(x)$ defined in (3.78) in the circumstances discussed in Section 3.3.3.*

happens at the boundary. We will show how this theorem substitutes the more complex theorems proved in Sections 2.5, 3.1.2 and 3.2.3.

3.3.4 Approximate Algorithms

In this section the ideas introduced so far are used to propose the three alternative algorithms of the CSC^a, the NSC^a, and the N$^+$SC^a. Here, we also show how the approximate calculation of C is incorporated into the proposed algorithms. In fact, for the algorithm XSC, which is one of the algorithms the CSC, the NSC, the N$'$SC, and the N$^+$SC, we replace the exact calculation of C with the approximate one in order to produce the algorithm XSC^a.

In each case, the exact formulations and the benefits of the proposed method in terms of computational cost will be presented. Also, we give new proofs for theorems for which more complicated proofs were given in the previous parts of this thesis. We show that the application of the approximations results in new shorter proofs for the equivalents of the theorems in the new framework. We again emphasize that after the approximate value of C is found, we calculate the exact C using a single run of the formulation which gives the precise C in terms of $\vec{\mathbf{p}}$. In the experimental results we will use the terms E, A, and E+A for the exact results, the crude results of the approximate algorithm and the recalculated results, respectively.

The CSC^a

According to the formulation for the solution to the CSC, given in Chapter 2, we have,

$$\vec{\mathbf{x}} = (l_1, \cdots, l_{k-1}, x_k, \varphi(1+T), \cdots, \varphi(1+T)) . \tag{3.80}$$

Hence,

$$C(\vec{\mathbf{x}}) \simeq \frac{1}{\ln 2}\left(\frac{L + x_k^2 + (M-k)\varphi^2(1+T)^2 - (1+T)}{(1+T)^2} + 1\right). \tag{3.81}$$

Here,

$$L = \sum_{i=1}^{k-1} l_i^2. \tag{3.82}$$

Now, using,

$$T = \psi^{-1}(x_k + l + 1), \tag{3.83}$$

where,

$$l = \sum_{i=1}^{k-1} l_i. \tag{3.84}$$

$$\psi = 1 - (M-k)\varphi. \tag{3.85}$$

we have,

$$C(\vec{\mathbf{x}}) \simeq \frac{1}{\ln 2}\left(\psi^2 \frac{x_k^2 - \frac{1}{\psi}x_k + L - \frac{1}{\psi}(l+1)}{(x_k + l + 1)^2} + 1 + (M-k)\varphi^2\right). \tag{3.86}$$

Hence, the problem translates into finding the maximum of (3.78) where,

$$a = -\psi^{-1}, b = L - \psi^{-1}(l+1), c = l + 1. \tag{3.87}$$

The search is performed in the interval given by (2.36) and (2.37).

Note that, we have,

$$c^2 - ac + b = l^2 + 2l + 1 + L > 0. \tag{3.88}$$

Hence, using the theorem proved in Section 3.3.3, x_k must accept one of the boundary values. We compare this short proof with the one given in Section 2.5.

Equation (3.86) is also important because it can be used in order to reduce the computational complexity of the solver. We compare this new algorithm to the previously proposed one which has to produce $\vec{\mathbf{C}}$ for every instance of k.

Analysis shows that the computational cost of the CSC^a equals $36M + 6$ flops, compared to the $8M^2 + 20M + 10$–flops cost of the CSC (refer to Section 2.7). Hence, a decrease in computational cost with ratio of $\frac{1}{5}M$ is observed. In fact, the computational cost drops from $O(M^2)$ to $O(M)$.

NSC^a

Analysis of the NSC in Section 3.1 showed that,

$$\vec{\mathbf{x}} = \Big(\omega(1+T), \cdots, \omega(1+T), l_{j+1}, \cdots, l_{k-1}, x_k, \varphi(1+T), \cdots, \varphi(1+T)\Big). \tag{3.89}$$

Hence,

$$C(\vec{\mathbf{x}}) \simeq \frac{1}{\ln 2}\left(\frac{j\omega^2(1+T)^2 + L + x_k^2 + (M-k)\varphi^2(1+T)^2 - (1+T)}{(1+T)^2} + 1\right), \tag{3.90}$$

which changes into,

$$C(\vec{\mathbf{x}}) \simeq \frac{1}{\ln 2}\left(\psi^2 \frac{x_k^2 - \frac{1}{\psi}x_k + L - \frac{1}{\psi}(l+1)}{(x_k + l + 1)^2} + 1 + (M-k)\varphi^2 + j\omega^2\right). \tag{3.91}$$

Here, we have defined,

$$L = \sum_{i=j+1}^{k-1} l_i^2, \tag{3.92}$$

$$l = \sum_{i=j+1}^{k-1} l_i. \tag{3.93}$$

Also, we have,

$$T = \psi^{-1}(x_k + l + 1), \tag{3.94}$$

where,

$$\psi = 1 - (j\omega + (M - k)\varphi). \tag{3.95}$$

Now, (3.91) decreases to a function of the type discussed in Section 3.3.3 with,

$$a = -\psi^{-1}, b = L - \psi^{-1}(l + 1), c = l + 1. \tag{3.96}$$

Again, $c^2 - ac + b$ is positive. Hence, x_k should accept one of the bounds given in (3.13) and (3.14).

Using the approximate closed form for $C(\vec{\mathbf{x}})$ given in (3.91) the computational cost of the NSC^a reduces to $23M^2 - 21M + 14$ flops compared to the $\frac{16}{3}M^3 + \frac{55}{3}M^2 - 23M + 6$–flop cost of the NSC (see Section 3.1.4). This makes the new algorithm about $\frac{1}{4}M$ times faster than the previous one and yields a computational cost of order of $O(M^2)$.

N$^+$SC^a

To analyze the N$^+$SC^a we first have to analyze the N$'$SC^a, for which we have (refer to Section 3.2.2),

$$\vec{\mathbf{x}} = \left(\frac{1}{M\mu}T, \cdots, \frac{1}{M\mu}T, l_{j+1}, \cdots, l_{k-1}, x_k, \varphi(1 + T), \cdots, \varphi(1 + T)\right), \tag{3.97}$$

which gives (L and l are defined in Section 3.2),

$$C(\vec{\mathbf{x}}) \simeq \frac{1}{\ln 2}\left(\frac{\frac{j}{M^2\mu^2}T^2 + L + x_k^2 + (M - k)\varphi^2(1 + T)^2 - (1 + T)}{(1 + T)^2} + 1\right). \tag{3.98}$$

Here,

$$1 + T = \psi^{-1}(x_k + l + \alpha), \tag{3.99}$$

$$\alpha = 1 - j(M\mu)^{-1}, \tag{3.100}$$

$$\psi = 1 - (j(M\mu)^{-1} + (M - k)\varphi). \tag{3.101}$$

Working on (3.98) we have,

$$C(\vec{\mathbf{x}}) \simeq \frac{1}{\ln 2}\left(\psi^2 \frac{x_k^2 - \frac{1}{\psi}\left(\frac{2j}{M^2\mu^2} + 1\right)x_k + L + \frac{j}{M^2\mu^2} - \frac{1}{\psi}\left(\frac{2j}{M^2\mu^2} + 1\right)(l + \alpha)}{(x_k + l + \alpha)^2}\right. \tag{3.102}$$
$$\left. +1 + (M - k)\varphi^2 + \frac{j}{M^2\mu^2}\right),$$

which is of the general form discussed in Section 3.3.3 if we substitute,

$$a = -\psi^{-1}(2jM^{-2}\mu^{-2} + 1), c = l + \alpha, \tag{3.103}$$

$$b = L + jM^{-2}\mu^{-2} - \psi^{-1}(2jM^{-2}\mu^{-2} + 1)(l + \alpha), \tag{3.104}$$

Here, we have,

$$c^2 - ac + b = (l + \alpha)^2 + L + jM^{-2}\mu^{-2} > 0. \tag{3.105}$$

Hence, the solution should be one of the boundary values given in Section 3.2.2. Using (3.103) the computational cost of the N′SC^a reduces from $\frac{16}{3}M^3 + \frac{67}{3}M^2 - 27M + 16$ flops to $26M^2 - 23M + 15$ flops, a decrease by $\frac{1}{5}M$.

Using these results and also the ones presented in Section 3.2 the computational cost of the

$\mathrm{N}^{+}\mathrm{SC}^{a}$ becomes $\tau_{N^{+}SC^{a}} = 51M^2 - 46M + 33$ flops, compared to the last cost of $\frac{32}{3}M^3 + \frac{128}{3}M^2 - 52M + 20$ flops for the $\mathrm{N}^{+}\mathrm{SC}$. Again, the computational cost is reduced by $\frac{1}{5}M$.

3.4 Utility Functions

As shown in Figure 3.1, the problems analyzed in Chapter 2 and Sections 3.1 and 3.2 use different sets of constraints, and thus reach different design goals. However, they all assume that the "benefit" of serving a mobile station at a certain capacity depends linearly on that capacity. In other words, looking at (1.8), the objective function, $C(\vec{\mathbf{p}})$, uses the utility function $f(x) \equiv x$, whilst, in real applications, being able to work with other utility functions gives the designer a significant degree of flexibility. In particular, according to the fact that all the algorithms discussed in the above tend to produce solutions in which all the elements of $\vec{\mathbf{p}}$ are at the margins, we may be able to produce more fair solutions using concave utility functions.

Here, we define a more general definition of the aggregate "satisfaction" as,

$$\hat{C}(\vec{\mathbf{p}}) = \sum_{i=1}^{M} f(C_i), \tag{3.106}$$

where, $f : \mathbb{R}^{+} \cup \{0\} \rightarrow \mathbb{R}^{+} \cup \{0\}$ is a doubly differentiable increasing function. Note that, $\hat{C}$ shows the aggregate satisfaction in the system, as opposed to C which shows the aggregate capacity. However, to comply with the history of the problem and also for consistency we address $\hat{C}$ as the aggregate "capacity".

In this section, we first show that the algorithms the CSC, the NSC, and the $\mathrm{N}^{+}\mathrm{SC}$ all remain functional if f is a convex function, while minor changes in the implementation is necessary. We emphasize that this proof only has theoretical importance. Because, given the behavior of the problem when the identity utility function is employed, there is no reason for using convex utility functions.

In the next step, we work on concave utility functions, and we show that given that a few conditions are met, the problem will be solved using a method proposed in this section. While

the proposed method could be further developed for the case of the N^+SC, we work on the NSC, because of mathematical convenience. To address problems produced by using (3.106), we use the superscripts $f-$ and $f+$ for the cases of concave and convex utility functions, respectively. For example, the NSC problem equipped with a concave utility function, given that a few other conditions are met, will be called the NSC^{f-}. Furthermore, as we focus on the utility functions defined as $f(x) \equiv x^{\alpha}$, we will also address the problems such as the NSC^{α}.

3.4.1 Convex Utility Functions

Assume that the convex utility function $f(x)$ is given. We also assume that for $x \geq 0$, both $f'(x)$ and $f''(x)$ are positive. Using (3.106) we have,

$$\hat{C}(\vec{\mathbf{x}}) = \sum_{i=1}^{M} f\left(\log_2\left(1+\gamma_i\right)\right) = \sum_{i=1}^{M} f\left(-\log_2\left(\frac{1+T-x_i}{1+T}\right)\right). \tag{3.107}$$

Defining

$$g(x) = f\left(-\log_2(x)\right), \tag{3.108}$$

we have,

$$\hat{C}(\vec{\mathbf{x}}) = \sum_{i=1}^{M} g\left(\frac{1+T-x_i}{1+T}\right). \tag{3.109}$$

Note that $g : (0,1) \rightarrow \mathbb{R}^+ \cup \{0\}$.

Lemma I: The function g is strictly convex ($g''(x) > 0$). Accordingly, g' is an increasing function, and thus it is one-to-one.

Proof: Analyzing $g(x)$, we have,

$$g''(x) = \frac{1}{\ln(2)} x^{-2} f'\left(-\log_2(x)\right) + \frac{1}{(\ln(2))^2} x^{-2} f''\left(-\log_2(x)\right) > 0. \tag{3.110}$$

■

Theorem I: In the solution to the NSC^{f+}, no extension is possible (refer to Section 2.3 for the definitions of extension and extending pairs).

Proof: Assume that $\vec{\mathbf{x}}$ is the maximizer of $\hat{C}$. Also assume that an extension engaging the two indexes i and j and the value of δ, resulting in a potential solution $\vec{\mathbf{x}}^{\star}$, is possible. Note that there is a value of T for which $\vec{\mathbf{x}}$ and $\vec{\mathbf{x}}^{\star}$ both lie on the same hyperplane defined as (2.13). Thus, writing $\hat{C}(\vec{\mathbf{x}})$ as,

$$\hat{C}(\vec{\mathbf{x}}) = \hat{C}^{\circ}(\vec{\mathbf{x}}) + g\left(\frac{1+T-x_i}{1+T}\right) + g\left(\frac{1+T-x_j}{1+T}\right), \tag{3.111}$$

where,

$$\hat{C}^{\circ}(\vec{\mathbf{x}}) = \sum_{\ell=1,\ell\neq i,j}^{M} g\left(\frac{1+T-x_\ell}{1+T}\right), \tag{3.112}$$

we have $\hat{C}^{\circ}(\vec{\mathbf{x}}) = \hat{C}^{\circ}(\vec{\mathbf{x}}^{\star})$. Thus, it is necessary to have,

$$g\left(\frac{1+T-x_i}{1+T}\right) + g\left(\frac{1+T-x_j}{1+T}\right) \geq g\left(\frac{1+T-x_i^{\star}}{1+T}\right) + g\left(\frac{1+T-x_j^{\star}}{1+T}\right). \tag{3.113}$$

Note that there is a value of $t \geq 0$ for which,

$$x_i + x_j = x_i^{\star} + x_j^{\star} = t. \tag{3.114}$$

Defining,

$$\Delta(x_i, x_j) = g\left(\frac{1+T-x_i}{1+T}\right) + g\left(\frac{1+T-x_j}{1+T}\right), \tag{3.115}$$

and using (3.114), where,

$$\frac{\partial \Delta}{\partial x_j} = -\frac{1}{T+1}g'\left(\frac{T+1-x_j}{T+1}\right) + \frac{1}{T+1}g'\left(\frac{T+1-t+x_j}{T+1}\right), \tag{3.116}$$

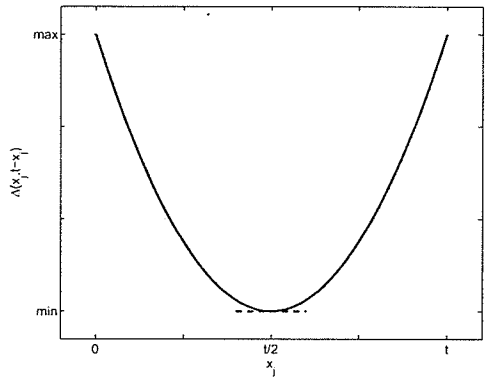

Figure 3.6: *Typical structure of* $\Delta(x_j, t - x_j)$.

which is an increasing function in terms of x_j. Thus, remembering that,

$$\Delta\left(x_i, x_j\right) = \Delta\left(x_j, x_i\right). \tag{3.117}$$

it can be shown that the curve $\Delta(x_j, t - x_j)$ has the structure shown in Figure 3.6. Thus, for $x_j \leq \frac{t}{2}$ ($x_j \geq \frac{t}{2}$), as x_j tends to the left (the right), $\Delta(x_j, t - x_j)$ increases. Hence it is impossible for (3.113) to happen ■

Having proved Theorem I, which is the general case of the similar theorem given in Section 2.3, the three resulting lemmas stated in Section 2.3 are valid in the NSC. Here, the lemmas are briefly reviewed. For any i, making x_j for $j \neq i$ fixed, x_i can accept values in an interval, which we call $[b_i, B_i]$. In this definition, x_i is called to be at the beginning, at the middle, or at the end, if $x_i = b_i$, $b_i < x_i < B_i$, or $x_i = B_i$, respectively. Using these definitions, the following lemmas are valid.

Lemma II In the solution to the NSC^{f+} there is at most one x_i at the middle.

Lemma III In the solution to the NSC^{f+}, if there is one x_i at the middle, every x_j for $j > i$ will be at the beginning.

Lemma IV In the solution to the NSC^{f+}, if x_k is at the middle and for a value of m, satisfying $m < k$, x_m is at the beginning, then for $m < i < k$, x_i cannot be at the end. Using Lemma III this implies that x_i must always be at the beginning.

Using these lemmas, a theorem similar to Theorem VI in Section 2.3 is concluded.

Theorem II: If there is any solution to the NSC^{f+}, then it has the structure shown below,

$$\vec{\mathbf{x}} = (\omega(1+T), \cdots, \omega(1+T), l_{j+1}, \cdots, l_{k-1}, x_k, \varphi(1+T), \cdots, \varphi(1+T)) . \tag{3.118}$$

Proof: Referring to Lemmas II, III, and IV, this is the only possible case ■

Thus, rather than searching for the optimal solution to the NSC^{f+} in $[0, p_{max}]^M$, the problem reduces to finding the proper j, k, and x_k. This yields a reduction of the dimension of the search space from M to 3. We will prove that in fact the search space can be further reduced to an order of M^2 individual points, for which we present closed forms. Here, first necessary and sufficient boundaries for x_k are given.

Theorem III: In the optimal solution to the NSC^{f+} we have,

$$T = \frac{1}{\psi}(x_k + L + 1) - 1, \tag{3.119}$$

where,

$$L = \sum_{i=j+1}^{k-1} l_i, \tag{3.120}$$

$$\psi = 1 - [j\omega + (M-k)\varphi] . \tag{3.121}$$

Furthermore, we must have $\psi > \varphi$ and,

$$x_k \leq max_{jk} = \min \left\{ \begin{array}{l} l_k \\ \dfrac{\omega}{\psi - \omega}(L+1)\dfrac{1}{1-[\psi < \omega]} \\ \psi \min \left\{ \begin{array}{l} \dfrac{1}{\omega} l_j \dfrac{1}{1-[j=0]} \\ \dfrac{1}{\varphi} l_M, X_{max} + 1 \end{array} \right\} - (L+1) \end{array} \right\} . \tag{3.122}$$

$$x_k \geq min_{jk} = \max \left\{ \begin{array}{l} \left(\frac{\psi}{\omega} l_{j+1} - (L+1)\right)(1 - [k \leq j+1]) \\ \frac{\varphi}{\psi - \varphi}(L+1) \end{array} \right\}. \tag{3.123}$$

Proof: Refer to the proof given in Section 2.4 ■

Now, the question is to find the best x_k, given k and j are known. This is carried out through Theorem IV.

Theorem IV: In the optimal solution to the NSC^{J+}, x_k must accept one of the marginal values given in (3.122) and (3.123).

Proof: Assume that the values of j and k are given, for which max_{jk} and min_{jk}, given in (3.122) and (3.123), satisfy $max_{jk} \geq min_{jk} \geq 0$. Now, the question is which value of $x_k \in [min_{ij}, max_{jk}]$ maximizes,

$$\hat{C}(x_k) = \sum_{i=1}^{M} g\left(\frac{1+T-x_i}{1+T}\right), \tag{3.124}$$

where the relationship between the elements of $\vec{\mathbf{x}}$ and x_k is given in (3.118). Routine substitution shows that,

$$\hat{C}(x_k) = jg(1-\omega) + \sum_{i=j+1}^{k-1} g\left(\frac{1+T-l_i}{1+T}\right) + g\left(\frac{1+T-x_k}{1+T}\right) + (M-k)g(1-\varphi). \tag{3.125}$$

Thus, the problem reduces to maximizing,

$$\hat{C}^{\circ}(x_k) = \sum_{i=j+1}^{k-1} g\left(\frac{1+T-l_i}{1+T}\right) + g\left(\frac{1+T-x_k}{1+T}\right). \tag{3.126}$$

Using Theorems II and III, (3.126) is rewritten as,

$$\hat{C}^{\circ}(x_k) = \sum_{i=1}^{n-1} g\left(\frac{x_k+\beta_i}{x_k+\beta}\right) + g\left((1-\psi)\frac{x_k+\beta_n}{x_k+\beta}\right), \tag{3.127}$$

where,

$$n = k - j, \beta = L + 1, \tag{3.128}$$

$$\beta_i = \begin{cases} L + 1 - \psi l_{i+j} & 1 \leq i \leq n-1 \\ \dfrac{L+1}{1-\psi} & i = n \end{cases}. \tag{3.129}$$

Note that $\beta_1 < \beta_2 < \cdots < \beta_{n-1} < \beta < \beta_n$.

We prove that there is at most one plausible solution to,

$$\frac{\partial \hat{C}^{\circ}}{\partial x_k} = 0. \tag{3.130}$$

Assuming otherwise, derivation shows that,

$$\frac{\partial \hat{C}^{\circ}}{\partial x_k} = \frac{1}{(x_k+\beta)^2}\left[\sum_{i=1}^{n-1}(\beta-\beta_i)\, g'\left(\frac{x_k+\beta_i}{x_k+\beta}\right) - (1-\psi)(\beta_n-\beta)\right. \tag{3.131}$$
$$\left. g'\left((1-\psi)\frac{x_k+\beta_n}{x_k+\beta}\right)\right].$$

Thus, assuming that there are two plausible solutions for (3.130), there must be at least two zero-crossings for,

$$\tilde{C}(x_k) = \sum_{i=1}^{n-1}(\beta-\beta_i)\, g'\left(\frac{x_k+\beta_i}{x_k+\beta}\right) - (1-\psi)(\beta_n-\beta)\, g'\left((1-\psi)\frac{x_k+\beta_n}{x_k+\beta}\right). \tag{3.132}$$

Hence, there must be at least one plausible solution to,

$$\frac{\partial \tilde{C}}{\partial x_k} = 0. \tag{3.133}$$

Routine calculations show that,

$$\frac{\partial \tilde{C}}{\partial x_k} = \sum_{i=1}^{n-1}(\beta-\beta_i)^2\, g''\left(\frac{x_k+\beta_i}{x_k+\beta}\right) + (1-\psi)^2(\beta_n-\beta)^2\, g''\left((1-\psi)\frac{x_k+\beta_n}{x_k+\beta}\right) > 0. \tag{3.134}$$

Thus, there is no plausible solution to (3.133) and hence there is at most only one plausible solution to (3.130).

It is convenient to prove that,

$$\lim_{x_k \to -\beta_1^+} \hat{C}^{\circ}(x_k) = +\infty, \tag{3.135}$$

$$\lim_{x_k \to -\beta_1^+} C^{\circ\prime}(x_k) = -\infty, \tag{3.136}$$

$$\lim_{x_k \to \infty} \hat{C}^{\circ}(x_k) = (n-1) \lim_{\varepsilon \to 1^-} g(\varepsilon) + g(1-\psi) > 0. \tag{3.137}$$

Also, we know that for $x_k > -\beta_1$, $\hat{C}^{\circ}(x_k)$ is always finite. Routine derivation shows that for $x_k \gg \beta_n$,

$$\left.\frac{\partial \hat{C}^{\circ}}{\partial x_k}\right|_{x_k} \simeq \frac{f'(0)}{(x_k+\beta)^2 \ln(2)} \Gamma, \tag{3.138}$$

where,

$$\Gamma = \left[\sum_{i=1}^{n-1} \beta_i - (n-1)\beta + (\beta_n - \beta)\nu\right], \tag{3.139}$$

$$\nu = \frac{f'(-\log_2(1-\psi))}{f'(0)} > 1. \tag{3.140}$$

Substituting (3.128) and (3.129) in (3.139) yields,

$$\Gamma = [(\nu - 1 + \psi)L + \nu]\frac{\psi}{1-\psi} > 0. \tag{3.141}$$

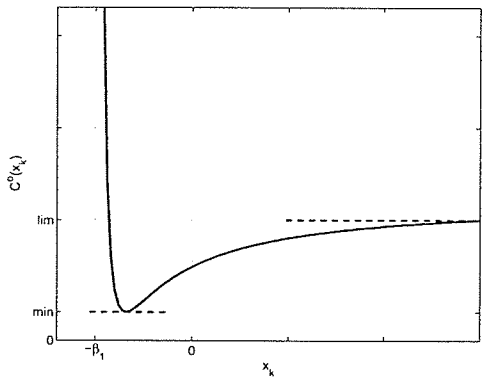

Figure 3.7: *Typical structure of* $\hat{C}^{\circ}(x_k)$.

Thus, according to (3.138),

$$\lim_{x_k \to \infty} \hat{C}^{\circ}(x_k) = 0^{+}. \tag{3.142}$$

Using (3.135), (3.136), (3.137), and (3.142), it could be shown that $\hat{C}^{\circ}(x_k)$ has the structure shown in Figure 3.7. Note that, although, in Figure 3.7 the minimizer of $\hat{C}^{\circ}(x_k)$ is shown to be negative, in fact, in some cases it is positive. Nevertheless, in any interval on the positive side, the maximum of $\hat{C}^{\circ}(x_k)$ happens on one of the boundaries ■

According to Theorem IV, in order to find the optimal solution to the NSC^{f+} it suffices to examine all values of j and k and to find max_{jk} and min_{jk}, as given in (3.122) and (3.123). Then, the value of $\hat{C}(\vec{\mathbf{x}})$ for the two alternatives of $x_k = max_{jk}$ and $x_k = min_{jk}$ should be independently calculated. From this list of solutions, which contains less than $2M^2$ potential points, finding the largest aggregate capacity retrieves the optimal solution. This algorithm is called the NSC^{f+} and is carried in detail in Figure 3.8.

Comparing the NSC^{f+} with the NSC reveals that the potential solutions of these two problems are identical. Therefore, the essential difference between the two algorithms is the objective function which is calculated for each candidate point.

Analysis shows that the computational cost of NSC^{f+} equals $\tau_{NSC^{f+}} = \frac{16+3\tau_f}{3}M^3$ flops. Here, τ_f is the cost of calculating $f(x)$ for one x. In the case of a power law ($f(x) = x^{\alpha}, \alpha > 1$)

1. Compute X_{max} using (2.11) and $\vec{\mathrm{I}}$ using (2.9).
2. Compute φ and ω using (2.5) and (3.6).
3. Report ''Error'' if $\omega < \varphi$.
4. For all j from 0 to M and for all k from $j + 1$ to M, do the followings,
   (a) Compute ψ using (3.121).
   (b) If not $\psi > \varphi$ then ignore this pair of j and k.
   (c) Compute L using (3.120).
   (d) Compute max_{jk} and min_{jk} using (3.122) and (3.123), respectively.
   (e) If not $max_{jk} \geq min_{jk} \geq 0$ then ignore this pair of j and k.
   (f) Do the followings for the two values of $x_k = min_{jk}$ and $x_k = max_{jk}$, independently. Store both $\hat{C}(\vec{\mathrm{x}})$ and $\vec{\mathrm{x}}$ for each trial.
      - Compute T using (3.119).
      - Produce $\vec{\mathrm{x}}$ using (3.118).
      - Compute $\hat{C}(\vec{\mathrm{x}})$ using (3.106).
5. Find the largest value of $\hat{C}$ produced at the above and retrieve the corresponding $\vec{\mathrm{x}}$.
6. Compute $\vec{\mathrm{p}}$, using (2.6), and return them as well as $\hat{C}$.

Figure 3.8: *Details of the algorithm NSC^{f+}.*

the computational cost will equal $\tau_{NSC^{f+}} = 6.3M^3$.

We emphasize that while the potential solutions to the NSC and the NSC^{f+} are the same, there is no claim that the final solutions to these two problems will also be the same. However, the author has no counterexample which would lead to different outcomes by the two algorithms.

3.4.2 Concave Utility Function

Assume that the increasing positive concave function $f(x)$ is given, based on which (3.108) yields the function $g(x)$.

Assume that a value of $0 < \theta < 1$ is given. Define the two functions $h(\varepsilon)$ and $t(\varepsilon)$ as,

$$h(\varepsilon) = g\left(1 - \theta\varepsilon\right) + g\left(1 - \theta + \theta\varepsilon\right), \tag{3.143}$$

$$t(\varepsilon) = g\left(1 - \frac{\theta}{2}\varepsilon\right), \tag{3.144}$$

where both functions are defined for $0 < \varepsilon < 1$. Note that $h(\varepsilon)$ is symmetric around $\theta = \frac{1}{2}$.

The algorithm proposed here demands the two conditions stated below to be satisfied. One, it is necessary that $h(\varepsilon)$ is increasing for $\varepsilon < \frac{1}{2}$ and decreasing for $\varepsilon > \frac{1}{2}$ and that hence it only has one local maximum, at $\varepsilon = \frac{1}{2}$. Two, $t(\varepsilon)$ must be strictly concave ($t''(\varepsilon) < 0$). Exploration of the category of functions which satisfy these two conditions is outside the scope of this thesis. Here, for notational convenience, we focus on the power-law utility functions. Note that the proposed method works for any other function which satisfies the above conditions as well. When an increasing concave utility function is given, which satisfies the above conditions, we will call the resulting problem as the NSC^{f-}.

A typical set of concave utility functions used in the literature is the class of power functions defined as,

$$f(x) = x^{\alpha}. 0 < \alpha < 1. \tag{3.145}$$

Theorem V proves that given that a condition on α is met, (3.145) will satisfy both conditions on $h(\varepsilon)$ and $t(\varepsilon)$.

Theorem V: If,

$$\theta \leq \sqrt{2}(1 - \alpha), \tag{3.146}$$

then the conditions on $h(\varepsilon)$ and $t(\varepsilon)$ will be satisfied.

Proof: To visually observe what the condition on $h(\varepsilon)$ implies, we fix α at 0.7 and then calculate the function for different values of θ and ε, as shown in Figure 3.9. This figure also

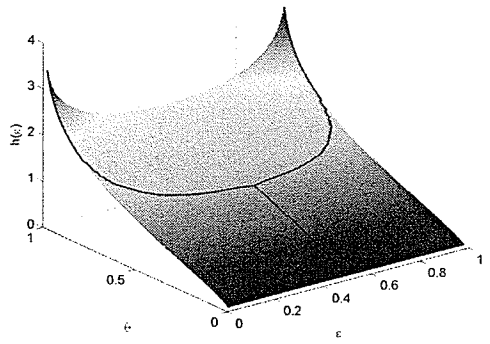

Figure 3.9: *Values of $h(\varepsilon)$ for $\alpha = 0.7$ and different values of θ. The solid line shows the loci of the peak for different values of θ.*

shows the loci of the maximizer for different values of θ, namely the solid curves. According to these curves, we are looking for the value of θ° for which if $\theta \leq \theta^\circ$ then the maximizer is at the middle. In other words, we are looking for the point at which the loci of the maximizers branches up into two curves. To find θ° for a known value of α, a numerical procedure is carried out which uses a bisection–style algorithm. The result is shown as the solid line in Figure 3.10. According to this curve, if the working point, identified by the pair (α, θ), is in the area denoted by the cross, then the condition on $h(\varepsilon)$ will be satisfied.

Carrying out the same operation for the second condition, $\alpha = 0.7$ is fixed and then the values of $t''(\varepsilon)$ for different values of θ and ε are calculated, as seen in Figure 3.11. The solid line in Figure 3.11 shows the set of points for which $t''(\varepsilon) = 0$, the existence of which indicates that there are values of ε satisfying $t''(\varepsilon) > 0$. Using another bisection–style algorithm, the value of θ°, similar to the one calculated for $h(\varepsilon)$, for each value of α are computed.

It is observed that in the case of $f(x)$ defined as (3.145), the two curves are identical. Note that the same may or may not be true for other definitions of $f(x)$. Analysis of this issue is outside the scope of this thesis.

Collecting the results produced for the two functions $h(\varepsilon)$ and $t(\varepsilon)$, we draw the curve shown in Figure 3.10. As mentioned before, any working point located in the area denoted by the cross

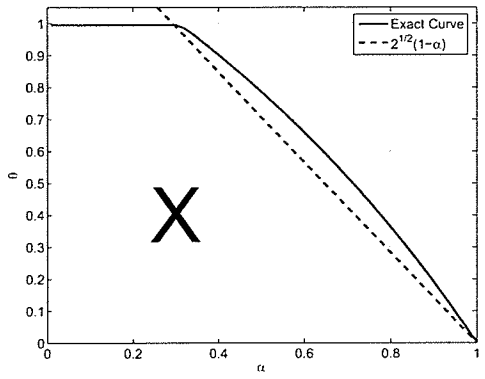

Figure 3.10: *If the (α, θ) pair is in the area denoted by the cross then the conditions on $h(\varepsilon)$ and $t(\varepsilon)$ will be satisfied.*

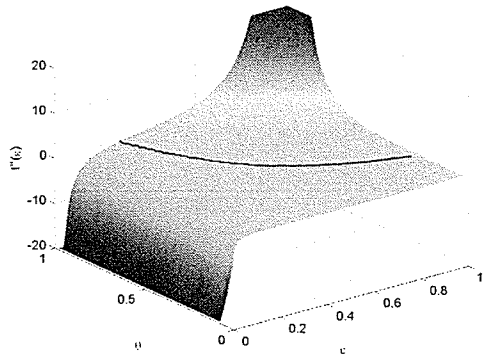

Figure 3.11: *Values of $t''(\varepsilon)$ for $\alpha = 0.7$ and different values of θ. The solid line shows the loci of points for which $t''(\varepsilon) = 0$.*

will satisfy the two conditions. For convenience, the curve is approximated by a line, shown as a dashed line in Figure 3.10 ■

Similar to the concept of extension, defined in Section 2.3, we define a contracting pair, and also a contraction. This way, if a potential solution could produce another one in which,

$$\left|x_i^\star - x_j^\star\right| < \left|x_i - x_j\right|, \tag{3.147}$$

then we will call i and j a contracting pair and the situation will be called a contraction.

Theorem VI: In the solution to the NSC^{f-}, no contraction is possible.

Proof: Fixing x_k for $k \neq i, j$, the problem reduces to maximizing,

$$\Delta(x_i, x_j) = g\left(\frac{1+T-x_i}{1+T}\right) + g\left(\frac{1+T-x_j}{1+T}\right), \tag{3.148}$$

subject to $x_i + x_j = t$. Writing $t = \theta(T+1)$ we have,

$$\theta \leq 2\omega. \tag{3.149}$$

Also, we write $x_i = \varepsilon t$ and also $x_j = t - x_i = t - \varepsilon t$. Now, we have,

$$\Delta(x_i, x_j) = h\left(\frac{x_i}{x_i + x_j}\right), \tag{3.150}$$

which using Theorem V shows that a contraction will produce a better solution, if (3.149) complies with (3.146) ■

Lemma V For the conditions on $h(\varepsilon)$ and $t(\varepsilon)$ to be satisfied it is sufficient to have $\alpha + \sqrt{2}\omega \leq 1$.

Proof: Routine manipulation of (3.149) and (3.146) gives the proof ■

Using Theorem VI the following lemmas are provable.

Lemma VI: In the solution to the NSC^{f-}, if x_i is at the beginning, no x_j can be not at the beginning. Thus, if one x_i is at the beginning, all others will be at the beginning as well.

Proof: We use the same graphical visualization used in Section 2.3. In fact, we show that x_i being at the beginning while x_j is at the end results in a contraction. The two possible cases are shown below.

$$\begin{aligned} x_j &: \left[\varphi(1+T)\cdots\cdots\cdots\leftarrow\times\cdots\cdots\cdots\cdots\tilde{l}_j\right] \\ x_i &: \left[\varphi(1+T)\times\rightarrow\cdots\cdots\cdots\cdots\cdots\cdots\cdots\tilde{l}_i\right] \end{aligned}$$

$$\begin{aligned} x_i &: \left[\varphi(1+T)\times\rightarrow\cdots\cdots\cdots\cdots\cdots\cdots\cdots\tilde{l}_i\right] \\ x_j &: \left[\varphi(1+T)\cdots\cdots\cdots\leftarrow\times\cdots\cdots\cdots\cdots\tilde{l}_j\right] \end{aligned}$$

Similarly, it can be shown that x_j cannot be at the end.

Lemma VII: In the solution to the NSC^{f-}, if x_i is at the end, for $j > i$, x_j will be at the end, too.

Proof: There are two possible situations in which for $j > i$, x_i is at the end but x_j is not at the end, both of which result in contractions.

$$\begin{aligned} x_i &: \left[\varphi(1+T)\cdots\cdots\cdots\cdots\cdots\cdots\leftarrow\times\tilde{l}_i\right] \\ x_j &: \left[\varphi(1+T)\times\rightarrow\cdots\cdots\cdots\cdots\cdots\cdots\tilde{l}_j\right] \end{aligned}$$

$$\begin{aligned} x_i &: \left[\varphi(1+T)\cdots\cdots\cdots\cdots\cdots\cdots\leftarrow\times\tilde{l}_i\right] \\ x_j &: \left[\varphi(1+T)\cdots\cdots\cdots\times\rightarrow\cdots\cdots\cdots\tilde{l}_j\right] \end{aligned}$$ ■

Lemma VIII: In the solution to the NSC^{f-}, if x_i and x_j are at the middle, $x_i = x_j$.

Proof: There are two possible situations in which $j > i$, x_i is at the end, and x_j is not at the end, both of which are contractions. One of them is shown below, and the other one is very similar.

$$\begin{aligned} x_i &: \left[\varphi(1+T)\cdots\cdots\cdots\cdots\leftarrow\times\cdots\cdots\cdots\tilde{l}_i\right] \\ x_j &: \left[\varphi(1+T)\cdots\cdots\cdots\times\rightarrow\cdots\cdots\cdots\cdots\tilde{l}_j\right] \end{aligned}$$ ■

Theorem VII: The solution to the NSC^{f-} has the following structure,

$$\vec{\mathbf{x}} = (x_k, \cdots, x_k, l_{k+1}, \cdots, l_M). \tag{3.151}$$

Proof: Referring to Lemmas VI, VII, and VIII, this is the only possible case ■

Theorem VII reduces the problem to finding the proper k and x_k. The next step is taken in Theorem VIII, which gives necessary and sufficient bounds for x_k.

Theorem VIII: In the solution to the NSC^{f-},

$$k \leq \frac{1}{\varphi}. \tag{3.152}$$

Also, if $k \neq 0$ is known, it is both necessary and sufficient for x_k to satisfy $min_k \leq x_k \leq max_k$, where,

$$max_k = \min \left\{ \begin{array}{l} \dfrac{X_{max} - L}{k} \\ \dfrac{1}{\left|\frac{1}{\omega} - k\right|}(L+1)\dfrac{1}{1 - \left[k \geq \frac{1}{\omega}\right]} \\ l_k \\ \dfrac{1}{k}\left(\dfrac{1}{\varphi} l_M - (L+1)\right) \end{array} \right\}, \tag{3.153}$$

$$min_k = \max \left\{ \begin{array}{l} l_{k+1} \\ \dfrac{1}{\frac{1}{\varphi} - k}(L+1) \end{array} \right\}. \tag{3.154}$$

Here,

$$L = \sum_{i=k+1}^{M} l_i. \tag{3.155}$$

Proof: Using (3.151) we know that,

$$T = kx_k + L. \tag{3.156}$$

Routine work on the set of all the conditions provides the proof ■

While Theorem VIII provides bounds for x_k, the actual value of x_k is still unknown. To facilitate the search for x_k, Theorem IX proves that either Golden Search [121] is able to find the proper solution or that the solution is known in closed form.

Theorem IX: If in the solution to the NSC^{f-}, $k \neq 0$ is known, either Golden Search can spot the optimal x_k, or x_k is at one of the boundaries.

Proof: We have,

$$\hat{C}\left(x_k\right) = \sum_{i=1}^{M} g\left(\frac{1+T-x_i}{1+T}\right), \tag{3.157}$$

which using (3.151) and (3.156) gives,

$$\hat{C}\left(x_k\right) = kg\left(\frac{(k-1)x_k+\beta}{kx_k+\beta}\right) + \sum_{i=1}^{n} g\left(\frac{kx_k+\beta_i}{kx_k+\beta}\right). \tag{3.158}$$

Here $n = M-k$, $\beta = L+1$, and $\beta_i = L+1-l_{i+k}$. Note that,

$$0 < \beta_1 < \beta_2 < \cdots < \beta_n < \beta. \tag{3.159}$$

Derivation shows that,

$$\frac{\partial \hat{C}}{\partial x_k} = \frac{1}{(kx_k+\beta)^2}\left[-k\beta g'\left(\frac{(k-1)x_k+\beta}{kx_k+\beta}\right) + \sum_{i=1}^{n} k(\beta-\beta_i)g'\left(\frac{kx_k+\beta_i}{kx_k+\beta}\right)\right]. \tag{3.160}$$

Thus, if for any x_k, $\frac{\partial \hat{C}}{\partial x_k}$ is zero, so will be,

$$\tilde{C}(x_k) = -\beta g'\left(\frac{(k-1)x_k+\beta}{kx_k+\beta}\right) + \sum_{i=1}^{n}(\beta-\beta_i)g'\left(\frac{kx_k+\beta_i}{kx_k+\beta}\right). \tag{3.161}$$

We also have,

$$\frac{\partial \tilde{C}}{\partial x_k} = \frac{1}{(kx_k+\beta)^2}\left[\beta^2 g''\left(\frac{(k-1)x_k+\beta}{kx_k+\beta}\right) + \sum_{i=1}^{n} k(\beta-\beta_i)^2 g''\left(\frac{kx_k+\beta_i}{kx_k+\beta}\right)\right]. \tag{3.162}$$

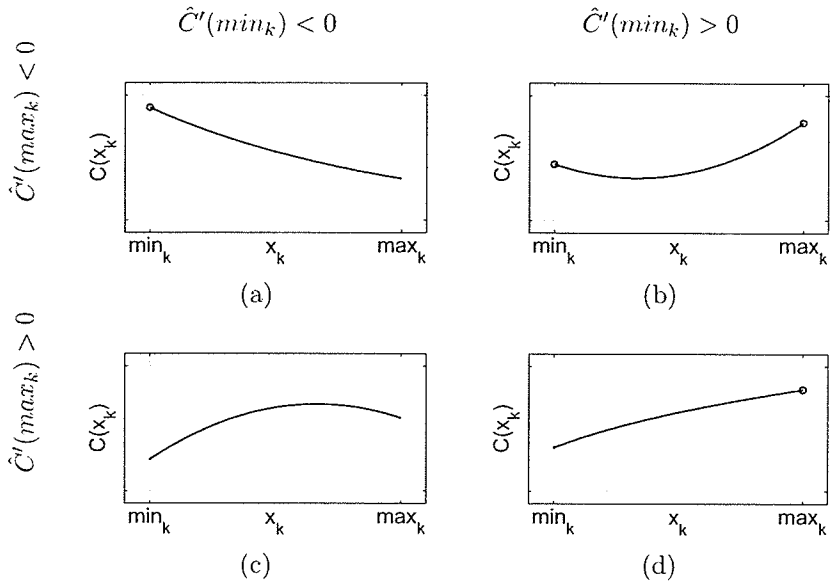

Figure 3.12: *The four possibilities for $\hat{C}(x_k)$. The candidates for the optimal solution are highlighted by circles.*

which according to the concavity of $t(\varepsilon)$ is always negative. Thus, $\tilde{C}(x_k)$ has at most one zero-crossing in the regarding domain. Hence, $\frac{\partial \hat{C}}{\partial x_k}$ becomes zero at most once. Looking at the values of $\hat{C}'(x_k)$ at the two ends of the boundary, given in (3.153) and (3.154), there are four possibilities, as shown in Figure 3.12. Note that in the cases shown in Figures 3.12-a, b, and d, the optimal point is one of the boundaries. In contrast, the case shown in Figure 3.12-c represents a unimodal concave function, for which Golden Search is able to approximately find the maximizer ■

Based on these results, we propose the algorithm the NSC^{J-}, as described in Figure 3.13. Analysis shows that if the relative precision of %0.01 is desired, Golden Search will need 20 function calculations in each run. Then, the maximum computational cost of the proposed algorithm, assuming that the Goldean search is utilized for every k, will be $20(\tau_f + 3)M^2$ flops. Here, τ_f is the cost of calculating $f(x)$ for one x. In the case of (3.145), the computational cost will equal $80M^2$. Note that this is a maximum bound because not for every value of k the case shown in Figure 3.12-c will occur.

1. Compute X_{max} using (2.11) and $\vec{\mathrm{I}}$ using (2.9).
2. Compute φ and ω using (2.5) and (3.6).
3. Report ''Error'' if $\omega < \varphi$.
4. If $\alpha + \sqrt{2}\omega > 1$ report ''Error''.
5. Set $\vec{\mathbf{x}} = (l_1, \cdots, l_M)$ and check if it complies with all the constraints. If so, calculate $\hat{C}(\vec{\mathbf{x}})$ and store it accompanied by $\vec{\mathbf{x}}$.
6. For all k from 1 to $\min\{M, \varphi^{-1}\}$ do the followings,
   (a) Compute L using (3.155).
   (b) Compute max_k and min_k using (3.153) and (3.154), respectively.
   (c) If not $max_k \geq min_k \geq 0$ then ignore this k.
   (d) Compute β and $\vec{\beta}$ using (3.128) and (3.129), respectively.
   (e) Calculate $\hat{C}'(min_k)$ and $\hat{C}'(max_k)$ using (3.160) and decide which one of the options shown in Figure 3.12 has occurred.
      i. Set $x_k = min_k$.
      ii. Set $x_k = min_k$ if $\hat{C}(min_k) > \hat{C}(max_k)$. Otherwise $x_k = max_k$.
      iii. Apply Golden Search on (3.158) in $[min_k, max_k]$ to find x_k.
      iv. Set $x_k = max_k$.
   (f) Produce $\vec{\mathbf{x}}$ using (3.151) and store it accompanied by $\hat{C}(\vec{\mathbf{x}})$.
7. Find the largest value of $\hat{C}$ produced at the above and retrieve the corresponding $\vec{\mathbf{x}}$.
8. Compute $\vec{\mathbf{p}}$, using (2.6), and return them as well as $\hat{C}$.

Figure 3.13: *Details of the algorithm NSC^{f-}.*

To compare the share of different mobile stations in the aggregate capacity, we use the capacity shares, as well as the ratio unfairness value, which we conveniently call the unfairness. Note that while in (1.32) the capacity share of the i–th mobile station was defined as its capacity over the aggregate capacity, in the existence of a utility function a more general definition is used,

$$\tilde{C}_i' = \frac{f(C_i)}{\hat{C}}. \tag{3.163}$$

Also, the unfairness of the system is defined as,

$$f' = \frac{f(C_{max})}{f(C_{min})}. \tag{3.164}$$

Thus we have,

$$f' \leq \frac{f(-\log_2(1-\omega))}{f(-\log_2(1-\varphi))}. \tag{3.165}$$

In the case of a power utility function,

$$f' \leq \left(\frac{-\log_2(1-\omega)}{-\log_2(1-\varphi)}\right)^{\alpha}. \tag{3.166}$$

which is less than the unfairness of the equivalent NSC (see Section 3.1.5).

3.5 Multiple–Class Systems (MSC)

The existence of different services in modern wireless systems has created the need for defining different classes of service [76]. This, for example, means potentially different guaranteed minimum QoS levels for different mobile stations. Moreover, different mobile stations may have different significances to the service provider, for example because of their premium rates. The fact that the constraints are met at different points for different mobile stations makes the application of many of the methods developed previously impossible, unless changes are made to

them to fulfill the new demand. This is essentially because a majority of the previous algorithm were designed for the case in which all the mobile stations reside in the same class [71, 73].

In this section, we analyze the problem of maximizing the aggregate capacity of the reverse link in a multiple-class CDMA network. The aggregate capacity here is defined as the weighted summation of the capacities of a group of mobile stations. Here, we consider the case in which there are different minimum SIR constraints for different mobile stations. The problem analyzed here also includes a maximum aggregate received power constraint and different limits on the transmit powers of different mobile stations. Furthermore, each mobile station has its own maximum capacity constraint. We will show how this problem can be approximately solved using linear or quadratic programming.

The rest of this section is organized as follows. First, in Section 3.5.1, the problem formulation is presented. Then, a set of substitute variables are defined in Section 3.5.2, from which, in Section 3.5.3, two approximations for the objective function are derived. These approximations are used for generating the canonical representations depicted in Section 3.5.4. Then, after the issue of the addition of other constraints into the problem is addressed in Section 3.5.5, Section 3.5.6 presents the proposed algorithms as well as a cost analysis.

3.5.1 Problem Formulation

In this section we consider the problem defined as maximizing,

$$C = \sum_{i=1}^{M} \alpha_i C_i, \alpha_i > 0, \tag{3.167}$$

subject to,

$$\begin{cases} \gamma_i \geq \gamma_i^{min}, \forall i, \\ C_i \leq C_i^{max}, \forall i, \\ \sum_{i=1}^{M} p_i g_i \leq P^{max}, \\ 0 \leq p_i \leq p_i^{max}, \forall i. \end{cases} \tag{3.168}$$

Here, the constants γ_i^{min}, C_i^{max}, and p_i^{max} are the minimum SIR, the maximum capacity, and the maximum transmission power of the i–th mobile station, respectively and α_i is the significance of mobile station i to the network. Through grouping the mobile stations into classes of identical values for these parameters this model will be applicable to a multiple–class scenario.

Setting $\alpha_i = 1$, $\gamma_i^{min} = \gamma$, $C_i^{max} = \eta$, and $p_i^{max} = p_{max}$ converts this problem to the single–class problem titled as the NSC in Section 3.1. In Section 3.1.3 an algorithm is proposed which solves the NSC in an M–station cell in $O(M^3)$ flops.

The goal of the rest of this section is to solve the more generalized problem of maximizing (3.167) subject to (3.168), in which different mobile stations not only have different significances, denoted by different values of α_i, but also have their own individual constraints. In these circumstances, the mathematical method developed in Chapter 2 and used for tackling the NSC (Section 3.1) and its single–class generalizations (see Section 3.2 for example) will not work, because the constraints are now specific to the mobile stations and therefore the methodology developed previously will fail.

3.5.2 Substitute Variables

Here, we propose a new set of substitute variables and then rewrite the optimization problem, using approximations, as a linear or a quadratic programming problem.

Define the new set of variables,

$$\varphi_i = \frac{\gamma_i}{1+\gamma_i} = \frac{p_i g_i}{\sum_{j=1}^{M} p_j g_j + I}, \forall i. \tag{3.169}$$

Derivation shows that,

$$C_i = -\log_2 (1 - \varphi_i), \tag{3.170}$$

$$p_i g_i = I \frac{\varphi_i}{1 - \sum_{j=1}^{M} \varphi_j}. \tag{3.171}$$

Thus, if $\sum_{i=1}^{M} \varphi_i < 1$, a positive $\vec{\varphi}$ will produce a positive $\vec{\mathbf{p}}$.

Using (3.169), the conditions given in (3.168) can be rewritten as linear constraints for $\vec{\varphi}$ as,

$$\begin{cases} \varphi_i^{min} \leq \varphi_i \leq \varphi_i^{max}, \forall i, \\ \sum_{i=1}^{M} \varphi_i \leq \dfrac{X^{max}}{X^{max}+1}, \\ l_i \sum_{j=1}^{M} \varphi_j + \varphi_i \leq l_i, \forall i. \end{cases} \tag{3.172}$$

Here,

$$\begin{cases} \varphi_i^{min} = \dfrac{\gamma_i^{min}}{\gamma_i^{min}+1}, \\ \varphi_i^{max} = 1 - 2^{-C_i^{max}}, \\ X^{max} = \dfrac{P^{max}}{I}, \\ l_i = \dfrac{p_i^{max} g_i}{I}. \end{cases} \tag{3.173}$$

Note that the second condition in (3.172) results in $\sum_{i=1}^{M} \varphi_i \leq 1$, satisfying the condition needed for (3.171) to produce a positive $\vec{\mathbf{p}}$. Defining,

$$\mathbf{A} = \begin{bmatrix} \vec{\mathbf{1}}_{1\times M} \\ \mathbf{1}_{M\times M} + diag\left[\dfrac{1}{l_1}, \cdots, \dfrac{1}{l_M}\right] \end{bmatrix}, \tag{3.174}$$

$$\vec{\mathbf{b}} = \begin{bmatrix} \dfrac{X^{max}}{X^{max}+1} \\ \vec{\mathbf{1}}_{M\times 1} \end{bmatrix}, \tag{3.175}$$

the set of inequalities given in (3.172) can be written as,

$$\begin{cases} \vec{\varphi^{\mathbf{min}}} \leq \vec{\varphi} \leq \vec{\varphi^{\mathbf{max}}}, \\ \mathbf{A}\vec{\varphi} \leq \vec{\mathbf{b}}. \end{cases} \tag{3.176}$$

While we will use (3.176) as the set of constraints for the optimization problem, to be given

later in the section, this set of inequalities can also be used for identifying the feasible region for $\vec{\varphi}$. This issue is not discussed in this thesis.

3.5.3 Approximation of the Objective Function

The depiction of the objective function in terms of $\vec{\varphi}$, in its present form includes fractional and logarithmic terms. Thus, we devise two methods, a linear and a quadratic one, in order to approximate C as a first–degree or a second–degree function of $\vec{\varphi}$. With the linear representation of the constraints, given in (3.176), this will make the application of standard linear and quadratic programming methods to the problem analyzed here possible.

For small γ_i, We have,

$$C_i = \log_2(1+\gamma_i) \simeq \frac{1}{ln2}\gamma_i \simeq \frac{1}{ln2}\varphi_i. \tag{3.177}$$

The approximation used here can be written as,

$$ln(1+x) \simeq \frac{x}{1+x}, x \in [\gamma, 2^\eta - 1], \tag{3.178}$$

and yields a linear approximation of C_i in terms of φ_i. A more appropriate approximation is given below,

$$C_i \simeq \frac{1}{ln2}\gamma_i = \frac{1}{ln2}\frac{\varphi_i}{1-\varphi_i} \simeq \frac{1}{ln2}\varphi_i(1+\varphi_i). \tag{3.179}$$

This is a second order approximation of C_i in terms of φ_i and is based on the following approximation,

$$ln(1+x) \simeq \frac{x}{1+x}\left(1+\frac{x}{1+x}\right), x \in [\gamma, 2^\eta - 1]. \tag{3.180}$$

The appropriateness of the two approximations demonstrated in (3.178) and (3.180) are investigated in Figure 3.14. Here, the nominal values of $\gamma = -30dB$ and $\eta = 0.3$ are used,

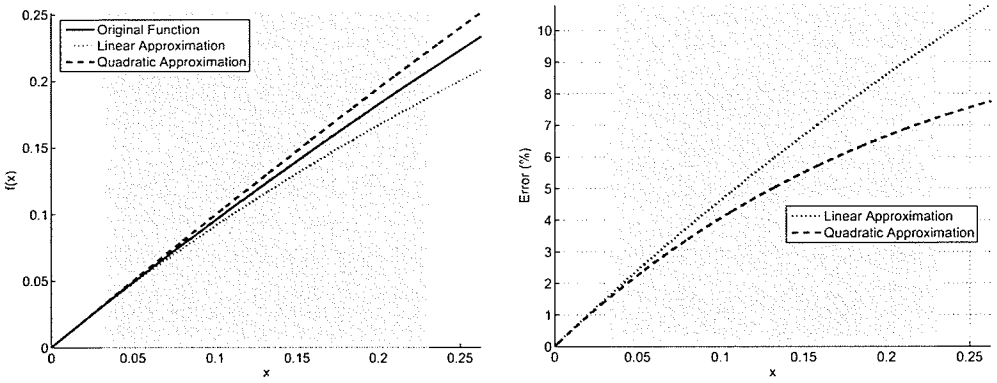

Figure 3.14: *Comparison of the exact form with the two different approximations given in (3.178) and (3.180). The shaded areas indicates the working point. (a) The values. (b) Relative error.*

shown as the shaded area. Based on Figure 3.14–(b), both approximations induce less than 10% error. Note that as p_i increases, and thus so do γ_i and φ_i, the error induced by either approximation goes up. However, the second order approximation is always more accurate than the linear approximation (see Figure 3.14–(a)). It is also important to emphasize that while the linear approximation is conservative, i.e. it produces smaller values than the exact formulation, the second order formula approximates the capacity by a larger value. Therefore, the second order approximation overestimates the aggregate capacity which it attempts at maximizing of.

3.5.4 Canonical Representation

We use the linear approximation, given in (3.177), to rewrite the objective function as,

$$C \simeq \frac{1}{ln2} \sum_{i=1}^{M} \alpha_i \varphi_i = \vec{\mathbf{f}}^T \vec{\varphi}. \tag{3.181}$$

Here,

$$\vec{\mathbf{f}} = \frac{1}{ln2} \vec{\alpha}. \tag{3.182}$$

Similarly, the quadratic approximation, given in (3.179), results in,

$$C \simeq \frac{1}{ln2}\sum_{i=1}^{M}\alpha_i\left(\varphi_i+\varphi_i^2\right)=\frac{1}{2}\vec{\varphi}^T\mathbf{H}\vec{\varphi}+\vec{\mathbf{f}}^T\vec{\varphi}, \tag{3.183}$$

where,

$$\mathbf{H}=\frac{2}{ln2}diag\left[\alpha_1,\cdots,\alpha_M\right]. \tag{3.184}$$

The maximization of either (3.181) or (3.183) should be carried out subject to the constraints given in (3.172), using linear or quadratic programming, respectively. We call these two algorithms the M^1SC and the M^2SC, respectively. These algorithms will be explicitly presented in Section 3.5.6.

3.5.5 Addition of Other Constraints

The approximations proposed here are also helpful when a a new constraint is to be added to the problem. For a better comparison, the reader is referred to the case of adding the new constraint to the NSC, addressed in Section 3.2, which led to the definition of the N^+SC. There, to tackle the unfairness of the solution to the NSC, a capacity share constraint was added to the problem, as,

$$\tilde{C}_i=\frac{C_i}{C}\leq\frac{1}{\mu}\frac{1}{M},0<\mu<1. \tag{3.185}$$

Adding this constraint to the NSC almost quadrupled the code complexity of the solver (see Section 3.2.4). Here, we demonstrate the straightforward approach which yields the addition of the new constraint to the approximate problems.

Using (3.167), Equation (3.185) can be approxmiated as,

$$\sum_{j=1}^{M}\alpha_j\vec{\varphi}_j\geq M\mu\varphi_i,\forall i. \tag{3.186}$$

This translates into,

$$\left(M\mu\vec{\mathbf{I}}_{M\times M} - \vec{\mathbf{1}}_{M\times 1}\vec{\alpha}^T\right)\vec{\varphi} \leq \vec{\mathbf{0}}_{M\times 1}. \tag{3.187}$$

This new constraint can now be added to either of the linear or quadratic approximations by writing the equivalent of (3.174) as,

$$\mathbf{A} = \begin{bmatrix} \vec{\mathbf{1}}_{1\times M} \\ \mathbf{1}_{M\times M} + diag\left[\frac{1}{l_1}, \cdots, \frac{1}{l_M}\right] \\ M\mu\vec{\mathbf{I}}_{M\times M} - \vec{\mathbf{1}}_{M\times 1}\vec{\alpha}^T \end{bmatrix}, \tag{3.188}$$

and the equivalent of (3.175) as,

$$\vec{\mathbf{b}} = \begin{bmatrix} \frac{X^{max}}{X^{max}+1} \\ \vec{\mathbf{1}}_{M\times 1} \\ \vec{\mathbf{0}}_{M\times 1} \end{bmatrix}. \tag{3.189}$$

We argue that the addition of any constraint which can be written as linear function of $\vec{\varphi}$ is as straightforward as this case is.

3.5.6 Details of the Proposed Algorithms

Using the developed formulation, the two algorithms the M^1SC and the M^2SC can be written as the three steps shown in Figure 3.15.

Note that, as the matrix $\mathbf{H}$, defined in (3.184), is positive–definite, the computational cost of the M^2SC is polynomial [122]. The linear programming–based approach, namely the M^1SC, will take up polynomial time as well [123].

3.6 Generalized MSC ($MSC^{\alpha\nu L_i}$)

The MSC and its ancestors all have particular dependence on the structure of the SIR given in (1.6). However, in the literature, more appropriate models for the SIR exist, many of which

1. Generate $\mathbf{A}$ using (3.174), $\vec{\mathbf{b}}$ using (3.175), $\vec{\mathbf{f}}$ using (3.182), and $\mathbf{H}$ using (3.184).
2. Solve either $\vec{\varphi}$=linprog($\vec{\mathbf{f}}$,$\mathbf{A}$,$\vec{\mathbf{b}}$,$\vec{\varphi}^{min}$,$\vec{\varphi}^{max}$), for the case of the M^1SC, or $\vec{\varphi}$=quadprog($\mathbf{H}$,$\vec{\mathbf{f}}$,$\mathbf{A}$,$\vec{\mathbf{b}}$, $\vec{\varphi}^{min}$,$\vec{\varphi}^{max}$), for the case of the M^2SC.
3. Calculate $\vec{\mathbf{C}}$ using (3.170), $\vec{\mathbf{p}}$ using (3.171), and C using (3.167).

Figure 3.15: *Details of the algorithms the M^1SC and the M^2SC.*

alter its conventional structure and thus make the previously developed methods fail. Some of these additions to the SIR model are presented in Section 1.3.2.

In this section, we incorporate the two parameters of α and ν as well as $\vec{\mathbf{L}}$ into the MSC problem. As a result, and in order to provide a solution to the new problem, which we call the $MSC^{\alpha\nu L_i}$, a new methodology has to be developed. This is mainly because the existence of the factors $\alpha\nu$ and L_i makes the constant-T method developed for solving the CSC fail. In this section we will propose a transformation which generates an imaginary problem out of the given $MSC^{\alpha\nu L_i}$. This imaginary problem is solvable using a generalized variant of the previously developed MSC. We then present the procedure for calculating the solution to the problem in hand using the one computed for the produced imaginary problem.

The rest of this section is organized as follows. First, in Section 3.6.1, the MSC algorithm, introduced in Section 3.5 is generalized. This generalization is used in Section 3.6.2 for implanting a more accurate model for the SIR inside the objective function. Then, in Section 3.6.3 some necessary mathematical tools are developed and, finally, in Section 3.6.4 the procedure through which the new problem can be solved is proposed.

3.6.1 Generalizing the MSC to the MSC*

As will be shown in Section 3.6.2, the MSC has to be generalized further in order to have the maximum capacity-share constraints be specific to the mobile stations as well. To comply with

this need, we rewrite (3.185) as,

$$\tilde{C}_i \leq \frac{1}{\mu_i}\frac{1}{M}, 0 < \mu_i < 1. \tag{3.190}$$

Derivation shows that this new set of constraints can be added to the optimization problem through rewriting (3.188) as,

$$\mathbf{A} = \begin{bmatrix} \vec{\mathbf{1}}_{1\times M} \\ \mathbf{1}_{M\times M} + diag\left[\frac{1}{l_1}, \cdots, \frac{1}{l_M}\right] \\ M diag\left[\mu_1, \cdots, \mu_M\right] - \vec{\mathbf{1}}_{M\times 1}\vec{\alpha}^T \end{bmatrix}, \tag{3.191}$$

For notational convenience, we call this problem the MSC*.

3.6.2 Solving the MSC*

Using,

$$\gamma_i = \frac{L_i p_i g_i}{I + \alpha\nu \sum_{j=1, j\neq i}^{M} p_j g_j}, \tag{3.192}$$

we know that,

$$1 + \gamma_i = \frac{I + \alpha\nu \sum_{j=1}^{M} p_j g_j + (L_i - \alpha\nu) p_i g_i}{I + \alpha\nu \sum_{j=1, j\neq i}^{M} p_j g_j}. \tag{3.193}$$

For the implications of the particular structure of (3.193) refer to Section 2.3 where the constant–T method ($T = I + \sum_{j=1}^{M} p_j g_j$) is developed and then used for dealing with the CSC and the NSC. Nevertheless, the presence of extra terms in the nominator of (3.193) prohibits the use of the previously developed method.

Consider rewriting (3.192) as,

$$\gamma_i = \frac{L_i}{\alpha\nu} \frac{p_i g_i}{\frac{1}{\alpha\nu} I + \sum_{j=1, j\neq i}^{M} p_j g_j}. \tag{3.194}$$

Now, we define

$$\chi_i = \frac{L_i}{\alpha\nu}, \chi = \frac{1}{\alpha\nu}, \hat{I} = \chi I, \tag{3.195}$$

and rewrite (3.194) as,

$$\gamma_i = \chi_i \hat{\gamma}_i, \tag{3.196}$$

where,

$$\hat{\gamma}_i = \frac{p_i g_i}{\hat{I} + \sum_{j=1, j\neq i}^{M} p_j g_j}. \tag{3.197}$$

As will be shown in Section 3.6.3, $\log_2(1+\gamma_i)$ can be approximated as a constant multiplier of $\log_2(1+\hat{\gamma}_i)$, and therefore, as (3.197) has the same structure as (1.6), the generalized problem can be approximately solved using an imaginary problem which has the structure the methods already developed in this thesis are capable of dealing with. The details of this process, as well as the utilized transformations, are presented in Section 3.6.4.

3.6.3 The Correction Function $\rho(\chi)$

As discussed in Section 3.6.2, the addition of new coefficients to either the nominator or the denominator of the SIR disrupts the application of the constant–T method developed earlier. However, due to the particular structure of the C_i–γ_i relationship, a linear approximation of $\log_2(1+\chi\gamma)$ in terms of $\log_2(1+\gamma)$ can provide a method for reducing the new problem to

one which is solvable using a method already developed in this thesis (as will be discussed in Section 3.6.4). This section is about this approximation.

Using first order Taylor Series approximation of $\ln(1+x) \sim x$, we can write,

$$\log_2(1+\chi\gamma) \simeq \frac{1}{\ln(2)}\chi\gamma \simeq \chi\log_2(1+\gamma). \tag{3.198}$$

Here, γ and $\chi\gamma$ are assumed to be small enough.

The approximation given in (3.198) is based on two consecutive linear approximations of logarithmic terms. Therefore, especially in the event of χ being large, the approximation may produce unacceptable values. However, due to the particular structure of the objective function and the constraints, a correction term ρ can be included in the approximation in order to yield more accuracy through using,

$$\log_2(1+\chi\gamma) \simeq \chi\rho\log_2(1+\gamma). \tag{3.199}$$

The choice of the best value of ρ for any particular χ is the main purpose of this section. Here, we define the correction function $\rho(\chi)$ as the one which produces the value of ρ which for a given χ minimizes the mean-square error of the approximation given in (3.199). In other words, $\rho(\chi)$ can be formally defined as,

$$\rho(\chi) = \arg_\rho \min \int_{\gamma_{min}}^{\gamma_{max}} \left[\log_2(1+\chi\gamma) - \chi\rho\log_2(1+\gamma)\right]^2 d\gamma. \tag{3.200}$$

Here, γ_{min} and γ_{max} denote the range of values γ can accept. We will discuss this issue later.

Using Leibniz Integral Rule, Equation (3.200) yields,

$$\rho(\chi) = \frac{\displaystyle\int_{\gamma_{min}}^{\gamma_{max}} \log_2(1+\chi\gamma)\log_2(1+\gamma)\,d\gamma}{\chi\displaystyle\int_{\gamma_{min}}^{\gamma_{max}} \left(\log_2(1+\gamma)\right)^2 d\gamma}. \tag{3.201}$$

In practice, the integrals are numerically calculated using recursive Adaptive Simpson Quadrature within an error of 10^{-6}.

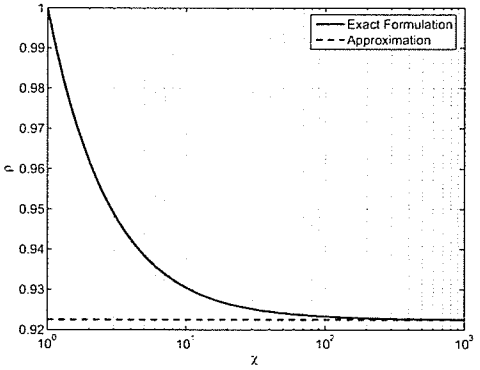

Figure 3.16: *Values of $\rho(\chi)$ for a nominal range of χ. Solid line shows the values given by (3.201) and the dashed line represents (3.204).*

Figure 3.17 demonstrates the case of $\chi = 7.5$, for which Equation (3.201) yields $\rho = 0.9332$. In Figure 3.17–(a), the solid line shows the original function and the dotted line represents the basic approximation given in (3.198). While this approximation yields more error as γ increases, the dashed line, which represents the improved form given in (3.199), produces more accurate results in most cases (see Figure 3.17–(b)). A comparative analysis of the relative error induced by the two functions is given in Figure 3.17–(c). As seen here, the introduction of the correction term cuts the maximum relative error in the working range in almost half. The solid line in Figure 3.16 shows the values of $\rho(\chi)$ for a nominal range of χ.

The calculation of $\rho(\chi)$ as given in Equation (3.201) is based on the computation of two integrals. Therefore, the existence of an alternative closed form for $\rho(\chi)$ could potentially result in reducing the computational complexity of the algorithm which utilizes this function. Here, we suggest the alternative function $\tilde{\rho}(\chi)$ by proposing an approximate closed form for (3.201).

Approximating $\ln(1+\gamma)$ by γ, and using (3.201), we write,

$$\rho(\chi) \simeq \tilde{\rho}(\chi) = \frac{3}{\chi\left(\gamma_{max}^3 - \gamma_{min}^3\right)} \int_{\gamma_{min}}^{\gamma_{max}} \gamma \ln\left(1+\chi\gamma\right) d\gamma. \tag{3.202}$$

Now, using a substitute variable we write,

$$\tilde{\rho}(\chi) = \frac{3}{\chi^3\left(\gamma_{max}^3 - \gamma_{min}^3\right)} \int_{1+\chi\gamma_{min}}^{1+\chi\gamma_{max}} (\tau - 1) \ln\tau d\tau, \tag{3.203}$$

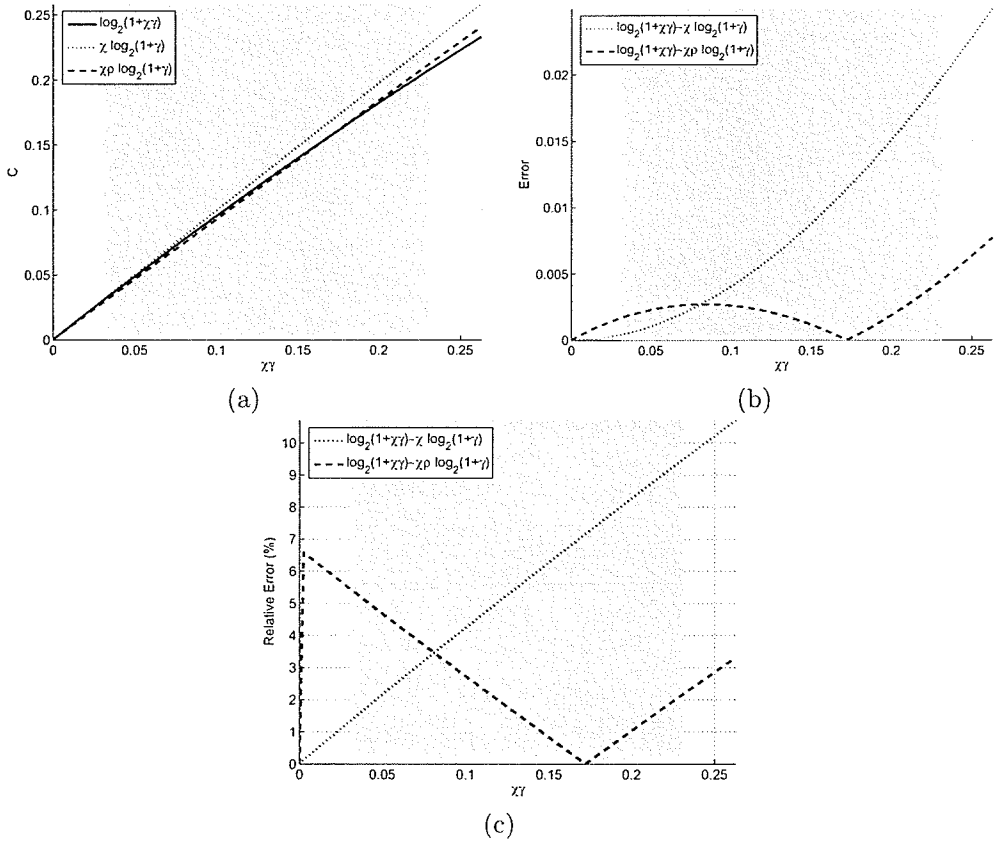

Figure 3.17: *The case of $\chi = 7.5$. (a) The original function compared to the two approximations. (b) The absolute error induced by the two approximations. (c) The relative error induced by the two approximations.*

and thus derive,

$$\tilde{\rho}(\chi) = \frac{\left(\frac{1}{2}\tau^2 \ln \tau - \tau \ln \tau - \frac{1}{4}\tau^2 + \tau\right)\Big|_{1+\chi\gamma_{min}}^{1+\chi\gamma_{max}}}{\chi^3\left(\gamma_{max}^3 - \gamma_{min}^3\right)}. \tag{3.204}$$

The dashed line in Figure 3.16 shows the values of $\tilde{\rho}(\chi)$ for a nominal range of values of χ.

In a practical implementation, both (3.201) and (3.204) depend on the two values of γ_{min} and γ_{max}. These values indicate the range of values the SIR can accept within the framework of the problem. As it will be shown in Section 3.6.4, for solving the problem devised and solved in this section, there is need for the calculation of ρ for M different values of χ. Therefore, it is important to realize that the bounds γ_{min} and γ_{max} are in fact the practical bounds on $\hat{\gamma}_i$ for which γ_i lies within what the parameters allow for (as described in Section 3.6.2). Therefore, defining γ_{min}° and γ_{max}° as the range for the SIR given by the system parameters, we have,

$$\gamma_{min} = \frac{1}{\chi}\gamma_{min}^{\circ}, \tag{3.205}$$

$$\gamma_{max} = \frac{1}{\chi}\gamma_{max}^{\circ}. \tag{3.206}$$

In practice, γ_{min}° is a given parameter for any particular problem and γ_{max}° is calculated using the given C_{max},

$$\gamma_{max}^{\circ} = 2^{C_{max}} - 1. \tag{3.207}$$

Using (3.205) and (3.206), we rewrite (3.201) and (3.204) as,

$$\rho(\chi) = \frac{\int_{\frac{1}{\chi}\gamma_{min}}^{\frac{1}{\chi}\gamma_{max}} \log_2(1+\chi\gamma)\log_2(1+\gamma)\,d\gamma}{\chi\int_{\frac{1}{\chi}\gamma_{min}}^{\frac{1}{\chi}\gamma_{max}} \left(\log_2(1+\gamma)\right)^2 d\gamma}. \tag{3.208}$$

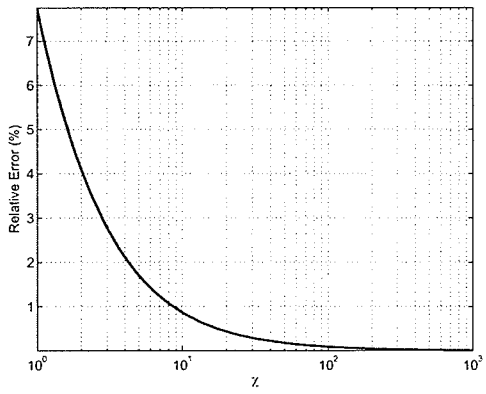

Figure 3.18: *Relative deviation of the values of ρ produced by the approximate form given in (3.209), compared to the what is generated by the exact formulation given in (3.208).*

$$\tilde{\rho}(\chi) = \frac{\left(\frac{1}{2}\tau^2 \ln \tau - \tau \ln \tau - \frac{1}{4}\tau^2 + \tau\right)\Big|_{1+\gamma_{min}}^{1+\gamma_{max}}}{\gamma_{max}^3 - \gamma_{min}^3}. \tag{3.209}$$

Note that the superscript $\circ$ is dropped for the sake of notational convenience but the bounds for the integrals in (3.208) are the original boundaries of the SIR as given by the system parameters. Also note that Equation (3.209) is independent of χ. This issue can be observed in Figure 3.16 as well, where for $\gamma_{min} = -30dB$ and $C_{max} = 0.3$, we have $\tilde{\rho}(\chi) \equiv 0.9225$, independent of χ. Note that the more intuitive depiction of (3.199) as,

$$\log_2(1+\gamma) \simeq \chi\rho \log_2\left(1 + \frac{1}{\chi}\gamma\right), \tag{3.210}$$

gives a better understanding why the approximation still holds as χ increases.

Comparing the two functions $\rho(\chi)$ and $\tilde{\rho}(\chi)$, and as seen in Figure 3.18, the application of the approximate form given in (3.209) causes less than 8% relative error in the working range. Practical implementation of the two formulations, however, shows a drastic reduction of the elapsed time from about $1ms$, for the exact form given in (3.208), compared to less than $0.01ms$ for the approximate formulation given in (3.209).

As an overall measure of integrity, Figure 3.19 shows the error bounds generated by the

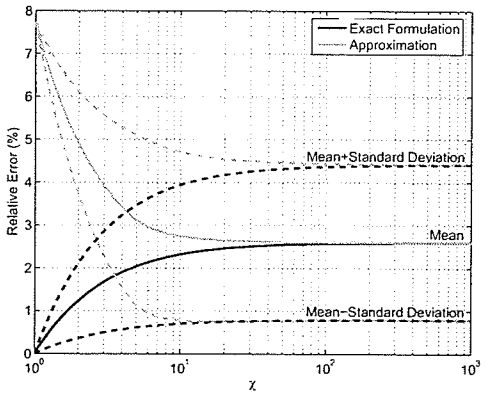

Figure 3.19: *Error bounds generated in the calculation of the capacity using the approximation given in (3.199). For details refer to the text.*

approximation given in (3.199). Here, the dark lines represent the exact formulation for $\rho(\chi)$, given in (3.208), and the gray lines show the outcome of using the approximation given in (3.209). For each case, the solid lines present the mean relative error, while the dashed lines indicate the mean plus the standard deviation curves and the mean minus the standard deviation curves. As observed here, for $\chi > 10$, the two formulations produce very similar results (the same effect seen in Figure 3.18). Furthermore, the relative error induced by using the more precise value of ρ, given by (3.208), is normally less than 5%. The approximate formulation for ρ, given by (3.209) on the other hand, causes a relative error of about 8% for smaller values of χ.

The correction term ρ developed here is used in Section 3.6.4 for producing an approximate solution to the generalized multiple-cell problem as well.

3.6.4 Application of $\rho(\chi)$ to Solving the Generalized Problem

Consider the problem defined as maximizing (3.167) subject to the revised version of (3.168) combined with (3.190) collectively written as,

$$\begin{cases} \gamma_i \geq \gamma_i^{min}, \forall i, \\ C_i \leq C_i^{max}, \forall i, \\ 0 \leq p_i \leq p_i^{max}, \forall i. \\ \tilde{C}_i = \dfrac{C_i}{C} \leq \dfrac{1}{\mu}\dfrac{1}{M}, 0 < \mu < 1 \\ \alpha\nu \displaystyle\sum_{i=1}^{M} p_i g_i \leq P_{max}, \end{cases} \tag{3.211}$$

Here, we consider the definition of the SIR as given in (3.192) and use (3.195) to yield (3.196) and (3.197). Through this procedure, we produce an imaginary problem which has the MSC* structure discussed in Section 3.6.1. We will denote the parameters related to this problem with a "hat" ($\hat{\gamma}$ for example). All the variables and parameters in the imaginary problem are identical to their counterparts in the original problem unless specified differently.

Routine derivation shows that $\hat{P}_{max} = \chi P_{max}$, $\hat{\alpha}_i = \rho_i \chi_i \alpha_i$, and,

$$\hat{\gamma}_i^{min} = \frac{1}{\chi_i}\gamma_i^{min}, \tag{3.212}$$

where $\rho_i = \rho(\chi_i)$. Also we have $\hat{\mu}_i = \rho_i \chi_i \mu$ and,

$$\hat{C}_i^{max} = \frac{1}{\rho_i \chi_i} C_i^{max}. \tag{3.213}$$

Now, the imaginary problem is a MSC* and thus can be solved using the method developed in Section 3.6.1. Then, the resulting values of p_i represent the corresponding values in an approximate solution to the original problem. The values of C_i, however, will be recalculated using the exact formulation as a final refinement stage. We call this method $MSC^{\alpha\nu L_i}$.

Chapter 4

Multiple–Cell Problem (MC)

In this chapter, the multiple–cell problem, as formulated in Section 1.3.3, will be analyzed. This analysis is essentially geared towards applying the two mathematical tools developed in Sections 3.5.3 and 3.6.3 on the problem in order to produce an approximate solution for it using quadratic programming.

This chapter is organized as follows. First, in Section 4.1 a set of substitute variables will presented. Subsequently, these variables are used in Section 4.2 for transforming the constraints into linear forms. Using a similar method, in Section 4.3, the objective function will be represented as a quadratic function. Both these transformations take advantage of a set of approximations and estimations. Then, Section 4.4 presents the details of the proposed algorithm.

4.1 Substitute Variables

Structural differences of γ_{ki}, given in (1.26), and its single–cell counterpart γ_i, given in (1.6), prohibit the direct application of the substitute variables as outlined in Section 3.5.2. Therefore, in order to restructure γ_{ki} in the way that makes the definition of appropriate substitute variables possible, Equation (1.26) will be rewritten and the $\rho(\cdot)$ function defined in Section 3.6.3 will be taken advantage of.

We first rewrite (1.26) as,

$$\gamma_{ki} = \frac{L_{ki}}{\alpha\nu} \frac{\zeta_{ki} p_{ki} g_{ki}}{I'_k + \sum_{k'=1}^{K} \left[\theta_{kk'} \sum_{i'=1}^{M_{k'}} p_{k'i'} g^k_{k'i'} \right] - \zeta'_{ki} p_{ki} g_{ki}}. \tag{4.1}$$

Here, we have defined,

$$I'_k = \frac{1}{\alpha\nu} I_k. \tag{4.2}$$

$$\zeta'_{ki} = 1 - \frac{1 - \zeta_{ki}}{\alpha\nu}. \tag{4.3}$$

Note that for $\alpha > 0.625$, as $\zeta_{ki} > 0.75$ and $\nu > 0.4$ (typical values taken from the references cited in Section 1.3.2), ζ'_{ki} will always be positive.

Continuing with (4.1) we write,

$$\gamma_{ki} = \chi_{ki} \gamma'_{ki}. \tag{4.4}$$

Here,

$$\chi_{ki} = \frac{L_{ki} \zeta_{ki}}{\alpha\nu \zeta'_{ki}}, \tag{4.5}$$

$$\gamma'_{ki} = \frac{\zeta'_{ki} p_{ki} g_{ki}}{I'_k + \sum_{k'=1}^{K} \left[\theta_{kk'} \sum_{i'=1}^{M_{k'}} p_{k'i'} g^k_{k'i'} \right] - \zeta'_{ki} p_{ki} g_{ki}}. \tag{4.6}$$

Note the similarity in the structure of γ'_{ki}, defined in (4.6), and γ_i, defined (1.6).

Now, similar to (3.169), we define,

$$\varphi'_{ki} = \frac{\gamma'_{ki}}{1+\gamma'_{ki}} = \frac{\zeta'_{ki} p_{ki} g_{ki}}{I'_k + \sum_{k'=1}^{K} \left[\theta_{kk'} \sum_{i'=1}^{M_{k'}} p_{k'i'} g^k_{k'i'} \right]}. \tag{4.7}$$

Note that, using (4.4), we have,

$$\varphi'_{ki} = \frac{\gamma_{ki}}{\chi_{ki} + \gamma_{ki}}. \tag{4.8}$$

4.2 Constraints

The second and the third constraints of the multiple–cell problem, as given in (1.29), impose a minimum and a maximum bound on the γ_{ki} and the C_{ki}, respectively. By defining,

$$\gamma^{max}_{ki} = 2^{C^{max}_{ki}} - 1, \tag{4.9}$$

these two constraints can be encapsulated in one double–bound constraint written as,

$$\gamma^{min}_{ki} \leq \gamma_{ki} \leq \gamma^{max}_{ki}, \forall i, k. \tag{4.10}$$

Now, using (4.8), and by defining,

$$\varphi^{min'}_{ki} = \frac{\gamma^{min}_{ki}}{\chi_{ki} + \gamma^{min}_{ki}}, \tag{4.11}$$

$$\varphi^{max'}_{ki} = \frac{\gamma^{max}_{ki}}{\chi_{ki} + \gamma^{max}_{ki}}, \tag{4.12}$$

Equation (4.10) will be written as,

$$\varphi^{min'}_{ki} \leq \varphi'_{ki} \leq \varphi^{max'}_{ki}, \forall i, k, \tag{4.13}$$

or, in vector format,

$$\vec{\varphi}^{min\prime} \leq \vec{\varphi}' \leq \vec{\varphi}^{max\prime}. \tag{4.14}$$

For addressing the first and the last constraints as listed in (1.29), we need a relationship similar to (3.171). However, Equation (4.7) has substantial differences with (3.169). These differences inhibit the use of a direct method. In order to resolve this issue, here, we propose an approximation.

As mentioned in Section 1.2, the intra-cell interference is in some works modeled as δ times the inter-cell interference [80]. Here, δ is the loading factor and the values of 0.6 [81] or 0.55 [74] are suggested for it. Another conservative approximation for δ is somewhere between 0.460 and 0.634 for nominal systems [80]. Adopting this approximate simplification, we rewrite (4.7) as,

$$\varphi'_{ki} \simeq \frac{\zeta'_{ki} p_{ki} g_{ki}}{I'_k + (1+\delta) \sum_{i'=1}^{M_k} p_{ki'} g_{ki'}}. \tag{4.15}$$

Now,

$$\sum_{i=1}^{M_k} \frac{\varphi'_{ki}}{\zeta'_{ki}} \simeq \frac{\sum_{i=1}^{M_k} p_{ki} g_{ki}}{I'_k + (1+\delta) \sum_{i=1}^{M_k} p_{ki} g_{ki}}, \tag{4.16}$$

or, equivalently,

$$\sum_{i=1}^{M_k} p_{ki} g_{ki} \simeq I'_k \frac{\sum_{i=1}^{M_k} \frac{\varphi'_{ki}}{\zeta'_{ki}}}{1 - (1+\delta) \sum_{i=1}^{M_k} \frac{\varphi'_{ki}}{\zeta'_{ki}}}. \tag{4.17}$$

Note that, here, the condition,

$$1 - (1+\delta)\sum_{i=1}^{M_k} \frac{\varphi'_{ki}}{\zeta'_{ki}} > 0, \tag{4.18}$$

is necessary for $\sum_{i=1}^{M_k} p_{ki} g_{ki}$ to be positive. We will show that another inequality, which has to be satisfied as well, in fact guarantees (4.18).

Using the concept of the loading factor, the last constraint in (1.29) can be approximated as,

$$\alpha\nu(1+\delta)\sum_{i=1}^{M_k} p_{ki} g_{ki} \leq P_k^{max}, \forall k. \tag{4.19}$$

Now, using (4.17), inequality (4.19) can be rewritten as,

$$I'_k \frac{\sum_{i=1}^{M_k} \frac{\varphi'_{ki}}{\zeta'_{ki}}}{1 - (1+\delta)\sum_{i=1}^{M_k} \frac{\varphi'_{ki}}{\zeta'_{ki}}} \leq P_k^{max\prime}, \forall k. \tag{4.20}$$

Here,

$$P_k^{max\prime} = \frac{P_k^{max}}{\alpha\nu(1+\delta)}. \tag{4.21}$$

Routine derivation reduces (4.20) to,

$$\sum_{i=1}^{M_k} \frac{\varphi'_{ki}}{\zeta'_{ki}} \leq X_k^{max\prime}, \forall k, \tag{4.22}$$

where,

$$X_k^{max\prime} = \frac{P_k^{max\prime}}{I'_k + (1+\delta)P_k^{max\prime}}. \tag{4.23}$$

Note that (4.22) yields,

$$\sum_{i=1}^{M_k} \frac{\varphi'_{ki}}{\zeta'_{ki}} < \frac{1}{1+\delta} \leq 1, \forall k, \tag{4.24}$$

which satisfies (4.18).

Combining the K constraints of the type given in (4.22) together, for all the cells, we write,

$$diag\left[\vec{\zeta}'_1, \cdots, \vec{\zeta}'_K\right] \vec{\varphi}' \leq \vec{\mathbf{X}}^{max\prime}. \tag{4.25}$$

Here,

$$\vec{\zeta}'_k = \left[{\zeta'_{k1}}^{-1}, \cdots, {\zeta'_{kM_k}}^{-1}\right], \tag{4.26}$$

is a $M_k \times 1$ vector and,

$$\vec{\mathbf{X}}^{max\prime} = \left[X_1^{max\prime}, \cdots, X_K^{max\prime}\right]^T, \tag{4.27}$$

is a $K \times 1$ vector.

Returning to (4.15), and using (4.17), we have,

$$\varphi'_{ki} \simeq \frac{\zeta'_{ki}}{I'_k} p_{ki} g_{ki} \left[1 - (1+\delta) \sum_{i'=1}^{M_k} \frac{\varphi'_{ki'}}{\zeta'_{ki'}}\right], \tag{4.28}$$

$$p_{ki} g_{ki} \simeq I'_k \frac{\dfrac{\varphi'_{ki}}{\zeta'_{ki}}}{1 - (1+\delta) \displaystyle\sum_{i'=1}^{M_k} \dfrac{\varphi'_{ki'}}{\zeta'_{ki'}}}. \tag{4.29}$$

Using (4.29), we approximate the first constraint in (1.29) as,

$$\frac{\varphi'_{ki}}{\zeta'_{ki}} \leq l_{ki} \left[1 - (1+\delta) \sum_{i'=1}^{M_k} \frac{\varphi'_{ki'}}{\zeta'_{ki'}}\right], \forall i, k. \tag{4.30}$$

Here,

$$l_{ki} = \frac{p_{ki}^{max} g_{ki}}{I'_k}. \tag{4.31}$$

Further derivation of (4.30) gives,

$$\frac{1}{l_{ki}} \frac{\varphi'_{ki}}{\zeta'_{ki}} + (1+\delta) \sum_{i'=1}^{M_k} \frac{\varphi'_{ki'}}{\zeta'_{ki'}} \leq 1, \forall i, k, \tag{4.32}$$

or in vector format,

$$\left[\mathbf{l}^{-1} \zeta'^{-1} + (1+\delta) diag \left[\zeta'_1, \cdots, \zeta'_K \right] \right] \vec{\varphi}' \leq \vec{\mathbf{1}}_{M \times 1}. \tag{4.33}$$

Here,

$$\mathbf{l} = diag \left[l_{11}, l_{12}, \cdots l_{KM_K} \right], \tag{4.34}$$

and,

$$\zeta' = diag \left[\zeta'_{11}, \zeta'_{12}, \cdots \zeta'_{KM_K} \right], \tag{4.35}$$

are both $M \times M$ matrices and,

$$\zeta'_k = \vec{\mathbf{1}}_{M_k \times 1} \vec{\zeta}'_k, \tag{4.36}$$

is a $M_k \times M_k$ matrix.

Combining (4.25) and (4.33) together we have,

$$\mathbf{A} \vec{\varphi}' \leq \vec{\mathbf{b}}. \tag{4.37}$$

Here,

$$\mathbf{A} = \begin{bmatrix} diag\left[\vec{\zeta}'_1, \cdots, \vec{\zeta}'_K\right] \\ \mathbf{I}^{-1}\zeta'^{-1} + (1+\delta)diag\left[\zeta'_1, \cdots, \zeta'_K\right] \end{bmatrix}. \tag{4.38}$$

$$\vec{\mathbf{b}} = \begin{bmatrix} \vec{\mathbf{X}}^{max\prime} \\ \vec{\mathbf{1}}_{M\times 1} \end{bmatrix}. \tag{4.39}$$

4.3 Objective Function

The formulation for the objective function C, given in (1.28), considers a general case in which each mobile station has its own utility function $f_{ki}(\cdot)$. Here, we assume that within the range of possible capacities, the function $f_{ki}(C)$ can be approximated as a second–degree form,

$$f_{ki}(C_{ki}) \simeq \alpha_{ki}C_{ki} + \beta_{ki}C_{ki}^2. \tag{4.40}$$

Here, we also assume that both α_{ki} and β_{ki} are non–negative. This is important in order to guarantee polynomial computational complexity for the quadratic programming–based solver to be developed as a result of this analysis.

Now, using (4.4), (1.27) and (3.199) we write,

$$C_{ki} \simeq \chi_{ki}\rho(\chi_{ki})\log_2\left(1+\gamma'_{ki}\right). \tag{4.41}$$

Using (4.7) and (3.179) we have,

$$C'_{ki} \simeq \frac{1}{ln2}\varphi'_{ki} + \frac{1}{ln2}\varphi'^2_{ki}. \tag{4.42}$$

Here,

$$C'_{ki} = \log_2\left(1+\gamma'_{ki}\right). \tag{4.43}$$

Therefore, combining (4.40), (4.41), (4.43), and (4.42), we have,

$$f_{ki}(C_{ki}) \simeq \alpha'_{ki}\varphi'_{ki} + \left(\alpha'_{ki} + \beta'_{ki}\right)\varphi'^2_{ki}, \tag{4.44}$$

where

$$\alpha'_{ki} = \frac{1}{\ln 2}\alpha_{ki}\chi_{ki}\rho(\chi_{ki}), \tag{4.45}$$

$$\beta'_{ki} = \left(\frac{1}{\ln 2}\right)^2 \beta_{ki}\chi^2_{ki}\rho(\chi_{ki})^2, \tag{4.46}$$

and powers of more than two of φ'_{ki} have been ignored. Note that as both α_{ki} and β_{ki} are non–negative, therefore $\alpha'_{ki} + \beta'_{ki}$ is non–negative as well.

Using (4.44) and (1.28) we have,

$$C \simeq \sum_{k=1}^{K}\sum_{i=1}^{M_k}\left[\alpha'_{ki}\varphi'_{ki} + \left(\alpha'_{ki} + \beta'_{ki}\right)\varphi'^2_{ki}\right]. \tag{4.47}$$

In other words, defining,

$$\vec{\mathbf{f}} = \vec{\alpha}', \tag{4.48}$$

as the multiple–cell version of (3.182),

$$\alpha' = diag\left[\alpha'_{11}, \alpha'_{12}, \cdots, \alpha'_{KM_K}\right], \tag{4.49}$$

$$\beta' = diag\left[\beta'_{11}, \beta'_{12}, \cdots, \beta'_{KM_K}\right], \tag{4.50}$$

and,

$$\mathbf{H} = 2\left[\alpha' + \beta'\right], \tag{4.51}$$

as the equivalent of (3.184) in multiple-cell systems, we have,

$$C \simeq \frac{1}{2}\vec{\varphi}'^T \mathbf{H}\vec{\varphi}' + \vec{\mathbf{f}}^T\vec{\varphi}', \tag{4.52}$$

which is the canonical form of the objective function in a quadratic programming problem. Note that $\mathbf{H}$ is positive-definite.

4.4 Details of the Proposed Algorithm

As a result of the discussion given in Sections 4.1, 4.2, and 4.3, the multiple-cell problem formulated in Section 1.3.3 can be approximately solved by applying quadratic programming for the maximization of,

$$\tilde{C} = \frac{1}{2}\vec{\varphi}'^T \mathbf{H}\vec{\varphi}' + \vec{\mathbf{f}}^T\vec{\varphi}', \tag{4.53}$$

subject to,

$$\begin{cases} \vec{\varphi}'^{min} \leq \vec{\varphi}' \leq \vec{\varphi}'^{max}, \\ \mathbf{A}\vec{\varphi}' \leq \vec{\mathbf{b}}. \end{cases} \tag{4.54}$$

The matrices and vectors $\vec{\mathbf{f}}$, $\mathbf{H}$, $\vec{\varphi}'^{min}$, $\vec{\varphi}'^{max}$, $\vec{\mathbf{A}}$, and $\vec{\mathbf{b}}$, are defined in (4.48), (4.51), (4.11), (4.12), (4.38), (4.39) respectively.

After the solution to this problem is produced, then, using (4.29), the optimal $\vec{\mathbf{p}}$ will be calculated.

Chapter 5

Experimental Results

This chapter contains the experimental results generated through execution of the algorithms proposed in the previous chapters. The results corresponding to each problem are discussed in a separate section.

5.1 Classical Single Cell (CSC)

Using the developed CSC algorithm, it takes less than $2ms$ to solve the CSC in a cell which contains 100 mobile stations. Here, we first analyze the effects of different parameters on the behavior of the system, in Section 5.1.1. Then, in Section 5.1.2, we carry out an extensive fairness analysis.

5.1.1 Effects of Different Parameters

Using a random sequence $\vec{\mathbf{g}}$, similar to what is shown in Figure 1.1–(b), we analyze the effects of different parameters on the solution to the single–cell problem. The analysis is conducted as follows. First the values of C, the aggregate capacity, are presented. Then, the unfairness measures f and $\tilde{f}$ are analyzed. This analysis will be followed in Section 5.1.2 by giving approximations which show how these three values, namely C, f, and $\tilde{f}$, are related to each other and what the practical implications of these relationships are.

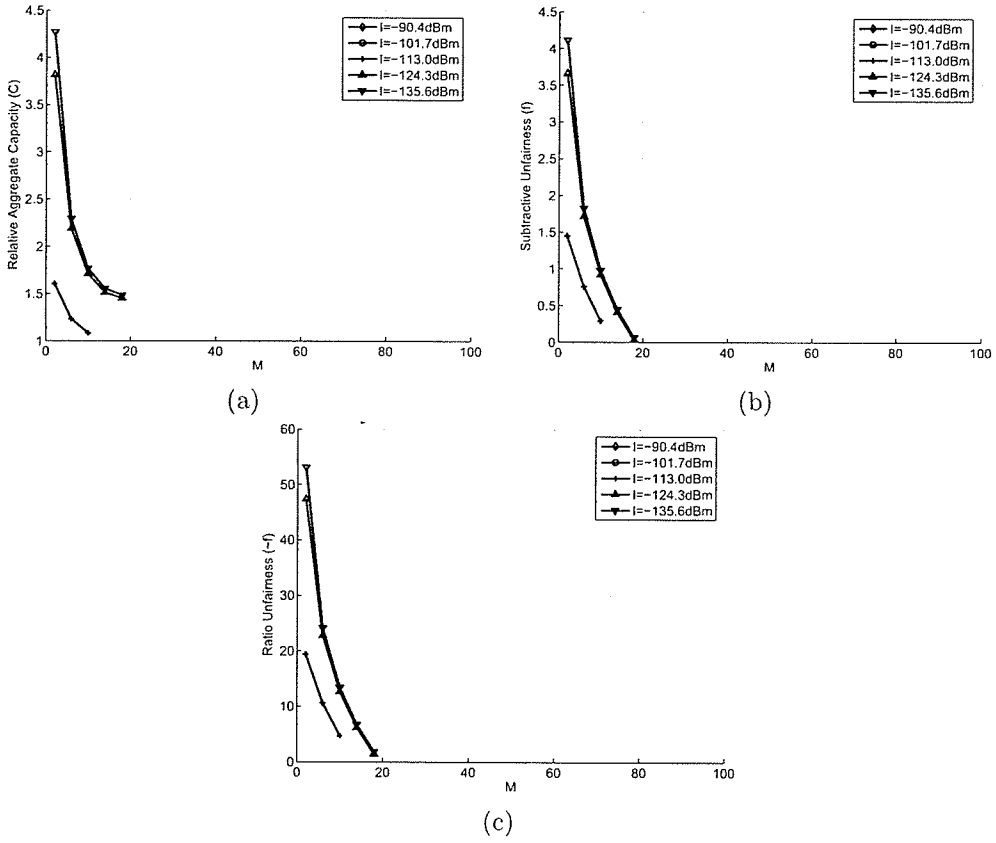

Figure 5.1: *Results for different number of mobile stations with $\gamma = -25dB$ and varying I in the CSC. (a) Aggregate capacity. (b) Subtractive unfairness. (c) Ratio unfairness.*

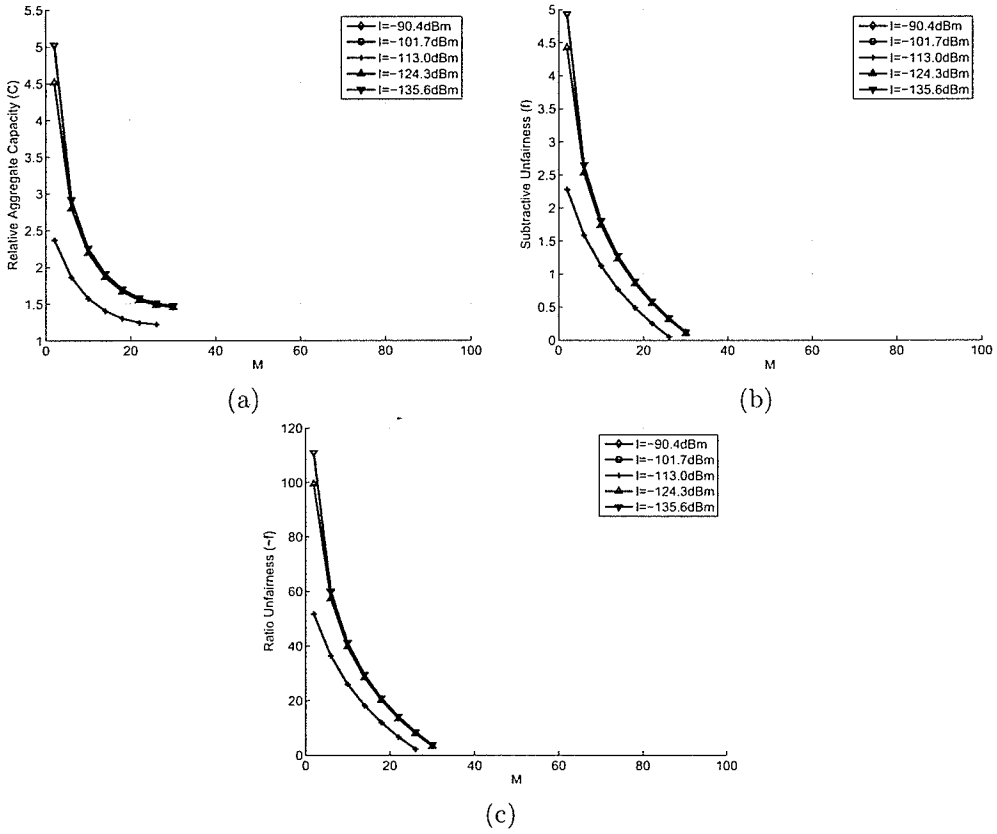

Figure 5.2: *Results for different number of mobile stations with $\gamma = -30dB$ and varying I in the CSC. (a) Aggregate capacity. (b) Subtractive unfairness. (c) Ratio unfairness.*

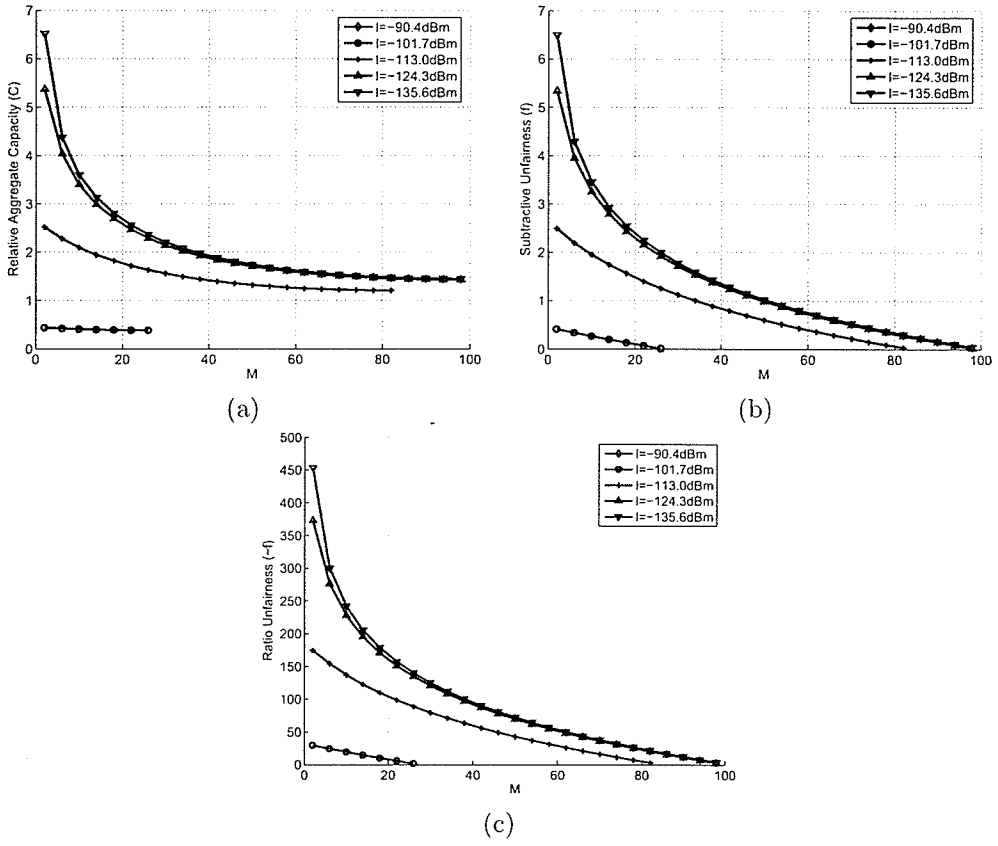

Figure 5.3: *Results for different number of mobile stations with $\gamma = -40dB$ and varying I in the CSC. (a) Aggregate capacity. (b) Subtractive unfairness. (c) Ratio unfairness.*

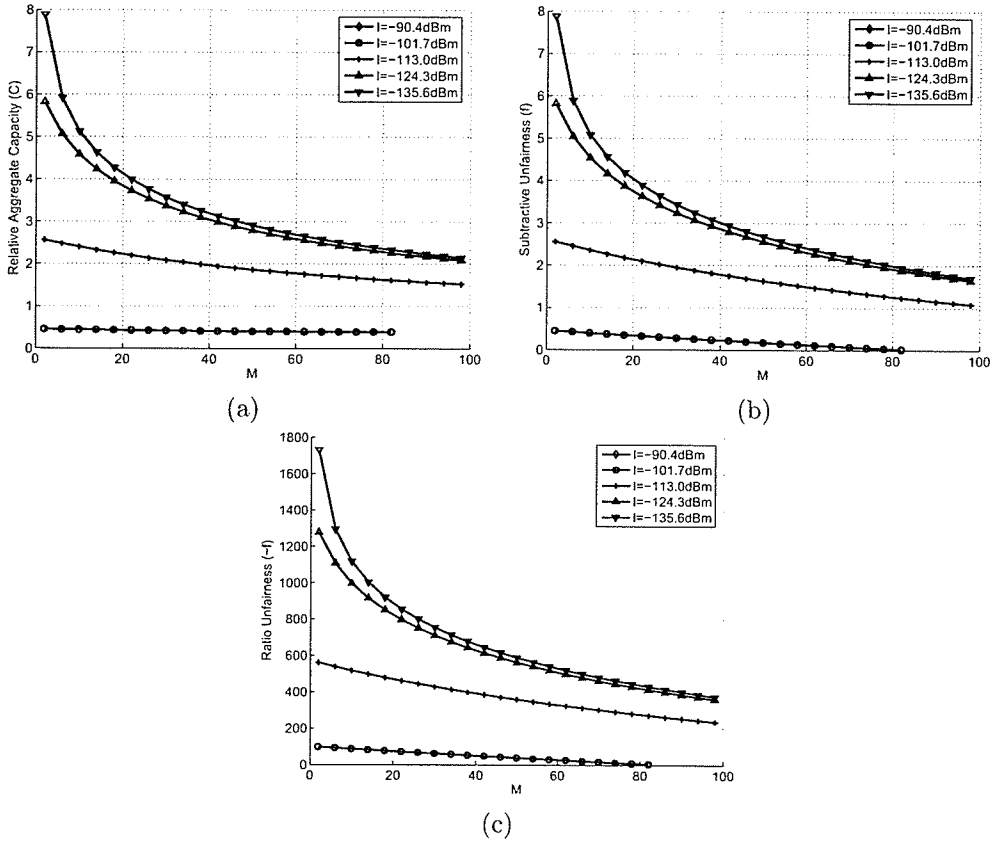

Figure 5.4: *Results for different number of mobile stations with and $\gamma = -50dB$ varying I in the CSC. (a) Aggregate capacity. (b) Subtractive unfairness. (c) Ratio unfairness.*

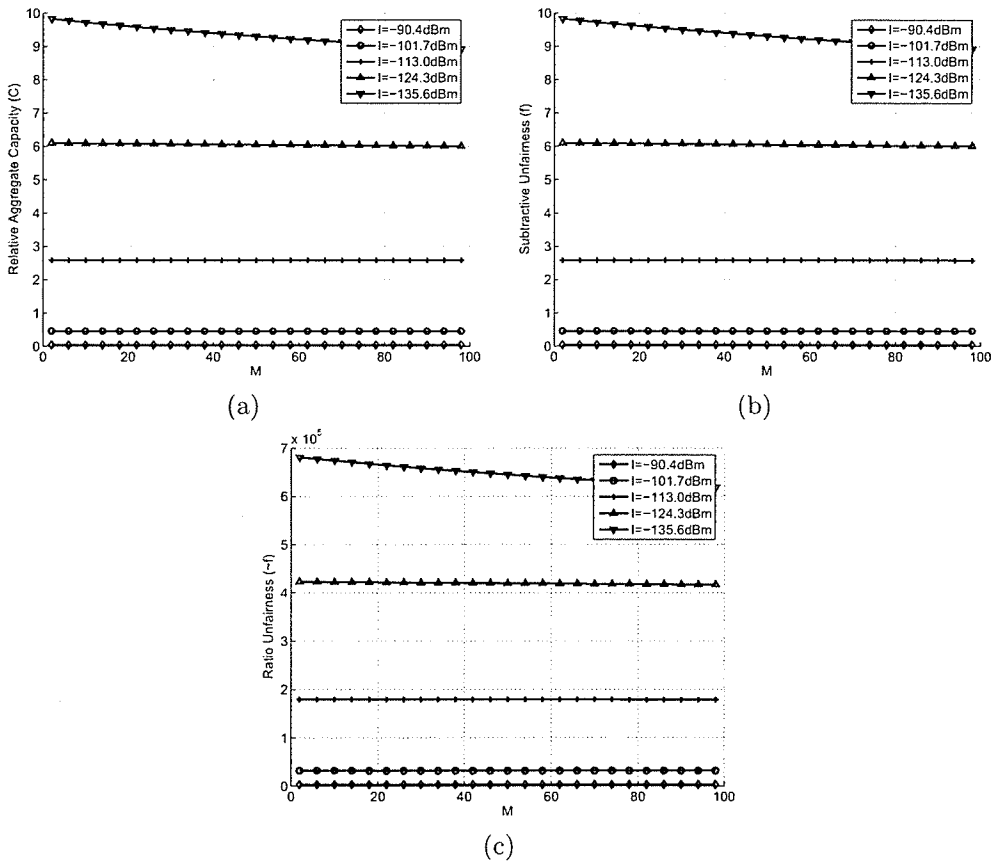

Figure 5.5: *Results for different number of mobile stations with varying I and $\gamma = 0$ in the CSC. (a) Aggregate capacity. (b) Subtractive unfairness. (c) Ratio unfairness.*

Figures 5.1–(a), 5.2–(a), 5.3–(a), and 5.4–(a) show the values of aggregate system capacity for different number of mobile stations, M, with varying I and γ. The vertical axis in each chart shows the number of mobile stations. Each graph also presents the effect of choosing between different candidates for I. As expected, choosing smaller background noise results in a larger aggregate system capacity. In any situation that the curves stop abruptly, it means that the set of parameters does not yield any result. Again, as expected, by easing the minimum quality of service bound, the aggregate system capacity increases. This effect is more significant in larger values of M, in which case the system becomes significantly partial.

We will first give an analytic justification for this situation. Later, when comparing the respective unfairness values, we will show how much unfair the system in fact is. To investigate this effect analytically, we use Figure 5.5–(a). This figure shows that by removing the minimum quality of service constraint, setting $\gamma = 0$, the aggregate system capacity does not change when the number of the mobile stations increases, except for the case of $I = -136dBm$. This is due to the fact that at this situation the system starts to handle one mobile station with maximum quality of service and to leave no resources for the others. In this situation, we will have,

$$x_2 = \cdots = x_M = 0, \tag{5.1}$$

therefore, using (2.7), we have,

$$C = \left(\frac{1+x_1}{1+x_1}\right)^{M-1}\left(\frac{1+x_1}{1+x_1-x_1}\right) = 1+x_1 = 1+\frac{p_1 g_1}{I}. \tag{5.2}$$

Here, the range of p_1 is dictated by p_{max} and P_{max}. Hence, we have,

$$C = 1+\frac{\min\{p_{max}g_1, P_{max}\}}{I}, \tag{5.3}$$

which is in fact what is seen in Figure 5.4–(a) for the first few values of M and in Figure 5.5–(a) for all values of M, except for $I = -136dBm$. We will return to the unfairness curves shortly.

As shown in Figure 5.6–(a), tightening the minimum quality of service bound has a declining effect on the aggregate system capacity. As M increases this effect is more severe. Finally,

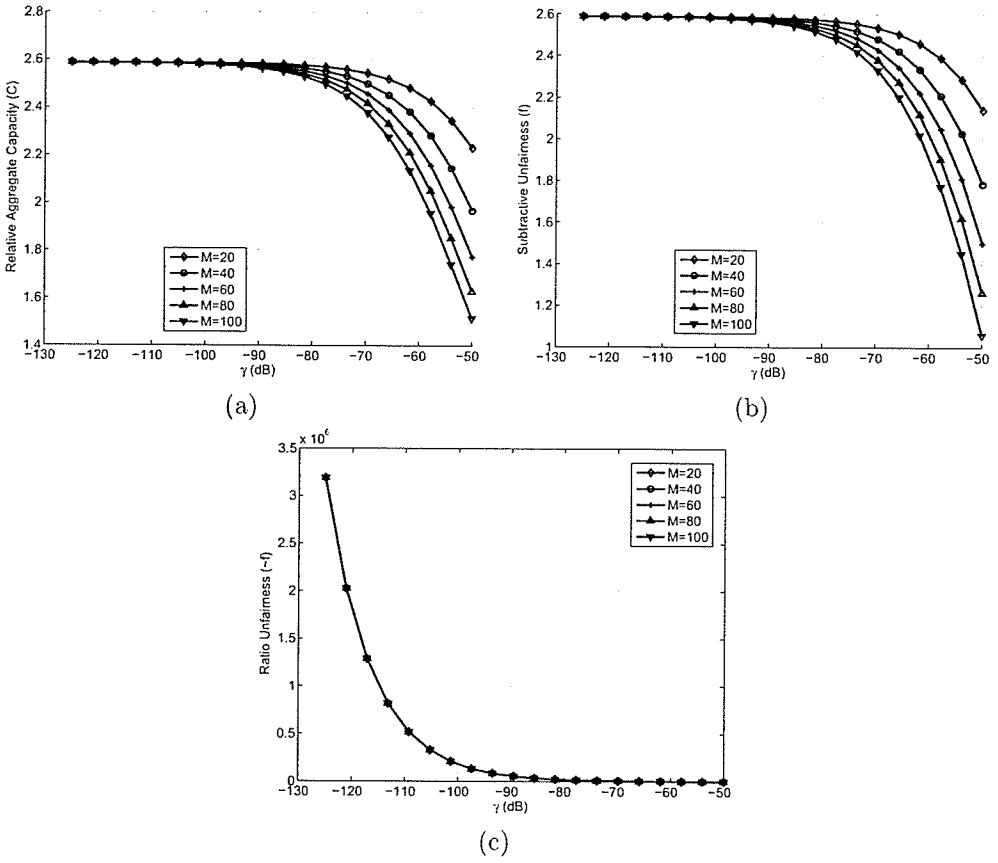

Figure 5.6: *Results for different number of mobile stations with varying γ in the CSC. (a) Aggregate capacity. (b) Subtractive unfairness. (c) Ratio unfairness.*

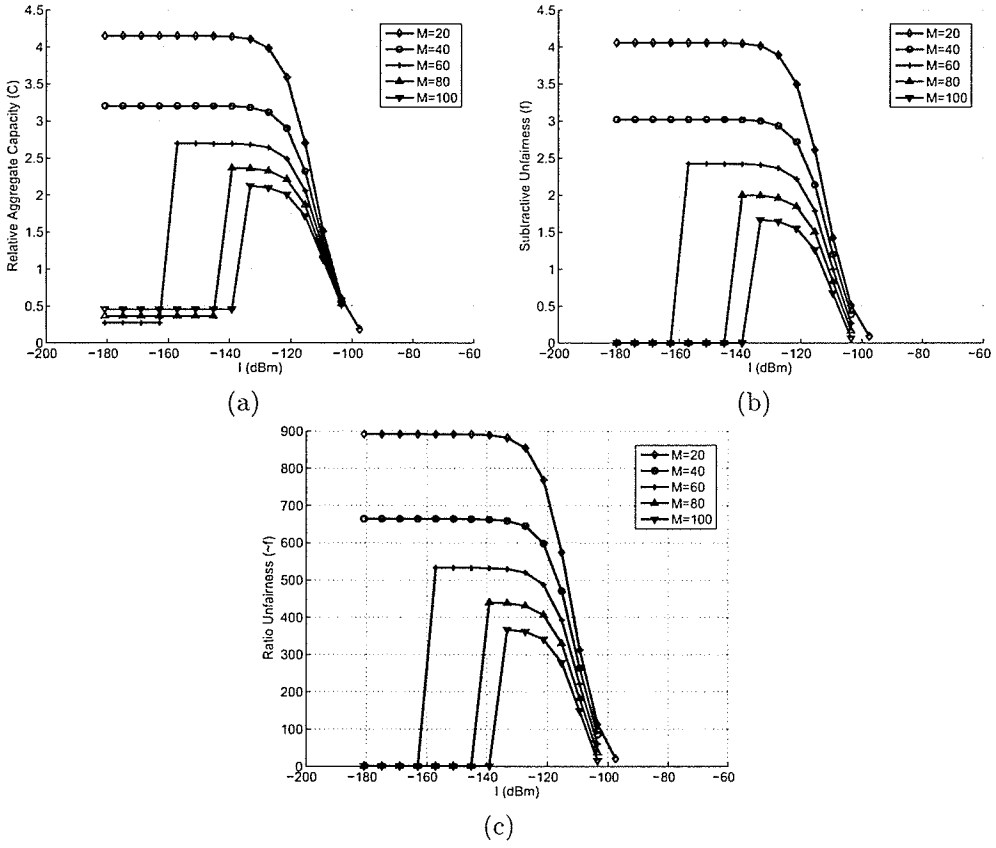

Figure 5.7: *Results for different number of mobile stations with varying I in the CSC. (a) Aggregate capacity. (b) Subtractive unfairness. (c) Ratio unfairness.*

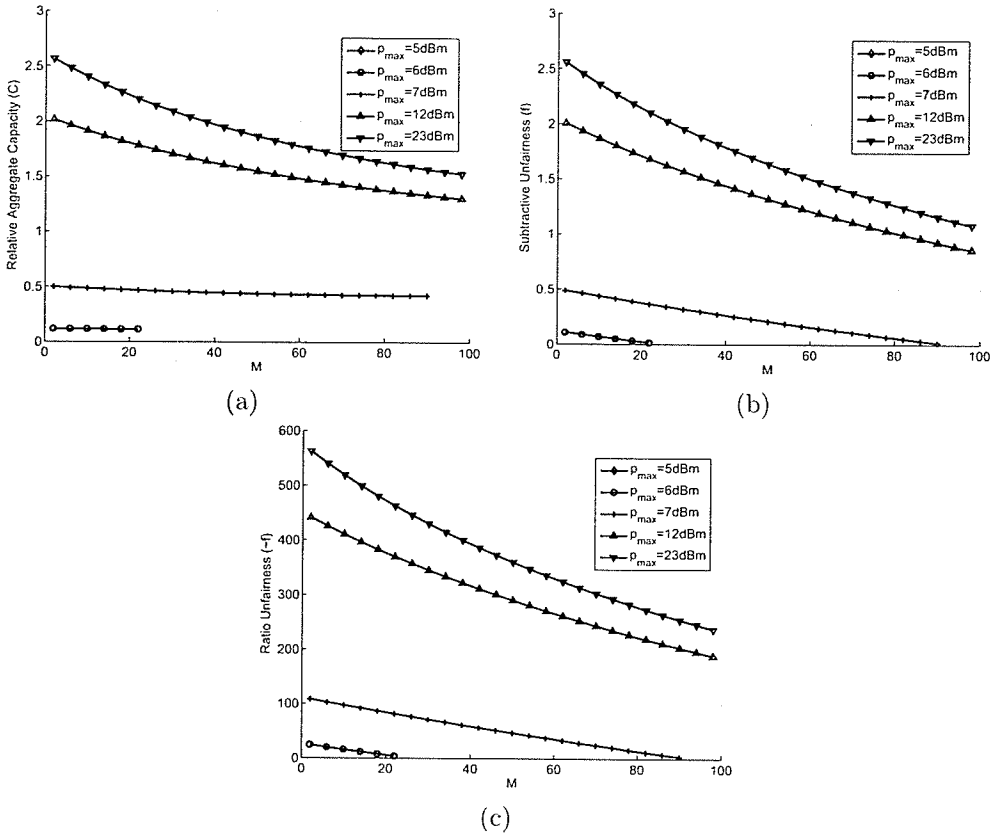

Figure 5.8: *Results for different number of mobile stations with varying p_{max} in the CSC. (a) Aggregate capacity. (b) Subtractive unfairness. (c) Ratio unfairness.*

note that as shown in Figure 5.7–(a) increasing I decreases the aggregate system capacity, as expected.

The effects of choosing different values of p_{max} is investigated in Figure 5.8–(a). As expected, small values of p_{max} lead to significant decrease in the aggregate system capacity or even makes the problem infeasible. A similar experiment is carried out in order to investigate the role of P_{max}. As the results shown in Figure 5.9–(a) demonstrate, a very small value of P_{max} reduces the aggregate system capacity, while larger values let the other constraints become active and control the final outcome.

Summarizing the effects of different parameters on the aggregate capacity, increasing I or γ has a declining effect. While the first parameter represents the amount of background noise

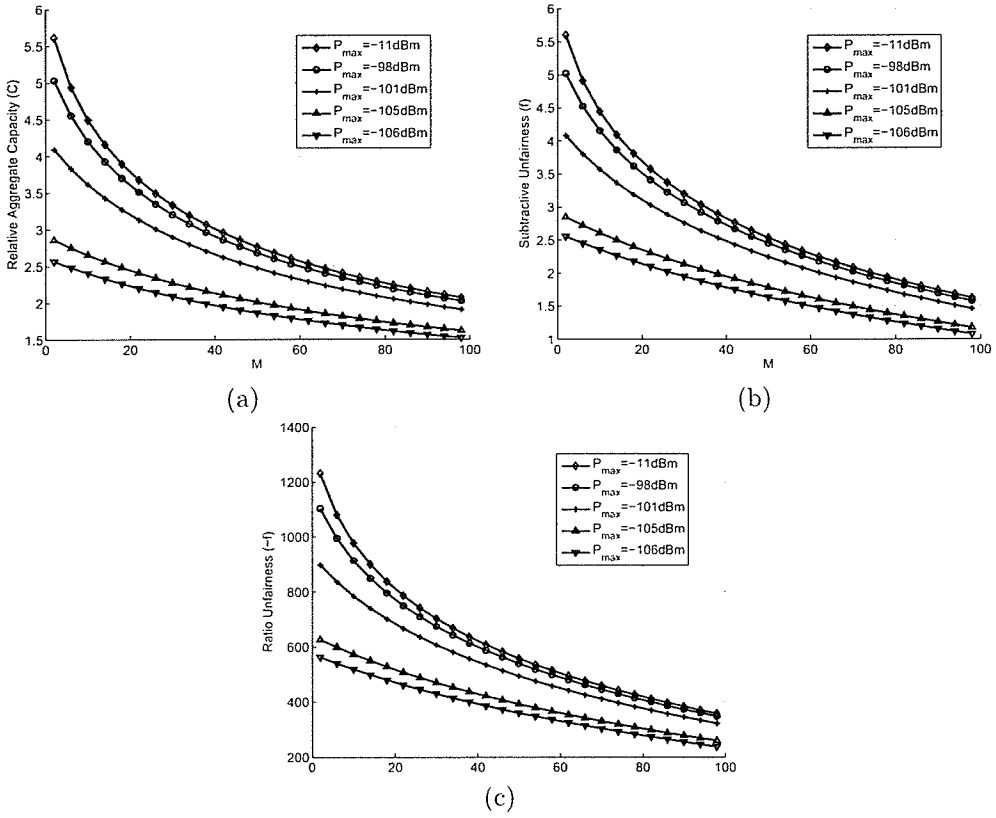

Figure 5.9: *Results for different number of mobile stations with varying P_{max} in the CSC. (a) Aggregate capacity. (b) Subtractive unfairness. (c) Ratio unfairness.*

and may be reduced using better engineering, reducing the second parameter will make the system more partial. Also, larger values of p_{max} and P_{max} are helpful. These values indicate the maximum power which one mobile station can afford to transmit at and the maximum total interference which is tolerated, respectively. Excessive increase of these two parameters is not practical, due to the fact that increasing p_{max} with fixed P_{max} may not result in a larger aggregate system capacity, because then the condition of total transmission power will push the maximum transmission power of each mobile station down. Also, generally, the system performance decreases as the number of the mobile stations increases. This issue will be looked at thoroughly in the next sections.

5.1.2 Fairness Analysis

In Figures 5.1–5.9, the first graph shows the aggregate capacity, while the second and the third graphs show the subtractive and ratio unfairness measures, respectively. Here, we observe that always the subtractive unfairness curves follow the same trend as the aggregate system capacity ones do. This issue will be looked at in this section.

Assume that x_1 is substantially larger than $x_2, \cdots, x_M$. For simplicity we assume that there is a $\varepsilon > 0$ for which,

$$x_i \simeq \varepsilon \ll x_1, \forall i > 1. \tag{5.4}$$

Hence, we can approximate (1.8) as,

$$C \simeq \log_2 \left\{ \left(\frac{1+(M-1)\varepsilon + x_1}{1+(M-2)\varepsilon + x_1} \right)^{M-1} \frac{1+(M-1)\varepsilon + x_1}{1+(M-1)\varepsilon} \right\}, \tag{5.5}$$

$$C \simeq \log_2 \frac{1+(M-1)\varepsilon + x_1}{1+(M-1)\varepsilon}. \tag{5.6}$$

Now, substituting (5.4) into (1.30) yields,

$$f \simeq \log_2 \frac{1+(M-2)\varepsilon + x_1}{1+(M-1)\varepsilon}. \tag{5.7}$$

Comparing (5.6) and (5.7) proves that at this drastically partial system we will have $f \simeq C$. This will describe the similarity of unfairness curves with aggregate system capacity ones if we can show that in these solutions x_1 is substantially larger than the rest of the elements of $\vec{\mathbf{x}}$.

When we analyze the structure of the best $\vec{\mathbf{x}}$ in the solution presented here, it is observed that k defined in (2.26) is always one (it happened in every single experiment shown at the above). This means that the system is supplying one customer with a very high capacity while others are kept at the minimum guaranteed quality of service. Note that although by increasing M the unfairness decreases, so does the aggregate capacity of the system. Hence, increasing M is not a good practice in this regard.

Here, we have compared the difference between capacities devoted to different customers, denoted by f, and not the ratio between them, denoted by $\tilde{f}$. In fact, $\tilde{f}$ curves show non-meaningful figures of orders of hundreds and more in many settings to give a better picture of this situation.

We analyze the ratio unfairness measures shown in the third graph in Figures 5.1, 5.2, 5.3, 5.4, 5.5, 5.6, 5.7, 5.8, and 5.9. Note that unless for the case of Figure 5.6-(c), the $\tilde{f}$ curve is following the same pattern the corresponding f curve does, and hence that of the corresponding C curve. In fact, $\tilde{f}$ seems to be solely a fixed multiplier of f. Assuming the condition in (5.4) we will show that this is in fact the case. Using (1.31) and (5.7) we have,

$$\tilde{f} = \frac{\log_2 \frac{1+(M-1)\varepsilon+x_1}{1+(M-1)\varepsilon}}{\log_2 \frac{1+(M-1)\varepsilon+x_1}{1+(M-2)\varepsilon+x_1}} \simeq \frac{C}{\log_2\left(1+\frac{\varepsilon}{1+(M-2)\varepsilon+x_1}\right)} = \frac{C}{\log_2(1+\gamma)} \simeq \frac{\ln 2}{\gamma} C. \tag{5.8}$$

Here, we have used the fact that for $|\delta| << 1$,

$$\ln(1+\delta) \simeq \delta. \tag{5.9}$$

Here, Equation (5.8) exhibits that if γ is kept constant, then $\tilde{f}$ and C only differ by the fixed, very large, constant $\gamma^{-1} \ln 2$. On the other hand, if γ too changes during the experiment, then (5.8) shows how $\tilde{f}$ and C are related. The ratio unfairness curves shown in Figures 5.1, 5.2,

5.3, 5.4, 5.5, 5.7, 5.8, and 5.9 show the situation in which γ is fixed during the experiment. Analyzing the curves for $\frac{\ln 2}{\gamma}C$ and $\tilde{f}$ demonstrates that for the case of Figure 5.6–(c), in which γ does change, Equation (5.8) is in fact valid.

It is worth to mention that, here, values of $\tilde{f}$ of orders of hundreds are observed. This demonstrates that the solution is utterly unfair, an observation which is in accordance with what is reported by other researchers [57, 58]. In fact, this unfairness was the main reason the authors in [71] devised the minimum SIR constraint. We argue that the impracticality of solution to the CSC comes from the fact the constraints neglect the unfairness of the solution. Furthermore, the formulation ignores the fact that while a minimum bound for the signal to noise ratio, and thus for the capacity, is vital, there should also exist a maximum capacity bound. lack of appropriate constraints on these two important aspects of the problem makes the final results partial and impractical. This issue has been the main reason for the proposal of the New Single Cell problem, as discussed in Section 3.1.

5.2 New Single Cell (NSC)

This section presents experimental results gathered through solving the NSC. Using the proposed algorithm, it takes less than $2ms$ to solve the NSC in a cell containing 100 mobile stations.

To compare the outcome of the CSC with the new one, we show the result of adding the new constraint in a sample problem. Table 5.1 shows the values of g_i for an example in which M is equal to 10. This table also shows the solutions to the CSC and the NSC with the set of parameters given in Section 1.3.1. For each problem, first the pattern of the solution is given.

The given structure of the solution, given in (2.26) and (3.9), for the CSC the NSC, respectively, it is informative to see where the breaking points are eventually placed. The location of these points in fact informs us of the number of the mobile stations which benefit from larger capacities. As expected from the results and discussions given in 5.1, the solution generated by the CSC serves the first mobile station with the maximum possible capacity while the others are left to the minimum guaranteed amount ($\log_2(1+\gamma)$). When we add the extra $C_i \leq \eta$ constraint,

we are in fact limiting the capacity of the first mobile station. As seen in the solutions to the NSC, this leads in the spread of the aggregate capacity between more mobile stations. In the new solution, presented in Table 5.1, nine mobile stations are served at the maximum possible capacity (either determined by η or l_i) while the tenth mobile station transmits at a capacity inside the range.

Table 5.1 also shows the capacity shares of different mobile stations in both problems. It is evident that the CSC dominantly depends on the first mobile station, while the dependence of the NSC on different mobile stations is more even. The high dependence of the CSC on one mobile station is not acceptable in practice if the system is to be deployed in the real world.

As expected both from the analysis and from the set of capacity values, the NSC is more fair than the CSC. In fact the ratio unfairness measure is about eighty times lower in the NSC compared to the CSC. Note that here we see the aggregate capacity becoming smaller in the NSC. This was expected, because by putting the maximum capacity constraint, we have in fact limited the objective function from going up-hill. By this, we have gained a more fair system.

Here, we in fact see the essential shortcoming of the CSC in detail. In fact, the solution given by the CSC will not be implementable if the first mobile station denies the high capacity which is decided for it. On the contrary, the NSC serves nine mobile stations with the highest possible capacity and then serves one with a midpoint capacity. In addition to its fairness, the NSC is also capable of supporting the aggregate capacity of above half the CSC.

Using a $\vec{\mathbf{g}}$ similar to what is shown in Figure 1.1–(b), we analyze the effects of different parameters on the solution. To carry out this analysis, first, we present the values of C, the aggregate capacity. Then, we analyze the unfairness measures f and $\tilde{f}$.

The first experiment analyzes how selecting between different values of I and γ affects the system while the number of the mobile stations changes from one to a hundred. It was shown in 5.1 that as γ decreases the aggregate capacity of the CSC increases. The interpretation for that effect was that decreasing γ means that the system is less engaged with the majority and can allocate more resources to a chosen mobile station. It was argued that this is not a practically acceptable performance.

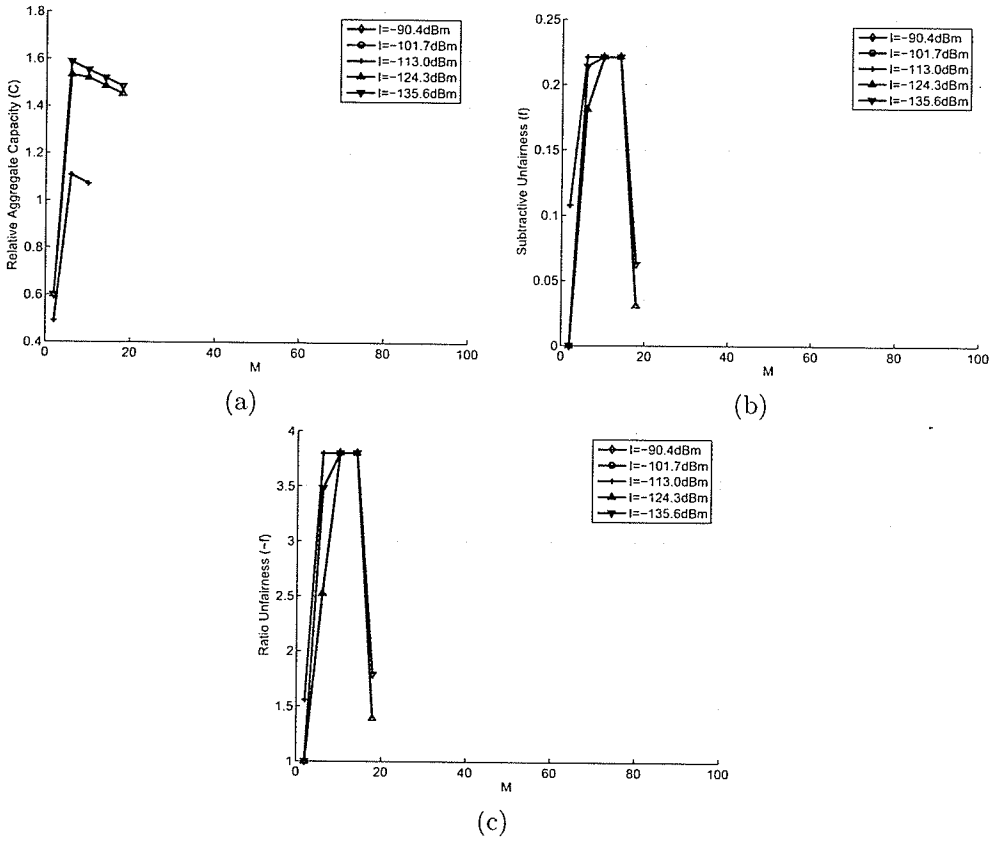

Figure 5.10: *Results for different number of mobile stations with varying I and $\gamma = -25dB$ in the NSC. (a) Aggregate capacity. (b) Subtractive unfairness. (c) Ratio unfairness.*

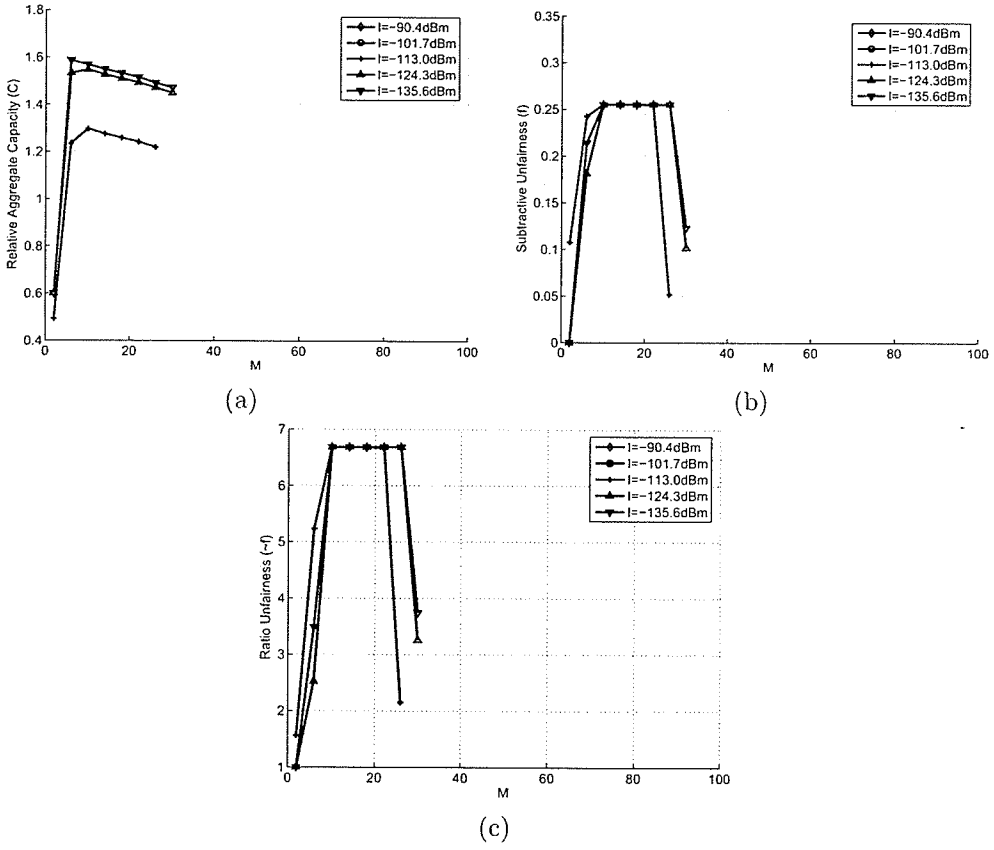

Figure 5.11: *Results for different number of mobile stations with varying I and $\gamma = -30dB$ in the NSC. (a) Aggregate capacity. (b) Subtractive unfairness. (c) Ratio unfairness.*

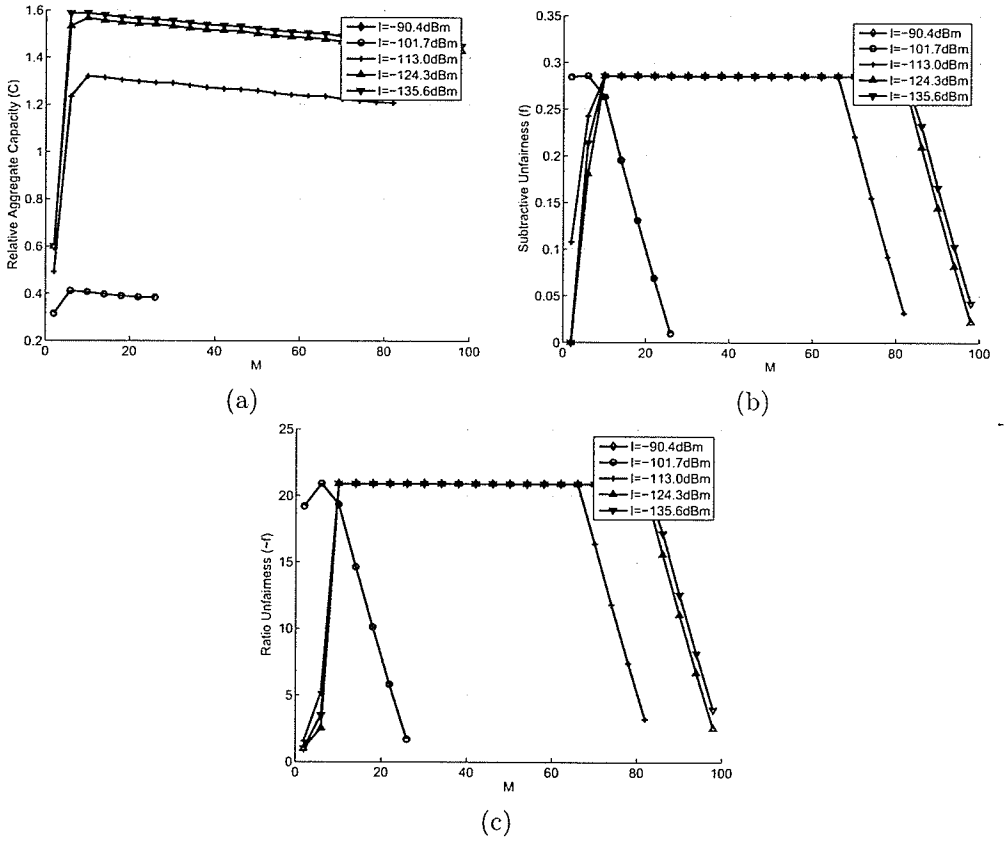

Figure 5.12: *Results for different number of mobile stations with varying I and $\gamma = -40dB$ in the NSC. (a) Aggregate capacity. (b) Subtractive unfairness. (c) Ratio unfairness.*

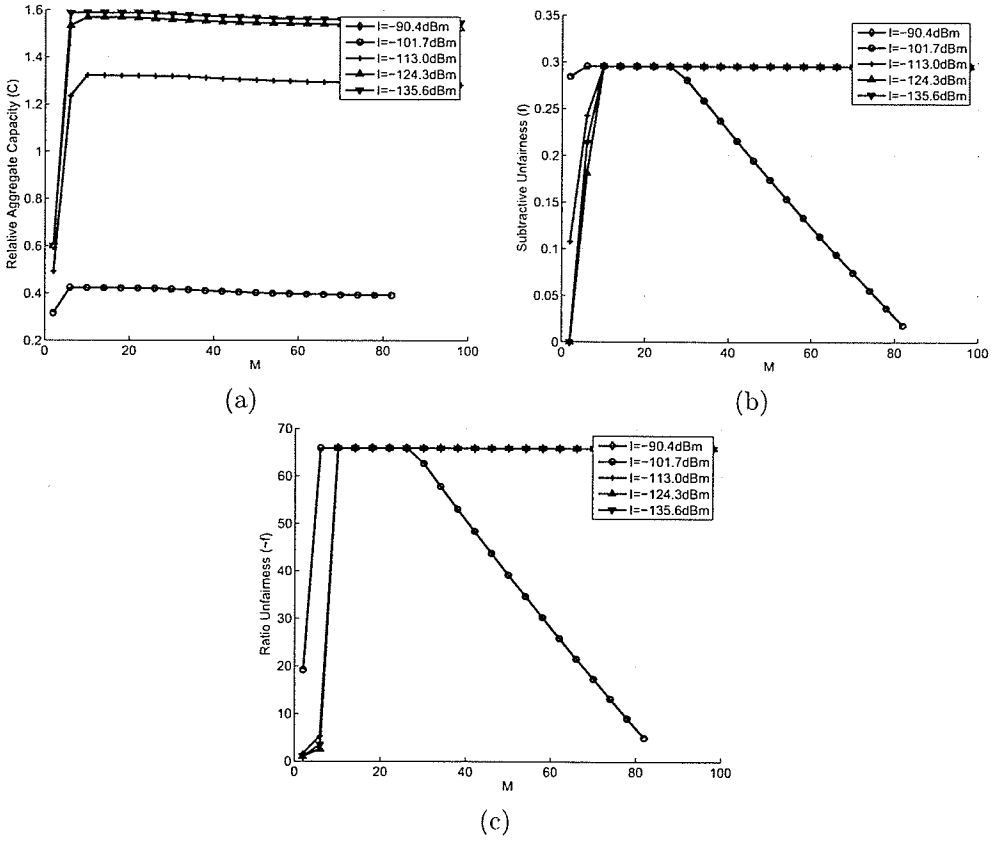

Figure 5.13: *Results for different number of mobile stations with varying I and $\gamma = -50dB$ in the NSC. (a) Aggregate capacity. (b) Subtractive unfairness. (c) Ratio unfairness.*

Figures 5.10, 5.11, 5.12, and 5.13 show the differences in the results generated by the NSC and the CSC. Here, γ has in fact negligible effect on the aggregate capacity, partly because not many mobile stations are treated at that low rate. Also, we see that in the NSC the aggregate capacity does not drop vastly when M increases. For example, looking at Figure 5.13–(a) we see that in the NSC the aggregate capacity of the new problem drops less than 0.1 when M goes from 1 to 100 (6.4% of the amplitude). At the same time the CSC results in a drop of 6 (75% of the amplitude) in the aggregate capacity (see Section 5.1). However, similar to the case of the CSC, we observe that increasing I does decreas the aggregate capacity. It should be mentioned that the aggregate capacity of the NSC is almost one third of that of the CSC and the difference increases vastly when γ reduces. We argue that the high aggregate capacity of the CSC does not mean that that system is in fact capable of producing that much revenue, because it is relying on one chosen mobile station which may not in fact exist in reality.

The ratio unfairness of the NSC is less than one tenth of that of the CSC and the gap increases as γ reduces, because the CSC becomes more partial.

Figure 5.14 shows the case in which γ is zero, meaning that there is no minimum guaranteed quality of service. In this situation the ratio unfairness increases to more than ten thousand, still one thirtieth of that of the CSC. Figure 5.15 shows the effects of varying γ. Here, it is observed that for $\gamma > -80dB$ the ratio unfairness is within a tactically acceptable interval. Also, note that the number of the mobile stations has no effect on either the subtractive or the ratio unfairness curves.

Figure 5.16 shows how varying I affects the solution. Note that increasing I over $-130dB$ drops the aggregate capacity curves to great extent. Again, contrary to the case of the CSC, the unfairness curves are independent of the number of the mobile stations. Figures 5.17 and 5.18 show the effects of p_{max} and P_{max} on the solution and, finally, Figure 5.19 shows that decreasing η decreases the aggregate capacity, because the maximum capacity of each mobile station is then limited. Moreover, as expected, reducing η decreases the unfairness.

To have a better insight about the NSC and its benefits over the CSC an experiment was carried out to compare their behavior in the long term. We assume that $M = 5$ mobile stations

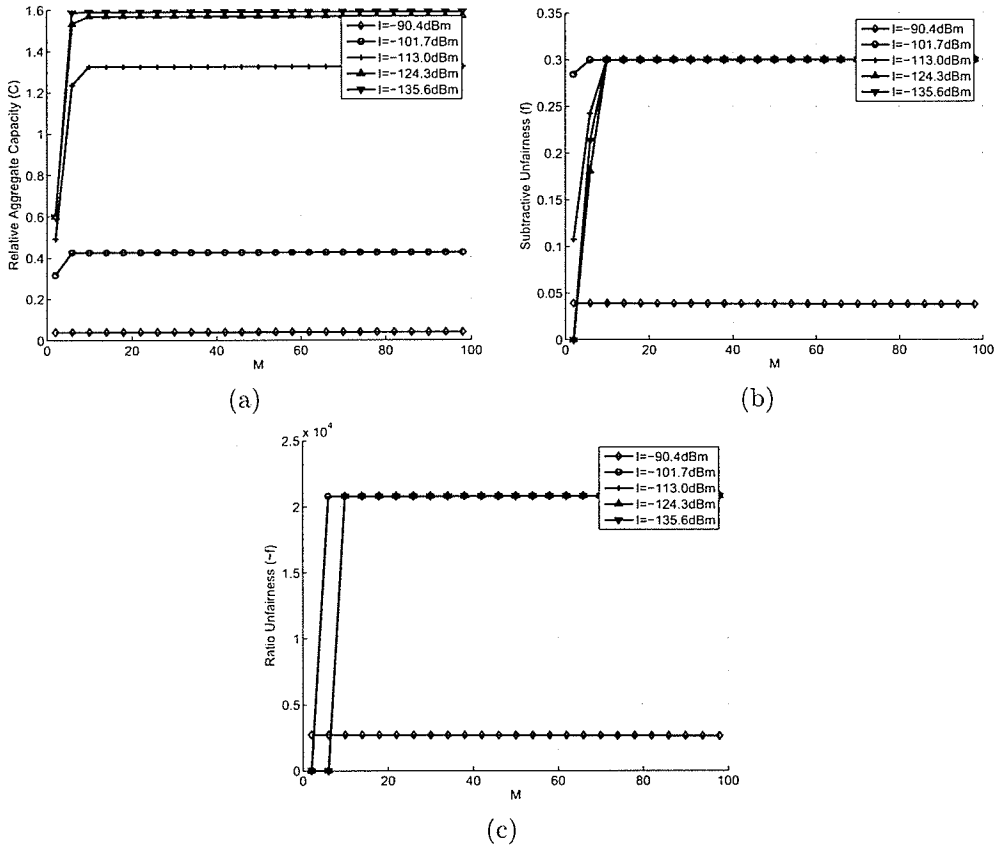

Figure 5.14: *Results for different number of mobile stations with varying I when γ equals zero in the NSC. (a) Aggregate capacity. (b) Subtractive unfairness. (c) Ratio unfairness.*

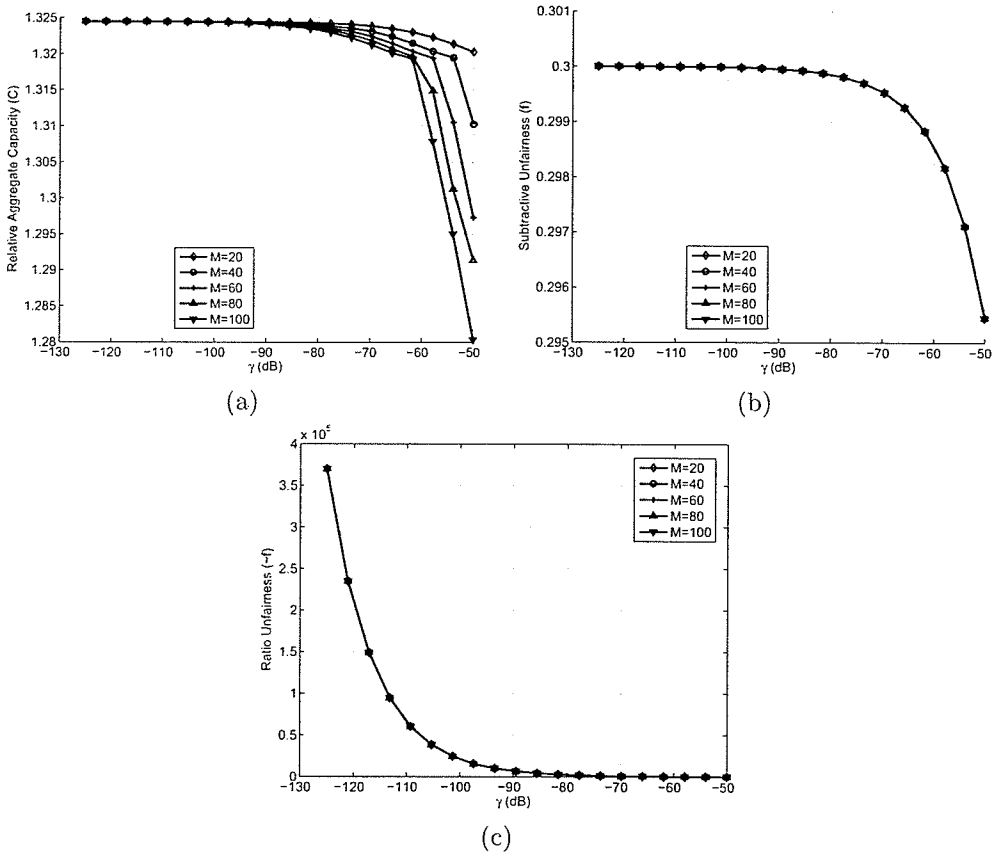

Figure 5.15: *Results for different number of mobile stations with varying γ in the NSC. (a) Aggregate capacity. (b) Subtractive unfairness. (c) Ratio unfairness.*

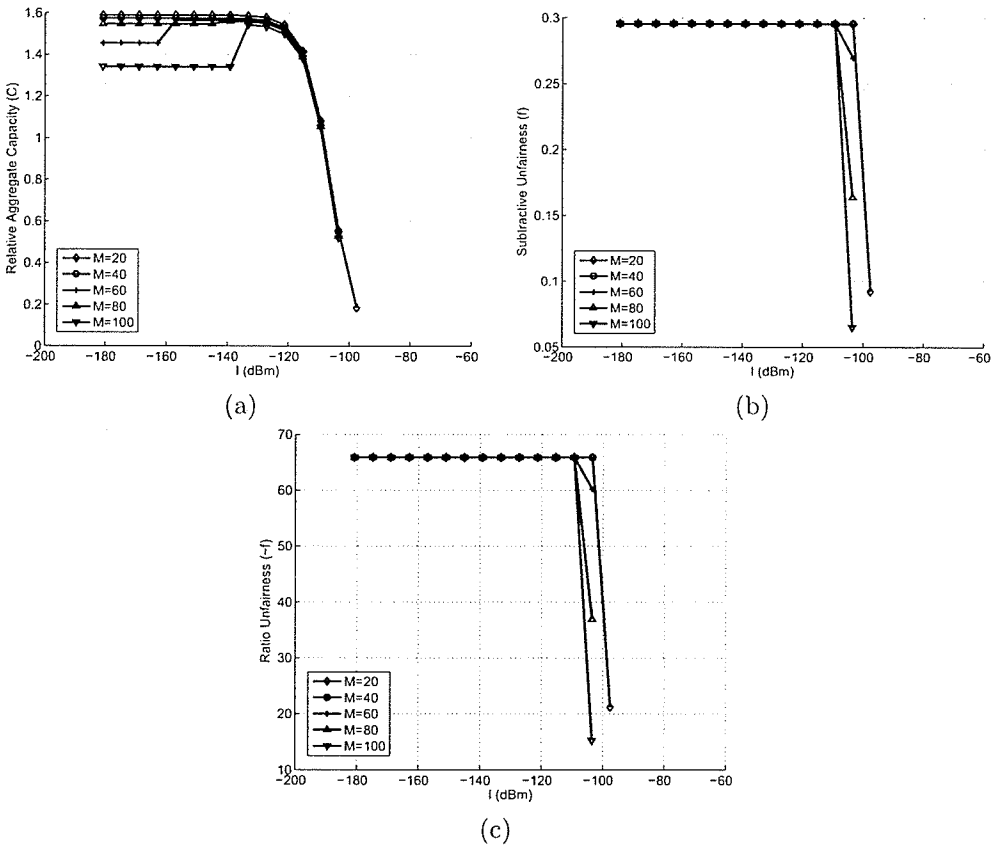

Figure 5.16: *Results for different number of mobile stations with varying I in the NSC. (a) Aggregate capacity. (b) Subtractive unfairness. (c) Ratio unfairness.*

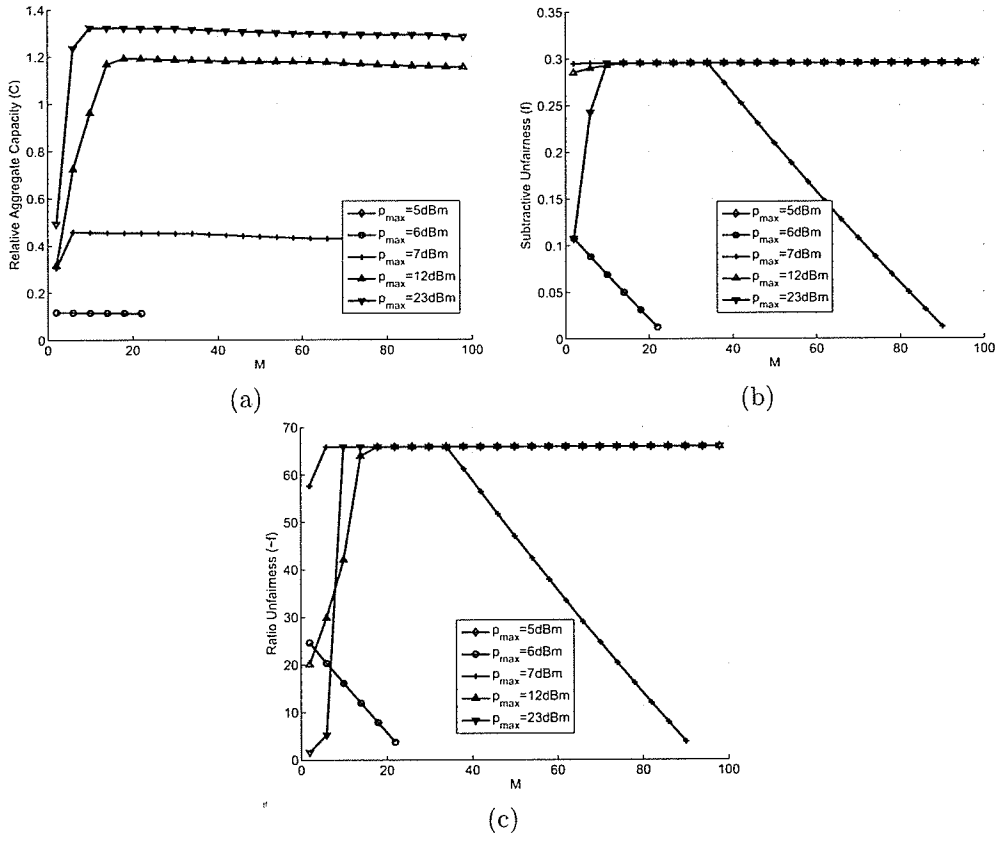

Figure 5.17: *Results for different number of mobile stations with varying p_{max} in the NSC. (a) Aggregate capacity. (b) Subtractive unfairness. (c) Ratio unfairness.*

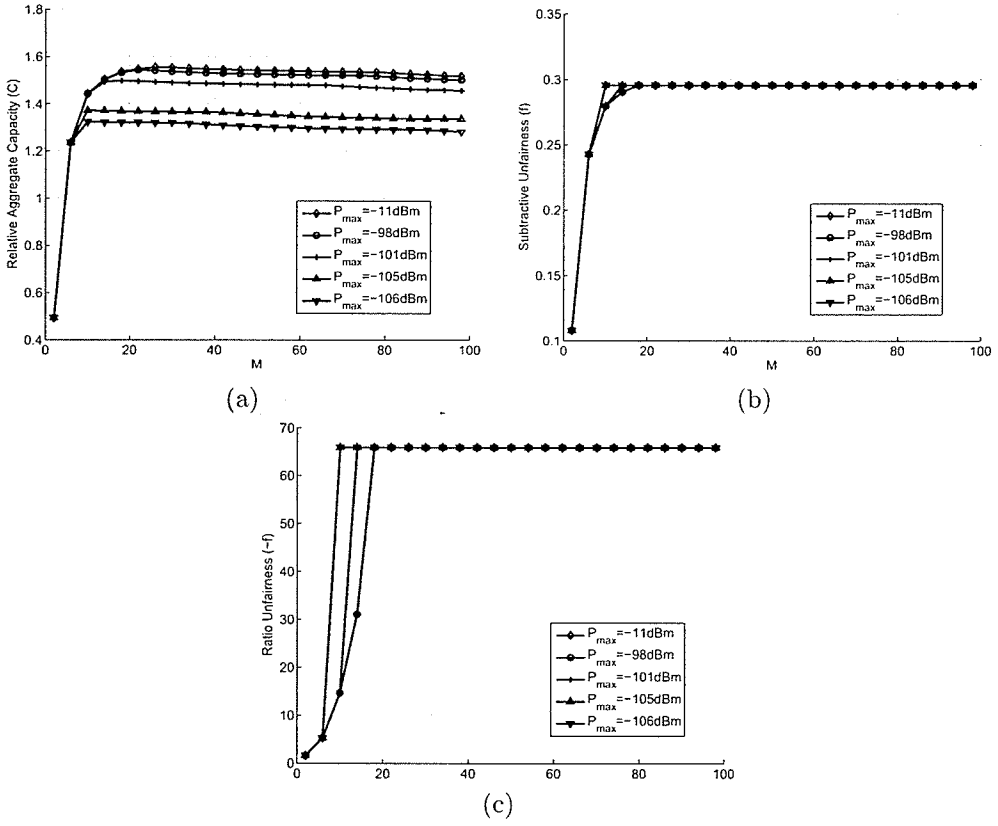

Figure 5.18: *Results for different number of mobile stations with varying P_{max} in the NSC. (a) Aggregate capacity. (b) Subtractive unfairness. (c) Ratio unfairness.*

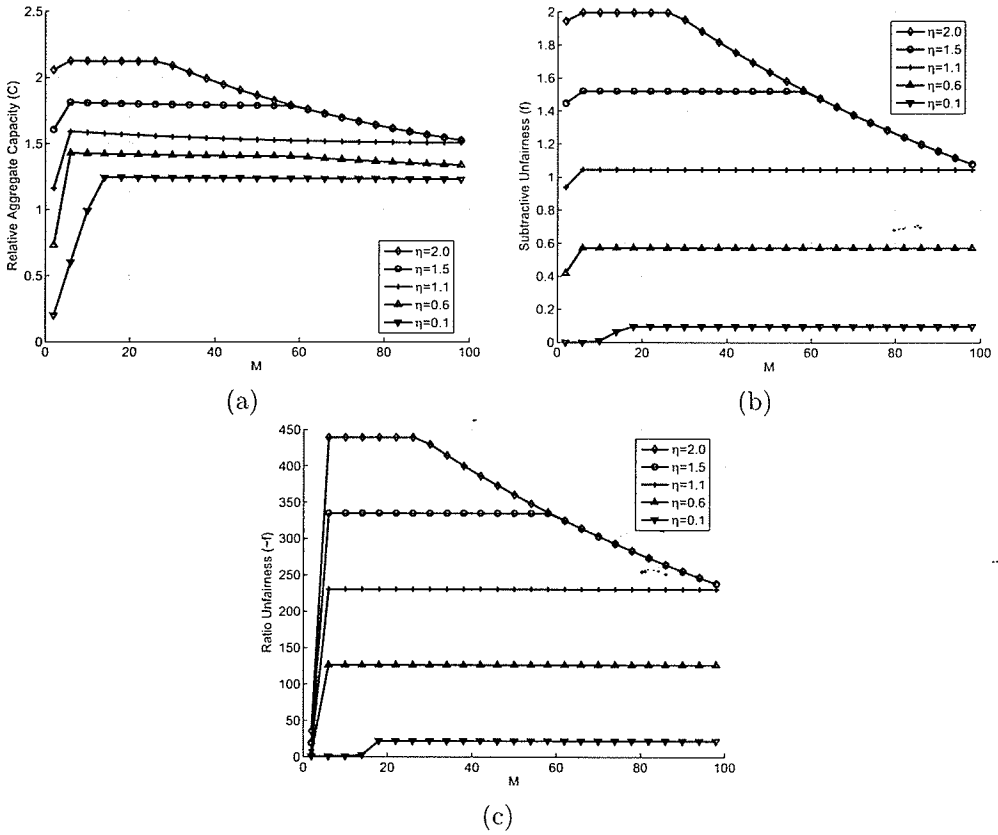

Figure 5.19: *Results for different number of mobile stations with varying η in the NSC. (a) Aggregate capacity. (b) Subtractive unfairness. (c) Ratio unfairness.*

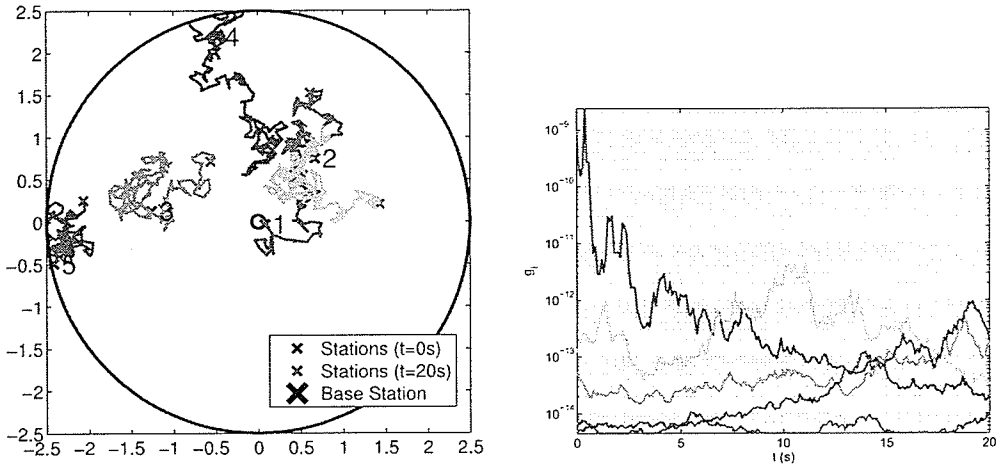

(a) (b)

Figure 5.20: *(a) Pattern of movement of mobile stations used in the simulation. (b) The corresponding values of g_i for different mobile stations over time.*

are in a cell and that each mobile station is originally randomly placed inside the cell. We also assume that each mobile station is a pedestrian and therefore the movements of each mobile station is modeled as a random walk. Denoting the position of the i–th mobile station at time t as $\vec{\mathbf{x}}_i(t)$ we calculate,

$$\vec{\mathbf{x}}_i(t+dt) = \vec{\mathbf{x}}_i(t) + s \begin{bmatrix} \cos\theta \\ \sin\theta \end{bmatrix} vdt. \tag{5.10}$$

Here, θ is a uniform random variable in the interval $[0, 2\pi]$ and v equals $5km/h$ [124]. Also, s is a uniform random variable in the interval $[0, 1]$. Here, we assume that no mobile station leaves the cell. Also, we do not consider the ones that enter it. Hence, at each time epoch we normalize the vectors $\vec{\mathbf{x}}_i(t)$ which leave the cell as,

$$\vec{\mathbf{x}}_i(t+dt) = \frac{R}{\|\vec{\mathbf{x}}_i(t-1)\|}\vec{\mathbf{x}}_i(t-1). \tag{5.11}$$

This model assumes that the boundaries of the cell inhibit the mobile stations from leaving it.

Selecting values of $T = 20s$ and $dt = 100ms$ and after generating sequences of the random variables θ and s we produce a pattern of movement for the mobile stations as seen in Figure 5.20–

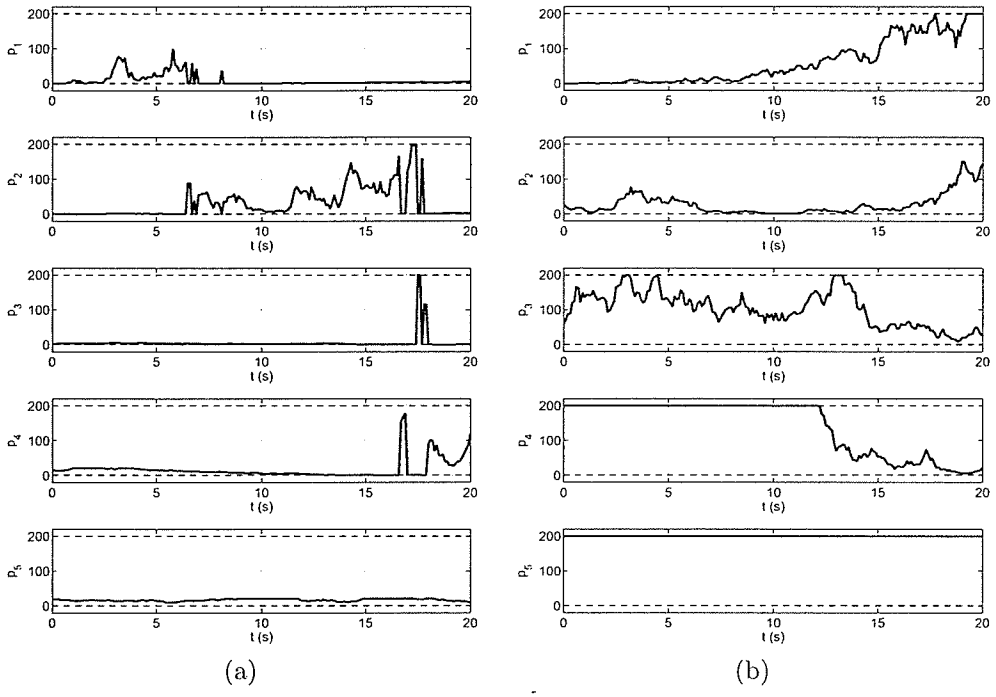

Figure 5.21: *Transmission power of different mobile stations over time. (a) The CSC. (b) The NSC.*

(a). This pattern of movement results in different values of g_i over time (see Figure 5.20–(b)). As a mobile station gets far from the base station the respective value of g_i decreases and vice versa.

Using the movement pattern generated in the above, we analyze the outcome of the CSC and the NSC in a period of time. First, note that while the system is sampled every $100ms$, the solutions take only $7ms$ and $36ms$ for the two problems, respectively. This means that the system is only being utilized 7% and 36% of the time for the CSC and the NSC, respectively.

Figure 5.21 compares the pattern of transmission powers of different mobile stations over time. Comparison shows that in the solution to the CSC, there is tendency to force the mobile stations to have rapid increase and decreases in the power. This phenomenon is mainly due the fact that the CSC tries to devote almost all the resources to the mobile station which is the closest to the base station. As the mobile stations move around they compete for this occasion. Having had this pattern of transmission powers, figure 5.22 shows the resulting capacities of

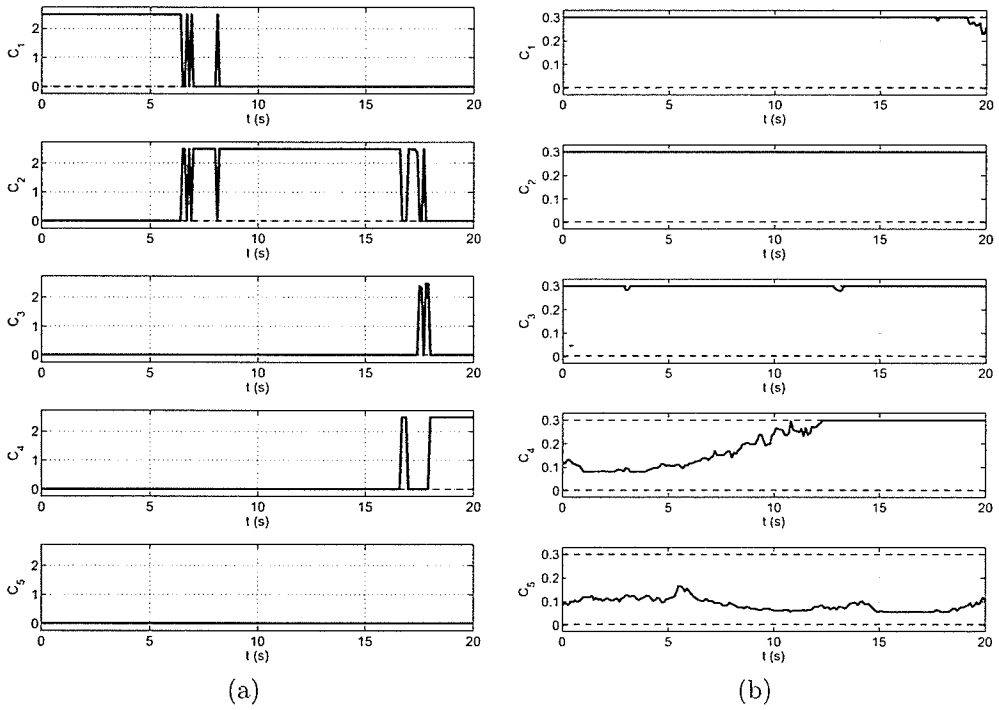

Figure 5.22: *Capacity of different mobile stations over time. (a) The CSC. (b) The NSC.*

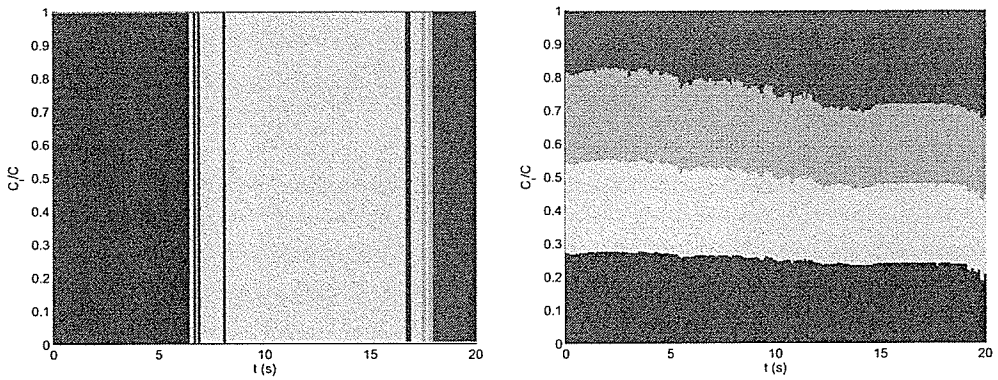

Figure 5.23: *Capacity share of different mobile stations over time. (a) The CSC. (b) The NSC.*

different mobile stations over time. The curves for the CSC show that the mobile stations are mostly oscillating between the two situations of minimum capacity and a very high one. This provides more evidence that the CSC does tend to serve one mobile station at a very high capacity. On the other hand, the NSC keeps the capacity of different mobile stations between the two specified bounds. The important observation here is that in the solution to the NSC, the capacity of none of the mobile stations is ever squeezed down to the minimum guaranteed limit (this may not always be true). The reduction in the oscillation of the capacities in the NSC is worth to mention, as well.

To better understand the difference between the two problems, we compare the capacity shares of different mobile stations in the two solutions. As the capacity shares of the mobile stations for each problem at any moment sum to one, we show their values using overlaid bar graphs (see Figure 5.23). As anticipated, we can see in Figure 5.23–(a) that almost all the capacity at each moment is devoted to the closest mobile station (compare Figure 5.23–(a) with figures 5.20–(b)). On the contrary, the NSC only increases its dependency upon each mobile station as it gets closer. Therefore, in the NSC, while the system tries to maximize the aggregate capacity, it does demand the mobile stations to transmit at capacities which are outside the range determined by γ and η. Also, no mobile station is ever served at the minimum guaranteed capacity. This should be looked at in comparison with Figure 5.22–(a) which shows

that the CSC very frequently serves mobile stations at the lowest allowed capacity.

Comparing Figures 5.24–(a) and 5.24–(b) we find out that the helpful results of the NSC cut the aggregate capacity to almost a half. On the other hand, comparing Figures 5.24–(c) and 5.24–(e) with Figures 5.24–(d) and 5.24–(f) shows that the NSC is substantially more fair (almost one hundred times better in ratio unfairness). Given this experiment and the other results presented in here we conclude that the NSC leads to a more practical solution to the QoS problem compared to the NSC.

5.3 New Enhanced Single Cell (N^+SC)

This section presents experimental results gathered through solving the N^+SC. Here, although the limit for $\tilde{C}_i$ is defined as $\frac{1}{M\mu}$ in (3.39), we choose to analyze the value of $\frac{1}{\mu}$, for reasons described below. The value of $M\tilde{C}_i$, which is one if all the mobile stations are transmitting at the same share of the total received power, represents the deviation of the power received from the i–th mobile station compared to the equilibrium. Hence, for example, setting $\mu = \frac{1}{1.2}$ means that no mobile station is allowed to exceed its capacity more than 20% above the value in equilibrium.

Table 5.2 compares the CSC, the NCS, and the N^+SC for a sample problem. This table shows that, compared to the CSC, the aggregate capacity given by the NSC had decreased fir about 37%. Consequently, the result of the N^+SC shows another 39% drop from the CSC. Equivalently, the N^+SC causes a less than 4% decrease in the aggregate capacity, compared to the NSC. In fact, we know that by imposing more constraints on the CSC we are reducing the aggregate capacity. This is performed for the sake of adding good properties, such as fairness and realistic range of capacity, to the solution. For example, in these three examples the highest capacity offered to one mobile station is 137. 21 and 13 times the lowest one, for the CSC, the NSC, and the N^+SC, respectively. This show that the NSC and the N^+SC are 7 and 10 times more fair compared to the CSC. Also, the N^+SC is two times more fair compared to the NSC. Similar observations are made regarding the ratio unfairness values.

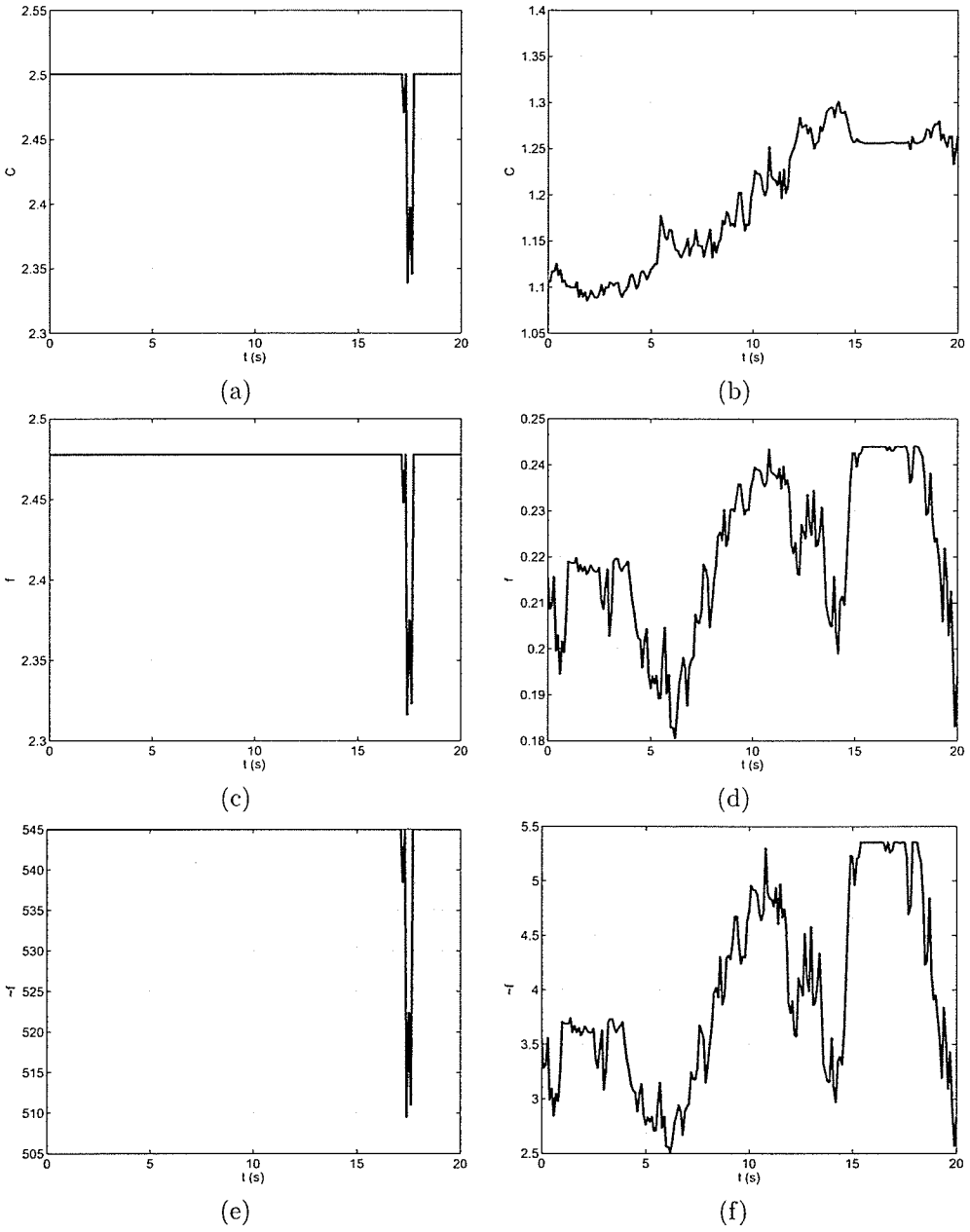

Figure 5.24: *Aggregate capacity and unfairness of the solutions over time. (a), (c), and (e), The CSC. (b), (d), and (f), The NSC. (a) and (b) Aggregate capacity. (c) and (d), Subtractive unfairness. (e) and (f), Ratio unfairness.*

These acceptable outcomes are gained with less than 4% loss in the aggregate capacity. Comparing the elapsed times, we see that the NSC elapses about ten times more than the CSC, something expected according to the difference in the order of the computational costs of the CSC and the NSC, namely $O(M^2)$ and $O(M^3)$. However, the N$^+$SC only elapses 20% more than the NSC. It is worth to mention that even for the most expensive algorithm, namely the N$^+$SC, the platform is able to run the code for about 140 times in a second, making the algorithm appropriate for a dynamic deployment.

One of the most important aspects of the N$^+$SC is its ability to control the dependency of the system on single mobile stations. While the dependency of the CSC on the first mobile station is about 90%, the NSC reduces the dependency to less than 23%, less than half. In fact, as expected, the dependency of the N$^+$SC on any mobile station is less than or equal to 15%, which equals $\frac{1}{M\mu}$. In Table 5.2, the values of the capacity shares, $\tilde{C}_i$, and the power shares, $\tilde{p}_i$, are shown alongside. Note that, the value of $\tilde{p}_i$ is idential to that of the $\tilde{x}_i$. However, in notation it also depends on g_i,

$$\tilde{p}_i = \tilde{x}_i = \frac{x_i}{\sum_{j=1}^{M} x_j} = \frac{p_i g_i}{\sum_{j=1}^{M} p_j g_j}. \tag{5.12}$$

The approximation used in Section 3.2.1, Equation (3.43), in fact claims,

$$\tilde{C}_i \simeq \tilde{p}_i. \tag{5.13}$$

Hence, while the equations control $\tilde{p}_i$, we are in fact implicitly controlling $\tilde{C}_i$. Looking at the case of the N$^+$SC in Table 5.2, it is observed that $\tilde{C}_i$ and $\tilde{p}_i$ are very close to each other. Also, we see that $\tilde{C}_i$ is in fact slightly exceeding the 15% bound, numerically less than 1%. Note that the relationship between $\tilde{C}_i$ and $\tilde{p}_i$ does not hold for large values of $\tilde{p}_i$, as expected. For example, in the case of the CSC with $\tilde{p}_1 = 89.3\%$ we have $\tilde{C}_i = 93.8\%$, more than 5% deviation. However, in the case of the N$^+$SC such monopolies of power do not exist and hence the use of the approximation is valid. In the coming parts of this section we will analyze the effects of μ in more details.

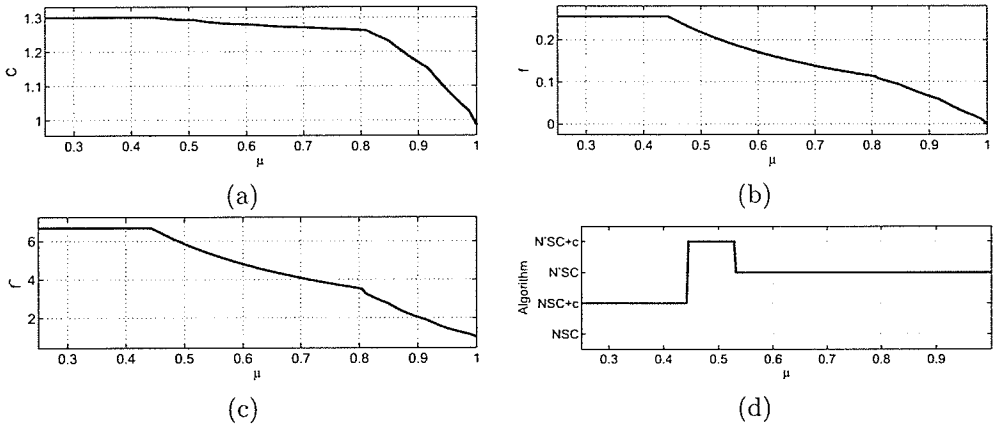

Figure 5.25: *System behavior for different values of μ corresponding to the N^+SC. (a) Aggregate capacity. (b) Subtractive unfairness. (c) Ratio unfairness. (d) The algorithm which gives the result.*

Using the same sequence of path gains as the one shown in Table 5.2 we investigate the behavior of the system as μ increases from $\frac{1}{3}$ to 1. Figure 5.25–(a) shows that as μ decreases, the aggregate capacity of the system increases. This is what we did expect prior to the experiment, because μ limits the capacities from reaching larger values. As Figure 5.25–(b) and c show, and as expected, when μ approaches one the subtractive and the ratio unfairness measures approach zero and one, respectively. Furthermore, decreasing μ forces the capacity shares to become more even, resulting in a more fair system. This is also visible in Figures 5.25–(b) and c.

Figure 5.25–d shows the algorithm which has given the solution for any value of μ. Looking at the flowchart given in Figure 3.3 this curve can be better understood. Here, the condition $M\mu\omega$ controls whether the solution will be sought for using the combination of the NSC+c and the N'SC+c or the N'SC. Having $(M\omega)^{-1} = 0.5326$ we will expect to have the early case for $\mu \leq 0.5326$. This is exactly what is observed in Figure 5.25–d.

To show the effects of different constraints, we refer to the curves shown in Figure 5.26. In these figures, dashed lines represent the constraints while colored lines indicate the behavior of a mobile station. This figure can be used in finding the values of parameters and their effects on the final result through finding the instance at which each constraint becomes active.

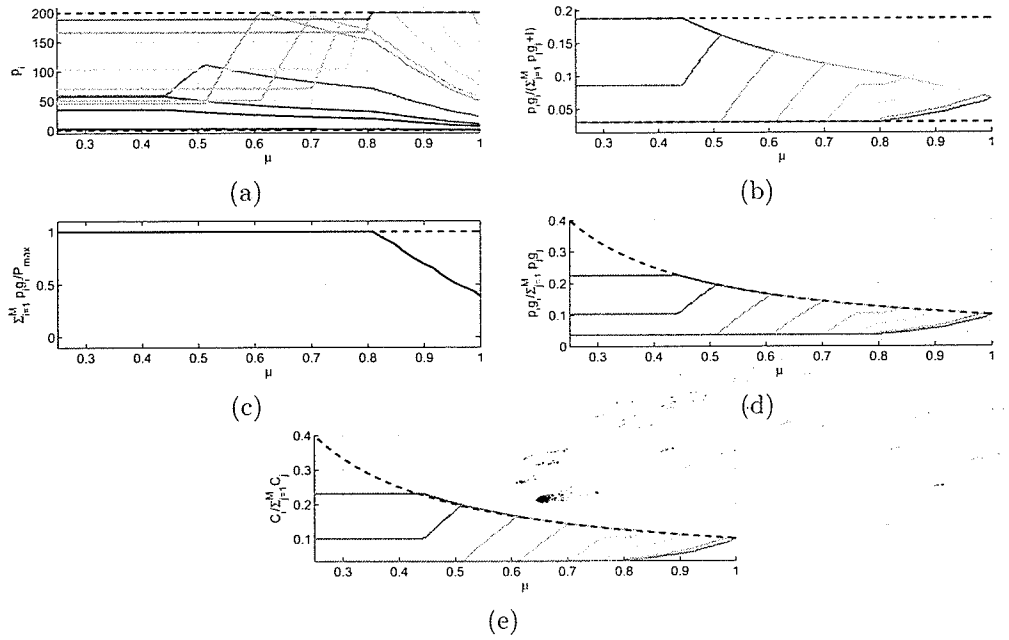

Figure 5.26: *Treatment of the constraints by different mobile stations in the solution produced by the N^+SC for different values of μ and a sample sequence $\mathbf{g}$. In each case the dashed line represents the constraint while colored lines indicate the status different mobile stations. (a)* $0 \leq p_i \leq p_{max}$. *(b)* $\varphi \leq \frac{p_i g_i}{\sum_{j=1}^{M} p_j g_j + I} \leq \omega$. *(c)* $\sum_{i=1}^{M} p_i g_i \leq P_{max}$. *(d)* $\frac{p_i g_i}{\sum_{j=1}^{M} p_j g_j} \leq \frac{1}{M\mu}$. *(e)* $\frac{C_i}{\sum_{j=1}^{M} C_j} \leq \frac{1}{M\mu}$.

Comparing Figure 5.26–(b) with Figure 5.26–(a) shows that the approximation used here, that $\tilde{p}_i \simeq \tilde{C}_i$, is in fact valid. Note that the values of capacity shares sometimes slightly exceed the constraint. However, comparison shows that the power share curves do follow the capacity share curves acceptably well.

Another method to research into the behavior of the system and the effects of the new constraint is to analyze the curves for the capacity shares for different values of μ. Figure 5.27 shows that as expected from the theory as μ tends to one the capacities shares become evenly distributed.

The experimental results discussed here show that adding the new maximum bound on the capacity share of the single mobile stations makes the dependency of the base station on them

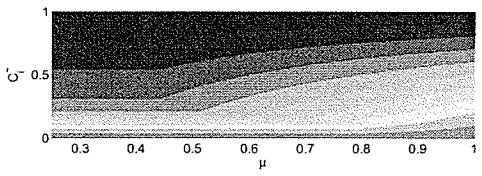

Figure 5.27: *Capacity share of the mobile stations for different values of μ corresponding to the N^+SC.*

more controllable. This contribution to the problem results in a slight drop in the aggregate capacity. Furthermore, it is observed, both theoretically and experimentally, that the computational cost of solving the QoS problem equipped with the new constraint is about twice as much as that of the NSC. Hence, we conclude that adding the new constraint to the problem causes an affordable increase in the computational cost while it provides more control over the results.

5.4 Application of Approximations

This section presents experimental results gathered through solving the CSC^a, the NSC^a, and the N^+SC^a. Here, we use the superscript a for all variables which are calculated using the approximation (in this section, we use $\gamma = -40dB$).

Table 5.3 investigates the properness of the applied approximation for a system solved in the three frameworks of the CSC^a, the NSC^a, and the N^+SC^a. Note that, as expected, the error in C_i^a is always less than 10% in all cases. The least amount of error is observed in the CSC for those mobile stations which transmit at the minimum capacity. This is in fact expected, because from Figure 3.4–(b) we know that smaller values of $\frac{x_i}{1+T}$ undergo smaller errors. Also, note that as again expected from the discussion given for Equation (3.74), the approximation always gives excessive results for the NSC and the N^+SC. The approximation is sometimes conservative in the case of the CSC, as also expected.

Table 5.3 approves that the proposed approximation results in less than 10% error. While this step was necessary, the actual purpose behind deriving the approximate C is not addressed in this expeirment. The success of this experiment however enables us to consider launching

the algorithms, namely the CSC^a, the NSC^a, and the N^+SC^a, which use the approximate C in carrying out the trials. This way, we can achieve considerable enhancement in terms of the comutational cost. In the next experiment we show the results of a sample run of the new algorithms.

Table 5.4 shows the results of solving a sample problem with the three algorithms. For each algorithm, first, the exact results are shown. Then, the crude results of the approximate algorithm are presented (row A). The, in row A+E the results of finding the exact results using the approximate solutions are shown. These last ones are the actual outputs of the algorithms called the CSC^a, the NSC^a, and the N^+SC^a. In this table, variables without a superscript denote the results of the exact algorithms, the ones with the superscript a represent the crude results of the proposed approximate algorithms, and the ones marked with $a\star$ holds the results of precise calculation using the approximate results (the final results of the proposed algorithms). The values in parentheses show the relative error and Italic and bold text show the final results of the exact and approximate algorithms, respectively.

As stated at the end of Section 3.3.2 as the proposed algorithms find precise values of the boundaries, $\vec{\mathbf{p}}^a$ is always identical to $\vec{\mathbf{p}}$. However, There exists a chance that the approximation may deviate the optimization process from finding the real maximum, due to the induced errors. In this experiment such an event was not observed.

In an effort to examine the probability of the approximation misleading the optimization process from finding the optimal point, the three algorithms were executed for ten thousand different positions of different number of mobile stations ($M \in [1, 25]$). Doing this experiment, once incident was in which the approximation disturbed the optimization process. With $M = 3$ and $g_1 = 0.39 \times 10^{-13}$, $g_2 = 0.23 \times 10^{-13}$, and $g_3 = 0.05 \times 10^{-13}$ the approximation in fact made an error in spotting the optimum point in the CSC^a. This error induced a 3% deviation in the final result. Based on this experiment we can roughly state that there is a less than 0.1% chance for a less than 5% error when the approximation is used. However, note that the error has occured when no maximum bound has been set for C_i. Here, we extensively analyze this case.

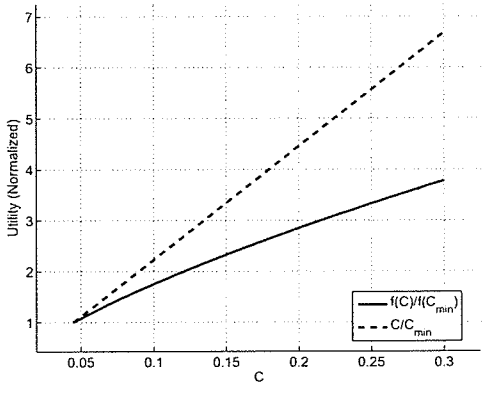

Figure 5.28: *Normalized utility function.*

Table 5.5 analyzes this error. The bold number in the C row shows the choice made by the CSC. Similarly, the bold number in C^a row shows the selection made by the CSC^a. The problem here is that the approximation has changed 1.296 into 1.413, causing about 8% error. Then, mistakenly, the CSC^a has rejected the value of 1.227 in delusion of having found a better value. Going to the root of this error we see that an error of magnitude 9% has occured in the calculation of C_1. The reason for this error is the high $\hat{x}_1$ of about 0.44. Looking at Figure 3.5-(b) we see that $\hat{x}_1$ is on the worst range in respect to the error induced by the approximation. One way to refrain from these approximation errors is to have smaller $\vec{\mathbf{x}}$, which means having more fair systems. In fact, in the case of the NSC^a and the N$^+$SC^a we do have $\hat{x} \in [\varphi, \omega] = [0.03, 0.19]$, the shaded area in Figure 3.5. This suggests an explanation for why the only case of erratic behavior happens in the CSC^a and not in the NSC^a or the N$^+$SC^a.

5.5 Incorporation of Utility Functions

This section presents experimental results gathered through solving the NSC^{f+} and the NSC^{f-}. Here, we use $\gamma = -45dB$. Setting $M = 10$, the two problems of the NSC^{f+} and the NSC^{f-} elapse less than $6ms$ and $10ms$, respectively. Thus, the current implementation could be used for solving the problem over a hundred times in a second, when a dynamic scheme is used.

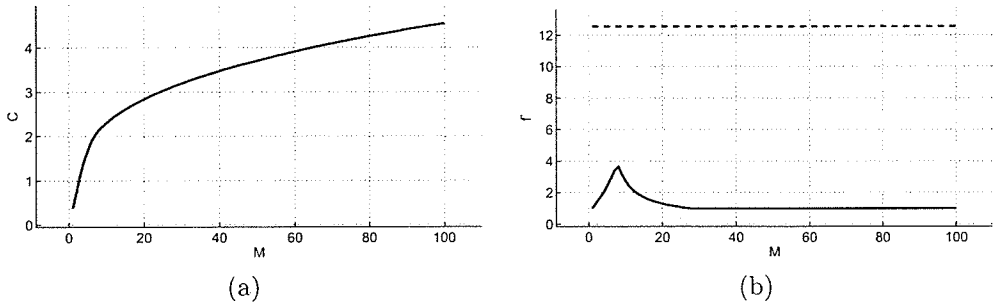

(a) (b)

Figure 5.29: *System parameters as M increases from one to a hundred for the NSC^{f-}. (a) Aggregate capacity. (b)Unfairness.*

As mentioned at the end of Section 3.4.1, the set of potential solutions to the NSC^{f+} is exactly identical to that of the NSC. Thus, we omit the detailed review the results of the NSC^{f+}. In fact, no further analysis of the NSC^{f+} will be given here, because the importance of this problem is solely theoretical. As pointed out in 5.2, the NSC does slightly inherit the unhelpful tendency of the CSC to serve all but one mobile station at the minimum possible capacity. Thus, the migration from the NSC to the NSC^{f+}, in which the utility function is pro larger capacities, will have no benefit.

Looking at concave utility functions, and according to the discussion given in the above, we expect the NSC^{f-} to generate more acceptable results. Because, as seen in Figure 5.28, the utility function reduces the relative importance of larger capacities. In the following parts of this section, we analyze the results of the NSC^{f-} in detail.

Figure 5.29–(a) shows the aggregate capacity as the number of the mobile stations increases form one to a hundred. As expected in practice, as M increases, so does the aggregate capacity. We emphasize that in the CSC increasing M decreases the aggregate capacity. For example, in similar situations, increasing M from one to a hundred drops the aggregate capacity to less than a third (see Section 5.1). Furthermore, the NSC had the positive property that increasing M, in most cases, did not decrease the aggregate capacity 5.1. In this context, the importance of the outcome of the NSC^{f-} is notable.

It is also informative to investigate the capacities of the individual mobile stations as M increases from one to a hundred. As seen in Figure 5.30–(a), as M increases, the mean capacity

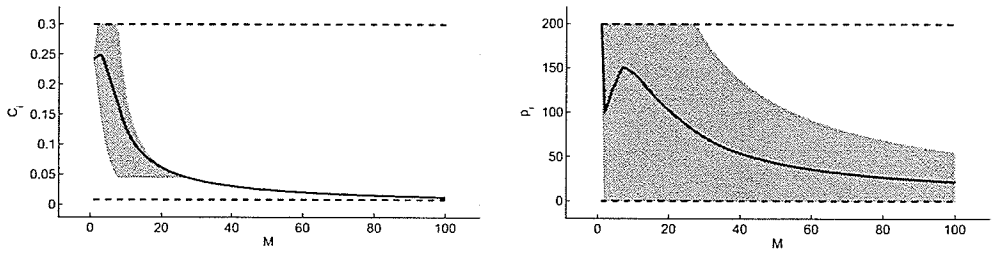

(a) (b)

Figure 5.30: *Parameters of the solution to the NSC^{f-} as M increases from one to a hundred. The dashed lines represent the constraints. In addition, the solid line shows the mean value and the shaded area indicates the range of variation . (a) Capacity. (b) Transmission power.*

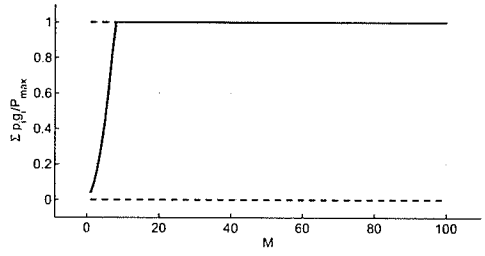

Figure 5.31: *Aggregate received power divided by P_{max} for the solution to the NSC^{f-} as M increases from one to a hundred.*

converges to the minimum guaranteed one. Also, looking at the shaded region, which shows the range of the elements of $\vec{\mathbf{C}}$, when there are thirty or more mobile stations in the cell, all the mobile station transmit at approximately the same capacity. This means that the power received from any mobile station at the base station will be approximately identical. Note that as Figure 5.30–(b) shows, the transmission powers of the mobile stations undergo a similar transformation. Also, looking at Figure 5.31, it is inferred that that after a certain value of M, the aggregate transmission power equals the maximum allowed value. However, it is worth to mention that this is not always the case, as assumed in some works.

To give a comparison between the NSC^{f-} and the NSC, Figure 5.29–(b) shows the values of unfairness for different values of M. It is worth to mention that while in the NSC^{f-} unfairness is always less than four and tends to one as M increases, in the CSC, the unfairness starts from a

few hundreds and converges to values around fifty. In this respect, the NSC shows more practical figures of about twenty, but it does not ever touch values around unity, i.e. total fairness. The dashed line in Figure 5.29–(b) shows the maximum unfairness calculated using (3.166). Note that the estimation is conservative, partly because there is never a pair of mobile stations being served at minimum and maximum simultaneously, as also seen in Figure 5.30–(a).

We argue that the fairness of the solution to the NSC^{f-} is essentially the result of the structure of $\vec{\mathbf{x}}$, as given in (3.151). Note that, compared to the cases of the CSC, the NSC, and the N^{+}SC, in which the mobile stations tended to produce a disperse pattern of transmission powers, the approach to maximizing the aggregate capacity in the NSC^{f-} is through pushing the transmission powers close to each other.

To analyze the behavior of the NSC^{f-} in a dynamic setting, an experiment was carried out to investigate the situation in which M mobile stations move around in a cell. The details of this experiment are as discussed in Section 5.2 and Figure 5.20–(a) and 5.20–(b), except for the fact that here $T = 200s$ is used (the pattern of movements is shown in Figure 5.32). Note that, while the system is sampled every $100ms$, the NSC^{f-} takes less than $10ms$. Thus, processor utilization is less than 10%. Figure 5.33 shows the transmission powers and the capacities of the mobile stations during the simulation.

Figure 5.34 shows how different parameters of the system change over time. We emphasize that as seen in Figure 5.34–(c), the aggregate transmission power is about half the given maximum bound. Also, according to Figure 5.34–(b), the unfairness of the system is far below the maximum bound. Figure 5.35 shows how the capacity shares of different mobile stations change during the simulation time.

5.6 Multiple–Class Systems (MSC)

In order to evaluate the performance of the M^{1}SC and the M^{2}SC, in comparison to each other as well as to the exact method, namely the NSC, first, a cell containing 15 mobile stations, as shown in Figure 5.36–(a), is considered (Here, we use system parameters as defined in Section 1.1, except for $P_{max} = -113dBm$).

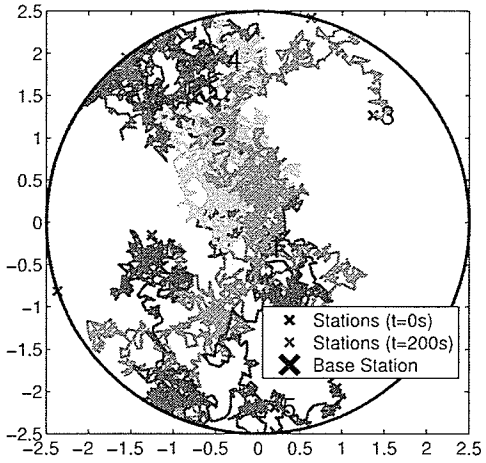

Figure 5.32: *Pattern of movement of the mobile stations used in dynamic simulation of the NSC^{f-}.*

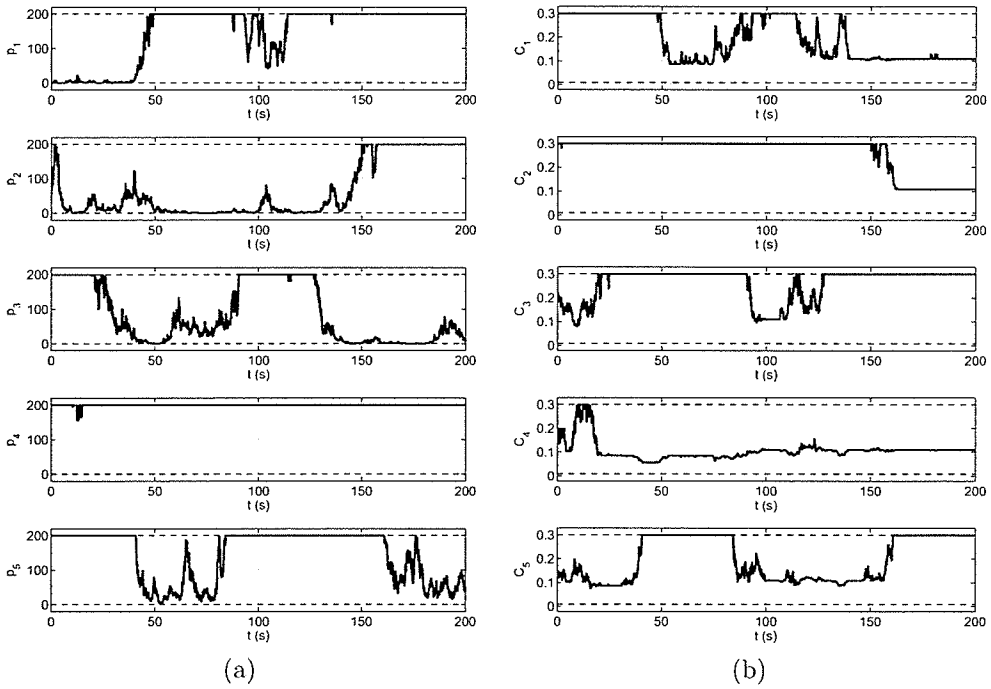

Figure 5.33: *Transmission powers and capacities of different mobile stations over time in the dynamic simulation of the NSC^{f-}. (a) Transmission powers. (b) Capacities.*

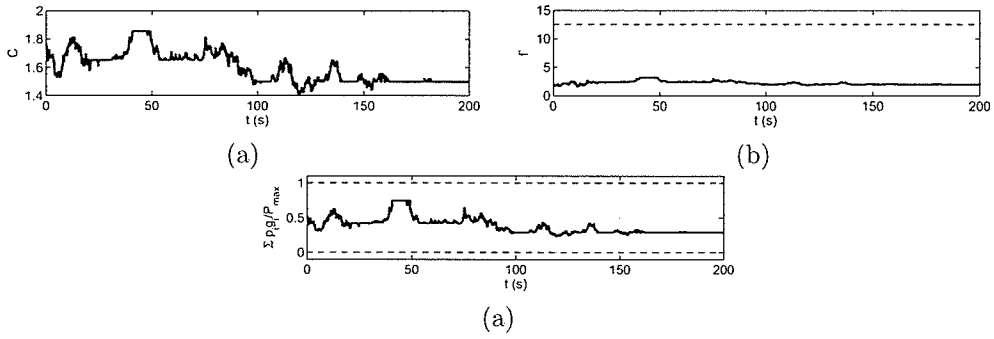

Figure 5.34: *Parameters of the solution to the NSC^{f-} during the simulation. (a) Aggregate capacity. (b) Unfairness. (c) Aggregate transmission power divided by P_{max}.*

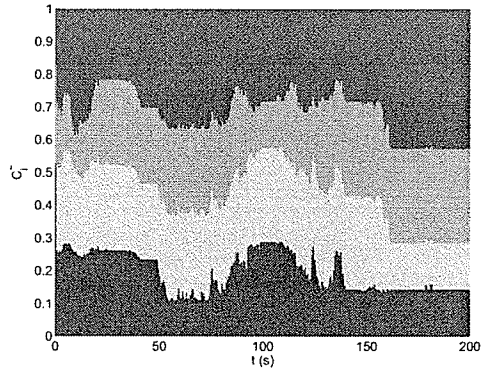

Figure 5.35: *Capacity shares of the mobile stations during the dynamic simulation of the NSC^{f-}.*

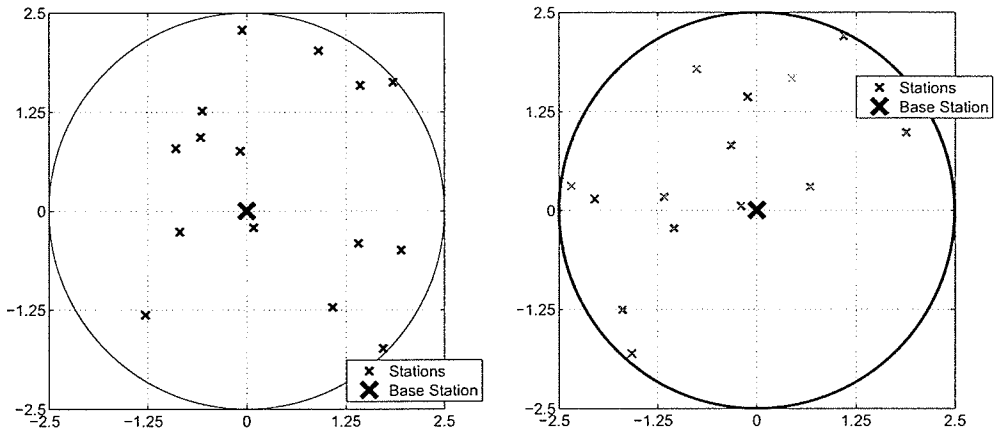

Figure 5.36: *Sample MSC problems defined in* 15*-mobile station cells. (a)* $\vec{\alpha} = \vec{1}$*. (b) The elements of* $\vec{\alpha}$ *have accepted values other than one. These values are visualized using different shades of gray.*

In order to be able to apply the NSC and the proposed algorithms on the same problem, we set $\alpha_i = 1$, $\gamma_i^{min} = \gamma$, $C_i^{max} = \eta$, and $p_i^{max} = p_{max}$, for all the mobile stations. Doing so, we are using the fact the NSC solves a special cases of the problems the M^1SC and the M^2SC are able to work on.

It takes $8.6ms$ for the NSC to produce a solution to the given problem. Using the first-order approximation, the M^1SC solves the same problem in $26.6ms$ and the M^2SC, which is based on a second-order approximation, takes $23.4ms$. Therefore, using the second-order approximation results in more than 10% decline in the computational complexity of the solver. Similar observation is made for problems with different sizes and locaitons of mobile stations. It is worth to mention that the application of the approximations almost triples the computational complexity. This is mainly due to the fact that the exact algorithms go through a list of candidate points (see Section 3.1), whereas the approximate algorithms use numerical search at their core. Nevertheless, the approximations enable us to solve the problem in a multiple-class framework, a scenario which is out of the scope of the exact algorithms.

Comparison of the aggregate capacity values generated by the three problems, we observe values of $C = 0.735$, $C = 0.734$, and $C = 0.735$, are produced by the NSC, the M^1SC, and

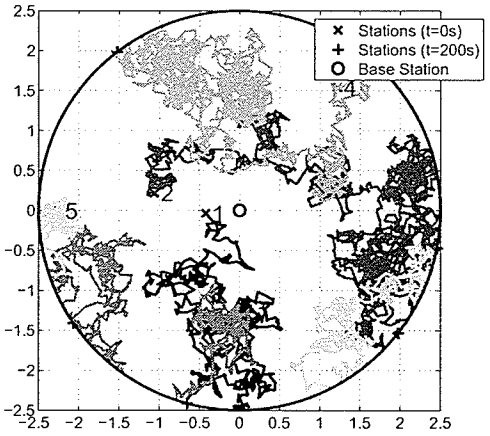

Figure 5.37: *Pattern of movement of the mobile stations used in the dynamic analysis of the M^2SC.*

the M^2SC, respectively (values are relative). The more accurate result of the M^2SC is notable. Numerically, the M^1SC has caused 0.16% error in the aggregate capacity whereas the M^2SC is accurate up to four decimal places.

Comparing the M^1SC with the exact algorithm, the mean deviation in values of p_i is 11.50%, in which case the minimum deviation is 0.08% and the maximum one is 52.08%. Similar figures are observed for values of C_i (mean of 11.70%, minimum of 0.085% and maximum of 53.00%). Analyzing the solution generated by the M^2SC, however, the deviation in the elements of $\vec{\mathbf{p}}$ and $\vec{\mathbf{C}}$ is zero per cent up to four decimal places.

In the next experiment, the performance of the two algorithms, the M^1SC and the M^2SC, in a truly multiple-class system are compared. In order to do so, a sample problem is generated, as shown in Figure 5.36-(b). Here, darkness of each mobile station demonstrates its corresponding value of α_i (the darker a mobile stations is, the higher the corresponding value of α_i is). Using the M^1SC, it takes about $29.7ms$ to solve this problem, whereas the M^2SC demands $28.1ms$ to find the solution to the same problem (about 5% less). Furthermore, there is 1.09% difference between the aggregate capacity values calculated by the two algorithms.

Based on the results stated in the above, another experiment is carried out in order to analyze the behavior of the M^2SC in a simulation which spans a given period of time. In this experiment,

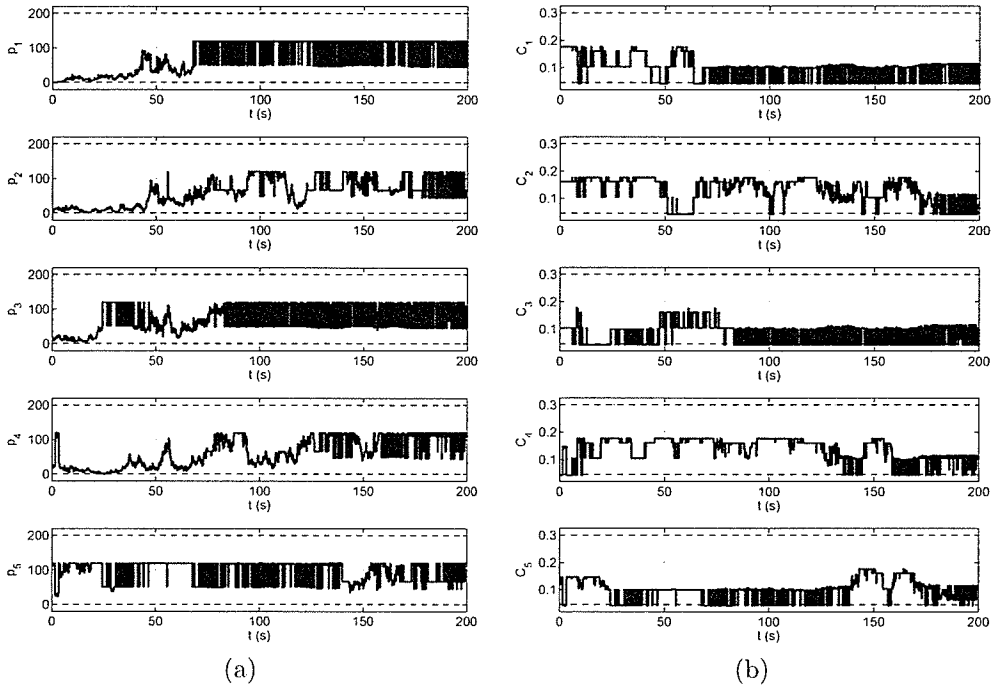

Figure 5.38: *Transmission powers and the capacities of different mobile stations over the time in the dynamic M^2SC experiment. (a) Transmission powers. (b) Capacities.*

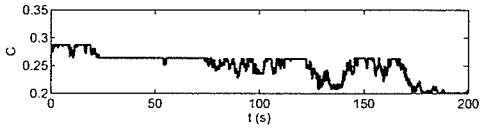

Figure 5.39: *Aggregate capacity during the M^2SC experiment.*

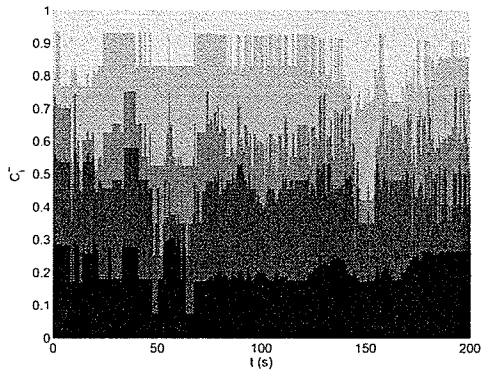

Figure 5.40: *Capacity shares of the mobile stations during the M^2SC experiment. Each shade of gray represents one mobile station.*

the movements of $M = 5$ mobile stations in a cell are simulated and the corresponding problems are solved. Here, the movements are modeled using a discrete random walk with the speed at each moment chosen based on a uniform random variable between zero and $5km/h$ ([124]). Here, we assume that no mobile station leaves the cell or enters it. In this setting, the system is analyzed in the time period of $T = 200s$, during which the resulting problem is solved every $dt = 100ms$. Figure 5.37 shows the random walk of the mobile stations during the experiment. The solutions produced for all the corresponding problems are aggregated in Figure 5.38. Here, each row represents one mobile station. The graphs on the left present the transmission powers of the mobile stations during this time period while the graphs to the right show the regarding capacities. Figure 5.39 shows the aggregate capacity of the system during the experiment and, finally, Figure 5.40 presents the capacity shares of the mobile stations during this experiment.

5.7 Generalized Multiple–Class Systems ($MSC^{\alpha\nu L_i}$)

This section holds the experimental results generated through using the proposed $MSC^{\alpha\nu L_i}$ algorithm. Here, we use the system parameters as discussed previously, except for $P_{max} = -113dBm$ and $\mu = 0.5$. Here, we have used $L = 100$ and $\alpha = 1$ as well.

As the first experiment, here, we go through the process of solving a sample $MSC^{\alpha\nu L_i}$ using the proposed method, as shown in Table 5.6. While the first two rows in this Table denote

the path gains in the sample problem, the transformation section in this table represents the material discussed in Section 3.6.3. It is worth to mention that all the values of ρ_i calculated in this problem, through using the exact formulation given in (3.208), are close to the 0.9225 approximation produced by (3.209). These values are used to generate the imaginary MSC* problem, the solution to which is carried in Table 5.6 as well. Note that, here, the values of $\chi_i \rho_i \hat{C}_i$ are mentioned, because based on (3.199) these values are what approximate the elements of $\vec{\mathbf{C}}$.

After the imaginary MSC* is solved, the corresponding values of p_i are exactly the transmission powers of the approximate solution to the original $MSC^{\alpha\nu L_i}$. The values of C_i, however, are recalculated, as shown in Table 5.6, thus leading to the recalculation of the aggregate capacity, C. As visible in Table 5.6, the values of $\chi_i \rho_i \hat{C}_i$ approximate the elements of $\vec{\mathbf{C}}$ within a less than 5% range of relative error. The aggregate capacity approximated by the imaginary problem is less than 3% off, as well. In the given framework, the code has taken $78ms$ to produce the presented solution.

Based on the results stated in the above, another experiment is carried out in order to analyze the behavior of the problem in a dynamic setting which spans a given period of time. In this experiment, the movements of $M = 5$ mobile stations in a cell are simulated and the corresponding problems are solved. Here, the movements are modeled using a discrete random walk with the speed at each moment chosen based on a uniform random variable between zero and $5km/h$ [124]. The underlying assumption of this experiment is that no mobile station leaves the cell or enters it.

In this setting, the system is analyzed in a time span of $T = 200s$, during which the resulting problem is solved every $dt = 100ms$. Figure 5.41 shows the random walk of the mobile stations during the experiment and the solutions produced for all the corresponding problems are aggregated in Figure 5.42. Here, each row represents one mobile station. The graphs on the left present the transmission powers of the mobile stations in the given time span while the graphs to the right show the regarding capacities. Note the different values of p_i^{max} and C_i^{max} for different mobile stations. Figure 5.43 shows the aggregate capacity of the system during the

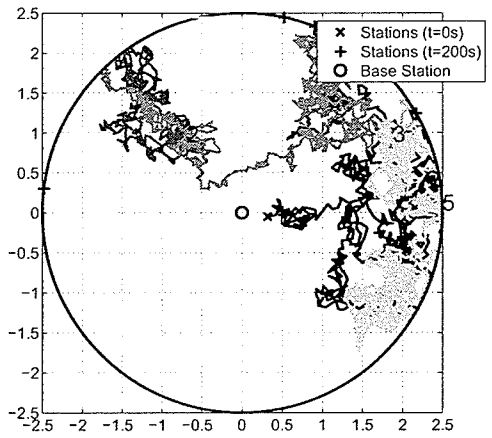

Figure 5.41: *Pattern of movement of the mobile stations used in the dynamic analysis of the* $MSC^{\alpha\nu L_i}$.

experiment and, finally, Figure 5.44 presents the capacity shares of the mobile stations during this experiment. Note that Figure 5.44 in fact shows the values of $\alpha_i \tilde{C}_i$.

5.8 Multiple–Cell Systems (MC)

In this section, we demonstrate two sets of experimental results gathered by solving sample MC problems using the proposed method. Here, first, the solution to a sample problem is presented and then analyzed in detail. Then, another system working under the same conditions is analyzed as the mobile stations move and cross the cell boundaries in the window of a known time period. The twin experiments are geared towards presenting the performance of the proposed method in both static and dynamic situations. Note that, running non-optimized code, solving the problem in a 5–cell problem which contains 50 mobile stations takes up about 1.2 seconds.

Here, we select the values of the parameters as denoted previsouly, except for C, for which the smaller value of 0.01 is adopted in order to increase the range for the elements of $\vec{\mathbf{p}}$ (see (1.25)). Also, the base stations are initially placed on a rectangular grid of size,

$$\left\lceil \sqrt{K} \right\rceil \times \left\lceil \frac{K}{\left\lceil \sqrt{K} \right\rceil} \right\rceil . \tag{5.14}$$

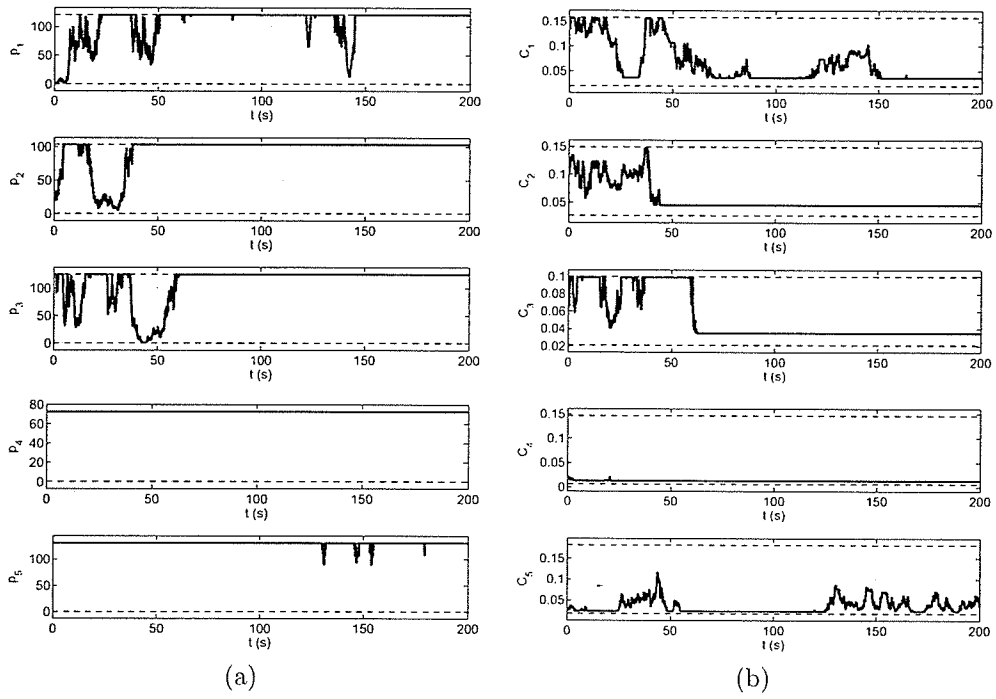

Figure 5.42: *Transmission powers and the capacities of different mobile stations over the time in the dynamic $MSC^{\alpha\nu L_i}$ experiment. (a) Transmission powers. (b) Capacities.*

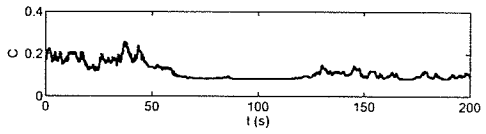

Figure 5.43: *Aggregate capacity during the experiment with the $MSC^{\alpha\nu L_i}$.*

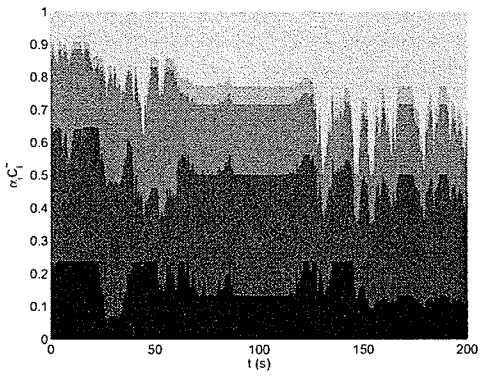

Figure 5.44: *Capacity shares of the mobile stations during the experiment with the* MSC^{avL_i}. *Each shade of gray represents one mobile station.*

and then altered along the two axes according to two independent uniform distributions. Subsequently, the mobile stations are placed according to a two-dimensional uniform distribution on the area designated by the base stations. Each mobile station is assigned to one base station at any moment and the borders of the cells are calculated.

The parameters used in this study not mentioned in previous sections are $\gamma = -25dB + 20log_{10}L$ and $P_{max} = -113dBm$ [112] plus $C_{max} = 1.3$ and $L = 16$. The regarding parameters for the individual cells and mobile stations follow uniform normal distributions with the given mean.

Figure 5.45 shows a sample 3-cell problem containing 12 mobile stations. The solution calculated by the proposed method for this problem is presented in Figure 5.46.

In Figure 5.46, the values of p_{ki} and C_{ki} corresponding to each mobile station are shown. The title of the figure shows the regarding values of C and $\tilde{f}$ as well. Note that here $\tilde{f} = 1.42$, exhibiting that the highest capacity offered in the system is only 42% more than the lowest in the same system. This is a direct result of the implementation of the maximum capacity constraint. The advantagous limiting effects of the maximum capacity constraint on the unfairness of the solution have been observed for single-cell systems as well (see Section 5.2).

Here, we analyze the solution shown in Figure 5.46 in detail. In this solution, the aggregate received power in the three cells equals 23%, 29%, and 31% of the corresponding values of P_k^{max}.

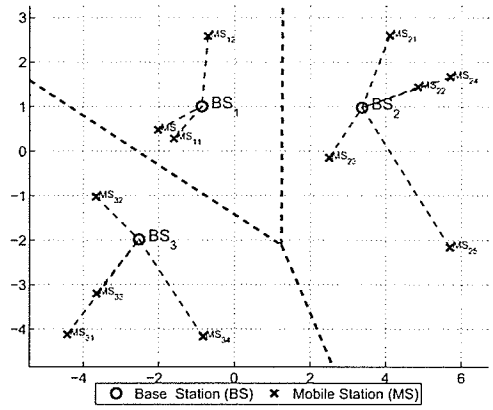

Figure 5.45: *Sample problem to be solved by the MC.*

Furthermore, the tramsnission powers of the mobile stations fall within the range of from 2% to 65% of what is allowed by the corresponding values of p_{ki}^{max}. In fact p_{23} is about 1.8% of p_{23}^{max} because of the relative closeness of the corresponding mobile station to the regarding base station and the better reception of its transmitted signal (the high value of g_{23}). On the contrary, MS_{22} and MS_{25} are transmitting at 65% and 52% of their allowed maximum transmission powers. While the condition for MS_{25} is mainly due to its larger distance to the corresponding base station, MS_{22} is experiencing a deep fade.

The regarding values of C_{ki}, on the other hand, demonstrate a maximum overshoot of 9% over the designated values of C_{ki}^{max}. This is due to the error induced by the use of the approximations. Among these sources of error is that while the loading factor is assumed to be equal to 0.55, direct calculation in fact produces values of 0.122, 0.000, and 0.177 for the three cells. Note that, in this experiment, the second cell is on a separate frequency band while the first and the third cells share the same band. The SIR of no mobile station in this experiment falls below the designated minimum SIR limit (all the elements of $\vec{\mathbf{g}}$ are at least 40% above their corresponding values of γ_{ki}^{min} in this experiment).

In the second experiment, a set of 12 mobile stations are placed in a 3-cell system. The resulting system is then analyzed in a 200s time period, during which the capacity maximization problem is solved every $\delta t = 200ms$. In this experiment the mobile stations move at the speed

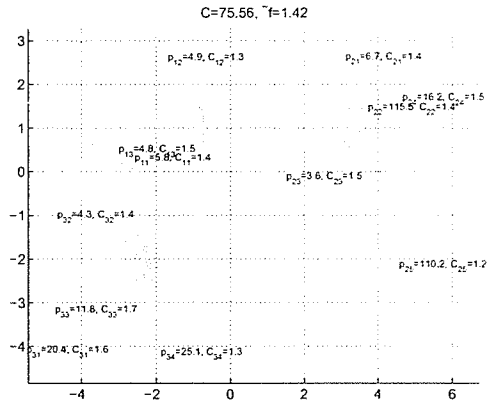

Figure 5.46: *The solution produced by the MC for the sample problem shown in Figure 5.45. Refer to the text for the analysis of this solution.*

of $36km/h$ [83]. Note that as the system is solved at the rate of $5Hz$, the values of Y_σ are regenerated at each refresh.

Figure 5.47 shows the produced problem. Here, three mobile stations undergo hand-offs. Note that as the base station to which each mobile station is communicating may change during the experiment, the double indexing of the mobile stations, as MS_{ki}, is not consistent during the time period of interest. Therefore, we label the mobile stations as one to twelve. Equivalently, double-indexing will be used for referring to mobile stations, in which case the indexes denote the status of the regarding mobile station at the end of the experiment.

Figure 5.48 shows the optimal transmission powers of the mobile stations as produced by the proposed method. In each graph, the two dashed lines indicate the bounds (enforced through the maximum and minimum transmission constraints). Note that in spite of the utilized approximations, including the assumption of the existence of a constant loading factor, the proposed algorithm is well capable of keeping the transmission powers inside the allowed range. As an example of the regulation of the transmission powers, note the rise in the transmission power of the third mobile station (MS_{22}) as its distance to the second base station increases. On the contrary, MS_{31} travels at almost the same distance to the third base station and thus exhibits an almost constant transmission power.

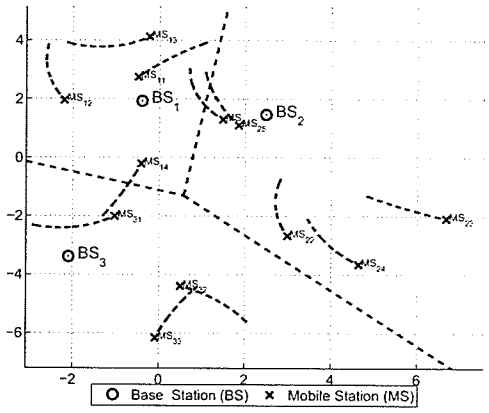

Figure 5.47: *Sample system investigated during a 200-second period to be solved by the MC.*

Figure 5.49 shows the capacity at which the mobile stations transmit, after they set their transmission powers as designated by the values shown in Figure 5.48. This figure shows that the approximations result in the capacities overshooting the allowed maximum capacities. In fact, in the implementation, a maximum error of 10% is set as the hard cut-off criterion for the integrity of the proposed method. Therfore, as each approximation is only valid within the ranges specified previously, these thresholds, as well as the other one on the accuracy of the aggregate capacity, act as validity checks for the proposed method. Nevertheless, note that the capacities do not exhibit the monopoly of capacity commonly observed in the classical formulation of the problem. The capacities do obey the maximum capacities within an acceptable range as well.

Finally, Figures 5.50–(a) and 5.50–(b) present the aggregate capacity of the system and the regarding values of ratio unfairness during the experiment. Note that as figure 5.50–(b) shows, the system normally operates within the range of $\tilde{f} = 1.2$ to $\tilde{f} = 1.6$. This shows that the highest capacity offered in the system is normally less than 60% more than the lowest in the same system.

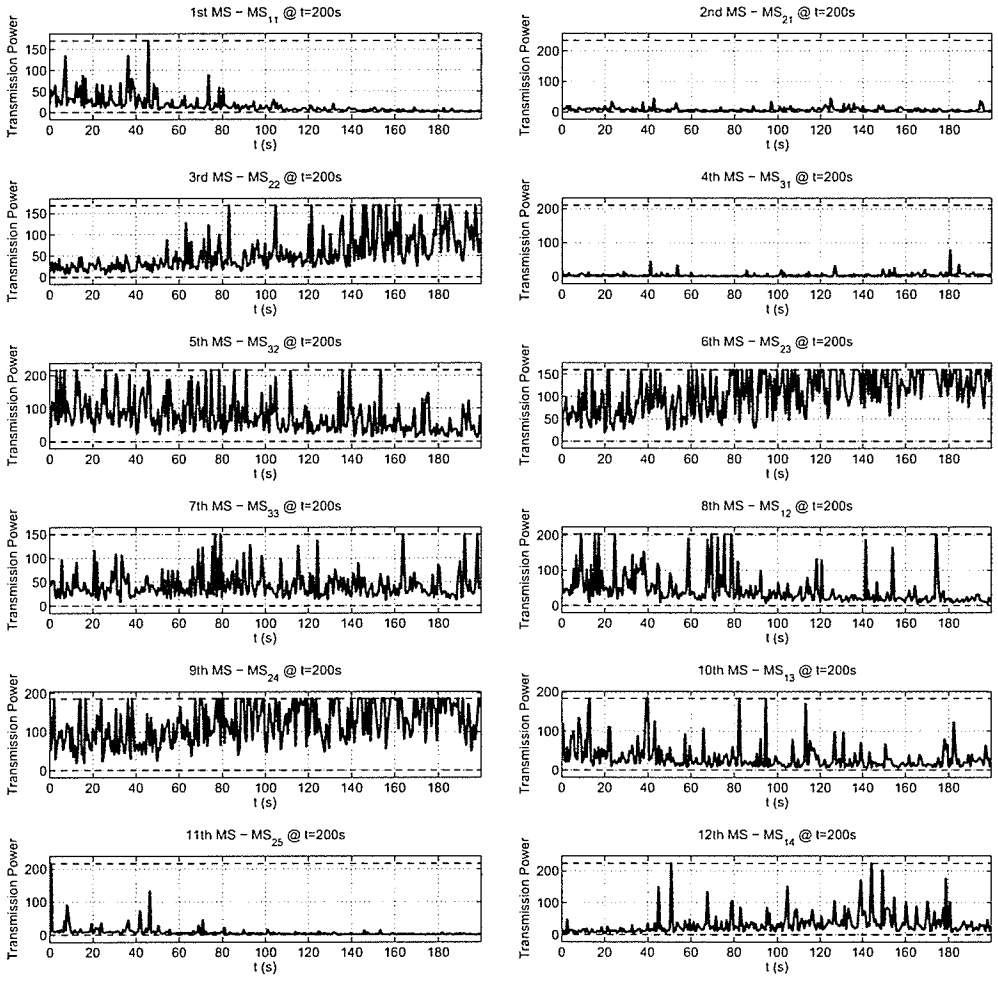

Figure 5.48: *Optimal transmission powers of the mobile stations as produced by the MC. Refer to the text for the analysis of this solution.*

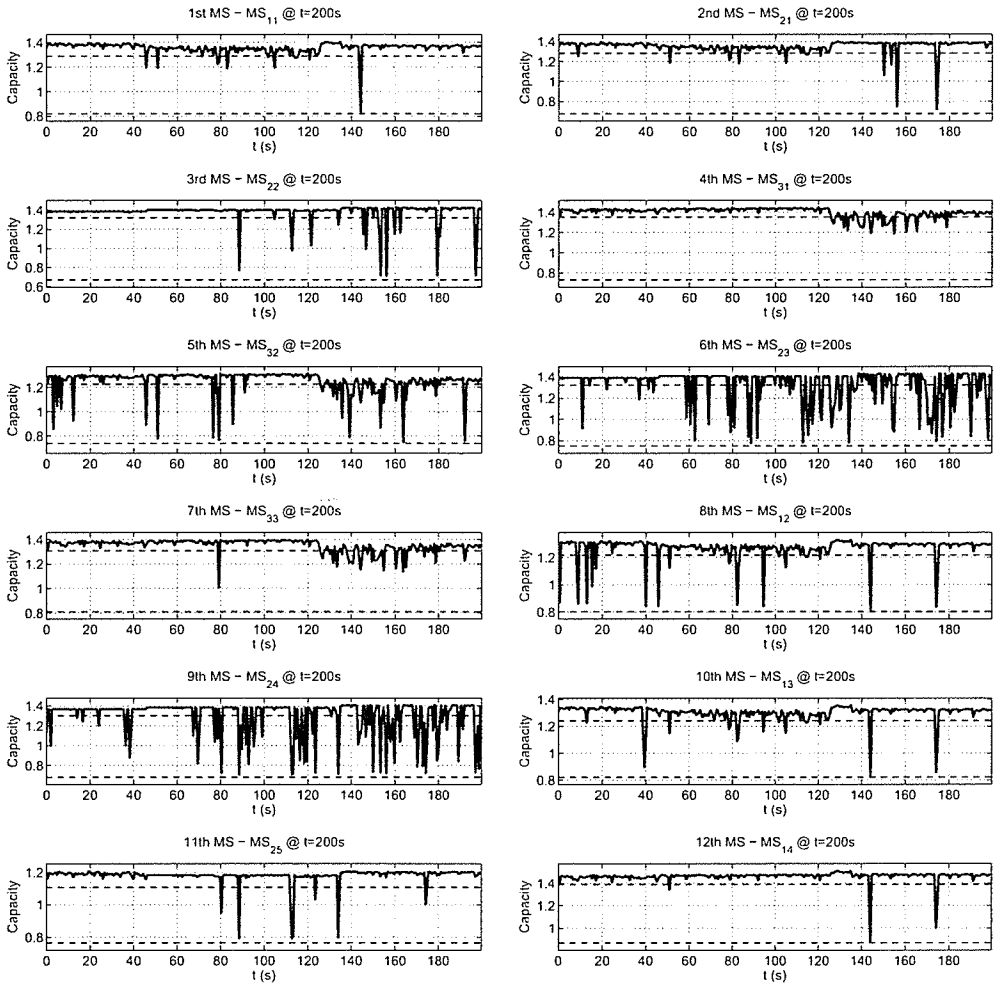

Figure 5.49: *Capacities of the mobile stations as produced by the MC. Refer to the text for the analysis of this solution.*

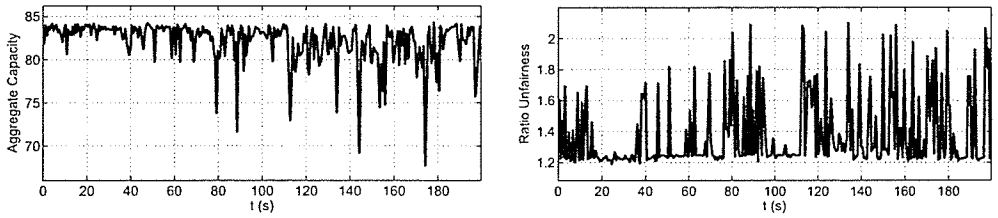

Figure 5.50: *System parameters as produced by the MC. (a) Aggregate capacity. (b) Unfairness.*

Table 5.1: Comparison of the CSC with the NSC. The row P denotes the pattern of the solution. Here, the symbols x and X denote that the corresponding mobile station is transmitting at the minimum and the maximum guaranteed capacities, respectively. Also, b and l denote that x_i is inside the allowed interval or equals l_i, respectively.

MS#		1	2	3	4	5	6	7	8	9	10
g_i ($\times 10^{-12}$)		0.52	0.018	0.016	0.0091	0.0082	0.0081	0.0075	0.0059	0.0059	0.0045
	P	b	x	x	x	x	x	x	x	x	x
	p_i	46.527	5.211	5.855	10.439	11.626	11.756	12.617	16.053	16.198	20.916
CSC	C_i	2.3606	0.0046	0.0046	0.0046	0.0046	0.0046	0.0046	0.0046	0.0046	0.0046
	$\tilde{C}_i$	98.2%	0.2%	0.2%	0.2%	0.2%	0.2%	0.2%	0.2%	0.2%	0.2%
		$C = 2.402$, $f = 2.356$, $\tilde{f} = 518.2$									
	P	X	l	l	l	l	l	l	l	l	b
	p_i	14.662	16.092	16.189	16.584	28.796	36.313	50.000	13.744	14.535	18.984
NSC	C_i	0.3000	0.2111	0.1863	0.1015	0.0908	0.0898	0.0835	0.0652	0.0646	0.0498
	$\tilde{C}_i$	24.1%	17.0%	15.0%	8.2%	7.3%	7.2%	6.7%	5.2%	5.2%	4.0%
	C	$C = 1.243$, $f = 0.2502$, $\tilde{f} = 6.027$									

Table 5.2: Comparison of the N^+SC with the CSC and the NSC. Refer to the caption of Table 5.1 for the definition of pattern identifiers.

MS#		1	2	3	4	5	6	7	8	9	10
g_i ($\times 10^{-11}$)		0.2	0.016	0.0099	0.0044	0.002	0.0018	0.0013	0.00089	0.00056	0.00049
	P	b	x	x	x	x	x	x	x	x	x
	p_i	11.33	1.86	3.02	6.79	14.63	16.21	22.80	33.39	53.60	60.93
	C_i	1.9689	0.0144	0.0144	0.0144	0.0144	0.0144	0.0144	0.0144	0.0144	0.0144
CSC	$\tilde{C}_i$	93.8%	0.7%	0.7%	0.7%	0.7%	0.7%	0.7%	0.7%	0.7%	0.7%
	$\tilde{p}_i$	89.3%	1.2%	1.2%	1.2%	1.2%	1.2%	1.2%	1.2%	1.2%	1.2%
		$C = 2.098$, $f = 1.955$, $\tilde{f} = 137.155$, $t = 0.6ms$									
	P	X	X	X	X	b	x	x	x	x	x
	p_i	2.86	35.22	57.30	128.81	49.01	16.21	22.80	33.39	53.60	60.93
	C_i	0.3000	0.3000	0.3000	0.3000	0.0487	0.0144	0.0144	0.0144	0.0144	0.0144
NSC	$\tilde{C}_i$	22.7%	22.7%	22.7%	22.7%	3.7%	1.1%	1.1%	1.1%	1.1%	1.1%
	$\tilde{p}_i$	22.5%	22.5%	22.5%	22.5%	4.0%	1.2%	1.2%	1.2%	1.2%	1.2%
		$C = 1.320$, $f = 0.286$, $\tilde{f} = 20.898$, $t = 5.6ms$									
	P	X	X	X	X	X	l	b	x	x	x
	p_i	1.90	23.46	38.17	85.79	184.78	199.53	130.86	33.39	53.60	60.93
	C_i	0.1927	0.1927	0.1927	0.1927	0.1927	0.1875	0.0844	0.0144	0.0144	0.0144
N^+SC	$\tilde{C}_i$	15.1%	15.1%	15.1%	15.1%	15.1%	14.7%	6.6%	1.1%	1.1%	1.1%
	$\tilde{p}_i$	15.0%	15.0%	15.0%	15.0%	15.0%	14.6%	6.8%	1.2%	1.2%	1.2%
		$C = 1.279$, $f = 0.178$, $\tilde{f} = 13.425$, $t = 7.2ms$									

Table 5.3: Investigating the properness of the approximation for the CSC^a, the NSC^a, and the N^+SC^a. The values in parentheses show relative error. Approximate values are shown in bold.

MS#		1	2	3	4	5	6	7
g_i ($\times 10^{-11}$)		0.11	0.031	0.0067	0.0018	0.0011	0.00069	0.00052
CSC	p_i	21.13	0.96	4.45	16.51	25.96	43.20	57.23
	γ_i	3.43	0.01	0.01	0.01	0.01	0.01	0.01
	$\hat{p}_i$	0.77	0.01	0.01	0.01	0.01	0.01	0.01
	C_i	2.14	0.01	0.01	0.01	0.01	0.01	0.01
	C_i^a	**1.98** (8%)	**0.01** (0%)	**0.01** (0%)	**0.01** (0%)	**0.01** (0%)	**0.01** (0%)	**0.01** (0%)
		$C = 2.23$, $C^a =$ **2.07** (7%)						
NSC	p_i	5.12	18.11	84.46	199.53	199.53	199.53	167.38
	γ_i	0.23	0.23	0.23	0.14	0.08	0.05	0.03
	$\hat{p}_i$	0.19	0.19	0.19	0.12	0.08	0.05	0.03
	C_i	0.30	0.30	0.30	0.18	0.11	0.07	0.04
	C_i^a	**0.32** (7%)	**0.32** (7%)	**0.32** (7%)	**0.19** (5%)	**0.12** (3%)	**0.07** (2%)	**0.04** (1%)
		$C = 1.31$, $C^a =$ **1.39** (6%)						
N^+SC	p_i	4.52	15.98	74.50	199.53	199.53	199.53	199.53
	γ_i	0.21	0.21	0.21	0.15	0.09	0.05	0.04
	$\hat{p}_i$	0.18	0.18	0.18	0.13	0.08	0.05	0.04
	C_i	0.28	0.28	0.28	0.20	0.12	0.07	0.05
	C_i^a	**0.30** (7%)	**0.30** (7%)	**0.30** (7%)	**0.21** (5%)	**0.13** (4%)	**0.07** (2%)	**0.05** (2%)
		$C = 1.28$, $C^a =$ **1.36** (6%)						

Table 5.4: Investigating the properness of the approximation utilized in the CSC^n, the NSC^n, and the N^+SC^n.

MS#			1	2	3	4	5	6	7
g_i ($\times 10^{-11}$)			0.4	0.0051	0.0038	0.0019	0.0014	0.0008	0.00052
CSC^a	E	p_i	*5.77*	*5.90*	*7.85*	*16.02*	*21.28*	*37.19*	*57.24*
		C_i	*2.15*	*0.01*	*0.01*	*0.01*	*0.01*	*0.01*	*0.01*
		C				*2.23*			
	A	p_i^a	5.77 (0%)	5.90 (0%)	7.85 (0%)	16.02 (0%)	21.28 (0%)	37.19 (0%)	57.24 (0%)
		C_i^a	1.98 (8%)	0.01 (0%)	0.01 (0%)	0.01 (0%)	0.01 (0%)	0.01 (0%)	0.01 (0%)
		C^a				2.07 (8%)			
	A+E	$C_i^{a\star}$	**2.15 (0%)**	**0.01 (0%)**	**0.01 (0%)**	**0.01 (0%)**	**0.01 (0%)**	**0.01 (0%)**	**0.01 (0%)**
		$C^{a\star}$				**2.23 (0%)**			
NSC^a	E	p_i	*1.40*	*111.86*	*148.95*	*199.53*	*199.53*	*166.60*	*57.24*
		C_i	*0.30*	*0.30*	*0.30*	*0.19*	*0.14*	*0.06*	*0.01*
		C				*1.31*			
	A	p_i^a	1.40 (0%)	111.86 (0%)	148.95 (0%)	199.53 (0%)	199.53 (0%)	166.60 (0%)	57.24 (0%)
		C_i^a	0.32 (7%)	0.32 (7%)	0.32 (7%)	0.20 (5%)	0.15 (4%)	0.07 (2%)	0.01 (0%)
		C^a				1.39 (6%)			
	A+E	$C_i^{a\star}$	**0.30 (0%)**	**0.30 (0%)**	**0.30 (0%)**	**0.19 (0%)**	**0.14 (0%)**	**0.06 (0%)**	**0.01 (0%)**
		$C^{a\star}$				**1.31 (0%)**			
N^+SC^a	E	p_i	*1.33*	*106.43*	*141.72*	*199.53*	*199.53*	*199.53*	*164.49*
		C_i	*0.28*	*0.28*	*0.28*	*0.19*	*0.14*	*0.08*	*0.04*
		C				*1.30*			
	A	p_i^a	1.33 (0%)	106.43 (0%)	141.72 (0%)	199.53 (0%)	199.53 (0%)	199.53 (0%)	164.49 (0%)
		C_i^a	0.30 (7%)	0.30 (7%)	0.30 (7%)	0.20 (5%)	0.15 (4%)	0.08 (2%)	0.04 (1%)
		C^a				1.30 (0%)			
	A+E	$C_i^{a\star}$	**0.28 (0%)**	**0.28 (0%)**	**0.28 (0%)**	**0.19 (0%)**	**0.14 (0%)**	**0.08 (0%)**	**0.04 (0%)**
		$C^{a\star}$				**1.30 (0%)**			

Table 5.5: *The case in which the approximation misleads the optimization process utilized within the CSC^a. Bold cases show the selected solutions by the two algorithms.*

Solution		**mobile station 1**				**mobile station 2**				**mobile station 3**				**Total**	
k	x_k	x_1	$\hat{x}_1$	C_1	C_1^a	x_2	$\hat{x}_2$	C_2	C_2^a	x_3	$\hat{x}_3$	C_3	C_3^a	C	C^a
1	0.01	0.01	0.01	0.01	0.01	0.01	0.01	0.01	0.01	0.01	0.01	0.01	0.01	0.043	0.042
1	1.55	1.55	0.60	1.31	1.37	0.03	0.01	0.01	0.01	0.03	0.01	0.01	0.01	1.337	1.402
2	0.03	1.55	0.60	1.31	1.37	0.03	0.01	0.01	0.01	0.03	0.01	0.01	0.01	**1.337**	1.402
2	0.92	1.55	0.44	0.84	0.92	0.92	0.26	0.44	0.48	0.04	0.01	0.01	0.01	1.296	**1.413**
3	0.04	1.55	0.44	0.84	0.92	0.92	0.26	0.44	0.48	0.04	0.01	0.01	0.01	1.296	1.413
3	0.20	1.55	0.42	0.79	0.87	0.92	0.25	0.41	0.45	0.20	0.05	0.08	0.08	1.289	1.402

Table 5.6: *Details of the solution to a 10-mobile station problem produced by the $MSC^{\alpha\nu L_i}$. Refer to the text for more details.*

MS#	1	2	3	4	5	6	7	8	9	10
g_i $(\times 10^{-15})$	2817.589	773.392	53.273	42.138	37.291	17.043	13.934	8.545	5.832	4.764
The Transformation										
χ_i	78.872	64.136	110.728	121.856	98.328	62.782	71.264	126.310	160.278	20.628
ρ_i	0.924	0.924	0.923	0.923	0.923	0.924	0.924	0.923	0.923	0.927
Solution to the Imaginary MSC*										
p_i	0.007	0.024	0.176	0.264	0.488	0.906	2.090	0.972	0.999	13.955
$\chi_i\rho_i\hat{C}_i$	0.152	0.124	0.109	0.142	0.187	0.102	0.218	0.110	0.098	0.144
$C = 0.815$										
Solution to the Original $MSC^{\alpha\nu L_i}$										
p_i	0.007	0.024	0.176	0.264	0.488	0.906	2.090	0.972	0.999	13.955
C_i	0.156	0.129	0.113	0.146	0.190	0.106	0.218	0.114	0.102	0.148
$C = 0.837$										
Relative Error										
C_i	2.516%	3.428%	3.968%	2.878%	1.367%	4.185%	0.377%	3.944%	4.359%	2.668%
C	2.634%									

Chapter 6

Conclusions

This chapter contains a summary of the work done in this thesis on the issue of the maximization of the capacity of the reverse link in CDMA systems. This research is based on the mathematical models developed in Chapters 2, 3, and 4. The experimental analysis of the developed methods is presented in Chapter 5.

The focal point of this research is the optimization of the aggregate capacity of the reverse link in a CDMA system. The formulations and the models used in this thesis capitalize on previously published results which indicate that the dimension of the search space of the problem can be efficiently decreased. One of the contributions of this research is that it eliminates the need for numerical search in most cases and yields closed–form solutions in many instances. Also, this thesis proposes solvers for problems not solvable by the previous approaches.

In the first stage, a new methodology is developed, based on which a closed-form solver algorithm for an existing problem is proposed. This problem is addressed as the classical problem in the text (CSC in short). Performance of the proposed solver for different sets of parameters is investigated and extensive computational cost analysis is given. As a result, it is shown that the proposed method is superior, both in terms of the computational complexity as well as the accuracy of the solution. It is found out, however, that in compliance with the available reports by other researchers, the solution to the CSC can potentially be vastly unfair towards the majority of the mobile stations, for the benefit of one "elite" mobile station.

In the next step, and in order to find a solution for the issue of the unfairness of the solution, a maximum capacity constraint is added to the problem. The resulting problem, which is referred to as the NSC in text, is then solved by using a methodology similar to the one developed for the CSC. Also, it is shown that the inclusion of the new constraint in the problem increases the computational cost of the solver from $O(M^2)$ to $O(M^3)$. Here, M is the number of the mobile stations. Subsequently, based on extensive experimental results, the performance of the NSC is analyzed and is compared with that of the CSC. This analysis contains cases of static systems, i.e. solving systems at a snapshot, and dynamic ones, i.e. solving a system iteratively as mobile stations move around in a cell. It is observed that the CSC does indeed separate the mobile stations into all but one which are served at the minimum allowed capacity and one elite, the closest mobile station to the base station. That particular mobile station is commonly served at the most possible capacity feasible in the search space. On the contrary, the NSC is observed to distribute the resources between the mobile stations evenly and also to correspondingly increase reliance on the mobile stations as they become closer to the base station. Based on all the collected evidence, it is suggested in this thesis that the incorporation of the maximum capacity constraint into the problem leads to a more practical solution with an affordable increase in the computational complexity. It is noted, however, that the favorable effects of the maximum capacity constraint on the fairness of the system are indirect influences. Therefore, it is suggested that through more explicit control of the fairness of the system better results could be achieved.

Following this line of research, in the next step, a maximum bound for the capacity share of each mobile station is added to the NSC. This new constraint directly limits the share of resources of the system used by each mobile station, therefore inhibiting monopolies of capacity, as commonly observed in the results of the CSC. It is shown that the methodology developed for the CSC and used for the NSC is also applicable to the new problem, which is addressed as the N^+SC for convenience. Through using an approximation, the effect of adding the new constraint to the problem on the performance of the solver is limited to doubling its computational cost, as opposed to increasing its order of complexity, as observed in the transition between the CSC and the NSC.

The solver for the N$^+$SC developed in this thesis capitalizes on an approximation of the aggregate capacity. As the previously suggested algorithms, namely the CSC and the NSC, calculate the aggregate capacity for numerous candidate points, it is suggested that through extending the use of this approximation, reduction in the complexity of the methods already developed in this thesis can be achieved. Before implementing these approximations, the error induced by their use is analyzed and mathematical guarantees for the appropriateness of their application within the framework of the problem are given. Furthermore, it is shown that there is a decrease of one in orders of M in the computational costs of the available algorithms after the approximation is integrated into them. Using examples and numerous safety checks it is observed that beyond a negligible probability, the solver is guaranteed to not generate false results induced by the error of the approximation. To calculate this probability, after running the exact algorithms alongside the ones which use the approximations, for an extensive number of randomly generated problems, the possibility of 5% error in the aggregate capacity being induced by the approximation is estimated to be less than 0.1%. Extensive investigation shows that this error occurs in the case of the classical formulation of the problem, in which the system is capable of becoming very unfair. In fact, the approximation is shown to be vulnerable to monopoly of power. Hence, it is concluded that, in more controlled environments provided by the NSC and the N$^+$SC, the approximation is capable of locating the exact solution while reducing the computational cost by a factor of more than $\frac{1}{5}M$.

In the steps summarized so far, it is assumed that the system operates based on the identity utility function, meaning the system benefits two times if the capacity offered to one mobile station is doubled. In practice, however, there always exists a utility function which maps capacity to revenue or "interest of the operator". Therefore, in the next step, the objective function is rewritten in order to calculate the sum of the utilities of the capacities. Then, it is shown that if the utility function is convex then the developed algorithms work with minor modifications. However, as it is shown next, in the case of a concave utility function, given that it meets a set of conditions, in order to achieve the maximum aggregate capacity the mobile stations have to make their transmission powers as close as possible to each other. This is

in contrast with the case of identity and convex utility functions in which the mobile stations work towards making their transmission powers as far from each other as permitted by the constraints. It is argued that the unfairness of the solution to those problems is primarily a result of this tendency. As anticipated, empirical results show that concave utility functions lead to extensively more fair systems than what is achieved by using convex utility functions. For problems which use concave utility functions, a solver is proposed which may use one-dimensional numerical search in some cases, depending on the values of the system parameters. Nevertheless, the computational complexity of the solver is of second degree, in terms of the number of the mobile stations. It is proved that the developed algorithm locates the global maximum in all cases as well.

After analyzing the incorporation of general utility functions into the problem, the case of multiple-class systems is investigated. It is argued that in practical systems service-providers tend to provide different classes of service, thus setting different bounds in the constraints for different mobile stations. Analysis of this problem is outside the scope of the methods available in the literature and the ones developed earlier in this research. Therefore, a previously proposed approximation is utilized in order to yield first- and second-order approximations of the objective function. Then, using further approximations, the search space is reduced to a set of linear inequalities, thus preparing the framework for the use of linear and quadratic programming. While utilizing a second-degree approximation yields a more accurate outcome, the developed quadratic objective function overestimates the capacities and therefore has the potential of producing spurious results. First-order approximation, on the other hand, is conservative but induces more error. Nevertheless, both algorithms are shown to be well within a 5% error margin. As a result, the approximate algorithms solve a more general problem at the cost of being computationally more demanding, partly due to the potential utilization of numerical optimization in them.

While the different problems discussed above differ in terms of the underlying objective functions or constraints, they are essentially based on the same model for the SIR. This is mainly due to the fact that the mathematical framework which is used inside the majority of

the developed algorithms heavily relies on one particular structure for the SIR model. In the next stage of this research, and in preparation for generalizing the problem to multiple–cell settings, the attention is shifted towards spotting the latest additions to the SIR model available in the literature and then embedding them in the work. Subsequently, and in order to solve the capacity maximization problem which is based on this inclusive SIR model, a set of approximations is proposed. These approximations take in a more advanced problem and generate an imaginary problem which complies with the conventional SIR model used in the classical formulation. In fact, this process approximates a symbol–level capacity maximization problem by a chip–level problem and then applies a slightly generalized version of an algorithm developed earlier in this thesis on it. Details of the approximations and the mathematical guarantees for the range of error caused by their application are presented in the regarding sections. Subsequently, after the imaginary problem is solved, the solution is transformed to one which approximates the solution to the generalized problem. In addition to the mathematical guarantees for the integrity of the developed algorithm, the performance of the proposed solver is empirically examined through presenting a set of experimental results as well.

The last stage of this research is the generalization of the work to the more realistic and the more challenging domain of multiple–cell capacity maximization. In fact, one of the core assumptions of the single–cell analysis of cellular systems, which inherently includes more than one cell, is that the inter–cell interference can be approximated as a constant background noise. Research shows that to be able to exploit the full capacity of the underlying systems this simplistic model has to be revised in favor of the more accurate definition of the capacity which considers a group of cells simultaneously.

In this thesis, the multiple–cell problem is constructed based on the most inclusive SIR model available to the author. Development of the problem also takes advantage of the constraints developed and examined in this research in single–cell settings. Proper utility functions, individually defined for the mobile stations, are included in the formulation as well. Therefore, the methods developed so far are unable to deal with the developed problem and new tools have to be proposed. In doing so, some of the approximations developed for single–cell problems are

reformulated and more approximations are developed. The combination of these approximations has the ability to reduce the complexity of the multiple–cell problem. To do so, these transformations approximate the objective function and the constraints as quadratic and linear forms, respectively. As a result, quadratic programming becomes applicable to the developed multiple–cell problem. Subsequently, after the resulting quadratic programming problem is solved, proper transformation for acquiring the transmission powers from the set of intermediate decision variables utilized in the procedure is devised. The proposed algorithm also includes a validity check in order to guarantee that the utilized approximations do not yield spurious results.

The performance of the proposed multiple–cell method is examined through the use of experimental results. This examination includes the analysis of a static system, in which the bounds of the error caused by the utilized approximations are discussed as well. Then, a dynamic scenario is investigated, in which a number of mobile stations move inside a multiple–cell system, thus undergoing hand–offs and other variations. The presented experimental results as well as the theoretical analysis exhibit the performance of the proposed method in solving the capacity maximization problem in true multiple–cell systems.

As outlined in this chapter, this thesis performs a step-by-step analysis of the capacity maximization in the reverse link of a CDMA system. At each step, one aspect of the model or the developed solver is examined and new improvements are made. These improvements include the addition of new constraints in order to yield better solutions, the employment of new approximations in order to reduce the computational complexity of the solver, and the addition of new features to the underlying model, among others. This research starts off from a classical definition of the problem in a single–cell system where all the stations are treated equally, both in terms of the constraints and their significance to the system. The problem is gradually equipped with more personalization of the system as well as a more realistic modeling. At the end of this research, the system is investigated in a true multiple–cell multiple–class form. Elaborate attention is also made to providing theorems and techniques which ease the addition of new features to the system.

Acknowledgments

This thesis would have not came into existence if it was not for the constant support I received from my advisor Prof. Attahiru Sule Alfa. He helped me throughout my studies as a Ph.D. student in University of Manitoba, both academically and also personally. I owe him my success in finishing my studies.

I thank Dr. Anthony C. K. Soong for suggesting the initial problem and for working with me in the early stages of this research. I also thank Mr. Haitham Abu Ghazaleh for guiding me to some of the data used in the simulations. I also wish to thank Ms. Azadeh Yadollahi for her encouragement and valuable discussions.

I was financially supported by TRLabs, Winnipeg, during my Ph.D. studies. I thank the administration of TRLabs, especially Dr. Jeff Diamond.

I thank Dr. Zahra Moussavi. She and her family were always there for me.

I thank my family and friends in Iran, in Winnipeg, Canada, and also all my e-friends throughout the world. It is in hard times that we appreciate the value of friendship. This thesis is dedicated to the help and support I received from all my friends.

Bibliography

[1] S. V. Hanly and D. Tse, "Power control and capacity of spread–spectrum wireless networks," *Automatica*, vol. 35 (12), pp. 1987–2012, 1999.

[2] D. Torrieri, *Principles of Spread-Spectrum Communication Systems.* Springer, 2004.

[3] J. Zhang, C. Wang, and B. Li, "Resource management in DS–CDMA cellular networks," in *Design and Analysis of Wireless Networks*, Y. Pan and Y. Xiao, Eds. Hauppauge, NY: Nova Science Publishers, Inc., 2005, pp. 99–111.

[4] S. Grandhi, R. Vijayan, D. Goodman, and J. Zander, "Centralized power control in cellular radio systems," *IEEE Transactions on Vehicular Technology*, vol. 42 (4), pp. 466–468, 1993.

[5] S. V. Hanly, "An algorithm of combined cell–site selection and power control to maximize cellular spread spectrum capacity," *IEEE Journals on Selected Areas in Communications*, vol. 13 (7), pp. 1332–1340, 1995.

[6] Y. Ishikawa and N. Umeda, "Capacity design and performance of call admission control in cellular CDMA systems," *IEEE Journal on Selected Areas in Communications*, vol. 15 (8), pp. 1627–1635, 1997.

[7] A. J. Viterbi, A. M. Viterbi, K. S. Gilhousen, and E. Zehavi, "Soft handoff extends CDMA cell coverage and increases reverse link capacity," *IEEE Journal on Selected Areas in Communications*, vol. 12 (8), pp. 1281–1288, 1994.

[8] S. M. Shin, C.-H. Cho, and D. K. Sung, "Interference-based channel assignment for DS–CDMA cellular systems," *IEEE Transactions on Vehicular Technology*, vol. 48 (1), pp. 233–239, 1999.

[9] R. D. Yates, "A framework for uplink power control in cellular radio systems," *IEEE Journal on Selected Areas in Communications*, vol. 13 (7), pp. 1341–1347, 1995.

[10] C. Smith and C. Gervelis, *Cellular System Design & Optimization.* McGraw–Hill Series on Telecommunications, 1996.

[11] J. Blom and F. Gunnarsson, "Power control in cellular radio systems," Ph.D. dissertation, Linkopings Universitet. Linkoping, Sweden, 1998.

[12] J. Zander, "Performance of optimum transmitter power control in cellular radio systems," *IEEE Transactions on Vehicular Technology*, vol. 41, pp. 57–62, 1992.

[13] G. J. Foschini and Z. Miljanic, "A simple distributed autonomous power control algorithm and its convergence," *IEEE Transactions on Vehicular Technology*, vol. 42, pp. 641–646, 1993.

[14] C. W. Sung and W. S. Wong, "A distributed fixed–step power control algorithm with quantization and active link quality protection," *IEEE Transactions on Vehicular Technologies*, vol. 48 (2), pp. 553–562, 1999.

[15] S. C. C. N. Bambos and G. J. Pottie, "Channel access algorithms with active link protection for wireless communication networks with power control," *IEEE/ACM Transactions on Networking*, vol. 8 (5), pp. 583–597, 2000.

[16] K. K. Leung, C. W. Sung, W. S. Wong, and T. M. Lok, "Convergence theorem for a general class of power control algorithms," *IEEE Transactions on Communications*, vol. 52 (9), pp. 1566–1574, 2004.

[17] V. Tralli, R. Veronesi, and M. Zorzi, "Power–shaped advanced resource assignment for fixed broadband wireless access systems," *IEEE Transactions on Wireless Communications*, vol. 3, pp. 2207–2220, 2004.

[18] K. Gilhousen, I. Jacobs, R. Padovani, A. Viterbi, L. Weaver Jr., and C. Wheatley III, "On the capacity of a cellular CDMA system," *IEEE Transactions on Vehicular Technology*, vol. 40 (2), pp. 303–312, 1991.

[19] S. Grandhi, R. Vijayan, and D. J. Goodman, "Distributed power control in cellular radio systems," *IEEE Transactions on Communications*, vol. 42, pp. 226–228, 1994.

[20] M. Xiao, N. B. Shroff, and E. K. P. Chong, "A utility–based power–control scheme in wireless cellular systems," *IEEE/ACM Transactions on Networking*, vol. 11 (2), pp. 210–221, 2003.

[21] C. W. Sung and W. S. Wong, "A noncooperative power control game for multirate CDMA data networks," *IEEE Transactions on Wireless Communications*, vol. 2 (1), pp. 186–194, 2003.

[22] X. Liu, E. K. P. Chong, and N. B. Shroff, "A framework for opportunistic scheduling in wireless networks," *Computer Networking*, vol. 41, pp. 451–474, 2003.

[23] D. I. Kim, E. Hossain, and V. K. Bhargava, "Dynamic rate and power adaptation for provisioning class–based QoS in cellular multirate WCDMA systems," *IEEE Transactions on Wireless Communications*, vol. 3 (5), pp. 1590–1601, 2004.

[24] N. Feng, Siun-ChuonMau, and N. B.Mandayam, "Joint network–centric and user–centric radio resource management in a multicell system," *IEEE Transactions on Communications*, vol. 53 (7), pp. 1114–1118, 2005.

[25] A. J. Goldsmith and P. P. Varaiya, "Capacity of fading channels with channel side information," *IEEE Transactions on Information Theory*, vol. 43 (6), pp. 1986–1992, 1997.

[26] S. G. Kiani and D. Gesbert, "Maximizing the capacity of large wireless networks: Optimal and distributed solutions," in *Proceedings of ISIT*, Seattle,USA, 2006, pp. 2501–2505.

[27] K.-K. Leung and C. W. Sung, "An opportunistic power control algorithm for cellular network," *IEEE/ACM Transactions ON Networking*, vol. 14 (3), pp. 470–478, 2006.

[28] P. Viswanath, D. Tse, and R. Laroia, "Opportunistic beamforming using dumb antennas," *IEEE Transactions on Information Theory*, vol. 48 (6), pp. 1277–1294, 2002.

[29] R. Rezaiifar, A. Makowski, and S. Kumar, "Stochastic control of handoffs in cellular networks," *IEEE Journal on Selected Areas in Communications*, vol. 13 (7), pp. 1348–1362, 1995.

[30] M. Asawa and W. Stark, "Optimal scheduling of handoffs in cellular networks," *IEEE/ACM Transactions on Networking*, vol. 4 (3), pp. 428–441, 1996.

[31] I. Koutsopoulos and L. Tassiulas, "Cross-layer adaptive techniques for throughput enhancement in wireless OFDM-based networks," *IEEE/ACM Transactions on Networking*, vol. 14 (5), pp. 1056–1066, 2006.

[32] S. Hamouda, S. Tabbane, and P. Godlewski, "Improved reuse partitioning and power control for downlink multi-cell OFDMA systems," in *Proceedings of the International Workshop on Broadband Wireless Access for ubiquitous Networking (BWAN'06)*, 2006.

[33] C. Wong, R. Cheng, K. Letaief, and R. Murch, "Multi-user subcarrier allocation for OFDM transmission using adaptive modulation," *IEEE Journal on Selected Area in Communications*, vol. 17, pp. 1747–1757, 1999.

[34] D. Kivanc, L. Guoqing, and L. Hui, "Computationally efficient bandwidth allocation and power control for OFDMA," *IEEE Transactions on Wireless Communications*, vol. 2 (6), pp. 1150–1158, 2003.

[35] S. Ulukus and L. Greenstein, "Throughput maximization in CDMA uplinks using adaptive spreading and power control," in *IEEE Sixth International Symposium on Spread Spectrum Techniques and Applications*, 2000, pp. 565–569.

[36] M. Frodigh, S. Parkvall, C. Roobol, P. Johansson, and P. Larsson, "Future-generation wireless networks," *IEEE Personal Communications*, vol. 8 (5), pp. 10–17, 2001.

[37] T. Ottosson and A. Svensson, "Multirate schemes in DS/CDMA systems," in *Proceedings of IEEE VTC*, 1995, pp. 1006–1010.

[38] A. Baier, U. C. Fiebig, W. Granzow, W. Koch, P. Teder, and J. Thielecke, "Design study for a CDMA–based third-generation mobile radio system," *IEEE Journal on Selected Areas in Communications*, vol. 12, pp. 733–743, 1994.

[39] I. Chih-Lin and K. K. Sabnani, "Variable spreading gain CDMA with adaptive control for integrated traffic in wireless networks." in *Proceedings of IEEE VTC*, 1995, pp. 794–798.

[40] R. Steele, *Mobile Radio Communications*. London, England: Pentech Press, 1992.

[41] G. L. Stuber, *Principles of Mobile Communication*. Boston, MA: Kluwer Academic Publisher, 1996.

[42] P. Bender, P. Black, M. Grob, R. Padovani, N. Sindhushayana, and A. Viterbi, "CDMA/HDR: A bandwidth–efficient high–speed wireless data service for nomadic users," *IEEE Communications Magazine*, vol. 38 (7), pp. 70–77, 2000.

[43] S. Parkvall, E. Dahlman, P. Frenger, P. Beming, and M. Persson, "The evolution of WCDMA toward higher speed downlink packet data access," in *Proceedings of IEEE VTC'01–Spring, Vol. 3*, 2001, pp. 2287–2291.

[44] S. Verdu, "The capacity region of the symbol–asynchronous Gaussian multiple–access channel," *IEEE Transactions on Information Theory*, vol. 35 (4), pp. 733–751, 1989.

[45] R. G. Akl, M. V. Hegde, M. Naraghi-Pour, and P. S. Min, "Multicell CDMA network design," *IEEE Transactions on Vehicular Technology*, vol. 50 (3), pp. 711–722, 2001.

[46] D. I. Kim, E. Hossain, and V. K. Bhargava, "Downlink joint rate and power allocation in cellular multirate WCDMA systems," *IEEE Transactions on Wireless Communications*, vol. 2 (1), pp. 69–80, 2003.

[47] R. Padovani, "Reverse link performance of IS–95 based cellular systems," *IEEE Personal Communications*, vol. Third Quarter, pp. 28–34, 1994.

[48] J. S. Evans and D. Everitt, "On the teletraffic capacity of CDMA cellular networks," *IEEE Transactions on Vehicular Technology*, vol. 48 (1), pp. 153–165, 1999.

[49] S. C. Yang, *CDMA RF System Engineering*. Boston, London: Artech House Publishers, 1998.

[50] R. Knopp and P. Humblet, "Information capacity and power control in single–cell multiuser communications," in *1995 IEEE International Conference on Communications*, Seattle, 1995, pp. 331–335.

[51] S. Hanly and D. Tse, "Multi–access fading channels: Part II: Delay–limited capacities," *IEEE Transactions on Information Theory*, vol. 44 (7), pp. 2816–2831, 1998.

[52] D. Tse and S. Hanly, "Multi–access fading channels: Part I: Polymatroid structure, optimal resource allocation and throughput capacities," *IEEE Transactions on Information Theory*, vol. 44 (7), pp. 2796–2815, 1998.

[53] K. Kumaran and L. Qian, "Uplink scheduling in CDMA packet data systems," Proceedings of the IEEE INFOCOM, 2003, pp. 292–300.

[54] Huawei, "Soft frequency reuse scheme for UTRAN LTE," 3GPP TSG RAN WG1 Meeting #41, R1–050507, 2005.

[55] S. Kandukuri and S. Boyd, "Simultaneous rate and power control in multirate multimedia CDMA systems," in *IEEE Sixth International Symposium on Spread Spectrum Techniques and Applications*, NJIT, NJ, 2000, pp. 570–574.

[56] S. V. Hanly and P. Whiting, "Information–theoretic capacity of multi-receiver networks," *Telecommunication Systems*, vol. 1, pp. 1–42, 1993.

[57] S.-J. Oh, D. Zhang, and K. M. Wasserman, "Optimal resource allocation in multi–service CDMA networks," *IEEE Transactions on Wireless Communications*, vol. 2, pp. 811–821, 2003.

[58] S. A. Jafar and A. Goldsmith, "Adaptive multirate CDMA for uplink throughput maximization," *IEEE Transactions on Wireless Communications*, vol. 2, pp. 218–228, 2003.

[59] D. N. Tse and S. V. Hanly, "Linear multiuser receivers: Effective interference, effective bandwidth and capacity," *IEEE Transactions in Information Theory*, vol. 45 (2), pp. 641–657, 1999.

[60] B. Sklar, "A structured overview of digital communications – a tutorial review – part I," *IEEE Communications Magazine*, vol. 21 (5), pp. 4–17, 1983.

[61] C. W. Sung and W. S. Wong, "Power control and rate management for wireless multimedia CDMA systems," *IEEE Transactions on Communications*, vol. 49 (7), pp. 1215–1226, 2001.

[62] J. T.-H. Wu and E. Geraniotis, "Power control in multi–media CDMA networks," in *Proceedings of IEEE VTC*, 1995, pp. 789–793.

[63] P. Hosein, "Optimality conditions for throughput maximization on the reverse link for a CDMA network," in *Proceedings of the IEEE Eighth International Symposium on Spread Spectrum Techniques and Applications*, 2004, pp. 764–768.

[64] C. W. Sung and W. S. Wong, "A distributed fixed–step power control algorithm with quantization and active link quality protection," *IEEE Transactions on Vehicular Technology*, vol. 48, pp. 553–562, 1999.

[65] C. W. Sung, K. K. Leung, and W. S. Wong. "A quality–based fixed–step power control algorithm with adaptive target threshold," *IEEE Transactions on Vehicular Technology*, vol. 49, pp. 1430–1439, 2000.

[66] S. Ramakrishna and J. M. Holtzman, "A scheme for throughput maximization in a dual–class CDMA system," *IEEE Journal on Selected Areas in Communication*, vol. 16 (6), pp. 830–844, 1998.

[67] A. Sampath, P. S. Kumar, and J. Holtzman, "Power control and resource management for a multimedia CDMA wireless system," in *Sixth IEEE International Symposium on Personal, Indoor and Mobile Radio Communications*, 1995, pp. 21–25.

[68] R. D. Yates and C.-Y. Huang, "Integrated power control and base station assignment," *IEEE Transactions on Vehicular Technology*, vol. 44 (3), pp. 638–644, 1995.

[69] J. Zender, "Performance of optimum transmitter control in cellular radio systems," *IEEE Transactions on Vehicular Technology*, vol. 41 (1), pp. 57–62, 1992.

[70] Q. Wu, "Performance of optimum transmitter control in CDMA cellular mobile systems," *IEEE Transactions on Vehicular Technology*, vol. 48 (2), pp. 571–575, 1999.

[71] S.-J. Oh and A. C. K. Soong, "QoS–constrained information–theoretic sum capacity of reverse link CDMA systems," *IEEE Transactions on Wireless Communications*, vol. 5 (1), pp. 3–7, 2006.

[72] D. Falomari, N. Mandayam, D. Goodman, and V. Shah, "A new framework for power control in wireless data networks: Games utility and pricing," in *Proceedings of the Allerton Conference on Communication, Control, and Computing*, Illinois, USA, September 1998, pp. 546–55.

[73] P. Hosein, "Optimal proportionally fair rate allocation for CDMA reverse links," in *Proceedings of the Sixth International Symposium on Wireless Personal Multimedia Communications*, Yokosuka, Japan, 2003.

[74] S. C. Yang, *CDMA RF System Design.* Boston: Artech House Publishing, 1998.

[75] T. Alpcan, X. Fan, T. Basar, M. Arcak, and J. Wen, "Power control for multicell CDMA wireless networks: a team optimization approach," in *Proceedings of Third International Symposium on Modeling and Optimization in Mobile, Ad Hoc, and Wireless Networks, 2005 (WIOPT 2005)*, 2005, pp. 379–388.

[76] J.-W. Lee, R. R. Mazumdar, and N. B. Shroff, "Downlink power allocation for multi-class wireless systems," *IEEE/ACM Transactions on Networking*, vol. 13 (4), pp. 854–867, 2005.

[77] ——, "Joint resource allocation and base-station assignment for the downlink in CDMA networks," *IEEE/ACM Transactions on Networking*, vol. 14 (1), pp. 1–14, 2006.

[78] A. Viterbi and A. Viterbi, "Erlang capacity of a power controlled CDMA system," *IEEE Journal on Selected Areas in Communications*, vol. 11 (6), pp. 892–900, 1993.

[79] T. Alpcan and T. Basar, "A hybrid systems model for power control in multicell wireless data networks," *Performance Evaluation*, vol. 57, pp. 477–495, 2004.

[80] D. Torrieri, "Instantaneous and local-mean power control for direct-sequence CDMA cellular networks," *IEEE Transactions on Communications*, vol. 50, pp. 1310–1315, 2002.

[81] A. J. Viterbi, *CDMA Principles of Spread Spectrum Communication.* Addison-Wesley Wireless Communications Series, 1995.

[82] D. Goodman and N. Mandayam, "Power control for wireless data," *IEEE Personal Communications Magazine*, vol. 7, pp. 48–54, 2000.

[83] T. Alpcan, T. Basar, and S. Dey, "A power control game based on outage probabilities for multicell wireless data networks," *IEEE Transactions on Wireless Communications*, vol. 5 (4), pp. 890–899, 2006.

[84] C. U. Saraydar, N. B. Mandayam, and D. J. Goodman, "Pricing and power control in a multicell wireless data network," *IEEE Journal on Selected Areas in Communications*, vol. 19 (10), pp. 1883–1892, 2001.

[85] C. Saraydar, N. Mandayam, and D. Goodman, "Power control in a multicell CDMA data system using pricing," in *Proceedings of the IEEE Conference on Vehicular Technology (IEEE VTS-Fall VTC 2000)*, vol. 2, 2000, pp. 484–491.

[86] S. Koskie and Z. Gajic, "A nash game algorithm for sir-based power control in 3G wireless CDMA networks," *IEEE/ACM Transactions on Networking*, vol. 13 (5), pp. 1017–1026, 2005.

[87] T. Alpcan, T. Basar, and R. Srikant, "CDMA uplink power control as a noncooperative game," *Wireless Networks*, vol. 8, pp. 659–670, 2002.

[88] H. Ji and C.-Y. Huang, "Non–cooperative uplink power control in cellular radio systems," *Wireless Networks*, vol. 4(3), pp. 233–240, April 1998.

[89] V. Siris, "Resource control for elastic traffic in CDMA networks," in *Proceedings of ACM MOBICOM*, Atlanta, GA, 2002, pp. 193–204.

[90] V. Shah, N. B. Mandayam, and D. J. Goodman, "Power control for wireless data based on utility and pricing," in *Proceedings of The Ninth IEEE International Symposium on Personal, Indoor and Mobile Radio Communications*, 1998, pp. 1427–1432.

[91] N. Feng, N. B. Mandayam, and D. J. Goodman, "Joint power and rate optimization for wireless data services based on utility functions," in *Proceedings of CISS*, 1999, pp. 109–113.

[92] C. U. Saraydar, N. B. Mandayam, and D. J. Goodman, "Efficient power control via pricing in wireless data networks," *IEEE Transactions on Communications*, vol. 50 (2), pp. 291–303, 2002.

[93] H.-K. Lim, J.-G. Choi, and S. Bahk, "Utility–based downlink power allocation in multicell wireless packet networks," in *Proceedings of Globecom 2004*, 2004, pp. 3321–3325.

[94] ——, "Utility–based downlink power allocation in multicell wireless packet networks," *Computer Communications*, vol. 29, pp. 3913–3920, 2006.

[95] S.-J. Oh and K. M. Wasserman, "Optimality of greedy power control and variable spreading gain in multi-class CDMA mobile networks," in *Proceedings of ACM Mobicom*, 1999, pp. 102–112.

[96] S.-J. Oh, T. L. Olsen, and K.M.Wasserman, "Distributed power control and spreading gain allocation in CDMA data networks," in *Proceedings of IEEE INFOCOM*, 2000, pp. 379–385, vol. 2.

[97] S. G. Kiani, G. E. Oien, and D. Gesbert, "Maximizing multicell capacity using distributed power allocation and scheduling," in *Proceedings of WCNC*, 2007, pp. 1692–1696.

[98] L. Papavassiliou and L. Tassiulas, "Joint optimal channel, base station and power assignment for wireless access," *IEEE/ACM Transactions on Networking*, vol. 4 (6), pp. 857–872, 1996.

[99] S. Kim and D. Kim, "Optimum transmitter power control in cellular radio systems," *Information Systems and Operational Research*, vol. 35 (1), 1997.

[100] M. Soleimanipour, W. Zhuang, and G. H. Freeman, "Optimal resource management in wireless multimedia wideband CDMA systems," *IEEE Transactions on Mobile Computing*, vol. 1 (2), pp. 143–160, 2002.

[101] A. Bedekar, S. Borst, K. Ramanan, P. Whiting, and E. Yeh, "Downlink scheduling in CDMA data networks," in *in Proceedings of IEEE GLOBECOM*, 1999, pp. 2653–2657, vol. 5.

[102] F. Berggren, S.-L. Kim, R. Jantti, and J. Zander, "Joint power control and intracell scheduling of DS-CDMA nonreal time data," *IEEE Journal on Selected Areas in Communications*, vol. 19 (10), pp. 1860–1870, 2001.

[103] "CDMA 2000 high rate packet data air interface specification, version 4, C.S0024-0 v 4.0, IS-856 TIA standard, 3GPP2," http://www.3gpp2.org, 2002.

[104] Y. Jou, "Developments in third generation (3G) CDMA technology," in *in Proceedings of IEEE ISSSTA00*, 2000, pp. 460–464.

[105] M. Andrews, K. Kumaran, K. Ramanan, A. Stolyar, P. Whiting, and R. Vijayakumar, "Providing quality of service over a shared wireless link," *IEEE Communications Magazine*, vol. 39 (2), pp. 150–154, 2001.

[106] T. Rappaport and L. Milstein, "Effects of radio propagation path loss on DS–CDMA cellular frequency reuse efficiency for the reverse channel," *IEEE Transactions on Vehicular Technology*, vol. 41 (3), pp. 231–242, 1992.

[107] Y. Okumura, E. Ohmori, T. Kawano, and K. Fukuda, "Field strength and its variability in VHF and UHF land–mobile radio service," *Review of the Electrical Communication Laboratory*, vol. 9–10, pp. 825–873, 1968.

[108] M. Hata, "Empirical formula for propagation loss in land mobile radio services," *IEEE Transactions on Vehicular Technology*, vol. 29(3), pp. 317–325, 1980.

[109] T. S. Rappaport, *Wireless Communications: Principles and Practice.* Upper Saddle River, N.J.: Prentice Hall, 2002.

[110] S.-J. Oh and K. Wasserman, "Adaptive resource allocation in power constrained CDMA mobile networks," in *IEEE Wireless Communications and Networking Conference*, 1999, pp. 510–514.

[111] J. Zander, "Transmitting power control for co–channel interference management in cellular radio systems," in *4th WinLab Workshop on 3G Information Networks*, 1993, pp. 241–247.

[112] D. J. Goodman, *Wireless Personal Communications Systems.* Reading, Massachusetts: Addison–Wesley Wireless Communications Series, 1997.

[113] J. Papandriopoulos, J. Evans, and S. Dey, "Optimal power control in CDMA networks with constraints on outage probability," in *Proceedings of the WiOpt03*, 2003, pp. 279–284.

[114] I. Koutsopoulos, U. C. Kozat, and L. Tassiulas, "Dynamic resource allocation in CDMA systems with deterministic codes and multirate provisioning," *IEEE Transactions on Mobile Computing*, vol. 5 (12), pp. 1780–1792, 2006.

[115] T. Chebaro and P. Godlewski, "Additional interference in a RAKE receiver implementation of a CDMA power control," in *Proceedings of IEEE Third International Symposium on Spread Spectrum Techniques and Applications (ISSSTA'94)*, 1994, pp. 425–429 vol.2.

[116] P. Godlewski and L. Nuaymi, "Auto–interference analysis in cellular systems," in *Proceedings of the 49th IEEE Vehicular Technology Conference*, 1999, pp. 1994–1998.

[117] S.-J. Oh, A. D. Damnjanovic, and A. C. K. Soong, "Information theoretic sum capacity of reverse link CDMA systems," in *Proceedings of The 57th IEEE Semiannual Vehicular Technology Conference (VTC 2003-Spring)*, 2003, pp. 93–97.

[118] S.-J. Oh and A. C. K. Soong, "QoS–constrained information–theoretic sum capacity of reverse link CDMA systems," in *Proceedings of IEEE Global Telecommunications Conference (GLOBECOM '03)*, 2003, pp. 190–194.

[119] R. L. Graham, D. E. Knuth, and O. Patashnik, *Concrete Mathematics: A Foundation for Computer Science*. Addison-Wesley Professional, 1994.

[120] M. R. Karim and M. Sarraf, *W-CDMA and CDMA2000 for 3G Mobile Networks*. McGraw–Hill Telecom, 2002.

[121] E. K. P. Chong and S. H. Zak, *An Introduction to Optimization*. Wiley Inter–Science Series in Discrete Mathematics and Optimization, 1996.

[122] M. K. Kozlov, S. P. Tarasov, and L. G. Khachiyan, "Polynomial solvability of convex quadratic programming," *Doklady Akademiia Nauk SSSR (translated in Soviet Mathematics Doklady, 20)*, vol. 248, pp. 1108–111, 1979.

[123] P. E. Gill, W. Murray, and M. H. Wright, *Practical Optimization*. Academic Press, 1982.

[124] B. Jabbari and W. F. Fuhrmann, "Teletraffic modeling and analysis of flexible hierarchical cellular networks with speed-sensitive handoff strategy," *IEEE Journal on Selected Areas in Telecommunications*, vol. 15 (8), pp. 1539–1548, 1997.

Appendix

Appendix A

Theorem

Theorem: For the function $f(x)$ defined as,

$$f(x) = \frac{\prod_{i=1}^{k}(x+\beta_i)}{(x+\beta)^k}, \tag{A.1}$$

where,

$$0 < \beta_1 < \beta_2 < \cdots < \beta_{k-1} < \beta < \beta_k, \tag{A.2}$$

and,

$$\sum_{i=1}^{k} \beta_i > k\beta, \tag{A.3}$$

the minimum of $f(x)$ for $x \in [a,b] \subset R^+ \cup \{0\}$ happens at either a or b.

Proof: We know that $\lim_{x\to\pm\infty} f(x) = 1$. We will now prove that ,

$$\lim_{x\to\pm\infty} f'(x) = 0^-, \tag{A.4}$$

which results in $\lim_{x\to\pm\infty} f(x) = 1^+$. We have,

$$f(x) = \frac{\prod_{i=1}^{k}(x+\beta_i)}{(x+\beta)^k} = \frac{x^k + \sum_{i=1}^{k}\beta_i x^{k-1} + F(x)}{(x+\beta)^k}, \tag{A.5}$$

where, $F(x)$ is a polynomial of degree $k-2$. Differentiating $f(x)$ in terms of x we have,

$$f'(x) = \left[\left(kx^{k-1} + (k-1)\sum_{i=1}^{k}\beta_i x^{k-2} + F'\right)(x+\beta)^k - k(x+\beta)^{k-1}\left(x^k + \sum_{i=1}^{k}\beta_i x^{k-1} + F\right)\right](x+\beta)^{-2k} = \frac{x^{k-1}\left(k\beta - \sum_{i=1}^{k}\beta_i\right) + G(x)}{(x+\beta)^{k+1}}, \tag{A.6}$$

where $G(x)$ is a polynomial of degree $k-2$. Hence, given (A.3), we have proved (A.4).

According to (A.2), we know that $-\beta_1$ is the largest zero of $f(x)$. We now prove that for $x > -\beta_1$, $f(x)$ has no local minimizer. If we prove this, as $-\beta_1$ is positive, we know that for any interval on the positive side, the minimum happens at the boundaries, exactly what the theorem suggests.

We define $h(x) = f(x-\beta_1)$, which yields,

$$h(x) = \frac{\prod_{i=1}^{k}(x-\beta_1+\beta_i)}{(x-\beta_1+\beta)^k} = \frac{x\prod_{i=1}^{k-1}(x+\theta_i)}{(x+\theta)^k}, \tag{A.7}$$

where,

$$\theta_i = \beta_{i+1} - \beta_1, i = 1, \cdots, k-1, \tag{A.8}$$

and $\theta = \beta - \beta_1$. Using (A.2) we have,

$$0 < \theta_1 < \theta_2 < \cdots < \theta_{k-2} < \theta < \theta_{k-1}. \tag{A.9}$$

We claim that if we prove that $h'(x)$ has one and only one zero for $x \geq 0$, then we have proved that $f(x)$ accepts its minimum at boundary point. For now, we assume that it is proved that $h'(x)$ has one and only one zero in $x \geq 0$. This claim will be proved later.

We know that $h'(0)$ is positive. If it is not, as $h(0) = 0$, for a small $\varepsilon > 0$ we have $h(\varepsilon) < 0$. Note that, $h(x)$, which is the shifted version of $f(x)$, converges to unity at infinity and is a continuous function in $R^+ \cup \{0\}$. Therefore, if $h(x)$ accepts both positive and negative values

inside $R^+ \cup \{0\}$, therefore it will have to have a zero in that interval, an impossible situation due to the fact that all the zeros of $h(x)$ occur on the negative side. Hence $h'(0) > 0$. As we proved that $h'(\infty) = 0^-$, so $h'(x)$ accepts both positive and negative values in $R^+ \cup \{0\}$ and is continuous in that interval, hence there should be a point inside $R^+ \cup \{0\}$ for ehich the value of $h'(x)$ is zero. If we prove that $h'(x)$ has no more zeros in $R^+ \cup \{0\}$, so there will be no local minimizer, leading to the proof we needed.

Now, we prove that there is at most one point at which the value of $h'(x)$ is zero.

Differentiating $h(x)$ given in (A.7) we have,

$$h'(x) = h(x)\left(\frac{-k}{x+\theta} + \frac{1}{x} + \sum_{i=1}^{k-1} \frac{1}{x+\theta_i}\right). \tag{A.10}$$

As for $x > 0$, $h(x)$ is positive, $h'(x)$ is zero if and only if the second term in (A.10) is zero,

$$\frac{1}{x} + \sum_{i=1}^{k-1} \frac{1}{x+\theta_i} = \frac{k}{x+\theta}, \tag{A.11}$$

$$\frac{x+\theta}{x} + \sum_{i=1}^{k-1} \frac{x+\theta}{x+\theta_i} = k, \tag{A.12}$$

$$1 + \frac{\theta}{x} + \sum_{i=1}^{k-2}\left(1 + \frac{\theta-\theta_i}{x+\theta_i}\right) + 1 - \frac{\theta_{k-1}-\theta}{x+\theta_{k-1}} = k, \tag{A.13}$$

$$\frac{\theta}{x} + \sum_{i=1}^{k-2} \frac{\theta-\theta_i}{x+\theta_i} = \frac{\theta_{k-1}-\theta}{x+\theta_{k-1}}. \tag{A.14}$$

Note that all the terms in the denominators of (A.14) are positive and that we have,

$$\frac{\mu}{x} + \sum_{i=1}^{k-2} \frac{\mu_i}{x+\theta_i} = \frac{1}{x+\theta_{k-1}}, \tag{A.15}$$

$$\mu_i = \frac{\theta-\theta_i}{\theta_{k-1}-\theta}, i = 1, \cdots, k-2, \tag{A.16}$$

$$\mu = \frac{\theta}{\theta_{k-1}-\theta}. \tag{A.17}$$

Note that,

$$\mu > \mu_1 > \mu_2 > \cdots > \mu_{k-2} > 0. \tag{A.18}$$

The equation in (A.15) leads to,

$$\left(\frac{\mu}{x} + \sum_{i=1}^{k-2} \frac{\mu_i}{x+\theta_i}\right)^{-1} = x + \theta_{k-1}. \tag{A.19}$$

We know that if $f(x) = g(x)$ has two solutions x_1 and x_2 for two continuous functions f and g, then there is a solution in $[x_1, x_2]$ for which $f'(x) = g'(x)$. The proof comes from working on the solutions to $h(x) = f(x) - g(x)$ and making sure that $h'(x) = f'(x) - g'(x)$ should have a zero inside $[x_1, x_2]$. Hence, if we are going to have two points which yield zero values of $h'(x)$, then thhere should be a solution to,

$$\frac{\partial}{\partial x}\left(\frac{\mu}{x} + \sum_{i=1}^{k-2} \frac{\mu_i}{x+\theta_i}\right)^{-1} = \frac{\partial}{\partial x}(x + \theta_{k-1}), \tag{A.20}$$

or equivalently,

$$\left(\frac{\mu}{x^2} + \sum_{i=1}^{k-2} \frac{\mu_i}{(x+\theta_i)^2}\right) = \left(\frac{\mu}{x} + \sum_{i=1}^{k-2} \frac{\mu_i}{x+\theta_i}\right)^2. \tag{A.21}$$

Here, we use the weighted power mean theorem stated as follows. Assume that the positive values of $\omega_1, \cdots, \omega_n$ and $\vec{\mathbf{x}} = (x_1, \cdots x_n)$ are given and define,

$$M_\omega^r(\vec{\mathbf{x}}) = \left(\sum_{i=1}^{n} \omega_i x_i^r\right)^{\frac{1}{r}}. \tag{A.22}$$

Now, the weighted power mean theorem states that for $r < s$ we have,

$$M_\omega^r(\vec{\mathbf{x}}) \leq M_\omega^s(\vec{\mathbf{x}}). \tag{A.23}$$

Now, using,

$$\omega_1 = \frac{\mu}{\mu + \sum_{j=1}^{k-2} \mu_j}, \tag{A.24}$$

$$\omega_i = \frac{\mu_{i-1}}{\mu + \sum_{j=1}^{k-2} \mu_j}, 2 \leq i \leq k-1, \tag{A.25}$$

for the set of numbers $\{x, x+\theta_1, x+\theta_2, \cdots, x+\theta_{k-2}\}$, we have,

$$\left(\mu + \sum_{j=1}^{k-2} \mu_j\right)\left(\frac{\mu}{x^2} + \sum_{i=1}^{k-2} \frac{\mu_i}{(x+\theta_i)^2}\right) \geq \left(\frac{\mu}{x} + \sum_{i=1}^{k-2} \frac{\mu_i}{x+\theta_i}\right)^2. \tag{A.26}$$

The question here is to determine the value of $\mu + \sum_{j=1}^{k-2} \mu_j$.

According to (A.3) with some manipulations we can show that $\mu + \sum_{j=1}^{k-2} \mu_j < 1$, which when substituted into (A.26) gives,

$$\left(\frac{\mu}{x^2} + \sum_{i=1}^{k-2} \frac{\mu_i}{(x+\theta_i)^2}\right) > \left(\frac{\mu}{x} + \sum_{i=1}^{k-2} \frac{\mu_i}{x+\theta_i}\right)^2, \tag{A.27}$$

contradicting (A.21).

Hence, $h'(x)$ has no two zeros in $R^+ \cup \{0\}$. This leads to a proof for the claim that the minimum value of $f(x)$ happens when x takes a value at the boundary ■

Appendix B

Publications

Parts of the material presented in this thesis have been previously used in these articles.

B.1 Conference Papers

- Arash Abadpour and Attahiru Sule Alfa, "Approximate Algorithms for Maximizing the Capacity of the Reverse Link in Multiple–Class CDMA System", Accepted for publication in the proceedings of the 11th INFORMS Computing Society Conference, Charleston 2009 (ICS'09).

- Arash Abadpour, Attahiru Sule Alfa, and Anthony C.K. Soong, "A More Realistic Approach to Information–Theoretic Sum Capacity of Reverse Link CDMA Systems in a Single Cell", In the IEEE International Conference on Communications (ICC 2007), Glasgow, Scotland.

- Arash Abadpour, Attahiru Sule Alfa, and Anthony C.K. Soong, "Capacity-Share Controlled Information–Theoretic Sum Capacity of Reverse Link Single–Cell CDMA Systems", In the 2007 IEEE 65th Vehicular Technology Conference, (VTC2007 Spring), Dublin, Ireland.

- Arash Abadpour, Attahiru Sule Alfa, and Anthony C.K. Soong, "Information-Theoretic Sum Capacity of Reverse Link CDMA Systems in A Single Cell, An Optimization Perspective", In the 8th Annual Conference for Canadian Queueing Theorists and Practitioners, CanQueue 2006, Banff, Calgary, Canada.

- Arash Abadpour, Attahiru Sule Alfa, and Anthony C.K. Soong, "Closed Form Solution for QoS–Constrained Information–Theoretic Sum Capacity of Reverse Link CDMA Systems", In the 2nd ACM Q2SWinet 2006, Torremolinos, Malaga, Spain.

B.2 Journal Papers

- Arash Abadpour, Attahiru Sule Alfa, "Approximate algorithms for maximizing the capacity of the reverse link in multiple–class CDMA systems", in Operations Research and Cyber–Infrastructure, M. J. Saltzman, J. W. Chinneck, and B. Kristjansson, Eds. Springer, 2008, Pages: 237–252.

- Arash Abadpour, Attahiru Sule Alfa, and Anthony C.K. Soong, "Closed Form Solution for Maximizing the Sum Capacity of Reverse–Link CDMA System with Rate Constraints", IEEE Transactions on Wireless Communications, Volume 7, Issue 4, April 2008, Pages:1179–1183.

- Arash Abadpour, Attahiru Sule Alfa, and Anthony C.K. Soong, "Approximation Algorithms For Maximizing The Information–Theoretic Sum Capacity of Reverse Link CDMA Systems", AEU - International Journal of Electronics and Communications, Volume 63, Issue 2, 4 February 2009, Pages 108–115.

B.3 In Progress

- Arash Abadpour, Attahiru Sule Alfa, "Generalized Maximization of the Aggregate Capacity of the CDMA Reverse Link".

- Arash Abadpour, Attahiru Sule Alfa, "Capacity Maximization in the Reverse Link CDMA for True Multiple–Cell Systems".

Appendix C

MATLAB Code Documentation

This chapter briefly discusses the implementation of the algorithms developed in this thesis in MATLAB 7.0. For more detailed instructions on how to use any particular function refer to the documentation enclosed in the regarding m–file. The information contained in the code is also more up–to–date than this document.

In this appendix, first, in Section C.1, the code developed for solving single–cell problems is reviewed. The single–cell methods proposed in this thesis are developed using different functions which carry out different tasks. Many of these functions operate on a large set of input arrays and matrices. In order to facilitate the use of the functions, however, different sample files are included in the developed code. These files act as usage examples for different functions. This appendix follows with the implementation of the multiple–cell algorithms developed in this thesis in Section C.2. This part of the code has been developed within a class–based framework, where different methods and handlers hide the unnecessary details from a non–interested user.

C.1 Single–Cell Methods

The implementation of the single–cell methods proposed in this thesis is carried out in a function–based framework. These implementations include the utility functions (discussed in Section C.1.1), the solvers (presented in Section C.1.2), and the interfaces (referred to in Section C.1.3). From a usage point of view, the interfaces help the potential user of the code bypass the details and run the code using a set of input parameters.

C.1.1 Utility Functions

QoSStatus

The file `QoSStatus` is not a function and does not accept any arguments. In fact, this code defines the structure of the status variables used in many other functions. In doing so, `QoSStatus` contains the indexes used by the solvers in reporting the status of the solution to a particular problem.

A status vector holds information such as the name of the algorithm which has produced the solution as well the values of k, and j if applicable.

QoSConst

A call to `QoSConst` will define constants which are used for designating which algorithm is to solve a particular problem.

PathGain

The function `PathGain` generates a set of path gains, thus producing the representation of one cell. This function can be called in a few different ways, the most basic one of which is as,

- `[g,X,Y,Z]=pathgain(M)`: A set of M mobile stations will be generated, the x–y coordinates of which will be stored at X and Y. The distances from the mobile stations to the base station will be stored in Z and g will hold the path gains.

In many cases, the cell is analyzed during a time period, thus raising the need for simulating the movements of the mobile stations. For these purposes, the function `PathGain` may be called as,

- `[g,X,Y,Z,I]=pathgain(x,y)`: Here, x and y hold the updated position of the mobile stations, most probably generated by a call to `PathGain` beforehand. The mobile stations, however, have to be reordered and the new values of g and Z have to be calculated.

The function `PathGain` can also be called in a few other different formats, in order to change model parameters and alike. For details refer to the instructions included in the header of the function.

QOSCalc

Function `QOSCalc` calculates some of the parameters of a solution. It is generally called inside the solvers in order to refresh the values of the parameters after a solution is produced.

QoSCheck and QoSCheckM

The function `QoSCheck` examines a solution to determine if it complies with all the required conditions. It can produce an overall result or a detailed error message. `QoSCheckM` is the multiple–class counterpart of `QoSCheck`.

QoSCheckConst

The function `QoSCheckConst` generates the constants used in `QoSCheck` and `QoSCheckM` for reporting the source of an error.

QoSVisualizeCell

The visualization of a cell is carried out through `QoSVisualizeCell`. This function can input different sets of parameters, enabling it, for example, to visualize cells in which different mobile stations have different significances.

chirho

The function `chirho` either calculates $\rho(\chi)$ or $\tilde{\rho}(\chi)$ for a scalar value of χ or an array of values of χ. For more information refer to Section 3.6.3.

C.1.2 Solver Functions

The solver functions constitute two categories. The first are the user callable functions, presented in the first part of Table C.1. In addition to these, there are internal functions which attempts to directly using them may result in spurious solutions. These functions are used inside other functions and are mentioned in the second half of table C.1.

Table C.1: *Single-cell solver functions and the corresponding problems they solve. For details refer to the references.*

Function	Problem(s)	Reference(s)
User Callable Functions		
`QoSCSC`	CSC	Chapter 2
`QoSNSC`	NSC, NSC^{f+}	Sections 3.1, 3.4
`QoSNplusSC`	N^{+}SC	Section 3.2
`QoSNSCa`	NSC^{a}	Section 3.3
`QoSNplusSCa`	$\text{N}^{+}\text{SC}^{a}$	Section 3.3
`QoSCSCa`	CSC^{a}	Section 3.3
`QoSNfmSC`	NSC^{f-}	Section 3.4
`QoSMSC`	M^{1}SC, M^{2}SC, $\text{MSC}^{\star}$	Sections 3.5, 3.6.2
`QoSMSCanL`	$\text{MSC}^{a\nu L_i}$	Section 3.6
Internal Functions		
`QoSNprimeSC`	$\text{N}'\text{SC}$	Section 3.2
`QoSNprimeSCa`	$\text{N}'\text{SC}^{a}$	Section 3.3
`internal_UaSCf`	NSC^{f-}	Section 3.4

C.1.3 Facilitating Interface

To facilitate the use of the functions listed in Table C.1, function `QoS` provides a unique interface, through which one can give in all the system parameters and descriptors. Then, through designating a type variable, the proper solver will be utilized. A sample usage of this function is given in the file `QoSTest`.

C.2 Multiple–Cell Methods

The code developed for solving multiple–cell problems takes advantage of MATLAB's support for class–based implementations. As a result, the corresponding code becomes encapsulated inside a class with a set of methods and there is no bulky parameter–passing involved in the usages.

The algorithm MC (see Section 4) is essentially implemented through the class MCP (stands for MC problem). This class will be surveyed in Section C.2.1. Then, as we also need to simulate multiple–cell systems in given time periods, the class MCPs is developed as well (discussed in Section C.2.2). The MCPs keeps of track of the system parameters of a MCP and provides the needed presentations and visualizations.

C.2.1 The Static Class MCP

The MCP class is initialized using the constructor `MCP` and has the following methods implemented in it.

get and set

The standard `get` and `set`, although minimally implemented.

load and save

Saving and loading a MCP class to and from a mat file are performed using the methods `save` and `load`, respectively.

randomize

A random MCP is generated through the use of the method `randomize`. This method fills all the parameters with random values within the respective ranges. These parameters can be later customized through the use of the method `set`.

prepare

After a problem is generated, it has to undergo a preprocessing stage in order to become ready for the method `solve`. To do so, a call to the method `prepare` will compute the assignment of the stations to the base stations as well as a few other preliminary stages necessary before producing a solution.

solve

The heart of the MCP class is the method `solve`. This method is the implementation of the algorithm MC.

check

After a call to `solve`, the method `check` will go through all the parameters and check the integrity of the solution, both in terms of the structure of the variables as well as the compliance to the constraints.

display and draw

The twin methods `display` and `draw` act as the visualizers of a MCP class. The method `display` gives an insider access to the class, letting the user cross the private boundary around the class properties, while `draw` provides different visualizations, including the ones presented in Section 5.6.

C.2.2 The Dynamic Class MCPs

The class MCPs contains a single MCP implemented in it, as well as a set of multi-dimensional matrices for logging the solution to a MC as the system undergoes change during a known time period. A MCPs class is initialized using the constructor `MCPs` and the following methods are applicable to it.

load and save

Saving and loading a MCPs class to and from a mat file are performed using the methods `save` and `load`, respectively.

randomize

The MCPs class is randomized using the method `randomize`. A call to this method will also invoke a call to the `randomize` method for the internal MCP class.

step

The method `step` simulates the change of the underlying MCP in a time step equal to δt. This will include a slight change in the position of the mobile stations as well as updating $\vec{\mathbf{g}}$.

simulate

The heart of the MCPs class is the `simulate` method. This method repeatedly utilizes the method `step` and then the method `solve` of the underlying MCP for the given time period and subsequently collects the produced results.

display and draw

The method `display` gives access to the private properties of the class and the method `draw` produces different visualizations of it, including the ones presented in Section 5.6.